INFORMATION TO USERS

This reproduction was made from a copy of a document sent to us for microfilming. While the most advanced technology has been used to photograph and reproduce this document, the quality of the reproduction is heavily dependent upon the quality of the material submitted.

The following explanation of techniques is provided to help clarify markings or notations which may appear on this reproduction.

1. The sign or "target" for pages apparently lacking from the document photographed is "Missing Page(s)". If it was possible to obtain the missing page(s) or section, they are spliced into the film along with adjacent pages. This may have necessitated cutting through an image and duplicating adjacent pages to assure complete continuity.

2. When an image on the film is obliterated with a round black mark, it is an indication of either blurred copy because of movement during exposure, duplicate copy, or copyrighted materials that should not have been filmed. For blurred pages, a good image of the page can be found in the adjacent frame. If copyrighted materials were deleted, a target note will appear listing the pages in the adjacent frame.

3. When a map, drawing or chart, etc., is part of the material being photographed, a definite method of "sectioning" the material has been followed. It is customary to begin filming at the upper left hand corner of a large sheet and to continue from left to right in equal sections with small overlaps. If necessary, sectioning is continued again—beginning below the first row and continuing on until complete.

4. For illustrations that cannot be satisfactorily reproduced by xerographic means, photographic prints can be purchased at additional cost and inserted into your xerographic copy. These prints are available upon request from the Dissertations Customer Services Department.

5. Some pages in any document may have indistinct print. In all cases the best available copy has been filmed.

University Microfilms International
300 N. Zeeb Road
Ann Arbor, MI 48106

Edwards, James Francis

IN SITU CHARACTERIZATION OF ADSORBED SPECIES ON METHANOL SYNTHESIS CATALYSTS BY FT-IR SPECTROSCOPY

Iowa State University PH.D. 1984

PLEASE NOTE:

In all cases this material has been filmed in the best possible way from the available copy. Problems encountered with this document have been identified here with a check mark _√_.

1. Glossy photographs or pages _____
2. Colored illustrations, paper or print _____
3. Photographs with dark background _____
4. Illustrations are poor copy _____
5. Pages with black marks, not original copy _____
6. Print shows through as there is text on both sides of page _____
7. Indistinct, broken or small print on several pages _✓_
8. Print exceeds margin requirements _____
9. Tightly bound copy with print lost in spine _____
10. Computer printout pages with indistinct print _____
11. Page(s) _____ lacking when material received, and not available from school or author.
12. Page(s) _____ seem to be missing in numbering only as text follows.
13. Two pages numbered _____. Text follows.
14. Curling and wrinkled pages _____
15. Other _____

In situ characterization of adsorbed species on methanol synthesis catalysts by FT-IR spectroscopy

by

James Francis Edwards

A Dissertation Submitted to the
Graduate Faculty in Partial Fulfillment of the
Requirements for the Degree of
DOCTOR OF PHILOSOPHY

Major: Chemical Engineering

Approved:

Signature was redacted for privacy.

In Charge of Major Work

Signature was redacted for privacy.

For the Major Department

Signature was redacted for privacy.

For the Graduate College

Iowa State University
Ames, Iowa

1984

TABLE OF CONTENTS

LIST OF TABLES

LIST OF FIGURES

NOMENCLATURE

a, b, c	lattice parameters, Å
c_p	heat capacity
$d_{h,k,l}$	interplanar distance, Å
E	energy, eV
f	fugacity
ΔG	free energy of formation
ΔH	heat of formation
H	dead-space pressure, mmHg
K	equilibrium constant
M	molecular weight; modulus of rupture
P	pressure
r	radius; reaction rate
R	ideal gas constant
S	surface area
t	thickness
T	temperature, °K
V	volume, cm^3
W	weight, g
y	mole fraction
α, β, γ	lattice angles, degrees
α	perfect gas law correction factor
γ	fugacity coefficient
θ	diffraction angle, degrees; contact angle condensate
λ	radiation wavelength, Å

ρ	density
σ	surface tension
ν	vibrational frequency, cm^{-1}
ϕ	correction term in XPS, eV

INTRODUCTION

One of the great challenges facing the chemical industry as the 21st century approaches will be making the adjustments in fuel and raw material sources as petroleum and natural gas reserves diminish. Coal is expected to become a major source for chemical feedstocks in this country because of its availability and abundance, but economic considerations have thus far restricted the development of coal-based industries for organic synthesis. There are two major approaches for coal utilization: 1) coal gasification to produce light hydrocarbons, carbon oxides, hydrogen, and water, and 2) coal liquefaction to produce heavier organics, especially aromatics. The technology involved in coal gasification is well-developed, e.g., the Winkler, Koppers-Totzek, or Lurgi processes, and has been used for many years on a large industrial scale in South Africa. Although the synthesis gas produced by gasification can be used in various processes for manufacturing organic compounds, this discussion will be limited to the use of synthesis gas to produce methanol. Coal gasification on a commercial scale for methanol synthesis is under development in North Dakota (Great Plains Coal Gasification Project) to make 17.5 tons/d of methanol for cleaning the raw-gas product, and in Tennessee (Tennessee Eastman Co.) to make acetic anhydride which involves methanol synthesis as an intermediate step. The Tennessee Valley Authority plans to construct a coal-to-methanol facility (North Alabama Coal Gasification Project) to produce 1 million gal/d of fuel-grade methanol.

Currently most methanol is produced from synthesis gas obtained

by steam reforming of natural gas:

$$CH_4 + H_2O \rightleftharpoons 3H_2 + CO$$

The CO/H_2 ratio is adjusted to 1/2 by adding carbon dioxide to the natural gas (combination of steam reforming and water-gas shift reactions):

$$CO_2 + CH_4 \rightleftharpoons 2CO + 2H_2$$

The synthesis gas is reacted over a highly selective mixed metal oxide catalyst at elevated pressures and temperatures to produce methanol:

$$CO + 2H_2 \rightleftharpoons CH_3OH$$

The initial technology for methanol synthesis was developed by Badische Anilin und Soda Fabrik in 1923 using a zinc chromite catalyst at pressures of several hundred atmospheres and temperatures between 300 and 450°C. During the 1960s, Imperial Chemical Industries developed a low-pressure process using a copper-zinc chromite catalyst at pressures of 50-100 atmospheres and temperatures of 250-300°C. The only significant change in catalyst composition since 1960 has been the substitution of alumina for chromia.

Annual methanol demand in this country has been projected to double during the 1980s to 8 million metric tons due mainly to rapid expansion in several developing applications (Weismantel, 1980). Major uses for methanol are the production of formaldehyde, dimethyl terephthalate (DMT), methyl methacrylate, methyl halides, methyl amines, and acetic acid. Large quantities of methanol are used as a gasoline blending

agent and as a solvent. Legislated reductions in the amount of tetraethyl lead allowed in gasoline have increased the demand for octane boosters such as methyl tert-butyl ether (MTBE) which is made from methanol and isobutylene. The recent development of a single-step catalytic distillation process (MTBE plus), which eliminates the methanol recovery section of the conventional process, provides an economically attractive alternative to isobutylene alkylation for octane enhancement (Lander et al., 1983). Methanol by itself can be used as an octane booster, but there are problems with methanol/gasoline mixtures due to their higher affinity for water, higher evaporative losses, and the need to modify the engine. Despite these problems, the TVA and ARCO will be testing a 6-7% methanol/gasoline mixture in 150 automobiles as part of the North Alabama Coal Gasification Project; West Germany has pursued a more ambitious program testing more than 1000 vehicles with a 15% methanol/gasoline mixture with only minor adjustments to the engines (Parkinson et al., 1982).

Future demand for methanol could expand multifold as coal assumes a greater proportion of our energy needs. Although methanol is presently economically unattractive as a substitute for gasoline, the State of California has begun a program to operate 550 vehicles with methanol because it produces fewer pollutants than gasoline. More than 300 privately-owned vehicles, converted by Future Fuels of America, Inc., are running on methanol in the Sacramento, San Francisco, and Los Angeles areas. Even if gasoline remains the major automotive fuel into the next century, methanol production could increase significantly if technology such as Mobil Oil's M-Gasoline process is used to produce gasoline. This

process uses a zeolite catalyst (ZSM-5) to convert methanol into a blend of paraffins, cycloparaffins, and aromatics with a research octane number of 93, i.e., an unleaded premium gasoline (Berry, 1980). New Zealand will use this technology to convert natural gas into approximately 12,500 bbl/d of gasoline. Utilities using coal gasification technology for power generation will probably also manufacture methanol. During off-peak hours, part of the syngas would be converted to methanol and stored; during peak hours, the methanol would be used as fuel in gas turbines to meet the high electrical demand. And finally, there is great potential for future development of methanol as a primary feedstock in the chemical industry, especially as supplies of ethylene and propylene decrease. An example is the manufacture of acetic acid, where methanol has replaced ethylene as the primary feedstock in new technologies by BASF and Monsanto (Kohn, 1979).

The key development in methanol synthesis technology has been the catalyst. Improvements in catalyst performance are usually obtained by trial-and-error methods: variations in composition or preparation technique are tried until a catalyst is found having greater activity, selectivity, or stability. Characterization of physical and chemical properties is often incomplete, and the reasons for the superiority of a particular catalyst are frequently unclear. Although methanol synthesis as a commercial process is fully developed, the specific function of the catalyst and the fundamentals of the elementary surface reactions are still highly speculative. The main objective of this investigation has been to prepare several different compositions of methanol synthesis catalysts and characterize these catalysts by physical

and chemical techniques, placing emphasis on the use of Fourier transform infrared (FT-IR) spectroscopy to identify the chemical species adsorbed on the catalyst surfaces under methanol synthesis conditions. Part I of this thesis describes the properties of the catalysts during the various stages of preparation (i.e., precursor, oxide, and reduced states) using the techniques of X-ray diffraction, atomic absorption, ESCA, surface area, and pore distribution measurements. Part II examines the adsorption of various organic molecules such as carbon monoxide, formic acid, formaldehyde, and methanol on oxidized and reduced catalysts to identify intermediate surface species and to observe the behavior of adsorbed species under various conditions using FT-IR spectroscopy. Part III evaluates the relative activities and selectivities of several catalysts for methanol synthesis and identifies the adsorbed species under reaction conditions. It should be emphasized that this study has focused on the FT-IR characterization of adsorbed surface species under in situ conditions with the objective of obtaining a better understanding of the molecular interactions occurring on the catalyst surface.

PART I.

PREPARATION AND CHARACTERIZATION OF METHANOL SYNTHESIS CATALYSTS

LITERATURE REVIEW

The development of an inorganic catalyst for the synthesis of methanol from hydrogen and carbon monoxide occurred during the early part of this century when catalysis was just beginning to play an important role in the chemical industry. This development was important because it enabled methanol to be produced on a larger scale and at a lower cost compared to synthesis by the destructive distillation of wood. Although there have been many improvements in the preparation of methanol catalysts during the succeeding years, the basic components – zinc oxide, copper oxide, and a promoter such as chromia or alumina – are unchanged. Methanol catalysts may be divided into two groups: (1) the high-pressure zinc catalysts composed of zinc oxide and a promoter, and (2) the low-pressure copper catalysts composed of zinc oxide, copper oxide, and a promoter. The developments in methanol catalysts are summarized in Table 1. Supported-metal catalysts for methanol synthesis have been developed in recent years but have not been applied commercially. Excellent reviews of methanol catalysts have been provided by Natta (1955) and Klier (1982).

Zinc Catalysts

The catalyst developed by BASF in 1923 for methanol synthesis was a highly selective, mixed metal oxide containing zinc oxide and chromia in a ratio of 9/1, respectively (BASF, 1923). Zinc oxide by itself is a fairly good catalyst for methanol synthesis, but it is quite susceptible to aging (crystallite growth) under reaction conditions

Table 1. Developments in methanol catalysts

Year	Inventor/assignee	Catalyst
1913	BASF G.P. 293,787	Oxides of Cr, Co, Mn, Mo, Pd, Ti, Zn
1923	BASF G.P. 415,686	90% ZnO - 10% Cr_2O_3
1923	Patart	90% CuO - 10% ZnO
1923	BASF F.P. 571,356	Oxides of Cu, Cr, Zn, Mn
1933	Dodge U.S. 1,908,696	ZnO - CuO (Cu)
1936	Larson U.S. 2,061,470	CuO-MnO_2; CuO-ZnO plus Cr_2O_3, Al_2O_3, ZrO_2, V_2O_3, TiO_2, ThO_2, SiO_2, or CeO_2
1967	ICI U.S. 3,326,956	ZnO - CuO - Cr_2O_3
1967	ICI F.P. 1,489,682	ZnO - CuO - Al_2O_3
1971	Metallgesellschaft F.P. 2,049,193	Oxides of Zn, Cu, Mn, V
1978	Stiles U.S. 4,111,847	ZnO - CuO

which reduces the catalytic activity. Chromia, a very poor hydrogenation catalyst which is also difficult to reduce, is added to zinc oxide to prevent aging. X-ray (Williams and Cunningham, 1974) and ESR (Rálek et al., 1968) studies of the mixed oxides have established that the active catalyst contains a mixture of zinc oxide and zinc chromite spinel, $ZnCr_2O_4$. The spinel is not catalytically active, but serves as a stabilizer for zinc oxide. The effect of chromia is mainly physical, as evident by comparing the activation energies of a $ZnO-Cr_2O_3$ catalyst with pure zinc oxide: both have a value of about 30 kcal/mol.

The optimum composition for a mixed $ZnO-Cr_2O_3$ catalyst depends greatly on the preparation method. Various values for the optimum Cr/Zn ratio have been determined by conversion tests to be 0.3-0.5 (Molstad and Dodge, 1935), 1.0 (Natta, 1955), 1.0-1.5 (Oba, 1965), 0.4-0.5 (Oba, 1965), and 0.5-1.4 (Vlasenko, 1966). The amount of chromia required appears to depend on the homogeneity of the catalyst components; less chromia is needed for catalysts which have small crystallites of each component in intimate contact with each other. The catalytic activity is poor below a Cr/Zn ratio of 0.3 because of crystallite growth, and is also poor at high ratios because of the decrease in the amount of the active component, zinc oxide. Lower amounts of chromia improve the catalyst selectivity. A catalyst with a Cr/Zn ratio of 0.1 produces methanol of greater than 99% purity (Natta et al., 1953).

Other metal oxides have been investigated as possible promoters for zinc oxide or zinc oxide-chromia catalysts. Alumina forms a spinel with zinc oxide (Kauffe and Pschera, 1950), but is less desirable as a stabilizer than chromia because alumina enhances the dehydration of

methanol to form dimethyl ether. Small quantities of thorium, zirconium, and tantalum oxides (Dolgov and Karpinskii, 1932) and vanadium oxide (Veltistova et al., 1934; Metallgesellschaft, 1971) act as stabilizers for $ZnO-Cr_2O_3$ catalysts.

The stabilizers which have been previously discussed are intercrystalline, i.e., they are external to the lattice structure of zinc oxide. There are also intracrystalline stabilizers such as magnesium, iron, and manganese oxides which form a solid solution with zinc oxide because of the similarities of the ionic radii.

Copper Catalysts

The high activity of a methanol synthesis catalyst containing copper oxide was discovered by Patart using a mixed metal oxide of 90% CuO-10% ZnO (Fenske and Frolich, 1929). However, catalysts containing copper were not applied commercially to methanol synthesis for many years because the sensitivity of copper sites to poisons such as sulfur was high. Copper oxide by itself is a very poor methanol catalyst, but when mixed with ZnO produces a combined oxide having greater activity than either oxide alone. The addition of copper oxide, unlike chromia, to zinc oxide has a truly synergistic effect since the activation energy decreases to about 18 kcal/mol (Natta, 1955). The promoting effect is believed to be both chemical and electronic.

The ternary catalysts composed of zinc oxide, copper oxide, and a stabilizer are of major interest. Early studies established that both chromia and alumina functioned as good stabilizers for methanol catalysts

(Frolich and Lewis, 1928; Ivanov, 1934a and 1934b; Plotnikov et al., 1931). However, there was great variety in proposed optimum compositions. Natta reported high activity for catalysts with Cu/Zn/Cr ratios of 3/6/1 and 1/8/1. Although X-ray patterns of reduced catalysts showed the presence of metallic copper, the active state of the copper was believed to be a partially reduced oxide (Natta, 1955).

Recently binary and ternary methanol catalysts have been extensively characterized by physical and kinetic measurements (Herman et al., 1979; Mehta et al., 1979; Bulko et al., 1979; Herman et al., 1981). A series of binary CuO-ZnO catalysts were prepared by coprecipitation from nitrate solution using sodium carbonate. X-ray analysis identified the precipitated compounds as mixtures of $Cu_2(OH)_3NO_3$, $Zn_5(OH)_6(CO_3)_2$, and $(Cu,Zn)_2(OH)_2CO_3$. These precursors were calcined in air at 350°C to form ZnO-CuO compounds. Oxides with more than 15 wt.% CuO had some copper (up to 6%) dissolved in the ZnO phase. Transmission electron microscopy established that the morphology of ZnO changed from thin crystallites to hexagonal platelets as the CuO content rose above 30 wt.%. The composition of the precipitate was believed to determine the nature of the ZnO morphology. The reduced catalysts were composed of zinc oxide, metallic copper, and an amorphous form of copper (based on X-ray diffraction). This amorphous copper was determined to be dissolved in the ZnO phase using scanning transmission electron microscopy. Diffuse reflectance spectra showed an absorption band at 17,500 cm^{-1} which was assigned to a Cu(I) species dissolved in ZnO. Maxima for greatest catalytic activity were found at ZnO/CuO ratios of 1/2 and 7/3, corresponding to compositions with maximum amounts (12%) of copper dissolved in the

zinc oxide particles. Surface analyses with XPS and Auger spectroscopies revealed surface compositions equal to the bulk catalyst composition. Ternary catalysts containing some chromia or alumina had a zinc oxide phase with both copper and the promoter cations dissolved in the lattice, although the effect of the promoter was mostly physical. A small amount of alumina caused an increase in the surface area and an increase in the amount of dissolved copper in the ZnO phase by 33%. The addition of ceria to a binary catalyst was found to decrease the amount of dissolved copper and decrease the catalytic activity. These investigators concluded that the active component of copper-containing methanol catalysts was a solid solution of Cu(I) ions in the zinc oxide phase.

Other investigators working with ZnO-CuO and ZnO-CuO-Al_2O_3 catalysts have found that copper and aluminum ions dissolve in the zinc oxide phase without the formation of spinels (Ketchik et al., 1982). In the binary compositions, a CuO phase appeared when the amount of copper exceeded 10 atomic %. Decomposition of these solid solutions produced water and carbon dioxide, indicating that the oxides normally have hydroxyl and carbonate groups incorporated into their structures. The function of the aluminum ions was to stabilize the catalyst, while the copper ions dissolved in the zinc oxide phase were active sites in methanol synthesis (Kuznetsova et al., 1982).

An X-ray diffraction analysis of the reduction process for a ZnO-CuO-Al_2O_3 catalyst identified a stabile Cu_2O intermediate at reduction temperatures under 200°C (Ruggeri et al., 1982).

The presence of gaseous CO_2 was found to retard the reduction of Cu_2O to metallic copper. Binary ZnO-CuO catalysts also formed an inter-

mediate Cu_2O phase during reduction (Himelfarb et al., 1983). The reduction rate was dependent on CuO crystallite size and CuO dispersion in these mixed metal oxides.

The valence states of copper in precursor, calcined, and reduced ZnO-CuO catalysts have been determined using X-ray photoelectron and Auger spectroscopies (Okamoto et al., 1982; Okamoto et al., 1983a and 1983b). The coprecipitated precursors had two types of Cu^{2+} species which were attributed to the copper ions in $Cu_2(OH)_2CO_3$ and $(Zn,Cu)_2(OH)_2CO_3$. The calcined oxides had three types of cupric ions: crystalline cupric oxide, an amorphous surface layer of copper oxide, and cupric oxide dissolved in the zinc oxide phase. The reduced catalysts contained copper metal particles and a two-dimensional monolayer of Cu^{o}-Cu^{+} species over zinc oxide. The two-dimensional layer, which had been formed from the cupric ions dissolved in zinc oxide, was believed to be the active site for methanol synthesis. The cuprous ions in these binary catalysts were very stable under reducing and mild oxidizing conditions.

Catalyst Preparation

Investigations to develop improved methanol catalysts have continued through the years as evident by the large number of patents issued. These developments have occurred because the method of catalyst preparation has a great effect on the catalytic activity. The metal oxides can be directly mixed and fused together to form a methanol catalyst (Larson, 1936), but the activity of this type of catalyst was low compared to

other types. Both catalytic activity and stability depended on the homogeneity of the phases in the catalyst. X-ray studies of several low-pressure catalysts have established that the most active catalysts have the greatest homogeneity of components (Shishkov et al., 1979). A ternary $ZnO-CuO-Al_2O_3$ catalyst prepared by kneading was less active than the same catalyst prepared by coprecipitation; the latter was found to have its components in a finely divided state (Kotera et al., 1976; Shimomura et al., 1978).

Preparation techniques can be critical in establishing the ultimate properties of the catalyst. The types of salts used, the precipitating agent, the precipitation temperature, the calcination conditions, and other factors have an impact on the eventual catalytic behavior. The general practice is to coprecipitate a solution of metal nitrates with a carbonate solution; the precipitate is then filtered and washed. The precipitated metal "carbonates" are then dried and calcined to form metal oxides. Salts of metal halides or sulfates produce catalysts with lower activities, presumably due to contamination of active sites (Natta, 1955). Sulfur will poison low-pressure catalysts by selectively adsorbing on copper sites (Wood et al., 1980). An alkali metal carbonate has been found to yield a more active catalyst than those precipitated with an alkali metal hydroxide or ammonium hydroxide (Dodge, 1933). It is important to thoroughly wash the precipitate because the presence of alkali metals in the catalyst will enhance the formation of higher alcohols. Ammonium carbonate or ammonium bicarbonate may be used as the precipitating agent to avoid this problem (Stiles, 1978). After the precipitate is dried, calcination should occur at a temperature

high enough to decompose the nitrate and carbonate components to the oxides, yet at a temperature low enough to minimize the growth of crystallites. Natta has shown that there was an inverse relationship between catalytic activity and crystallite size for zinc oxide (Natta, 1955). Calcination temperatures generally fall within the 300-500°C range. The final step in catalyst preparation is the reduction of the oxides, usually performed in the reactor just prior to actual use (catalyst activation). A hydrogen/inert gas mixture with a hydrogen content of 2-5% is passed over the catalyst at the reduction temperature until the reduction is complete. It is important that local temperatures during reduction remain low to avoid crystallite growth and also to prevent the complete reduction of copper to the zero valent oxidation state.

A novel methanol catalyst has been prepared by leaching an alumina-zinc-copper alloy with aqueous NaOH to produce a Raney catalyst (Friedrich et al., 1983a and 1983b). These catalysts were highly selective to methanol formation (99%) and quite resistant to copper sintering. The greatest activity was related to both surface area and the concentration of zinc oxide on the catalyst surface (these catalysts were mostly copper). Although metallic copper was ascribed to the most active component of the Raney catalysts, these investigators also suggested that the catalytic activity depended on a complex interaction between the copper and zinc oxide.

EXPERIMENTAL APPARATUS AND METHODS

Catalyst Preparation

A series of binary copper-zinc oxide catalysts with relatively low copper content was prepared by coprecipitating the metal nitrates with ammonium bicarbonate according to the method developed by Stiles (1978). A 1 liter solution of the mixed metal nitrates (1N) and 1/2 liter of distilled water were poured into a 4 liter glass kettle and gradually heated to 60°C. The initial pH of the solution was typically between 3 and 4. When the precipitation temperature was reached, a slow flow of CO_2 was bubbled through the nitrate solution and mild stirring was begun. A 1 liter solution of 1 N ammonium bicarbonate was added dropwise to the nitrate solution in the region near the CO_2 sparger. The temperature of the solution was measured continuously via a thermocouple well and the pH was monitored periodically by inserting a probe into the solution manually. The pH probe could not be kept in the solution continuously without forming a film on the glass membrane which resulted in erroneous readings. After the bicarbonate solution was completely added, some solid ammonium bicarbonate was gradually added to the solution until a pH of approximately 7 was reached. The total amount of ammonium bicarbonate added to the solution was approximately 2.5 moles per mole of metal nitrates in the initial solution. The solution was stirred for an additional half hour before removing the kettle and filtering its contents through a 50 micron fritted glass filter. The precipitate was washed with 1 liter of distilled water. The binary precipitates were light blue and the filtrates were navy blue. Pure

precipitated zinc oxide had a white precipitate and a clear filtrate. Precipitates were dried in air overnight at 110°C and then were calcined in flowing oxygen at 400°C for 8 hours.

Some ternary oxides containing chromia or alumina were prepared in the same manner, starting with a mixture of three metal nitrates. These precipitates were composed of smaller crystallites that did not settle as readily as binary particles, and were more difficult to filter and wash. The ternary precipitates were also light blue with navy blue filtrates. Pure precipitated alumina had a white gel-like precipitate and clear filtrate, while pure precipitated chromia had a fine grey precipitate and clear filtrate. The precipitated alumina was calcined at the slightly higher temperature of 450°C.

An impregnated 95/5 ZnO/CuO catalyst was prepared by mixing a copper nitrate solution with Kadox 25. This slurry was dried at 110°C to yield a light blue solid which was subsequently calcined in oxygen at 400°C for 8 hours.

Catalyst Characterization

X-Ray diffraction

A Picker powder diffractometer was used to identify the solid-state crystalline phases in the precipitates, oxides, and reduced oxides. Thin powder films were placed on glass slides and exposed to Mo Kα X-rays, using a step size of 0.05° during scanning. The detector signals were collected and processed by computer facilities which used a plotting routine to present the data as intensity versus 2θ value.

Compounds were identified by comparing the patterns with standards for pure crystalline phases.

The Guinier X-ray patterns were taken with an Enraf Nonius Delft camera. Approximately 0.05 g of each sample was mixed with 0.02 g silica powder (an internal standard) and this mixture was spread lightly over a piece of adhesive tape. Three samples were mounted adjacent to each other in the sample compartment of the Guinier instrument and the film was exposed to radiation for five hours.

X-Ray photoelectron and Auger electron spectroscopies

The techniques of X-ray photoelectron spectroscopy (XPS), also known as electron spectroscopy for chemical analysis (ESCA), and Auger electron spectroscopy (AES) can provide information about the elemental composition, oxidation state, bonding, and electronic structure of the surface of a solid. These spectroscopies have been used very successfully to increase the knowledge of surface phenomena in heterogeneous catalysis.

XPS uses X-rays to excite core electrons with enough energy to cause ionization. The kinetic energies of the emitted electrons are measured with a magnetic or electrostatic analyzer. Binding energies are calculated from the Einstein relation:

$$E_B = h\nu - E_k - \phi$$

The binding energy equals the incident energy minus the kinetic energy minus a correction term taking into account the spectrometer work function and sample charging effects. This process is depicted in Figure 1;

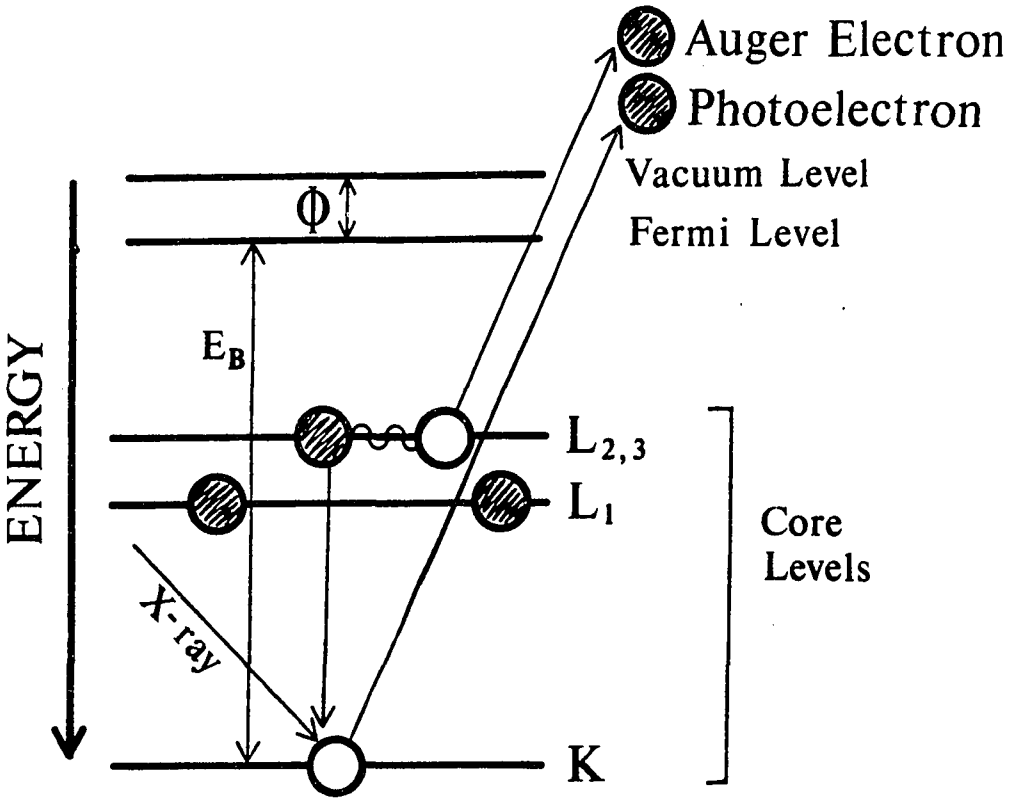

Figure 1. Energy level diagram of photoelectron and Auger electron generation

incident X-rays excite a core electron resulting in the ejection of that electron.

Subsequent relaxation of electrons in the sample can cause the emission of Auger electrons. As an electron from a more energetic level replaces a core electron ejected by the X-ray source, some energy is transferred to other electrons in the same principle electron level. If this energy is sufficient, an electron in this higher level is ejected. Figure 1 shows how a $KL_{2,3}L_{2,3}$ Auger electron is generated. Since Auger electrons result from a secondary process, their kinetic energies are independent of the incident excitation source. Auger transitions are unique for the various elements, thus making this technique popular for elemental analysis; information on oxidation states can also be obtained.

Both X-ray photoelectron and Auger spectra were obtained from an AEI 200B spectrometer coupled with a Nicolet 1180 computer for data manipulation. The X-ray source was Al $K\alpha_{1,2}$ radiation which has an energy of 1486.6 eV. After pretreatment, samples were tightly sealed and transferred via a dry box to avoid atmospheric contamination or oxidation. Sample were prepared for analysis by lightly dusting some powder on adhesive tape.

Surface area and micropore distribution

A Micromeritics AccuSorb 2100E analyzer was used to determine BET surface areas and micropore distributions. All samples were heated at 200°C under vacuum ($< 10^{-4}$ torr) overnight to remove adsorbed gases on the surfaces. Measurements were taken using nitrogen gas at liquid

nitrogen temperature (-195°C). A value of 16.2 $\mathring{A}^2$ was used for the area of a nitrogen molecule in BET determinations. The micropore distribution was determined from the desorption isotherm of each sample, using a cylindrical pore model to estimate pore radii.

RESULTS OF CATALYST CHARACTERIZATION

Cation Composition of the Binary Oxides

The relative amount of zinc and copper in the precipitated oxides does not necessarily equal the relative amount in the initial nitrate solution because the precipitation kinetics and/or thermodynamics might allow one of the cations to preferentially remain in solution. The analytical technique of atomic absorption was used to determine the relative amount of zinc and copper in the binary oxides.

Standard solutions of zinc and copper were prepared by dissolving the oxide in hydrochloric acid and diluting the sample with distilled, deionized water. The zinc standard had 0.95 ppm Zn and the copper standard had 4.8 ppm Cu. The usual method for preparing the precipitated oxides involved dissolving approximately 0.5 g of the oxide in hydrochloric acid and diluting the sample in a 1000 ml volumetric flask. The solution for copper analysis was made by taking 10 ml of the diluted solution and further diluting this aliquot in a 250 ml volumetric flask. The solution for zinc analysis was made by taking 10 ml of the copper solution and diluting it in a 250 ml volumetric flask. These solutions made from the binary oxides must have cation concentrations less than those in the standard solutions to ensure the accuracy of the results because the zinc and copper standards have cation concentrations near the upper limit of a linear range (concentration vs signal intensity). Distilled water is used to establish the lower limit (0 ppm) and the standards establish the upper limits for the particular conditions used in this analysis. A linear relationship between these limits is then

used to determine the cation concentrations in the precipitated oxides. In some cases, the filtrate from the precipitation reaction was analyzed to check for consistency in the results by making a material balance; generally the filtrate was diluted by a factor of 100 for both zinc and copper analyses. Instrumentation parameters and cation ratios are given in Table 2. Both zinc and copper concentrations are based on the average of ten readings.

Using the preparation of 86/14 Zn/Cu oxide as an example, the cation ratio in the precipitate can be calculated by determining the amounts of zinc and copper lost in the filtrate and subtracting these amounts from the original nitrate composition. The filtrate had a much higher proportion of copper to zinc than the initial solution in all the cases examined. Because the amount of filtrate was approximately 2.5 liters, the amount of copper lost can be calculated as:

$$(1.41 \text{ ppm})(100)(2500 \text{ ml}) = 0.35 \text{ g Cu}$$

and the amount of zinc lost was:

$$(0.55 \text{ ppm})(100)(2500 \text{ ml}) = 0.14 \text{ g Zn}$$

The amounts of copper and zinc in the original nitrate solution were:

$$(0.14 \text{ mole Cu})(63.5 \text{ g/mol}) = 8.89 \text{ g Cu}$$
$$(0.86 \text{ mole Zn})(65.4 \text{ g/mol}) = 56.2 \text{ g Zn}$$

Thus, the amounts of copper and zinc in the precipitate should be:

Table 2. Atomic absorption parameters and binary oxide compositions

	Zn lamp	Cu lamp
Wavelength	213.9 nm	324.8 nm
Current	15 mA	15 mA
Time constant	0.5 s	0.5 s
Slit height	0.7 nm	0.7 nm
Fuel flowrate	2.5 l/min	2.5 l/min
Air flowrate	17.5 l/min	17.5 l/min

Binary oxide	Zn, ppm (dilution)	Cu, ppm	Zn/Cu
95/5 Zn/Cu	0.631 ± .005 (25)	0.72 ± 0.02	96/4
filtrate	0.821 ± .006 (2)	0.98 ± 0.01	63/37
90/10 Zn/Cu	0.91 ± .02 (20)	1.5 ± 0.00	92/8
85/15 Zn/Cu	0.63 ± .01 (25)	2.68 ± 0.04	85/15
86/14 Zn/Cu	0.64 ± .01 (25)	2.61 ± 0.04	86/14
filtrate	0.55 ± .01	1.41 ± 0.05	28/72
80/20 Zn/Cu	0.81 ± .02 (20)	4.1 ± 0.05	80/20
2/1 Zn/Cu	0.681 ± .004	0.31 ± 0.02	69/31
filtrate	0.580 ± .004	3.64 ± 0.03	14/86

8.89 - 0.35 = 8.54 g Cu

56.2 - 0.14 = 56.1 g Zn

The Zn/Cu ratio corresponds to 87/13 which is consistent with the result of 86/14 for the precipitate. The material balances for the other oxides were also consistent. Even though an enrichment of copper in the filtrate occurred, the amount was not enough to significantly alter the precipitate composition. However, if less concentrated nitrate solutions had been used, the cation ratio in the precipitates could have been changed considerably.

X-Ray Powder Diffraction

Identification of the precursors for methanol catalysts proved to be most difficult because samples were partially amorphous and comparisons with pure crystalline phases did not match exactly. The precursor of precipitated zinc oxide (Figure 2) was composed of smithsonite, $ZnCO_3$, and hydrozincite, $Zn_5(CO_3)_2(OH)_6$. The precursor of precipitated copper oxide (Figure 3) was malachite, $CuCO_3 \cdot Cu(OH)_2$. The precursor of 80/20 Zn/Cu oxide was typical of the binary oxides with relatively high zinc contents; although an exact identification of crystalline phases could not be determined with certainty, it appeared that hydrozincite was the major phase with some smithsonite and some rosalite, $(Cu,Zn)_2(OH)_2CO_3$, present (Figure 4). Because these precipitates were prepared with CO_2 bubbling through the solution, carbonates rather than nitrates were favored in the formation of the precursors.

After calcining the precursors in oxygen at 400°C for 8 hours, the oxidized materials showed only zinc oxide and cupric oxide. The presence of CuO ($2\theta = 17.56°$) did not become apparent until the copper content exceeded that of the 90/10 Zn/Cu oxide (Figure 5). Reduction of these oxides in carbon monoxide at 200°C did not affect the ZnO phase but some copper metal ($2\theta = 19.56°$) was formed (Figure 6). There was no evidence of a cuprous oxide phase.

The powder patterns of ternary oxides were very similar to the binary oxide patterns. As indicated in Figure 7, ZnO was the only distinct phase observed in $ZnO/CuO/Cr_2O_3$ precipitated oxides with copper and chromium contents up to 10% (metal atom %). Pure metal oxides of

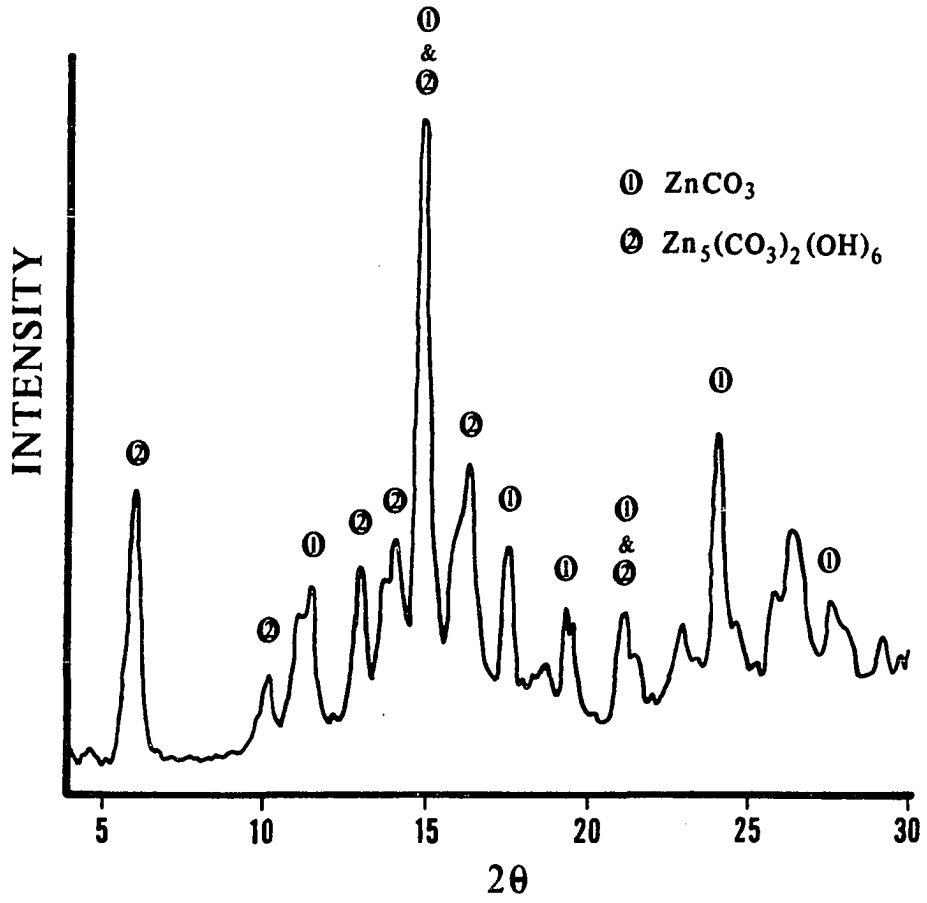

Figure 2. Powder diffraction pattern of zinc oxide precursor

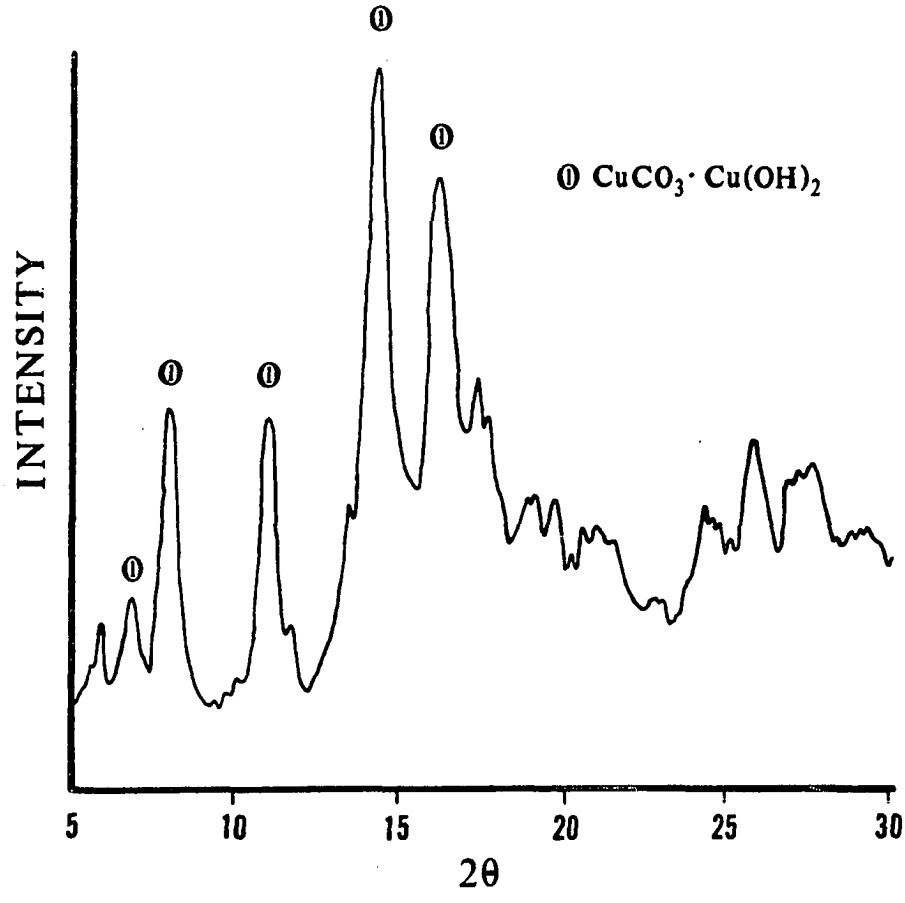

Figure 3. Powder diffraction pattern of copper oxide precursor

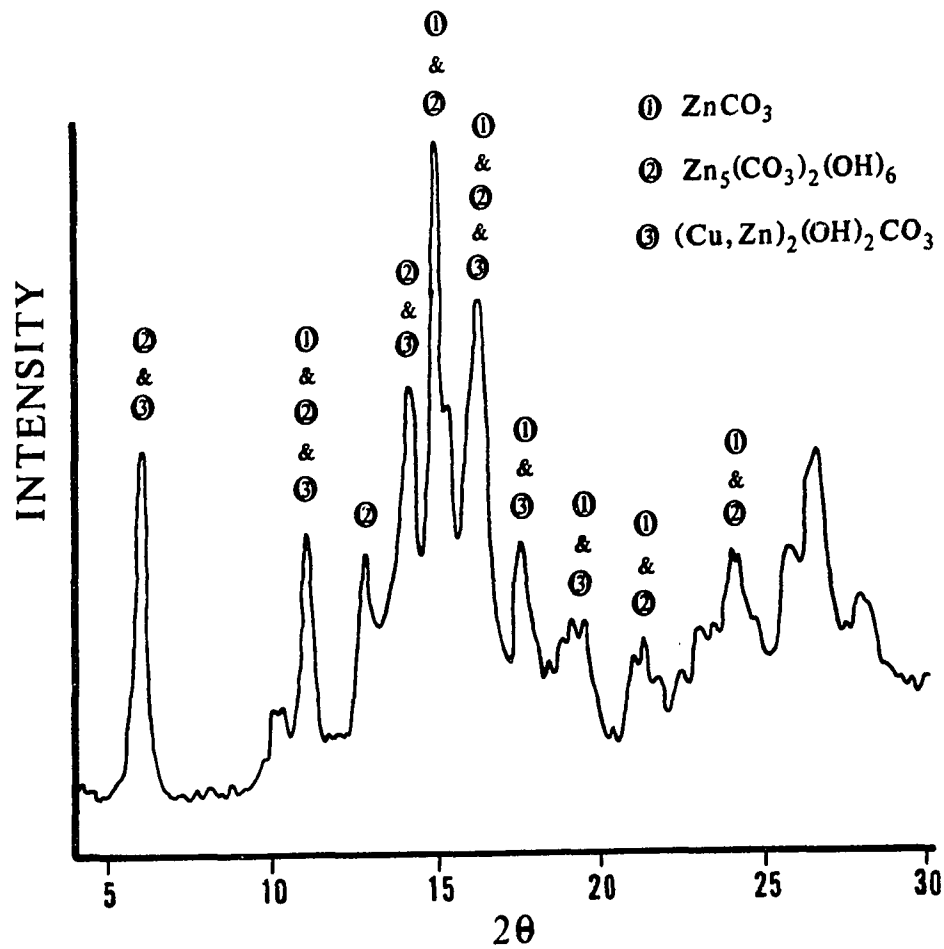

Figure 4. Powder diffraction pattern of a binary precursor

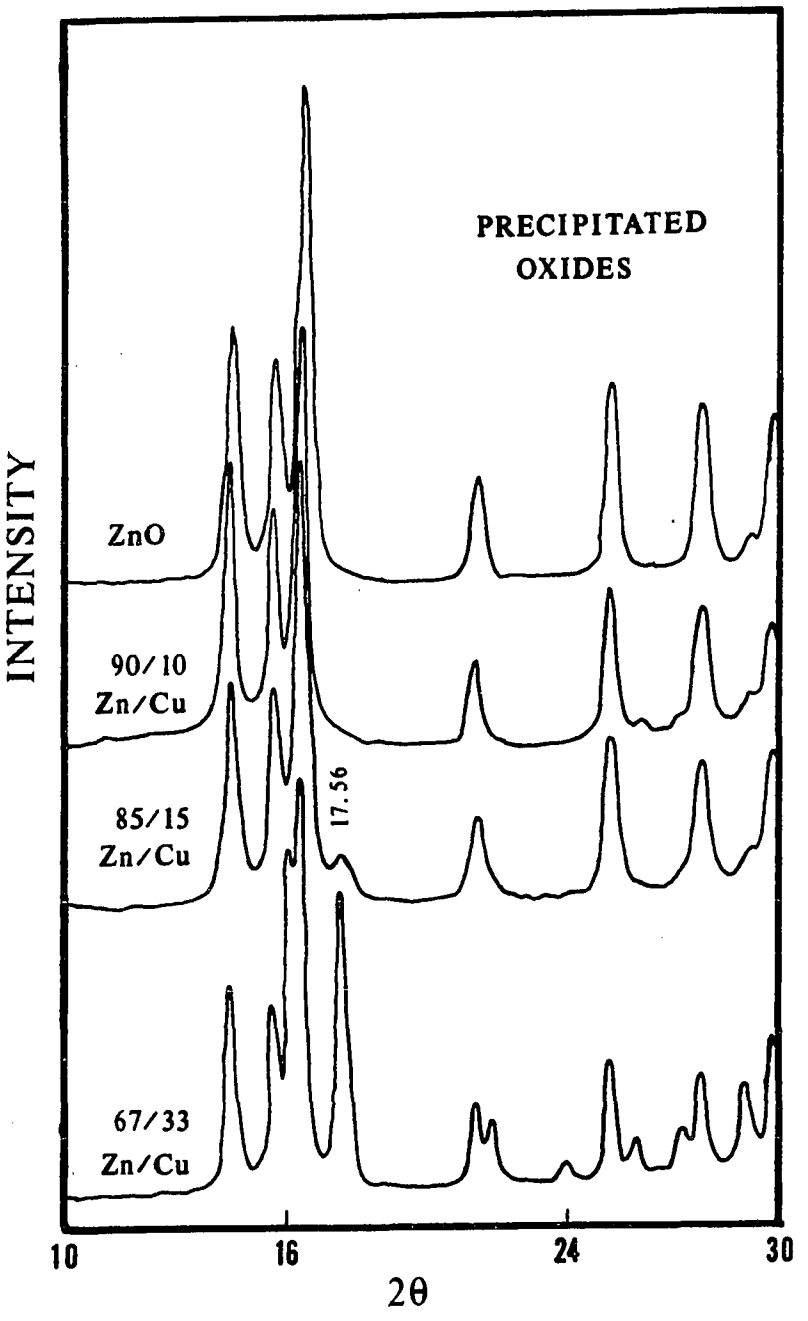

Figure 5. Powder diffraction patterns of precipitated oxides

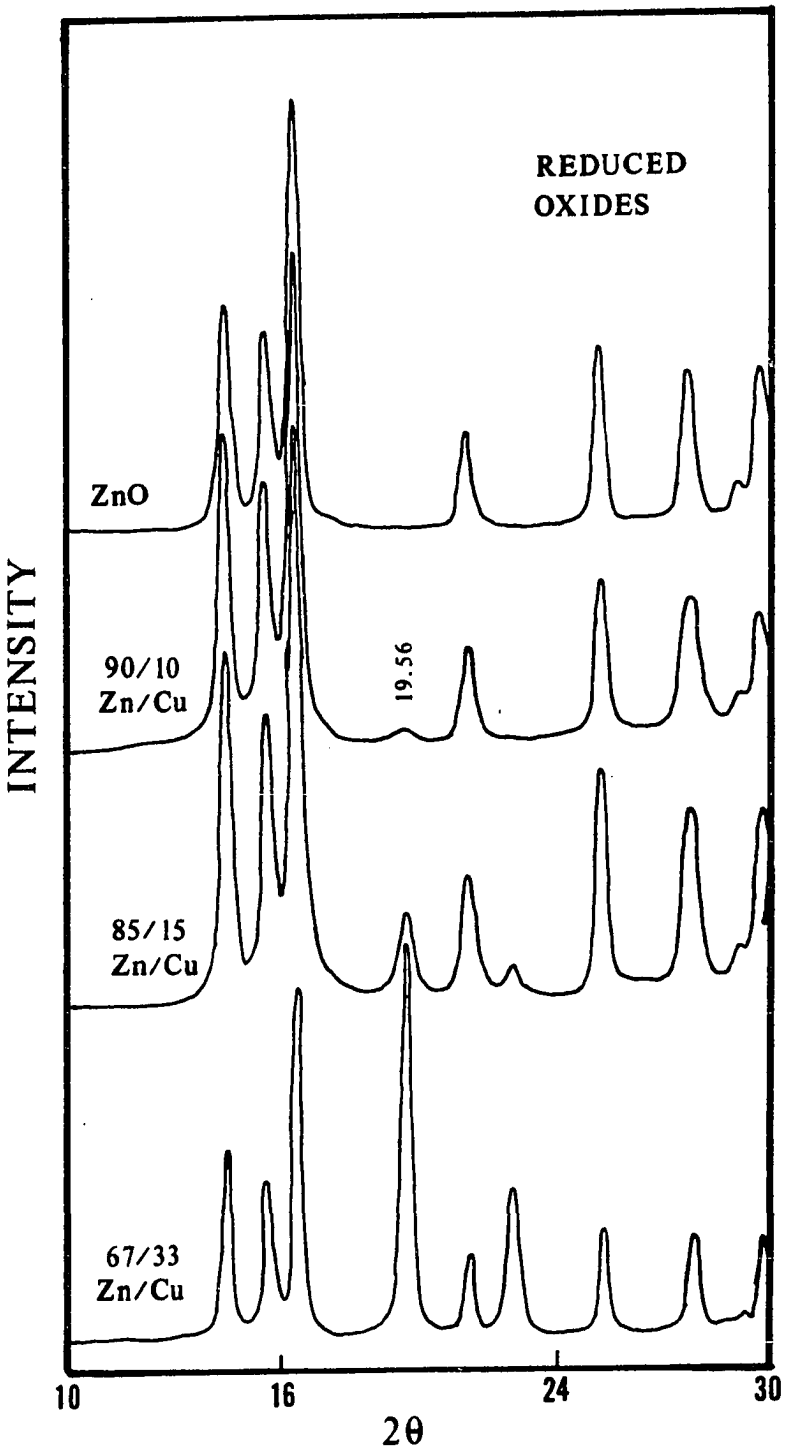

Figure 6. Powder diffraction patterns of reduced oxides

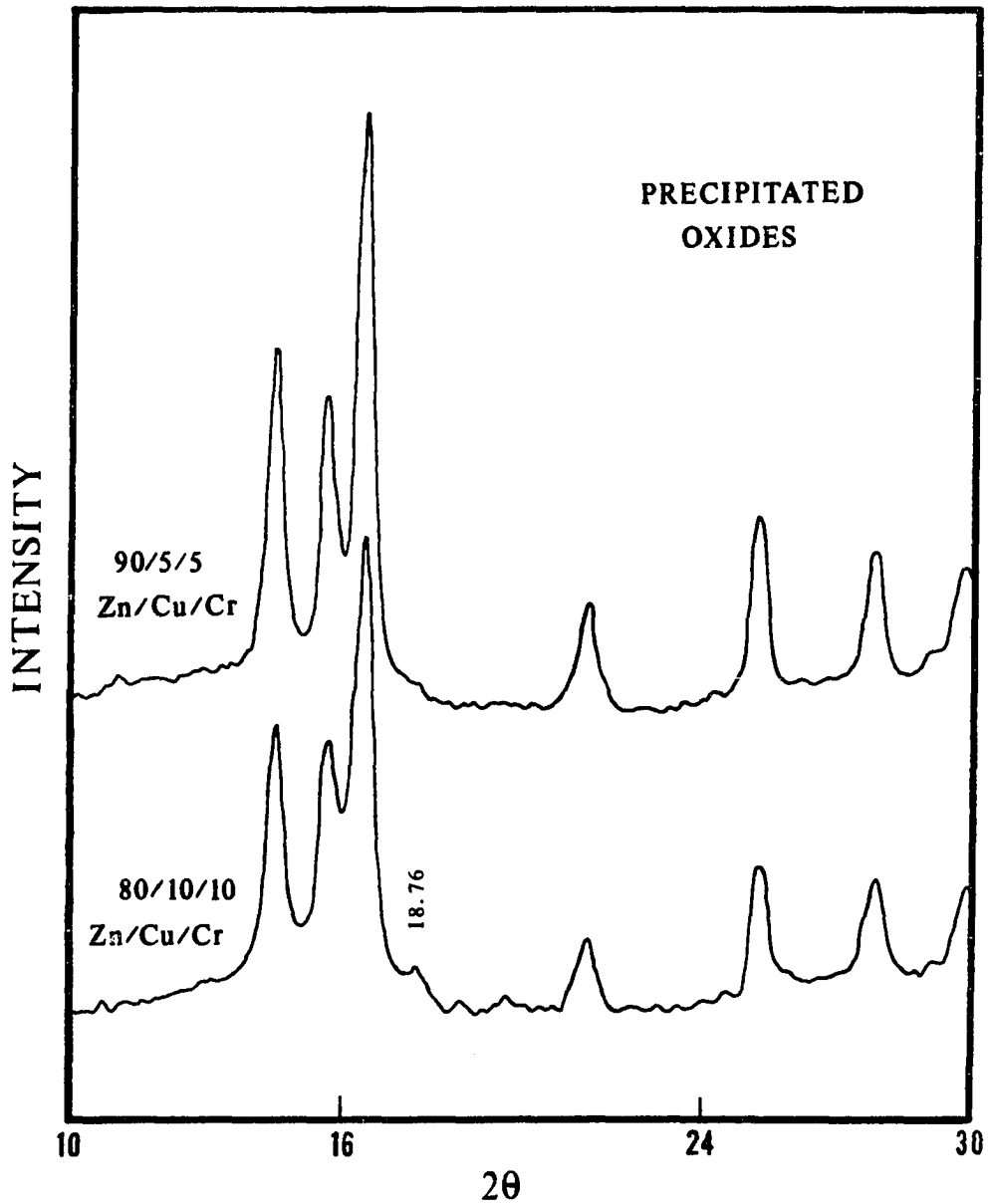

Figure 7. Powder diffraction patterns of ternary oxides

chromium and aluminum were prepared under the precipitation conditions used in the preparation of ternary catalysts to identify the crystal phases formed. After precipitating chromium nitrate with ammonium bicarbonate in the standard manner, the calcined precipitate was identified as Cr_2O_3 (Figure 8). There was some indication in Figure 7 that a Cr_2O_3 phase ($2\theta = 18.76^{o}$) had begun to appear for the 80/10/10 Zn/Cu/Cr oxide composition. A preparation using aluminum nitrate precipitated with ammonium bicarbonate and calcined to the oxide yielded the pattern shown in Figure 9. Although the oxide can be seen to be quite amorphous, the two distinct peaks identify the oxide as γ-Al_2O_3.

Guinier X-Ray

Copper and zinc can form a solid solution known as brass, but little is known about the solubility of the oxides. The results of the atomic absorption analysis showed that copper contents in the precipitated oxides were very close to the original composition of the nitrate solutions. However, the powder diffraction patterns have indicated that some of the copper may be incorporated in the ZnO phase before a cupric oxide phase develops. The patterns of mixtures of ZnO and CuO were not conclusive in establishing whether or not the amounts of cupric oxide in the precipitated oxides were less than would be expected if all the copper were in the CuO phase. Another approach to address this question was Guinier X-ray analysis, which was utilized to determine the lattice dimensions of the ZnO crystallites as the copper content of the precipitated oxides was increased.

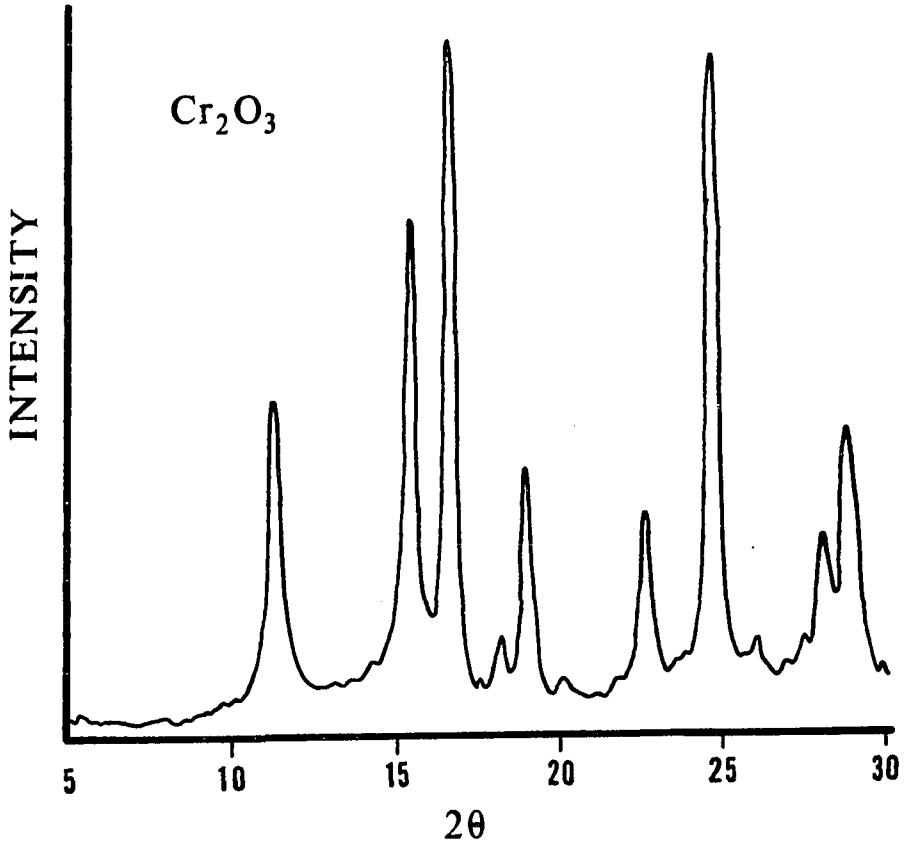

Figure 8. Powder diffraction pattern of chromium oxide

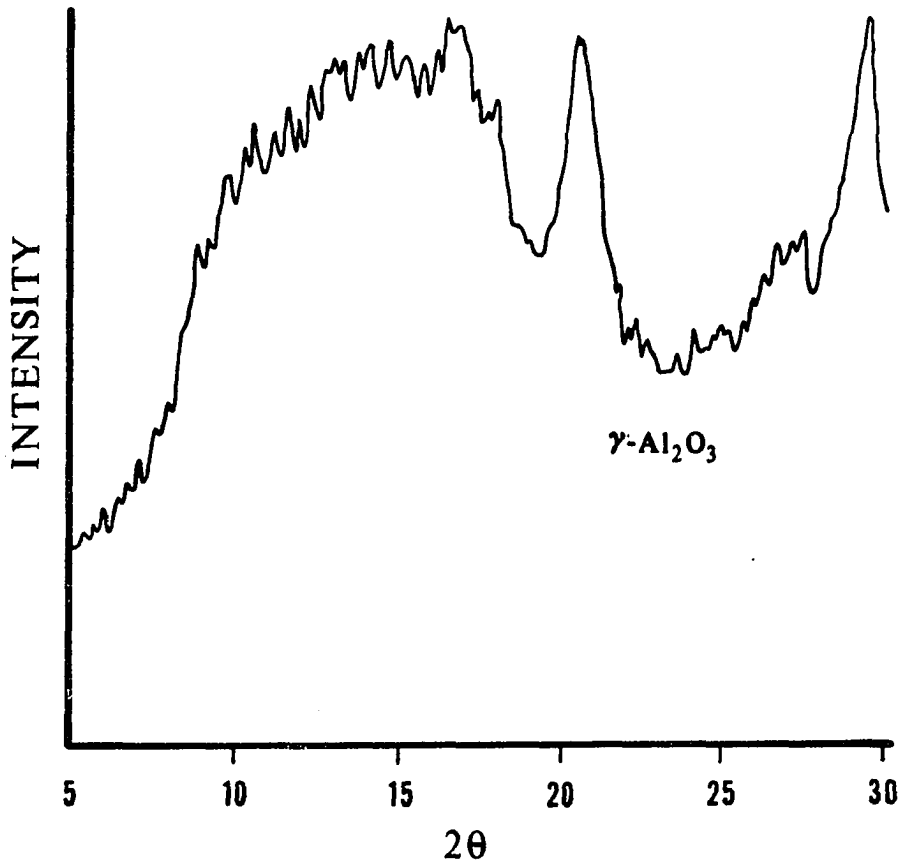

Figure 9. Powder diffraction pattern of aluminum oxide

Precipitated oxides of pure ZnO, 95/5 Zn/Cu oxide, and 90/10 Zn/Cu oxide were analyzed with the Guinier X-ray technique. The positions of the diffraction lines on the developed film were measured, using the Si lines as an internal standard to correspond line positions with 2θ values. The interplanar distances were calculated from Bragg's law:

$$d_{hkl} = \lambda/2 \sin\theta$$

where λ is 1.54051 Å for the X-rays used in these experiments. Because ZnO has a hexagonal lattice structure, the lattice parameters are $a = b \neq c$ and $\alpha = \beta = 90^{o}$ with $\gamma = 120^{o}$. This information combined with the Miller indices and interplanar spacings, given in Table 3, led to the determination of lattice parameters a and c from the computer program LATT (Ames Laboratory). The values of a and c did not change as the copper content of the precipitated oxides was increased (Table 4). These three oxides were also reduced in CO at 200°C and analyzed in the same manner as the oxides except that these samples were prepared in a dry box to avoid any oxidation after the reduction step. These results, given in Tables 3 and 4, also showed no change in the lattice paramters as the copper content increased; the values for a and c were the same as those for the oxides. The diffraction patterns for the reduced oxides did not show any lines for copper metal.

Surface Oxidation States

XPS and AES were utilized to identify the oxidation states of Cu and Zn in binary oxides subjected to various treatments, with the

Table 3. Data from Guinier X-ray analysis

Oxides			ZnO		95/5 Zn/Cu		90/10 Zn/Cu	
h	k	l	2θ	d_{hkl}	2θ	d_{hkl}	2θ	d_{hkl}
1	0	0	31.786	2.8130	31.768	2.8145	31.790	2.8126
0	0	2	34.454	2.6010	34.438	2.6021	34.455	2.6009
1	0	1	36.280	2.4742	36.275	2.4745	36.289	2.4736
1	1	0	56.613	1.6245	56.604	1.6247	56.610	1.6245
1	0	3	62.882	1.4767	62.848	1.4775	62.852	1.4774
1	1	2	67.898	1.3793	67.958	1.3783	67.962	1.3782
Reduced oxides			**ZnO**		**95/5 Zn/Cu**		**90/10 Zn/Cu**	
h	k	l	2θ	d_{hkl}	2θ	d_{hkl}	2θ	d_{hkl}
1	0	0	31.730	2.8178	31.726	2.8181	31.750	2.8161
0	0	2	34.378	2.6065	34.423	2.6032	34.416	2.6037
1	0	1	36.225	2.4778	36.238	2.4769	36.211	2.4787
1	1	0	56.593	1.6250	56.584	1.6252	56.580	1.6253
1	0	3	62.844	1.4775	62.842	1.4776	62.835	1.4777
1	1	2	67.981	1.3778	67.946	1.3785	67.948	1.3785

Table 4. Lattice parameters

Oxides	a	c
ZnO	3.250 ± .001	5.205 ± .003
95/5 Zn/Cu	3.2491 ± .0004	5.207 ± .001
90/10 Zn/Cu	3.250 ± .001	5.205 ± .002
Reduced oxides	**a**	**c**
ZnO	3.249 ± .001	5.208 ± .003
95/5 Zn/Cu	3.250 ± .001	5.207 ± .001
90/10 Zn/Cu	3.250 ± .001	5.208 ± .001

intention to establish what oxidation states likely exist on an active catalyst. Because methanol synthesis is a high-pressure process and these techniques involve high-vacuum conditions, no direct determination of actual surface oxidation states during methanol synthesis conditions was possible.

Two samples of 90/10 Zn/Cu oxide were heated overnight at 200°C under vacuum to remove residual surface impurities. One sample was cooled and removed in a fully oxidized state, while the other sample was reduced in carbon monoxide at 200°C for 8 hours, cooled, and removed for analysis. The kinetic energies of the photoelectrons from the oxidized and reduced samples were recorded. The kinetic energies of the C 1s, Zn $2p_{3/2}$, and Cu $2p_{3/2}$ photoelectrons are given in Table 5. The most obvious difference between these two samples was the absence of the broad, short peak (the copper shake-up satellite) in the reduced sample as shown in Figure 10. The shake-up peak results from the promotion of a valence electron to an unfilled higher energy level when the photoelectron leaves the atom. Because Cu(II) has an intense shake-up satellite and reduced states of copper do not, the reduced sample has only reduced states of copper. This conclusion was supported by the calculated binding energies of the Cu $2p_{3/2}$ electrons. The binding energies reported in Table 5 were calculated using the Einstein relation. The correction term for each sample was determined from the kinetic energy of the C 1s electron and a value of 285.0 eV for the binding energy of this electron (the carbon in the adhesive tape was used as an internal standard). Correction terms of 9.2 and 9.7 eV were calculated for the oxidized and reduced samples, respectively. Some reported binding energies for various states

Table 5. Results from X-ray photoelectron and Auger electron spectroscopies

Photoelectron kinetic energy (eV)	C 1s	Zn $2p_{3/2}$	Cu $2p_{3/2}$
oxidized 90/10 Zn/Cu	1192.4	454.8	543.4
partially reduced 90/10 Zn/Cu	1191.9	454.4	543.6
oxidized 67/33 Zn/Cu	1191.2	454.4	542.8
partially reduced 67/33 Zn/Cu	1192.9	455.4	545.0
fully reduced 67/33 Zn/Cu	1193.5	456.0	545.7

Photoelectron binding energy (eV)	Zn $2p_{3/2}$	Cu $2p_{3/2}$
oxidized 90/10 Zn/Cu	1022.6	934.0
partially reduced 90/10 Zn/Cu	1022.5	933.3
oxidized 67/33 Zn/Cu	1021.8	933.4
partially reduced 67/33 Zn/Cu	1022.5	932.9
fully reduced 67/33 Zn/Cu	1022.5	932.8

Auger kinetic energy (eV)	Cu $L_3M_{4,5}M_{4,5}$
oxidized 67/33 Zn/Cu	918.6
partially reduced 67/33 Zn/Cu	916.5
fully reduced 67/33 Zn/Cu	915.7, 917.7

of zinc and copper are given in Table 6. Comparing experimental binding energies from Table 5 with the literature values from Table 6, it was determined that the oxidized samples had both zinc and copper in the 2+ oxidation state, whereas the reduced sample had zinc in the 2+ oxidation state and copper in either the 1+ or metallic state. The binding energies of Cu_2O and Cu metal are too close to be able to distinguish between them. However, the measurement of the kinetic energies of the X-ray induced Auger electrons can readily differentiate between Cu_2O and Cu metal. Unfortunately the Zn Auger electrons were so much more intense

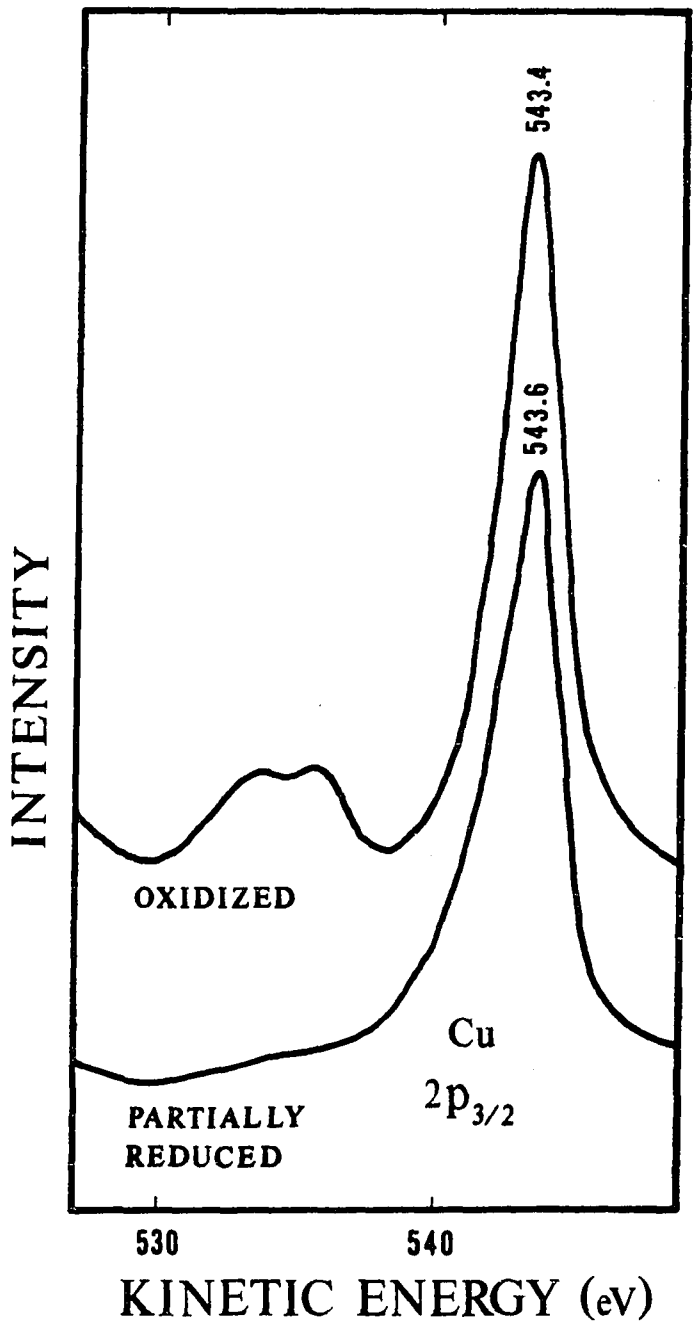

Figure 10. XPS spectra for 90/10 Zn/Cu oxide

Table 6. Literature XPS and AES energies for various states of copper and zinc

	Photoelectron binding energy (eV)[a]
	$2p_{3/2}$
ZnO	1022.5
Zn metal	1021.7
CuO	933.5
Cu_2O	932.2
Cu metal	932.4

	Auger electron energy (eV)[b]
	$L_3M_{4,5}M_{4,5}$
CuO	918.2
Cu_2O	916.7
Cu metal	919.0

[a]Wagner et al., 1979.

[b]McIntyre, 1982.

than the Cu Auger electrons from this reduced sample that the Cu Auger electrons were not observed.

The intensity of the Cu Auger electrons was increased by using a catalyst with a higher copper content. Three samples of 67/33 Zn/Cu oxide were heated overnight at 200°C under vacuum to remove surface impurities. One sample was cooled and removed. Another sample was reduced in hydrogen for 2 hours; since this system was static, the gas phase contained water at its saturation point of 200°C and 1 atmosphere. The remaining sample was subjected to several cycles of reduction in hydrogen followed by evacuation of the gas phase, until reduction of the sample was complete (no water was present in the gas phase). Figure 11

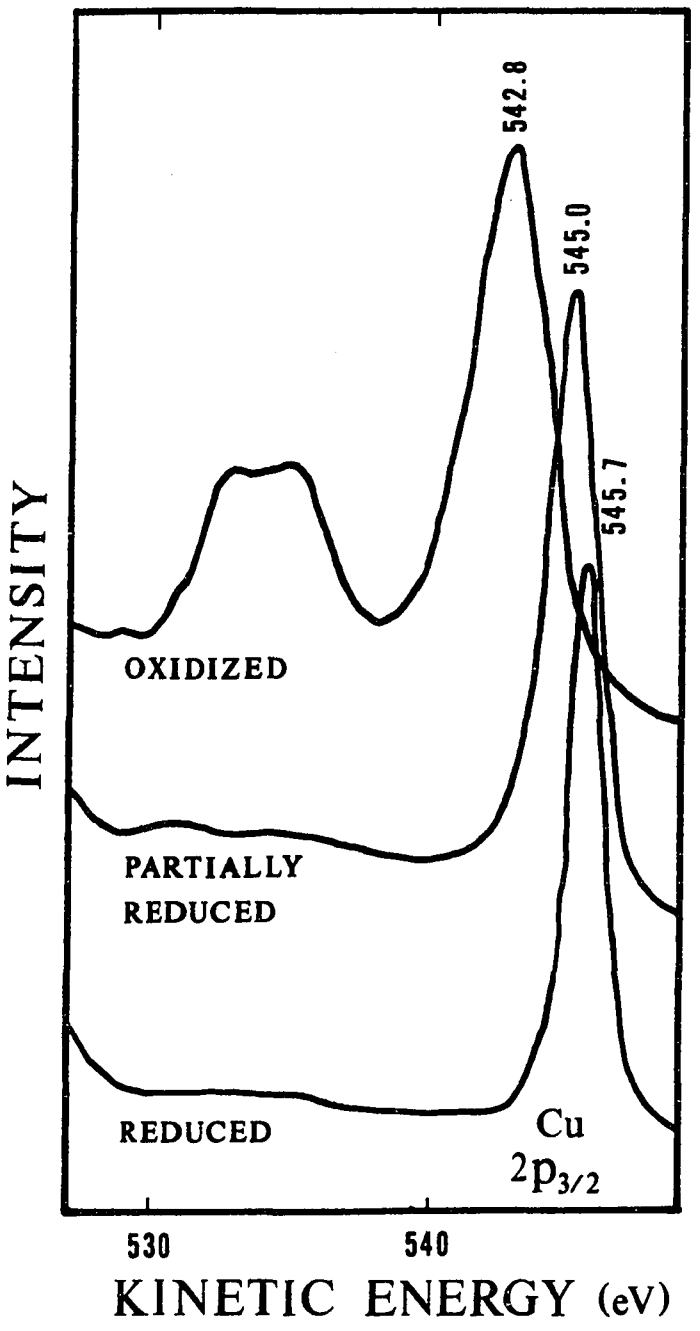

Figure 11. XPS spectra for 67/33 Zn/Cu oxide

shows the kinetic energies of the Cu $2p_{3/2}$ electrons in the oxidized, partially reduced, and fully reduced samples. Neither the partially reduced nor fully reduced samples have the Cu shake-up satellite, indicating that these samples contain no CuO. Correction terms of 10.4, 8.7, and 8.1 eV were calculated for the oxidized, partially reduced, and fully reduced samples, respectively, using the Einstein relation and the kinetic energies in Table 5. These kinetic energies and correction terms were used to determine the binding energies reported in Table 5. Comparing experimental and literature values, the oxidized sample had both zinc and copper in the 2+ oxidation state, while both reduced samples had zinc in the 2+ oxidation state and copper in either the first oxidation or metallic state. This time the Cu Auger electrons were sufficiently intense to permit identification of the reduced oxidation states. Figure 12 shows the kinetic energies of the $L_3M_{4,5}M_{4,5}$ Auger electrons for Cu in these three samples. Because the kinetic energies of Auger electrons reported in the literature were relative to the Fermi level, whereas the experimental kinetic energies were relative to the vacuum level, the correction term of the Einstein relation was added to the experimental values to yield the Auger kinetic energies given in Table 5. When these values were compared to literature values given in Table 6, the following conclusions were reached. In agreement with the XPS results, the oxidized sample had Cu in the 2+ oxidation state. The partially reduced sample had all the Cu in the 1+ oxidation state. The fully reduced sample had two types of Cu present, corresponding to copper in the 1+ oxidation state and metallic copper. The energy difference of 2 eV between these two peaks as well as the absence of a

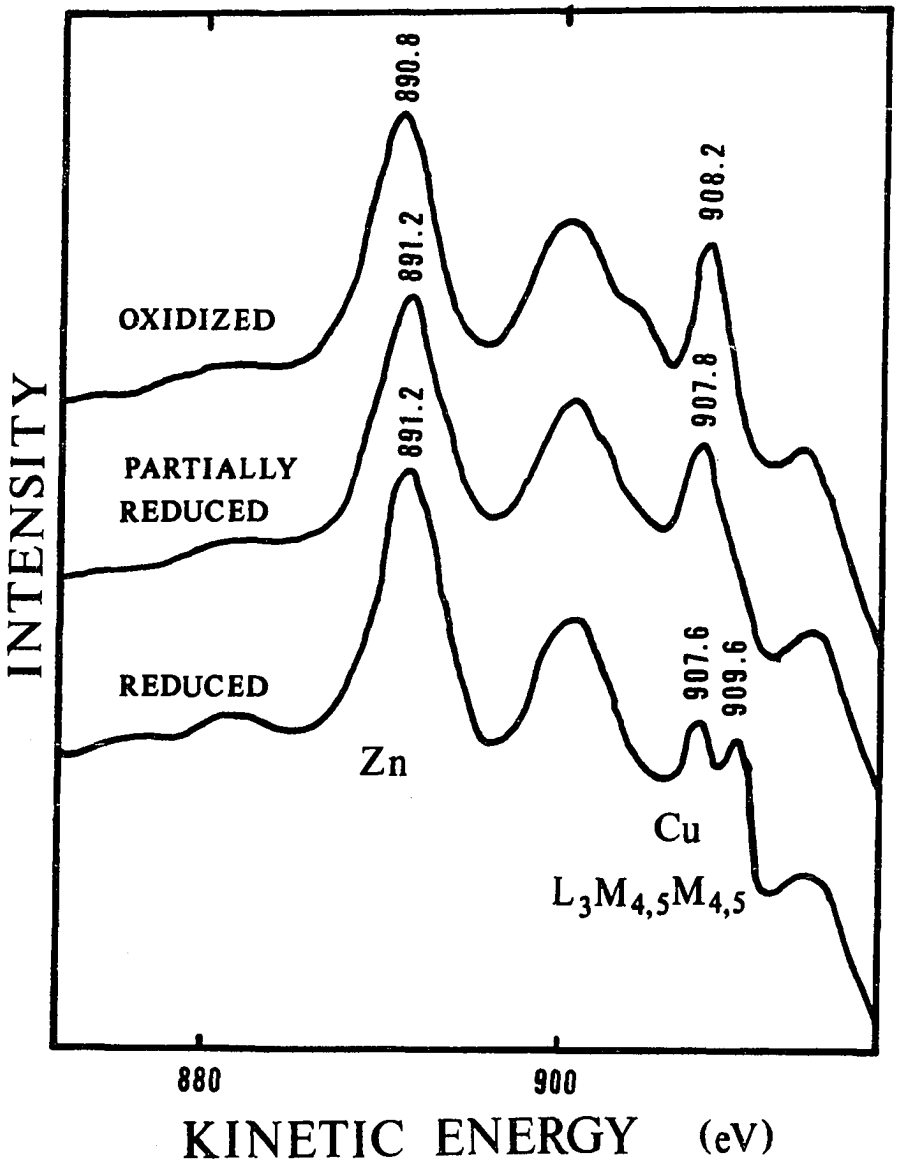

Figure 12. Auger spectra for 67/33 Zn/Cu oxide

shake-up satellite in the XPS plot supported this conclusion.

A sample calculation for determining binding energies and Auger kinetic energies can be found in Appendix A.

Surface Area and Micropore Distribution

The BET surface areas reported in Table 7 were measured on powdered oxides prepared by precipitation at 60°C and calcination at 400°C. The precipitated oxides of copper and zinc had surface areas of 15 and 20 m^2/g, respectively. Coprecipitated binary oxides of zinc and copper had surface areas in the range of 20-30 m^2/g, the value increasing as the zinc content increased. The coprecipitated ternary oxides containing small amounts of chromia or alumina had surface areas twice the magnitude of binary oxides. Because infrared and reactivity measurements were conducted with compressed powders, the surface areas of some oxides pressed into wafers were determined. The surface areas of 90/10 ZnO/CuO and 80/20 ZnO/CuO were 28 and 22 m^2/g, respectively, showing that compression of the powders at the load used in this work (1200 kg/cm^2) had no observable effect on the surface area. The calcination process was found to significantly affect the surface area of the oxide. The surface area of the precipitate of 67/33 ZnO/CuO was reduced from 29 to 20 m^2/g when calcined at 400°C and was reduced to 1.5 m^2/g when calcined at 600°C, indicating that severe sintering had occurred at the higher temperature. The surface area of Kadox 25 was measured as 9.1 m^2/g, in agreement with values determined by other investigators (Amberg and Seanor, 1965; Ueno et al., 1971; Boccuzzi et al., 1978a). The impregnated 95/5 ZnO/CuO

Table 7. BET surface areas of metal oxides

Catalyst (molar ratio)	Surface area (m^2/g)
ZnO/CuO	
100/0	20
95/5	27
90/10	27
85/15	26
80/20	23
67/33	20
0/100	15
$ZnO/CuO/Cr_2O_3$	
90/5/2.5	49
80/10/5	58
$ZnO/CuO/Al_2O_3$	
80/10/5	65

prepared from Kadox 25 had a surface area of 4.7 m^2/g.

By continuing adsorption isotherms to the saturation pressure of nitrogen at liquid nitrogen temperature, pore distribution analyses of the micropores could be obtained from the desorption isotherms. The results for two binary and two ternary oxides are given in Figure 13. The distribution of micropore radii was quite narrow for binary oxides and slightly broader for ternary oxides. All of these oxides had a most probable micropore radius in the range of 100-120 Å. Micropore volumes and surface areas calculated from the desorption isotherms are given in Table 8. All of these oxides had very similar micropore volumes. The surface areas of the binary oxides were larger than the BET values, suggesting that the cylindrical pore model used in these calculations needs to be modified to better represent these catalysts. A sample calculation

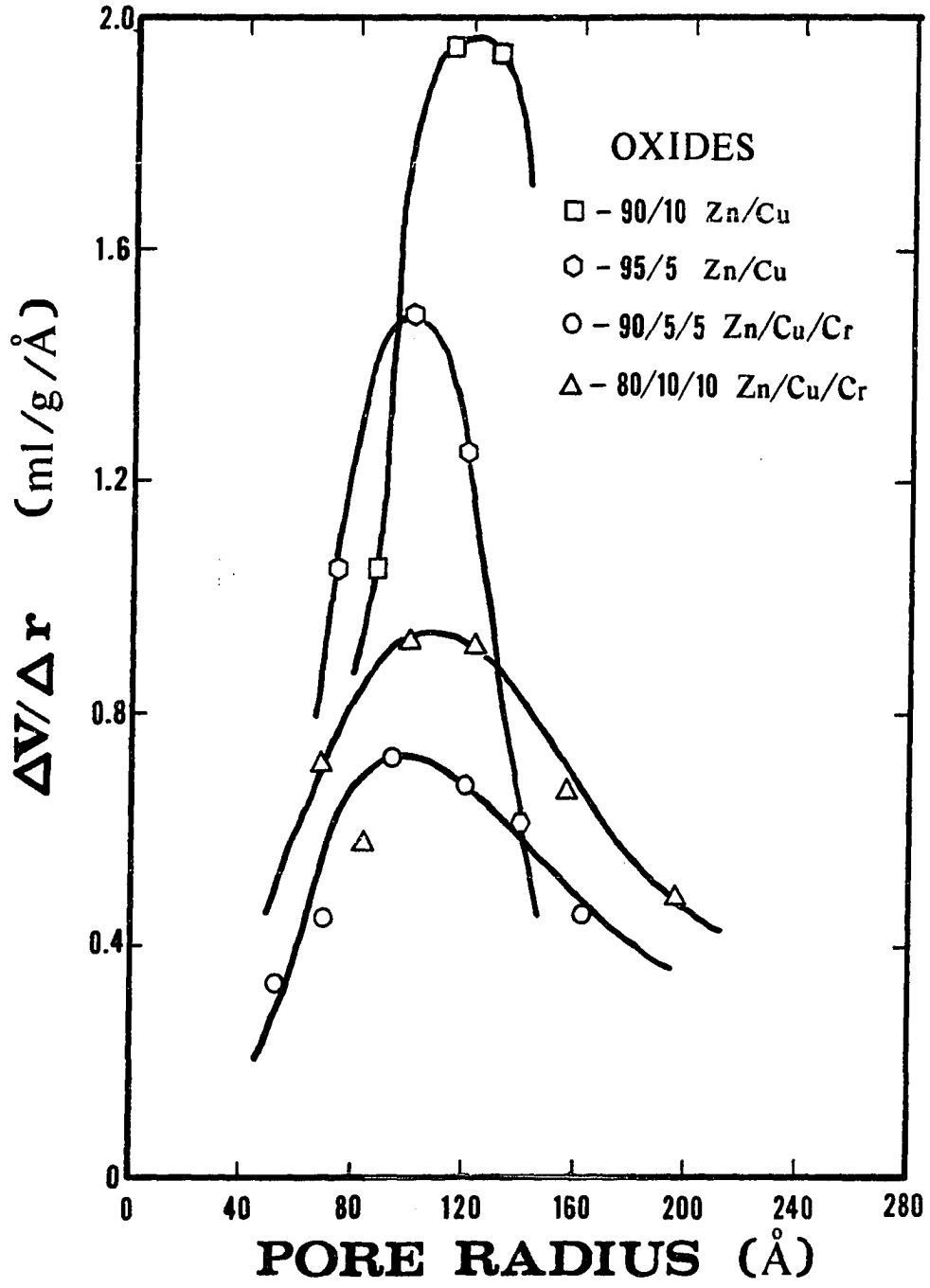

Figure 13. Micropore size distribution

Table 8. Micropore volume and surface area

Catalyst (mole %)	Pore volume (ml/g)	Surface area (m^2/g)
ZnO/CuO		
95/5	0.22	45
90/10	0.21	42
$ZnO/CuO/Cr_2O_3$		
90/5/2.5	0.23	36
80/10/5	0.27	44

of a BET surface area and pore distribution analysis can be found in Appendix B.

DISCUSSION OF RESULTS

The primary objective in catalyst preparation was to develop suitable mixed metal oxide catalysts for methanol synthesis which were also amenable to transmission infrared studies. The color of the oxide was a good indicator of whether or not the oxide could satisfactorily transmit infrared radiation. Precipitated zinc oxide was white whereas precipitated copper oxide was black; the former oxide was very good while the latter was very poor in transmitting infrared radiation when the sample was a thin wafer. Binary and ternary oxides with less than 14 atomic % copper oxide were brown and transmitted infrared radiation as well as pure zinc oxide. Oxides with greater amounts of copper oxide appeared dark brown or black and were nearly opaque to infrared radiation. Apparently, the black coloration developed as a cupric oxide phase was formed. The brown color arose from an intimate mixture of copper oxide and zinc oxide, possibly a solid solution of copper oxide in the zinc oxide phase. Mechanical mixtures of copper oxide and zinc oxide, as well as the impregnated 95/5 ZnO/CuO, were grey rather than brown. The Guinier X-ray patterns showed that the zinc oxide lattice was unaffected by copper contents up to 10 metal atom %. This result was consistent with values given for the ionic radii of Zn^{2+} and Cu^{2+}, which are 0.60 Å and 0.62 Å, respectively (Shannon and Prewitt, 1969). Since these radii are nearly equal, the lattice dimensions of zinc oxide would not be expected to change if some copper ions were incorporated in the ZnO crystallites.

The existence of some copper in an X-ray amorphous state has been

proposed to explain the observation that less cupric oxide was detected in coprecipitated oxides than would be expected if all the copper were in this phase (Semenova et al., 1977; Herman et al., 1979). One possible explanation for this deficiency of cupric oxide not previously considered would be a loss of copper during precipitation via the filtrate. The coprecipitation method used in this investigation yielded a dark blue filtrate, suggesting that part of the copper had complexed with ammonia to form soluble complexes of the type $Cu(NH_3)_x(H_2O)_{6-x}$, where x has values from 1 to 4. Precipitates and filtrates were analyzed for zinc and copper contents by atomic absorption. Although the amount of copper lost in the filtrate exceeded the amount of zinc, the total amount in the filtrate was sufficiently small to have negligible effect on the composition of the precipitates. Therefore, the copper composition in the oxides was very close to the copper composition in the original nitrate solutions.

The catalyst precursors were identified as hydrozincite, smithsonite, rosalite, and malachite. With the exception of smithsonite, these precipitated compounds have been observed in previous studies which attributed the formation of the precursors to the reactions (Herman et al., 1979):

$$Zn^{2+} + 2OH^- \rightarrow Zn(OH)_2$$

$$2Zn^{2+} + 4HCO_3^- + 3Zn(OH)_2 \rightarrow Zn_5(OH)_6(CO_3)_2 + 2H_2O + 2CO_2$$

$$Zn^{2+} + 2HCO_3^- + Cu(OH)_2 \rightarrow CuZn(OH)_2CO_3 + H_2O + CO_2$$

Unlike the previous studies, the precipitation reactions were conducted with carbon dioxide bubbling through the solution. The presence of carbon dioxide inhibited the formation of hydrozincite and rosalite, while promoting the formation of smithsonite:

$$Zn^{2+} + HCO_3^- + OH^- \rightarrow ZnCO_3 + H_2O$$

The effect of smithsonite on the morphology of the zinc oxide crystallites has not been determined.

The X-ray patterns of the precipitated oxides showed only zinc oxide and cupric oxide; the amount of alumina or chromia in the ternary compositions was too low to observe these phases. The surface areas of the binary oxides were in the 20-30 m^2/g range, while ternary oxides had approximately double the surface area of binary oxides. The addition of small amounts of alumina or chromia to a binary composition brought about a large change in surface area without changing the crystal phase. Compression of the powdered oxides into thin wafers, which reduced the bulk volume by approximately an order of magnitude, did not change the BET surface area. It seems that most of the surface area was in the micropores ($r < 200$ Å). Both binary and ternary oxides had a most probable micropore radius near 100 Å, indicating that the increase in surface area of ternary oxides arose from an increase in the number of pores rather than a decrease in pore radius relative to pore volume.

Reduction of the catalysts did not change surface areas. X-ray spectra showed some formation of metallic copper but no cuprous oxide phase. The XPS-Auger spectra revealed a very different result. Reduction of a 67/33 Zn/Cu binary oxide reduced all the cupric ions. When reduction

took place without removal of reaction products from the gas phase, the copper was found exclusively in the +1 oxidation state. When reduction took place with the removal of reaction products, a comparable amount of copper was detected in both the +1 oxidation and metallic states. Therefore, a small amount of oxidant in the gas phase during reducing conditions favored the formation of the cuprous ion. Even during severely reducing conditions (at 200°C), the cuprous ion was stable.

The location of the copper in reduced coprecipitated oxides might be shown by determining the effect of copper content on the lattice dimensions of zinc oxide. An increase in the lattice dimensions would occur if copper existing as a solid solution in zinc oxide was reduced. Copper in the +1 oxidation state (coordination number 4) would have an ionic radius of 0.90 Å and copper in the zero valent oxidation state (metallic copper) would have a radius of 1.28 Å (Lange's Handbook of Chemistry, 1973). The Guinier X-ray results have indicated, however, that the lattice dimensions of the zinc oxide crystallites for reduced binary oxides did not change for oxides with copper contents up to 10%. The metallic copper must be a separate phase or on the surface of the zinc oxide crystallites to explain the observed result. The cuprous ion could be within the zinc oxide crystallite if the coordination number was 2; the ionic radius would be about 0.60 Å (Shannon and Prewitt, 1969). Further experimentation will be necessary to clarify the precise location of copper ions.

PART II.

CHEMISORPTION ON METHANOL SYNTHESIS CATALYSTS

LITERATURE REVIEW

In heterogeneous catalysis, the interactions between reactants and the catalyst which lead to the formation of products can be very complex. Often the catalyst surface contains many different adsorbed species. The first objective in studies of reaction intermediates is the identification of adsorbed species. In this study, the emphasis has been placed on the use of infrared spectroscopy for the characterization of surface species on methanol synthesis catalysts. Various gaseous compounds have been adsorbed on zinc oxide and mixed metal oxides during spectroscopic measurements.

Adsorption on Zinc Oxide

Zinc oxide has been one of the most extensively studied oxides over the past two decades. The strong interest in zinc oxide has been mainly due to its high transparency to infrared radiation which, combined with a controlled-atmosphere cell, has provided a very successful technique for identifying adsorbed species under reaction conditions. The catalytic behavior and nature of adsorbed compounds on zinc oxide, recently reviewed by John (1980), will be addressed in the next several sections.

Zinc oxide is an n-type semiconductor with both zinc and oxygen ions tetrahedrally coordinated. Contrary to an earlier assumption that the surface of ZnO powders were mostly composed of equal areas of polar (0001) and nonpolar ($10\bar{1}0$) planes (Morimoto and Morishige, 1975), the ratio of polar to nonpolar planes was determined to be 1:6, respectively,

by transmission electron microscopy (Bowker et al., 1981).

The (0001) plane consists of surface zinc ions coordinated to three lattice oxygens, whereas the $(10\bar{1}0)$ plane contains rows of zinc and oxygen ions arranged in pairs.

In normal practice, the ZnO surfaces are crystallographically imperfect and contain impurities. Atmospheric water and carbon dioxide form an amorphous layer of $Zn_5(OH)_6(CO_3)_2$ on zinc oxide which can be decomposed by heating the sample above 200°C in vacuo (Nagao et al., 1974). Residual surface carbonates can be removed by successive oxidation and evacuation steps, producing a "clean" surface containing hydroxyl groups observed in an infrared spectrum as bands at 3670, 3640, 3620, 3555, and 3440 cm^{-1} (Atherton et al., 1971). The first three bands were assigned to isolated hydroxyls on polar planes, while the latter two bands were assigned to hydrogen-bonded hydroxyls on nonpolar planes. The surface could be gradually dehydroxylated by increasing the outgassing temperature above 200°C, causing a decrease in the intensity of the hydrogen-bonded hydroxyls. The chemisorption of water on several types of ZnO which had received various surface pretreatments was found to be associated mostly with the nonpolar $(10\bar{1}0)$ plane (Morimoto and Nagao, 1974; Nagao et al., 1978), supporting the infrared results. The water adsorption isotherms and heats of immersion for the different oxides were correlated with the area of various planes estimated with scanning electron microscopy. Photoelectron studies have determined that the interaction of water with the polar (0001) plane of ZnO near ambient temperatures was insignificant, although at lower temperatures (80-200°K), an oxygenated surface will undergo additional hydroxylation (Abbati

et al., 1978; Au et al., 1982).

A summary of infrared bands assigned to residual hydroxyl bands on ZnO is presented in Table 9.

Table 9. Residual hydroxyl groups on zinc oxide

Hydroxyl infrared bands, cm^{-1}	Reference
3670, 3640, 3620, 3555, 3440	Atherton et al., 1971
3670, 3642, 3620, 3595, 3450	Nguyen and Sheppard, 1981
3640, 3575, 3530, 3440	Morimoto et al., 1976
3660, 3610, 3550, 3439	Scholten and van Montfoort, 1973

The adsorption of hydrogen on zinc oxide produces several types of surface complexes that are infrared active. Eischens, Pliskin, and Low (1962) established that a reversible type of adsorption occurring at 30°C (Type I) formed two infrared bands. Hydrogen adsorbs dissociatively at ambient temperature on zinc oxide pair sites to produce bands at 1710 and 3500 cm^{-1}, due to ZnH and OH species, respectively. This type of adsorption was found to be reversible, covering between 5 and 10% of the surface (Dent and Kokes, 1969a). Also at ambient temperature an irreversible adsorption (Type II) occurred that was infrared inactive and unreactive in ethylene hydrogenation. A reversible type of adsorption occurring at -195°C (Type III) is believed to be molecularly adsorbed hydrogen which produces a band at 4019 cm^{-1} (Chang et al., 1973). A recent infrared study of hydrogen adsorption on zinc oxide at ambient temperature identified two additional bands associated with Type I

adsorption; bands at 817 and 845-850 cm^{-1} were assigned to bending frequencies for ZnH and OH species, respectively (Boccuzzi et al., 1978a). More significant was the assignment of broad bands near 3400 and 1475 cm^{-1} to dissociated hydrogen atoms bridged between neighboring oxygen and zinc ions, respectively (Type II).

Deuteration of Type I species shifted the bands to 1232 and 2584 cm^{-1} for ZnD and OD, respectively (Kokes et al., 1972). The electrical conductivity of ZnO can increase when hydrogen is adsorbed in an infrared inactive form (Cimino et al., 1962). This adsorption has been proposed to occur on interstitital zinc atoms (Scholten and van Montfoort, 1973), but other studies have found that the amount of adsorbed hydrogen did not relate to the interstitial zinc concentration (Gerasimova et al., 1973).

Carbon monoxide adsorption on zinc oxide at ambient temperature occurs as two types: a reversible, weakly adsorbed species which produces a band in the 2174-2212 cm^{-1} region depending on the degree of oxidation of zinc oxide, and a strongly adsorbed species producing bands in the 1300-1600 cm^{-1} region which desorbs as carbon dioxide (Taylor and Amberg, 1961; Amberg and Seanor, 1965). The band near 2200 cm^{-1} was believed to be a weakly adsorbed carbon monoxide molecule that, due to polarization, had a CO stretching frequency well above that for gaseous carbon monoxide. Bands near 1530, 1470, and 1330 cm^{-1} were assigned to surface carbonate species, and other bands at 1575, 1342, and 1287 cm^{-1} were

assigned to a carboxylate species (see Figure 14). A similar study of CO_2 adsorption on ZnO dispersed in Aerosil found bidentate and unidentate carbonate bands at 1640 and 1430 cm^{-1}, respectively; at 200°C, bands at 1570 and 1380 cm^{-1} were assigned to a carboxylate species (Matsushita and Nakata, 1962). Carbon dioxide was strongly adsorbed on sites formed by partial dehydroxylation of the surface, and was displaced by gaseous H_2O (Atherton et al., 1971; Morimoto and Morishige, 1974; Morimoto and Morishige, 1975).

The interaction of CO and CO_2 with specific planes of ZnO has been examined with a variety of techniques. Low temperature (90°K) chemisorption of CO occurred on both polar and nonpolar planes by σ interaction of the carbon end of the molecule to zinc ions (Gay et al., 1980; Sayers et al., 1980; McClellan et al., 1981). At higher temperatures (25-200°C), CO adsorbed irreversibly on nonpolar surfaces, yielding CO_2 when desorbed (Hotan et al., 1979). Two types of adsorbed CO_2 were identified by temperature programmed desorption on nonpolar and stepped planes: the weaker species was assumed to occur on zinc-oxygen pairs, while the stronger species occurred on anion vacancies or steps (Cheng and Kung, 1982). The CO_2 desorbed as a result of CO adsorption was the stronger species. Reversible CO adsorption took place on polar and stepped planes. At higher temperatures, CO adsorption on polar, stepped, and nonpolar planes resulted in CO_2 desorption.

When carbon monoxide was adsorbed on ZnO in the presence of hydrogen, significant shifts were observed in Type I hydrogen adsorption bands (Dent and Kokes, 1969b; Boccuzzi et al., 1978b). The stretch frequency of the OH band shifted continuously to higher wavenumbers with increasing

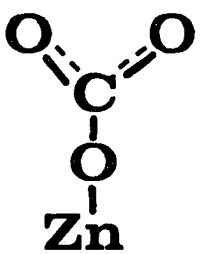

UNIDENTATE
CARBONATE

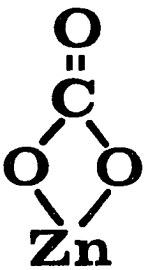

BIDENTATE
CARBONATE

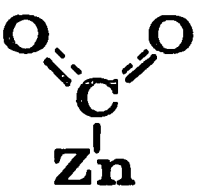

CARBOXYLATE

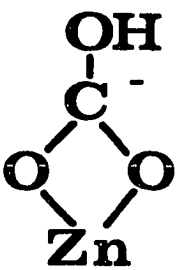

BICARBONATE

Figure 14. Adsorbed carbonates on ZnO

carbon monoxide pressure; the maximum value observed by Boccuzzi was 3523 cm^{-1}. The ZnH band transformed into a triplet structure which gradually shifted to lower wavenumbers with increasing carbon monoxide pressure. The triplet arose from interactions caused by carbon monoxide adsorption on zinc ions adjacent to the ZnH species. Additional weak bands have been observed at 2770 and 2661 cm^{-1} which were assigned to a formyl species (see Figure 15) (Saussey et al., 1982). An interaction occurred between CO and a weakly adsorbed species of hydrogen at room temperature, although the exact nature of this surface product was unknown (Giamello and Fubini, 1981).

The reaction of carbon dioxide and hydrogen on ZnO at 230°C was studied using simultaneous infrared and kinetic measurements (Ueno et al., 1970). An intermediate adsorbed species identified as a formate ion produced infrared bands at 2870, 1572, 1369, and 1379 cm^{-1}; these bands were assigned to the C-H stretching frequency, the asymmetric and symmetric O-C-O stretching frequencies, and the in-plane C-H bending frequency, respectively. Formic acid adsorption on ZnO formed formate ions which decomposed to yield ZnH and gaseous CO_2 (Noto et al., 1967). Formic acid decomposition on a nonpolar $(1\bar{1}00)$ plane produced adsorbed CO and atomic oxygen; the carbon end of the CO molecule was proposed to be bonded to an oxygen ion rather than zinc (Lüth et al., 1976).

The adsorption and decomposition of methanol on ZnO have been investigated. At room temperature, dissociative adsorption produced hydroxyl and methoxy groups (Nagao and Morimoto, 1980). At 200°C, methoxy groups decomposed to formate ions and hydrogen; formate ions decomposed to yield CO (Ueno et al., 1971). Formate ions also reacted

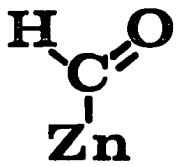

FORMYL

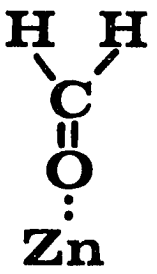

FORMALDEHYDE

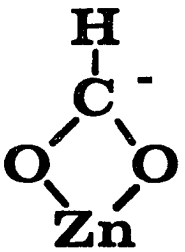

FORMATE

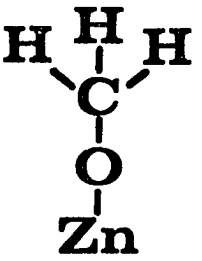

METHOXY

Figure 15. Adsorbed hydrocarbons on ZnO

with gaseous methanol to produce CO_2 and H_2. Methoxy groups can be displaced by gaseous water to form hydroxyl groups. The adsorption of methanol on a nonpolar $(1\bar{1}00)$ surface produced a methoxy species bonded to the surface through the oxygen atom (Rubloff et al., 1976). Methanol decomposition on polar, stepped, and nonpolar planes of ZnO was investigated using temperature programmed desorption (Cheng et al., 1983). The product composition from the various surfaces indicated that the decomposition reaction was structure-sensitive. Nonpolar planes with anion vacancies and stepped planes produced methane, hydrogen, carbon monoxide, and carbon dioxide. The polar plane produced formaldehyde, water, hydrogen, carbon monoxide, and carbon dioxide.

Summaries of formate and methoxy infrared band assignments are presented in Tables 10 and 11, respectively.

Adsorption on Copper and Copper Oxide

The huge success of utilizing transmission infrared spectroscopy for characterizing surface species on ZnO has not been enjoyed in the characterization of copper and copper oxide because of strong infrared absorption. To overcome this problem, some studies have used infrared-transmitting supports such as silica or alumina to obtain a spectrum. Carbon monoxide adsorption on copper oxide (CuO) supported by silica produced bands near 2170 and 2140 cm^{-1} which were assigned to chemisorbed and physically adsorbed CO, respectively (London and Bell, 1973). Reflection-absorption spectroscopy has been utilized successfully in studies of adsorbed CO on copper. Initial investigations on copper

Table 10. Infrared bands of surface formates on zinc oxide

Fundamental frequencies, cm^{-1}	HCOOH adsorption[a]	CH_3OH decomposition[b]
$\nu_1(A_1)$ C-H stretching	2870	2870
$\nu_2(A_1)$ symmetric C-O stretching	1369	1367
$\nu_3(A_1)$ symmetric C-O bending	–	–
$\nu_4(B_1)$ asymmetric C-O stretching	1572	1571
$\nu_5(B_1)$ in-plane C-H bending	1379	1382
$\nu_6(B_2)$ out-of-plane C-H bending	–	–

[a]Ueno et al., 1970.

[b]Ueno et al., 1971.

[c]Miyata et al., 1981.

[d]Hata et al., 1977.

Butanol oxidation[c]	Methylpropene oxidation[c]	Propene oxidation[d]	DCOOD adsorption[a]
2870	2872	2870	2190
1364	1364	1365	1342
–	–	–	–
1578	1574	1572	1572
–	–	–	–
–	–	–	–

Table 11. Infrared bands of surface methoxides on zinc oxide

Fundamental frequencies, cm^{-1}	CH_3OH adsorption[a]	CH_3OH adsorption[b]	CD_3OD adsorption[a]
Asymmetric CH_3 stretching	2930	2930	2200
Symmetric CH_3 stretching	2830	2813	2050
Asymmetric CH_3 bending	–	–	–
Symmetric CH_3 bending	1470	–	–
CH_3 rocking	–	–	–
C-O stretching	–	–	–

[a]Ueno et al., 1971.

[b]Nagao and Morimoto, 1980.

films revealed a band in the 2100-2110 cm^{-1} region (Pritchard and Sims, 1970). The frequency of adsorbed CO has been found to depend on the crystal face (Pritchard et al., 1975) and on the surface coverage of CO (Horn and Pritchard, 1976; Hollins and Pritchard, 1979; Ryberg, 1982). The effects of dipole-dipole interactions and the extent of π bonding tend to offset each other. The bonding geometry of CO can range from perpendicular on the (100) face to parallel on the (311) face (Sayers et al., 1981).

Formic acid adsorption on copper at room temperature formed both monodentate (1640 cm^{-1}) and bidentate (1350 cm^{-1}) formates characterized with a polarization modulation infrared technique (Wadayama et al., 1983). Methanol adsorbed on oxidized copper surfaces to yield a methoxy species; formaldehyde and hydrogen were formed by the decomposition of

methoxy groups (Wachs and Madix, 1978; Sexton, 1979; Bowker and Madix, 1980). Formaldehyde reacted with adsorbed oxygen on a copper surface to form a very stable formate species which ultimately decomposed to H_2 and CO_2 (Wachs and Madix, 1979).

Adsorption on Alumina and Chromia

Although alumina and chromia were minor components in the mixed metal oxides investigated in this work, some infrared studies have been reviewed to demonstrate that the types of adsorption on these oxides have much in common with adsorption on zinc oxide. Alumina has been one of the most extensively studied oxides because of its importance in catalytic applications. Residual hydroxyl groups have been observed on γ-alumina with bands at 3800, 3780, 3744, 3733, and 3700 cm^{-1} (Peri, 1965). Band positions were affected by temperature and the extent of surface hydration. Carbon monoxide adsorbed weakly to produce a band at 2200 cm^{-1} and was also oxidized to yield surface carbonates (Parkyns, 1967). These same carbonates were produced by CO_2 adsorption (Parkyns, 1969). Bicarbonate species formed bands at 3605, 1640, 1480, and 1233 cm^{-1} while a bidentate carbonate species was assigned to bands at 1850 and 1180 cm^{-1}. Physically adsorbed CO_2 produced a band in the 2346-2367 cm^{-1} region. Other investigators have also observed these surface compounds during CO_2 adsorption (Fink, 1967; Gregg and Ramsay, 1969; Morterra et al., 1977; King, 1980).

Formic acid adsorption on alumina produced a formate ion and a surface proton (Noto et al., 1967). Only the C-H stretching frequency

at 2915 cm^{-1} was identified. Methanol adsorption produced methoxy groups and physically adsorbed methanol at room temperature, while at higher temperatures (above 150°C), a formate species was also formed (Greenler, 1962; Kagel, 1967; Hertl and Cuenca, 1973). It was proposed that a methoxy group reacted with an adjacent hydroxyl group to produce hydrogen and a bidentate formate species.

The adsorption of water, carbon monoxide, and carbon dioxide on chromia has been investigated using transmission infrared spectroscopy (Zecchina et al., 1971a and 1971b). Light scattering was a major problem at higher wavenumbers, obscuring detail in the hydroxyl region. Five OD bands were observed at 2700, 2675, 2600, 2535, and 2430 cm^{-1} which arose from the dissociative chemisorption of D_2O; the coordinative chemisorption and physical adsorption of water also occurred on the surface. Carbon monoxide adsorption at room temperature produced two types of species: a σ-bonded species with a band frequency of 2170-2184 cm^{-1}, depending on the surface coverage, and an adsorbed CO species with partial π bonding having a stretching frequency near 2130 cm^{-1}. Water and carbon monoxide were adsorbed on the same sites. Carbon dioxide adsorption formed bicarbonate and carbonate species as well as a physically adsorbed CO_2 species.

The decomposition of olefins over chromia has been found to produce an adsorbed formate species with bands in the regions of 2800-3000 cm^{-1}, 1560-1565 cm^{-1}, and 1360 cm^{-1} which correspond to the C-H stretching frequency, the O-C-O asymmetric stretching frequency, and O-C-O symmetric stretching frequency of the formate, respectively (Budneva et al., 1975; Kuznetsov et al., 1977). Methanol adsorption produced physically ad-

sorbed methanol, methoxy groups, and formate groups on chromia (Davydov et al., 1971). Methanol decomposition on an oxygenated surface yielded a band at 1620 cm^{-1} which was assigned to the C=O stretching frequency of a formaldehyde species on the surface.

Adsorption on Mixed Metal Oxides

Infrared spectroscopy has not been utilized in adsorption studies on mixed metal oxides for methanol synthesis. The formation of surface species generally has been based on the amount of a gaseous compound adsorbed on the surface and the nature of desorbed species. A study of CO adsorption on a Cu-Zn-Al oxide catalyst as a function of the oxygen content of the oxide indicated that CO formed a surface carbonate at temperatures above 40°C (Ostrovskii et al., 1978). Carbon monoxide adsorption on a strongly reduced surface was very slow. Hydrogen adsorption on a Cu-Zn-Cr oxide catalyst was found to increase with increasing copper content (Rudnitskii et al., 1973). This hydrogen was not associated with reduction of the catalyst and could be directly related to the activity for methanol synthesis. The simultaneous adsorption of carbon monoxide and hydrogen on a Cu-Zn-Cr oxide catalyst at atmospheric pressure showed that each reactant enhanced the adsorption of the other (Tsuchiya and Shiba, 1965). An intermediate surface species having the formula $-OCH_3$ was proposed based on the amounts of each reactant adsorbed. A critical assumption in this approach was that the methoxy species dominated the surface.

Fourier Transform Infrared Spectroscopy

The use of infrared spectroscopy for the observation and identification of adsorbed species on solid surfaces, especially heterogeneous catalysts, has been very popular in experimental research (Little, 1966; Hair, 1967; Kiselev and Lygin, 1975). Advances in optics and computer technologies have made Fourier transform infrared (FT-IR) spectroscopy a practical alternative to dispersive infrared methods. The basic components of an FT-IR spectrometer consist of an interferometer with the associated optical components and a dedicated computer for performing a Fourier transformation of the data and for executing spectral manipulations of the data. FT-IR spectroscopy offers several advantages compared to dispersive methods (Bell, 1972; Griffiths, 1975; Green and Reedy, 1978). Faster scanning times are possible since all wavelengths are measured simultaneously (Felgett's advantage). The utilization of an internal helium-neon reference laser permits a more accurate wavelength calibration (Connes' advantage). Other advantages include greater energy throughput (Jacquinot's advantage), no interference by stray light or sample emission, and better mechanical reliability (the interferometer mirror is the only moving part during the measurement scans). Infrared spectra of adsorbed species under <u>in situ</u> conditions frequently require that spectral contributions due to gaseous species and the catalyst itself be removed. The computer capabilities of the FT-IR spectrometer can be utilized to remove these background effects. FT-IR spectroscopy is advantageous in transmission infrared spectroscopy for

samples having low transmittance of radiation and for studying transients involving limited data acquisition time (Bell, 1980).

EXPERIMENTAL APPARATUS AND METHODS

Fourier Transform Infrared Spectrometer

A Bruker-Physik AG Model IFS 113 spectrometer was used to obtain infrared spectra. Both the spectrometer and the data system were supplied by USA Bruker Instruments and serviced by IBM. The spectrometer, shown in Figure 16, is divided into four compartments; the detector, sample, interferometer, and source sections. During use, the sample compartment can be isolated from the other sections. The source chamber has both a Globar and a mercury arc lamp source. The radiation from the source is directed through an aperature into the interferometer chamber to a filter assembly, and through to the beamsplitter. Because the infrared beam comes to a focus at this point, the beamsplitters for both mid- and far-IR are sufficiently small to be placed on a single rotatable wheel controlled by the computer. The two beams leaving the beamsplitter are reflected on opposite sides of a movable double-sided plane mirror. The modulated beam combines at the beamsplitter and is directed to the sample chamber; rotatable mirrors permit beam switching. The radiation passes through the sample chamber to the detector chamber. Two DTS detectors, optimized for either far-IR or mid-IR radiation, measure the intensity of the infrared beam.

The resolution can be varied from 0.05 to 8.0 cm^{-1}, with a minimum scanning time at 8.0 cm^{-1} of 0.2 sec. The data system utilizes a special 24-bit word. Data are stored either on a removable disc or on a floppy disc. Preprogrammed experiments can be executed. The control board permits scope display of inferograms and spectra, which may be

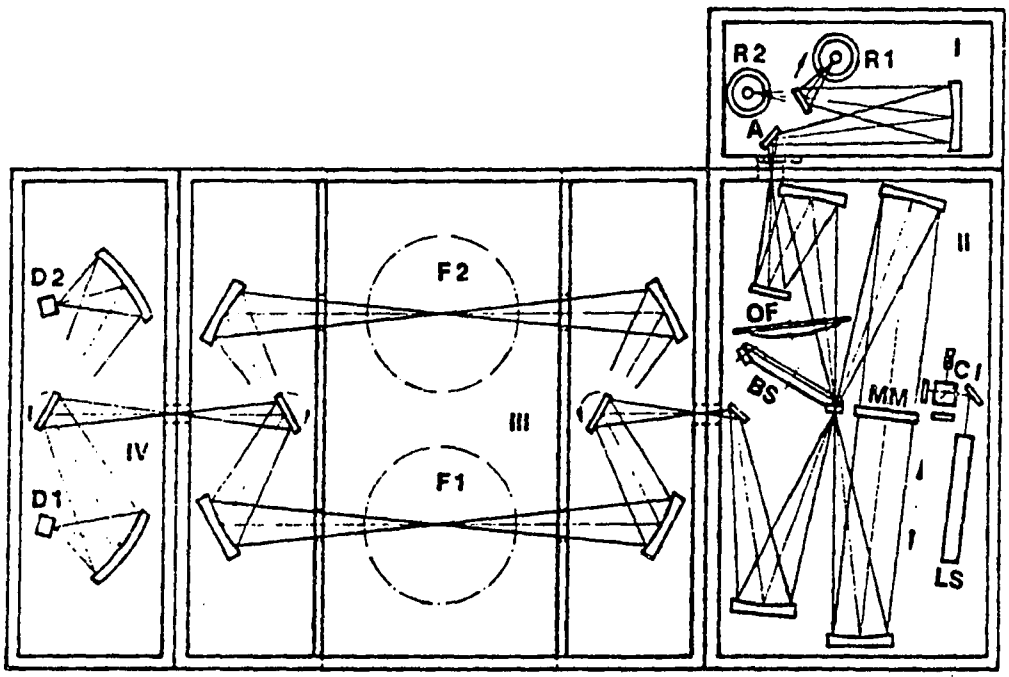

R1	Globar source	MM	Moving mirror
R2	Mercury arc lamp	LS	Laser source
A	Variable aperature	F1	Sample
OF	Optical filter	F2	Reference
BS	Beam splitter	D1, D2	Detectors

Figure 16. Bruker IFS 113 FT-IR spectrometer

manipulated using role and zoom controls. The computer can operate in three task regions simultaneously; data acquisition, data manipulation, and data output (plots) can be undertaken at the same time.

Infrared Photoacoustic Spectroscopy

Although methanol synthesis catalysis typically have a copper content above 30% (metal atom %), these catalysts cannot be studied in their pure state by transmission infrared techniques due to very poor transmittance. Infrared radiation striking a solid that does not transmit photons may either reflect or be absorbed. Recent advancements in the practical application of photoacoustic spectroscopy (PAS) to the characterization of solids provide a method for detecting the radiation absorbed by a sample. This technique is under development in this laboratory, and offers a possible means to characterize those methanol catalysts with high copper contents.

When PAS is combined with FT-IR spectroscopy, a sensitive and relatively quick analytical system is formed. The modulated infrared beam passes through a window into the sample chamber and is absorbed by the sample (Figure 17). The radiation is converted to heat by nonradiative de-excitation of the sample. Because the infrared energy is modulated, the surface heats and cools as the incident energy rises and falls. This thermal cycle causes the gaseous boundary layer next to the surface to expand and contract, producing sound waves detected by a sensitive microphone. The signal is then processed by the FT-IR data system into an infrared spectrum.

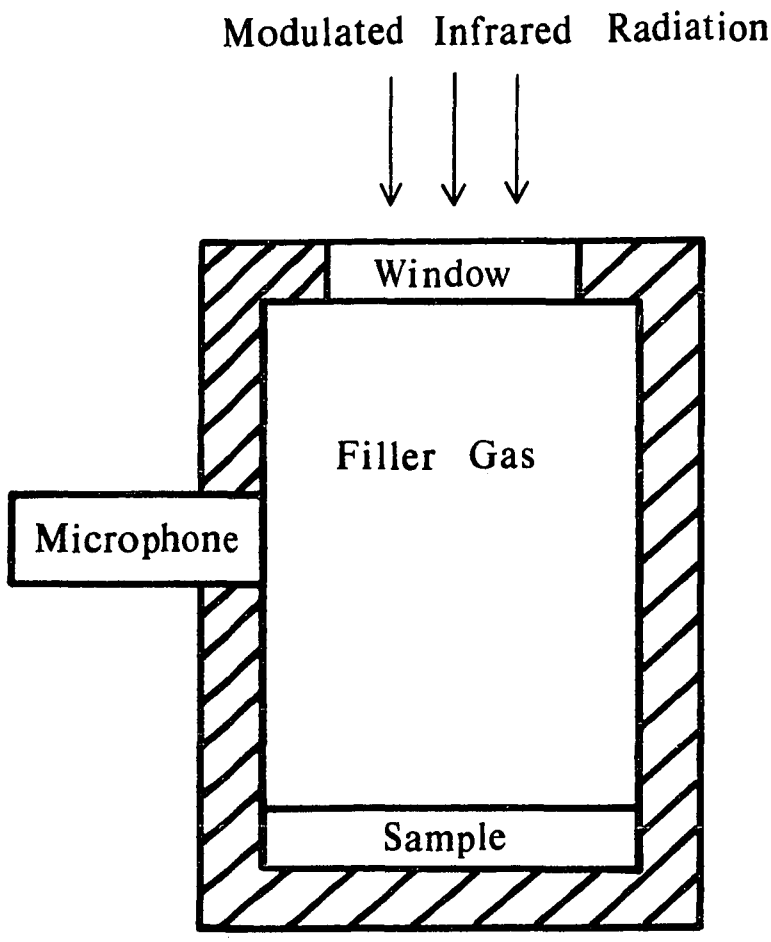

Figure 17. Photoacoustic cell

Sample Preparation for Transmission Infrared Studies

All oxides used in transmission infrared studies were heated at 350°C overnight under a vacuum of 10^{-4} torr to remove adsorbed carbonates and water. After cooling the oxide to room temperature in helium, this powder was transferred in air to a vial and capped to prevent contamination by atmospheric CO_2. Samples could be taken from a vial over a period of several months before this treatment needed to be repeated. Zinc oxide wafers were prepared by pressing some powder under a load of 3200 kg into a wafer 20.6 mm in diameter and 0.2-0.3 mm thick. Binary and ternary oxides were pressed under a load of 4500 kg into wafers 0.06-0.12 mm thick. Zinc oxide wafers were relatively thick because thinner wafers were too brittle to handle; binary and ternary wafers were made as thin as possible to achieve sufficient transmittance for in situ studies. All these oxides tended to adhere to the metal faces of the die; thin sheets of Mylar were placed on the die faces when ZnO and binary oxides were compressed, whereas thin sheets of glassine paper were used with ternary oxides. Wafers were carefully transferred into the infrared cell and placed in the spectrometer. Details of the infrared cell design will be presented in Part III. Adsorbed water on the catalyst wafer was removed by flowing nitrogen gas through the cell overnight (about 12 hours) at atmospheric pressure and 200°C (pretreatment #1). In some cases, the nitrogen gas was passed through water before entering the cell during an overnight treatment at atmospheric pressure and 200°C (pretreatment #2). In some experiments, the catalyst was reduced by flowing a 5% hydrogen stream (the balance was nitrogen) through

the cell for 1 hour at atmospheric pressure and 200°C (pretreatment #3).

All adsorption experiments were conducted in a continuous flow mode. Gaseous adsorbates were passed through the cell at 60 cc/min STP. Liquids such as water, methanol, or formic acid solution were introduced to the cell in low concentrations by passing a carrier gas (normally nitrogen) through the liquid when the liquid was enclosed in a glass container (saturator). Formaldehyde was introduced to the cell at its vapor pressure (1.4 torr at 25°C) by heating solid paraformaldehyde in the saturator while carrier gas flowed through. The outlet line from the saturator developed some paraformaldehyde on the inner walls, indicating that the formaldehyde was at saturation. Flow conditions in the line to the cell were 60 cc/min, 25°C, and 1 atmosphere. High purity gases were used and the adsorbates are listed in Table 12.

Table 12. Adsorbate specifications

1.	Eastman Formic Acid (88%), Reagent ACS
2.	Kodak Paraformaldehyde, 90% min.
3.	Fisher Scientific Methanol, Reagent ACS
4.	Aldrich Chemical Methanol-d, 99.5% + D
5.	Aldrich Chemical Methanol-d_4, 99.5% + D

RESULTS OF ATMOSPHERIC ADSORPTION

Adsorption on Zinc Oxide

The method of preparation of zinc oxide has a very strong effect on its infrared transmission property. Zinc oxide made by the oxidation of metallic zinc (dry process) transmits infrared radiation well, whereas precipitated zinc oxide (wet process) rapidly loses transmittance when the oxide is reduced. Reduction involves the removal of some oxygen creating excess zinc (possibly interstitial zinc) and releasing electrons to the conduction band of the oxide. A commercially available ZnO compound (Kadox 25) prepared by the dry process was used in these adsorption studies to avoid excessive transmission losses.

An oxidized (pretreatment #1) zinc oxide wafer was reduced in a 5% hydrogen-95% nitrogen stream at 200°C for an hour (pretreatment #3). Figure 18 shows that some of the residual surface carbonate species (bands at 1512, 1466, 1383, and 1326 cm^{-1}) were reduced to surface formate groups (bands at 2976, 2879, 2738, 1582, and 1370 cm^{-1}). The residual surface hydroxyl groups (bands at 3668, 3620, 3565, and 3450 cm^{-1}) were unaffected by the exposure to hydrogen.

The adsorption of carbon monoxide on zinc oxide (pretreatment #1) at 200°C and 1 atmosphere is shown in Figure 19. The transmission was strongly reduced by carbon monoxide (band at 2143 cm^{-1}) making it very difficult to observe infrared bands under 2000 cm^{-1} (Figure 19b). After 8 hours of exposure to carbon monoxide, the cell was flushed with nitrogen to reveal a significant increase in formate groups (bands at 2970, 2875, 2738, 1572, 1381, and 1366 cm^{-1}). The bidentate carbonate

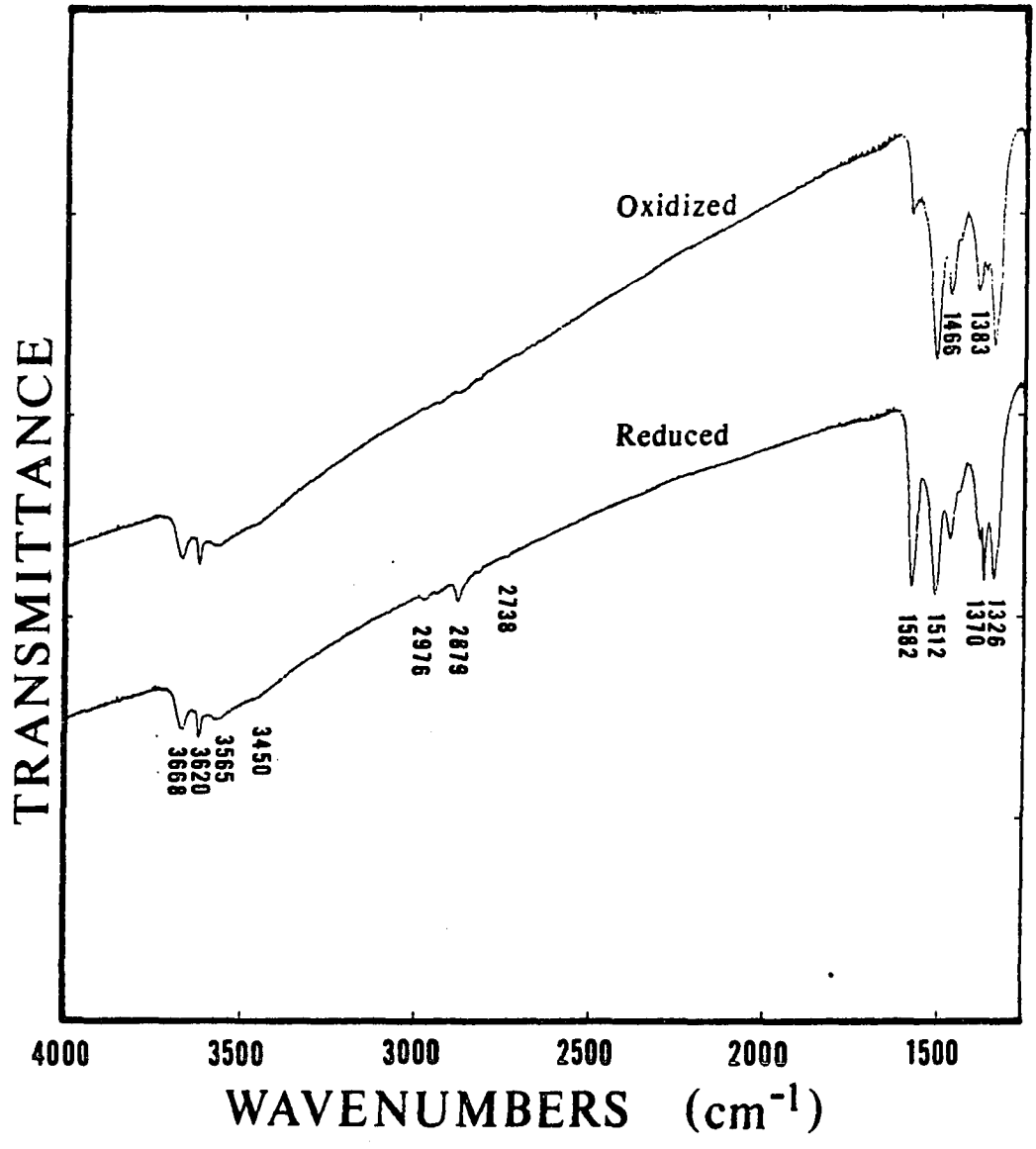

Figure 18. Reduction of Kadox 25 in hydrogen at 200°C

Figure 19. Carbon monoxide adsorption on Kadox 25 at 200°C

a) oxidized surface

b) exposure to CO for 5 minutes

c) purged sample after 8 hours of CO exposure

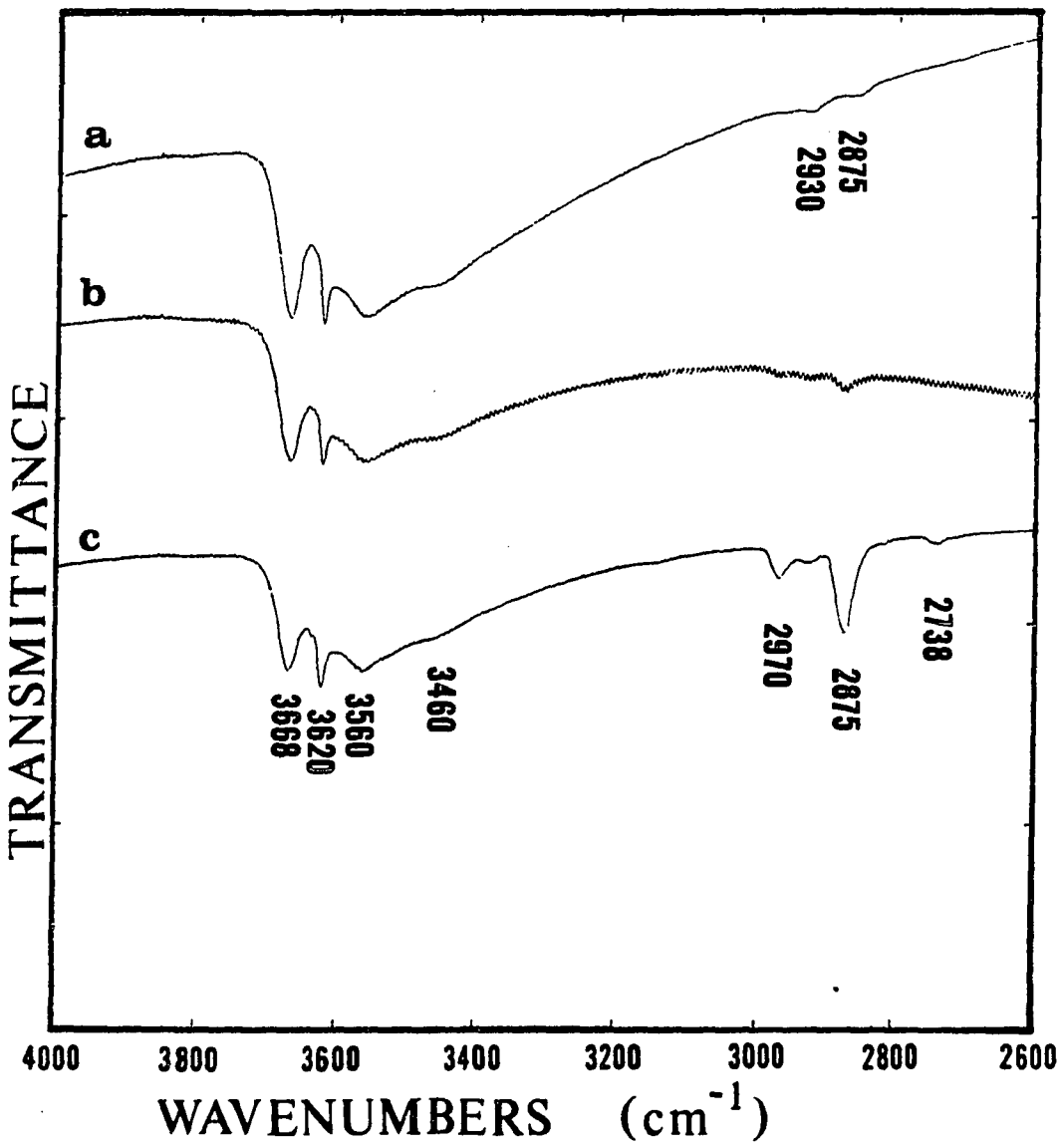
a
b
c
2875
2930
2970
2875
2738
3460
3560
3620
3668
TRANSMITTANCE
4000
3800
3600
3400
3200
3000
2800
2600
WAVENUMBERS (cm-1)

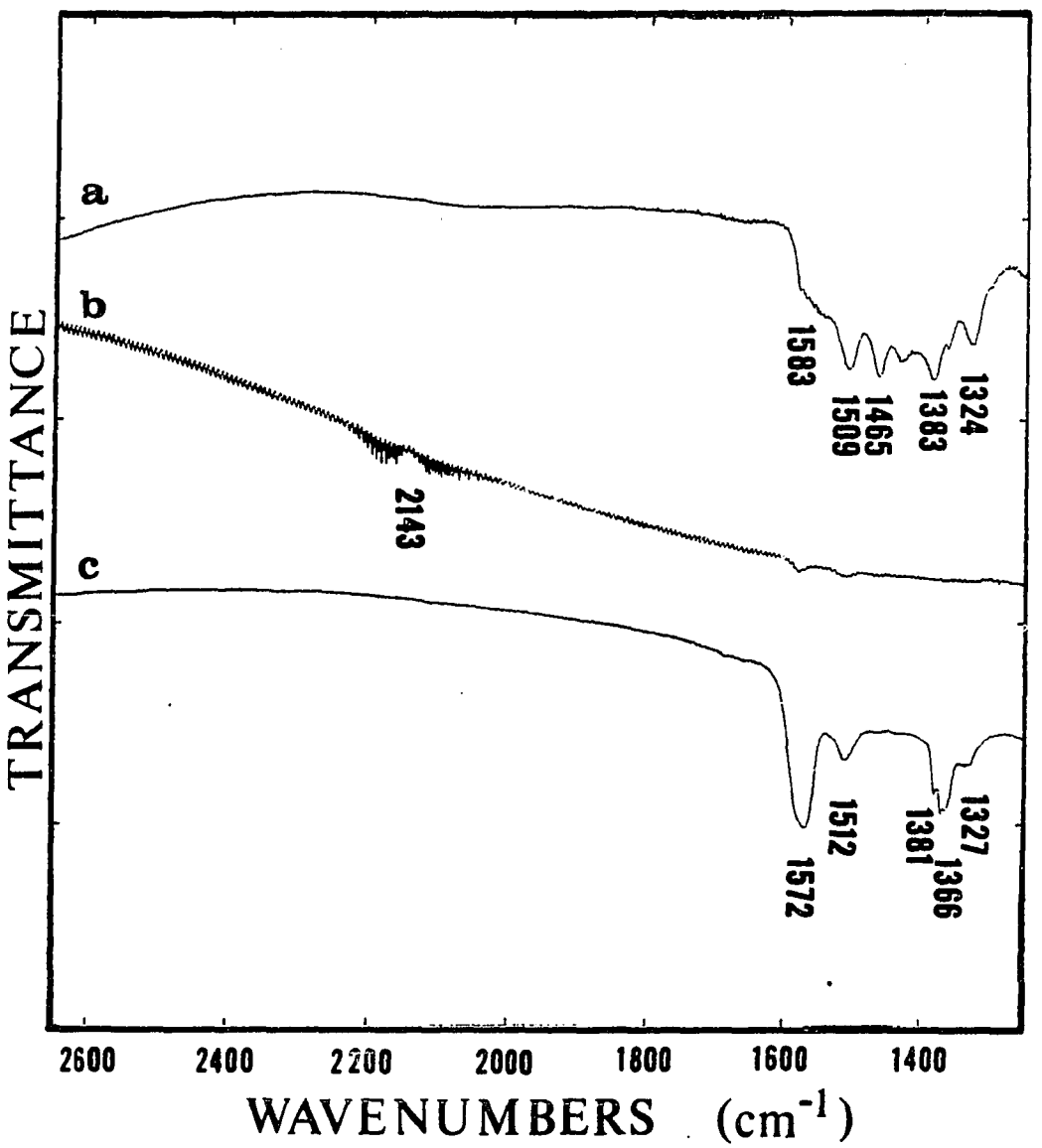

Figure 19. Continued

species (bands at 1512 and 1327 cm^{-1}) have diminished and the unidentate carbonate (bands at 1465 and 1383 cm^{-1}) has disappeared. The hydroxyl region (4000-3000 cm^{-1}) was unaffected by the exposure to carbon monoxide.

The adsorption of carbon monoxide and hydrogen ($H_2/CO = 2/1$) on zinc oxide (pretreatment #1) at 200°C and 1 atmosphere is shown in Figure 20. The infrared spectra were quite similar to those for carbon monoxide adsorption; the transmission was very low causing a loss of information at lower frequencies. The development of formate groups was indicated by the growth of bands at 2970 and 2875 cm^{-1}.

The presence of stable formate species on Kadox 25 was verified by exposing the oxide to formic acid. The adsorption of formic acid solution (88% HCOOH, 12% H_2O) on zinc oxide (pretreatment #3) at 165°C and 1 atmosphere is shown in Figure 21. The lower adsorption temperature was used to slow the decomposition rate of surface species. Exposure to formic acid solution caused a formate species (bands at 2970, 2882, 2737, 1576, and 1382 cm^{-1}) to form which lacks the sharp detail of the initial formate groups on the reduced surface, possibly because of interactions among species at relatively high concentrations. The hydroxyl groups have been displaced by formate and adsorbed water (bands at 3430 and 1660 cm^{-1}). The formation of gaseous carbon dioxide (vibrational-rotational bands at 2350 cm^{-1}) occurred when the cell was isolated (no flow through the cell), indicating that carbon dioxide rather than carbon monoxide was the primary product of surface formate decomposition.

Figure 20. Adsorption of a CO-H_2 mixture on Kadox 25 at 200°C

a) oxidized surface

b) exposure for 5 minutes

c) exposure for 1 hour

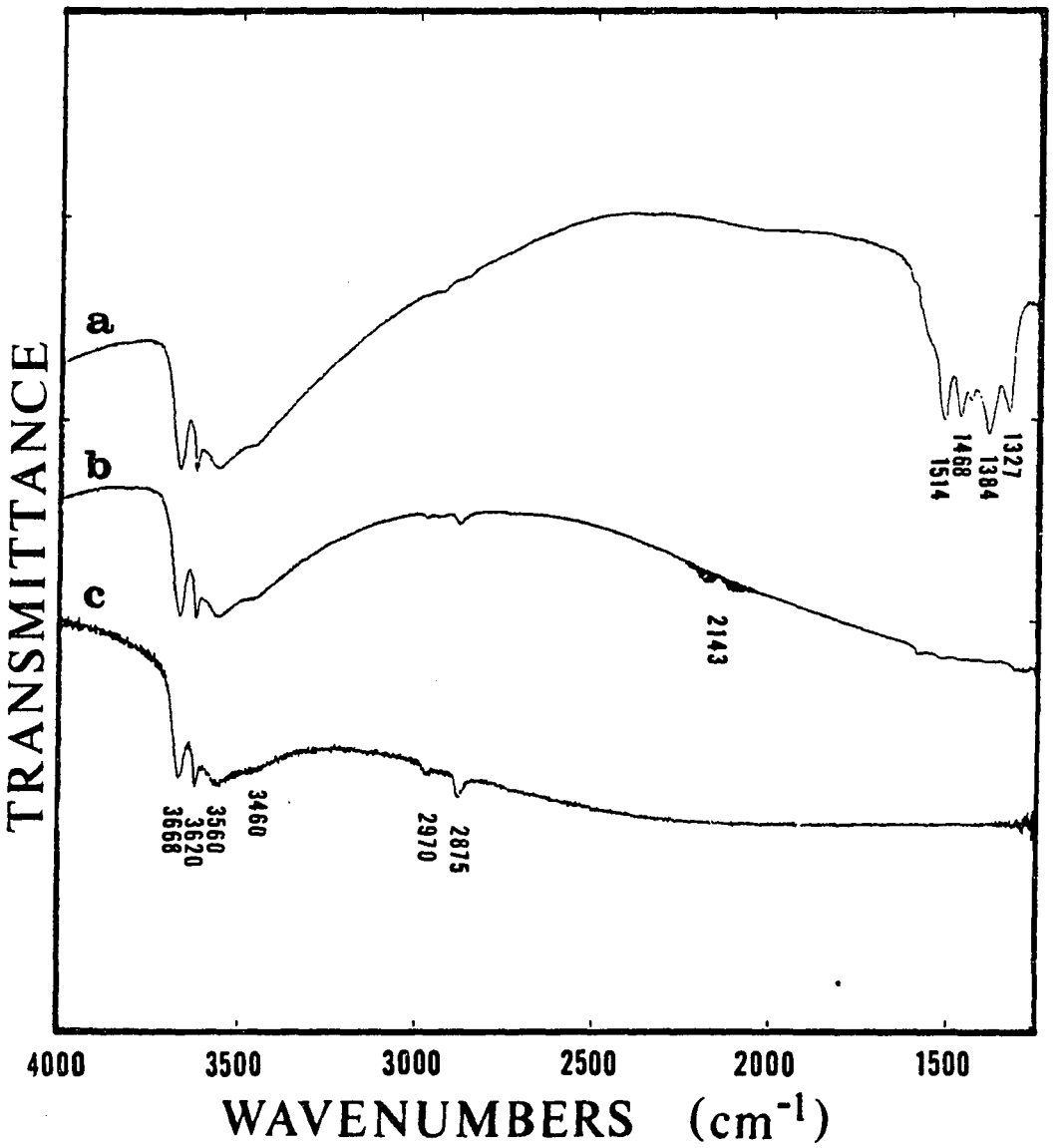
TRANSMITTANCE
a
b
c
1327
1384
1468
1514
2143
3460
3560
3620
3668
2875
2970
4000
3500
3000
2500
2000
1500
WAVENUMBERS (cm-1)

Figure 21. Formic acid adsorption on Kadox 25 at 165°C

a) reduced surface

b) exposure to formic acid solution

c) decomposition of surface formate species in an isolated cell

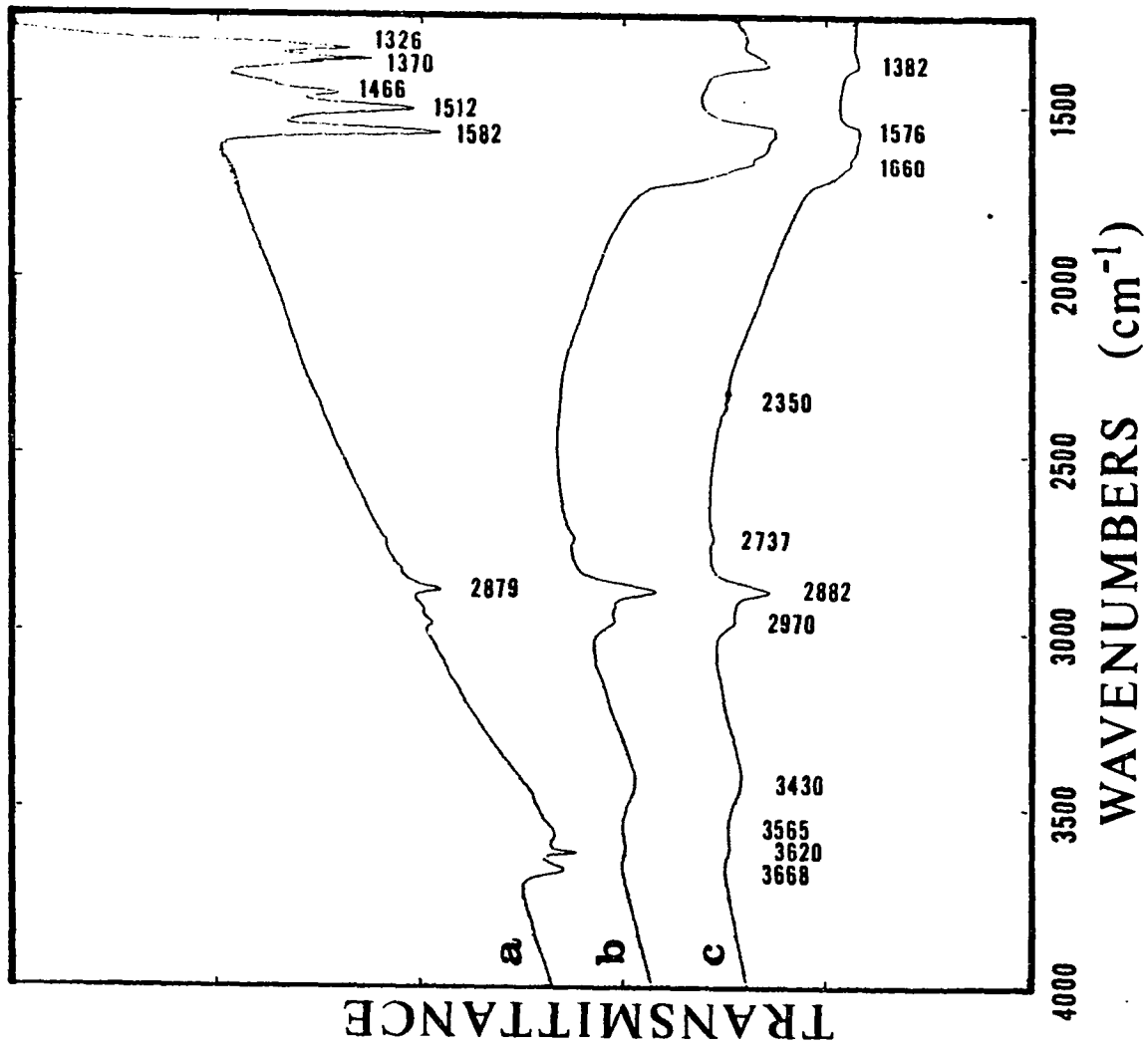
1326
1370
1466
1512
1582
1382
1576
1660
2350
2737
2879
2882
2970
3430
3565
3620
3668
a
b
c
TRANSMITTANCE
1500
2000
2500
3000
3500
4000
WAVENUMBERS (cm-1)

Adsorption on Binary Oxides

Two precipitated binary oxides, 95/5 Zn/Cu and 90/10 Zn/Cu oxides, transmitted sufficient radiation for infrared studies. These binary oxides had the same residual hydroxyl groups as those found on pure zinc oxide and had some residual surface carbonate groups. The reduction of a 95/5 Zn/Cu oxide in a 5% H_2-95% N_2 stream at 200°C (pretreatment #3) is shown in Figure 22. Surface carbonate groups (bands at 1516, 1469, 1380, and 1322 cm^{-1}) were partially reduced to formate species (bands at 2970, 2878, 1576, 1381, and 1366 cm^{-1}). A new hydroxyl band developed at 3252 cm^{-1}. Reduction with deuterium shifted the residual hydroxyl groups to OD groups (bands at 2706, 2667, 2630, and 2560 cm^{-1}) and created a new OD group at 2420 cm^{-1}. If a binary oxide was reduced with hydrogen and subsequently exposed to deuterium, all the hydroxyl groups except the species at 3252 cm^{-1} were rapidly shifted to OD groups.

The adsorption of carbon monoxide on the binary oxides was affected by the condition of the catalyst surface. Figures 23 and 24 show the adsorption of carbon monoxide at 200°C and 1 atmosphere on an oxidized 95/5 and 90/10 Zn/Cu catalyst, respectively. Carbon monoxide adsorbed as a carbonyl species (band at 2093 cm^{-1}) and caused gradual reduction of the oxide. The unidentate carbonate groups quickly disappeared and formate species slowly developed. The vibrational-rotational bands for gaseous carbon monoxide occurred at 2143 cm^{-1}.

The adsorption of a carbon monoxide and hydrogen mixture (CO/H_2 = 1/2) on oxidized 95/5 and 90/10 Zn/Cu catalysts at 200°C and 1 atmosphere is shown in Figures 25 and 26, respectively. Reduction of the oxide

Figure 22. Reduction of 95/5 Zn/Cu oxide at 200°C

a) oxidized surface

b) exposure to 5% H_2 for 30 minutes

c) exposure to 5% H_2 for 2 hours

d) exposure of an oxidized surface to deuterium for 30 minutes

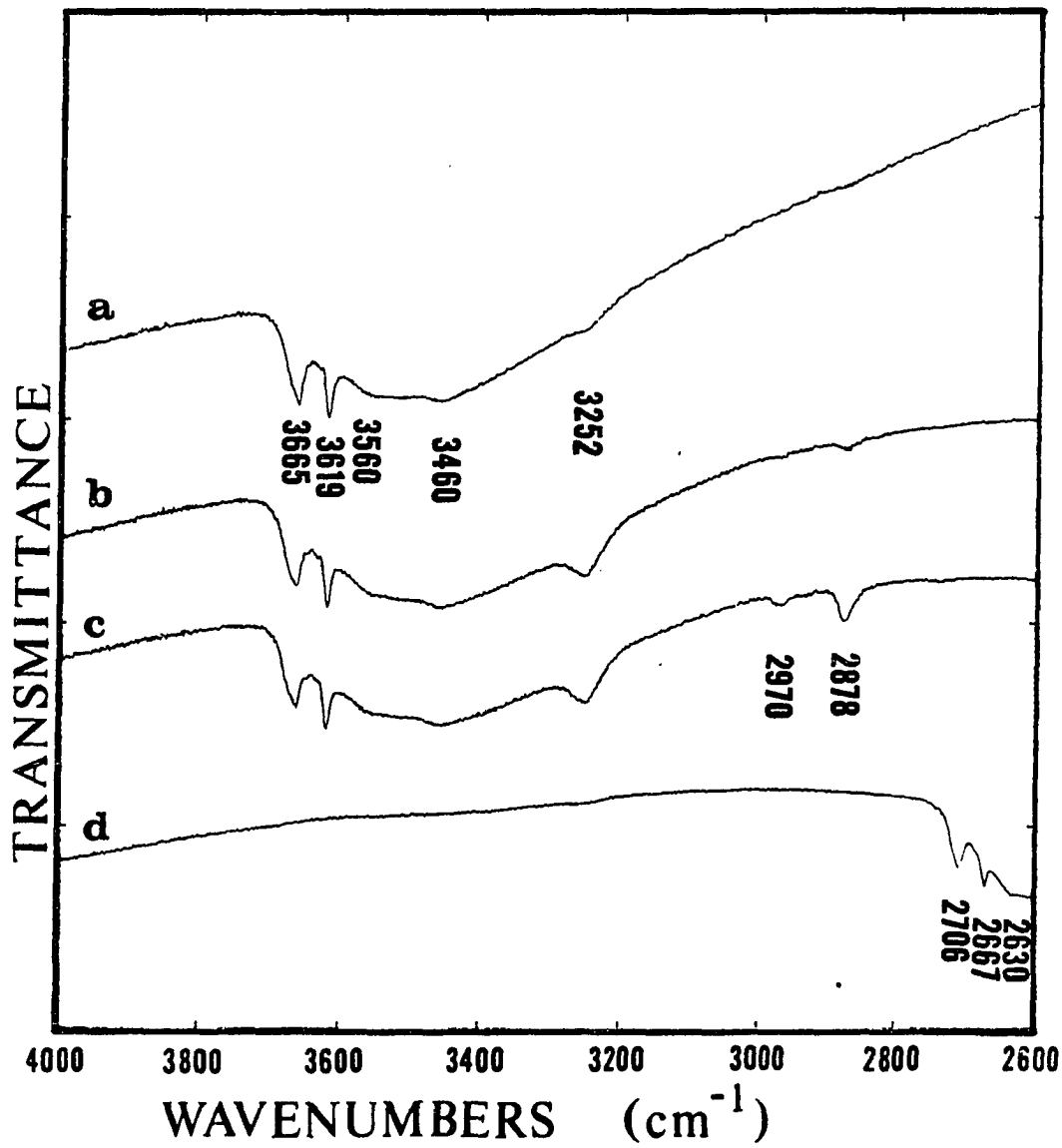
a
b
c
d
3665
3619
3560
3460
3252
2970
2878
2630
2667
2706
TRANSMITTANCE
4000
3800
3600
3400
3200
3000
2800
2600
WAVENUMBERS (cm-1)

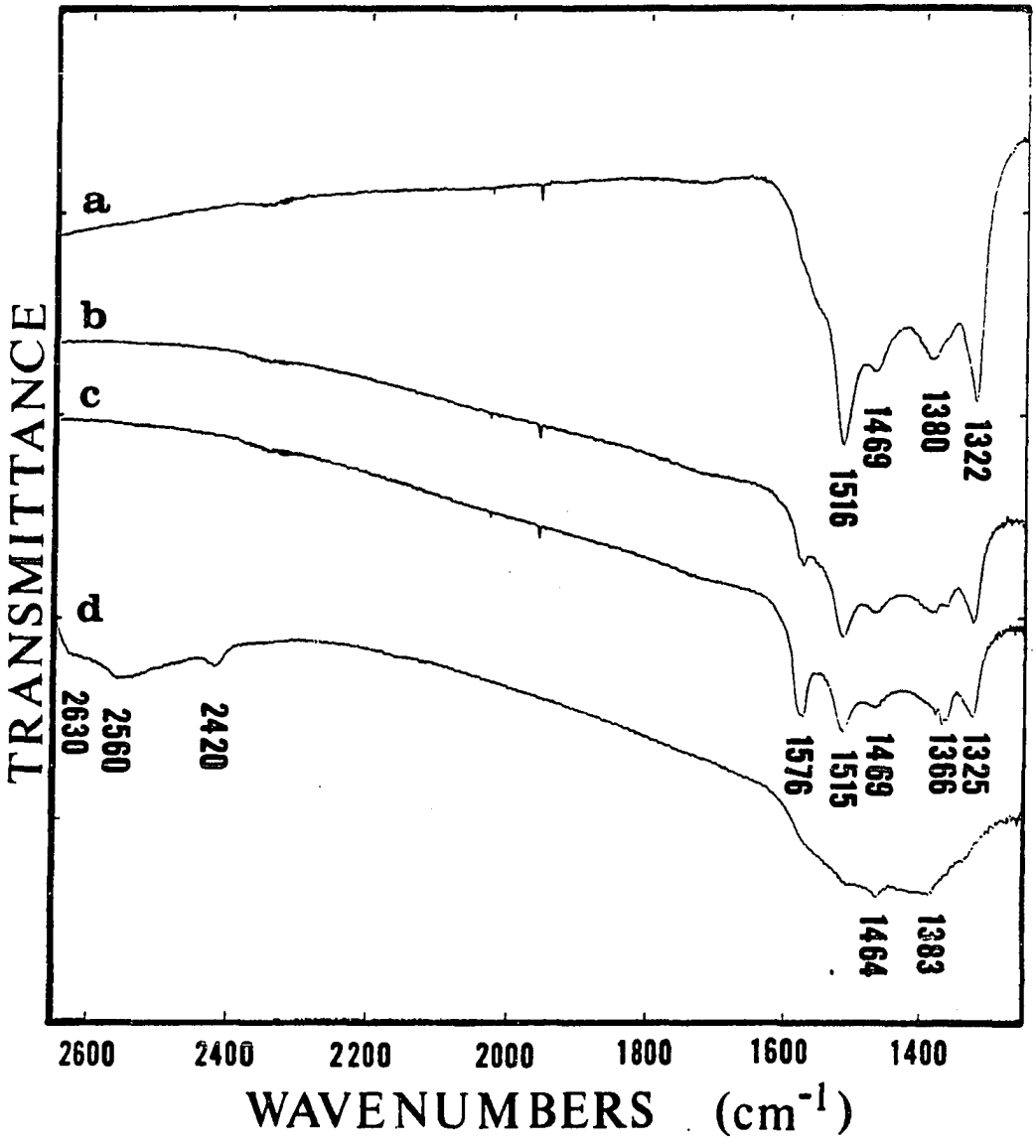

Figure 22. Continued

Figure 23. Carbon monoxide adsorption on 95/5 Zn/Cu oxide at 200°C

a) oxidized surface

b) exposure for 5 minutes

c) exposure for 1 hour

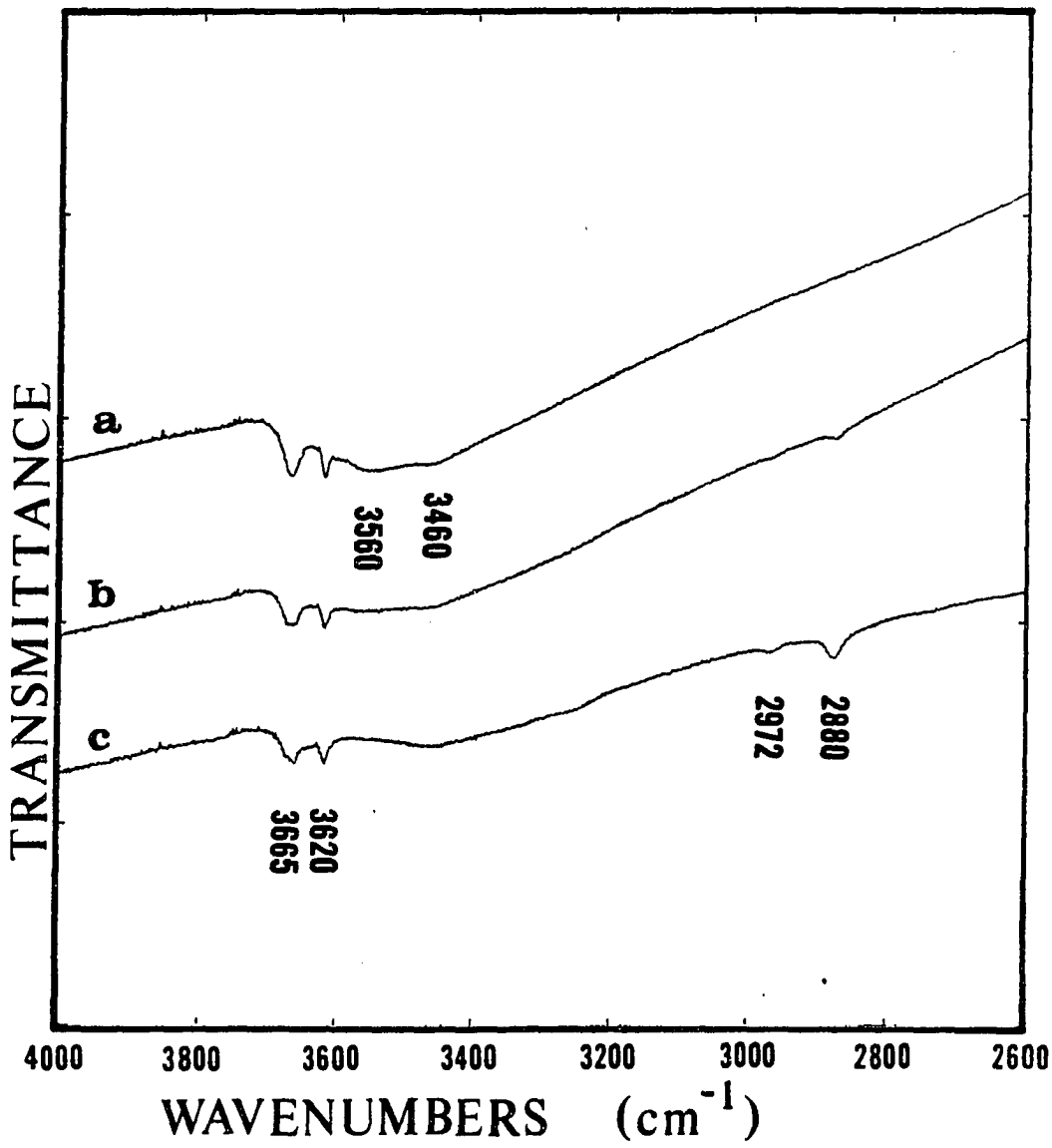
TRANSMITTANCE
a
b
c
3560
3490
3620
3665
2972
2880
4000
3800
3600
3400
3200
3000
2800
2600
WAVENUMBERS (cm-1)

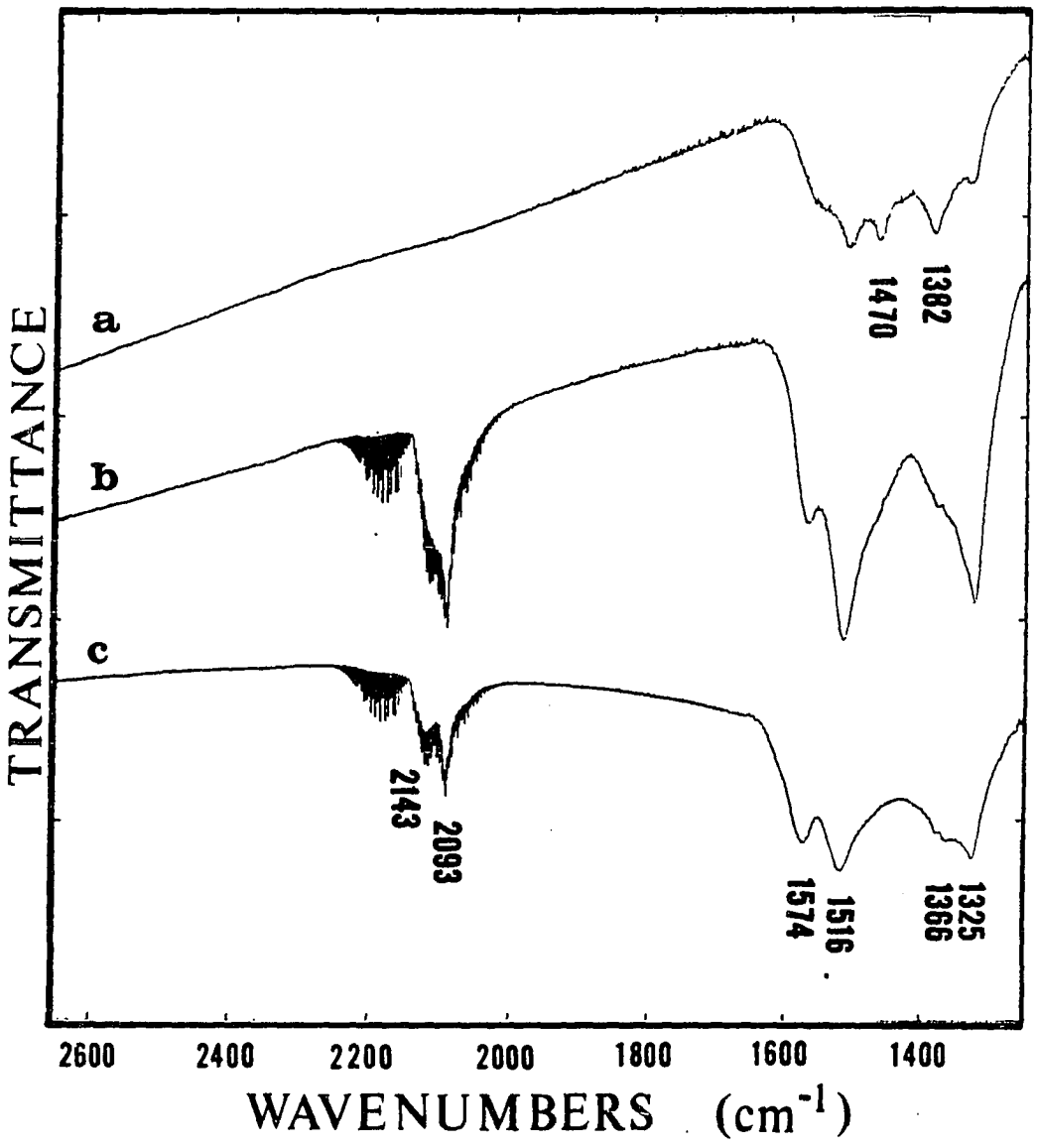

Figure 23. Continued

Figure 24. Carbon monoxide adsorption on 90/10 Zn/Cu oxide at 200°C

a) oxidized surface

b) exposure for 5 minutes

c) exposure for 1 hour

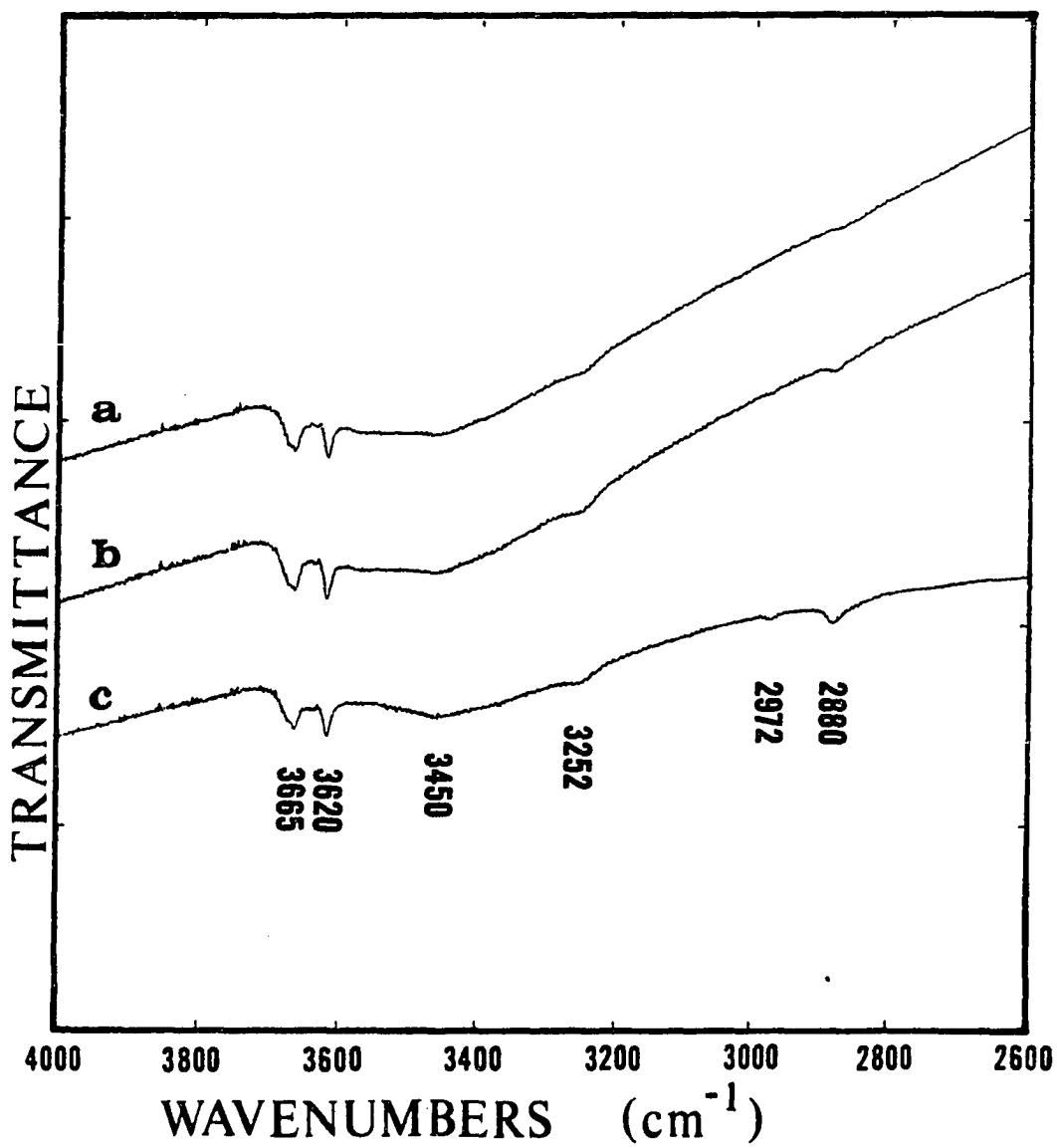
TRANSMITTANCE
a
b
c
3665
3620
3450
3252
2972
2880
4000
3800
3600
3400
3200
3000
2800
2600
WAVENUMBERS (cm-1)

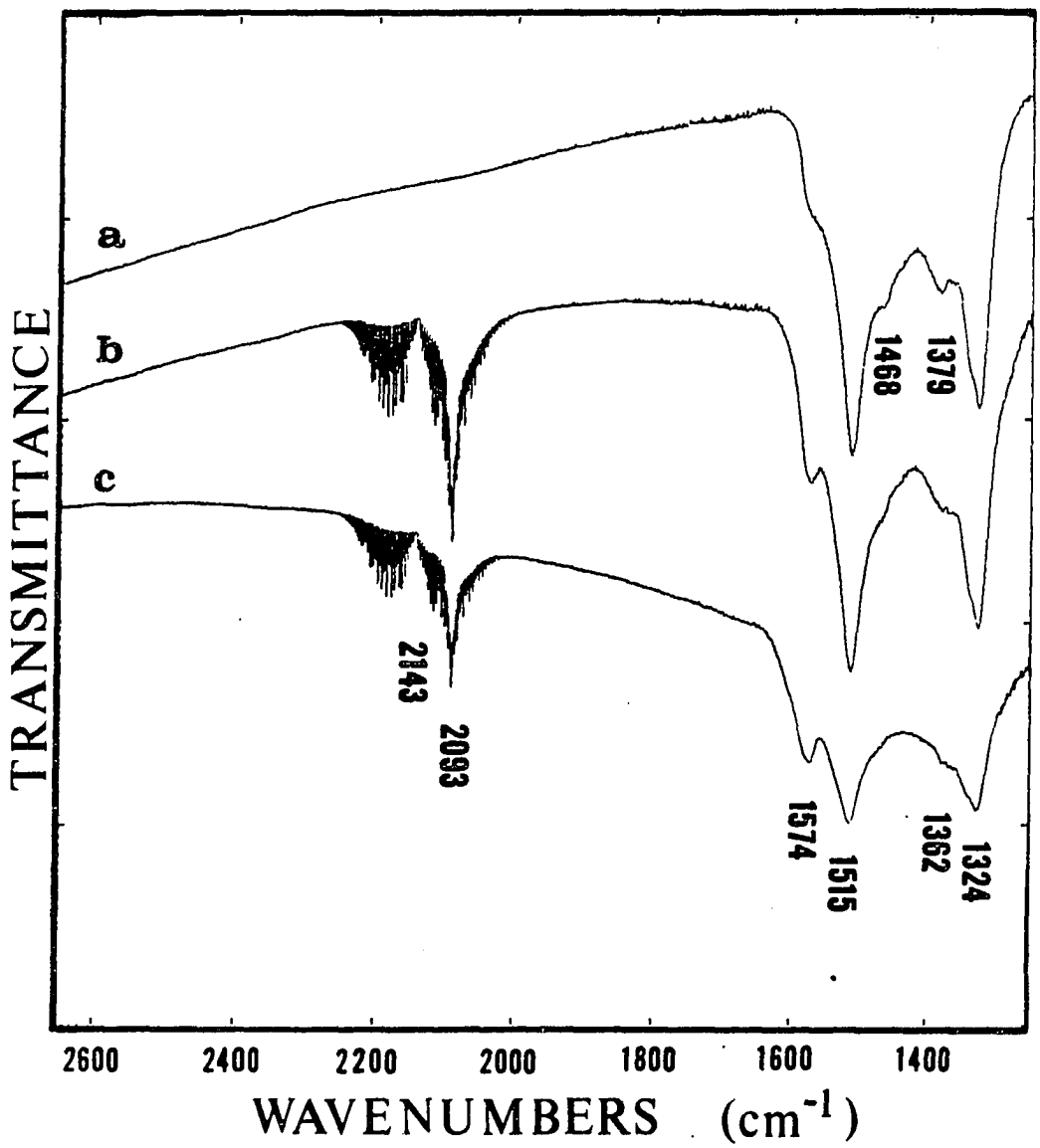

Figure 24. Continued

Figure 25. Adsorption of CO-H_2 mixture on 95/5 Zn/Cu oxide at 200°C

a) oxidized surface

b) exposure for 5 minutes

c) exposure for 1 hour

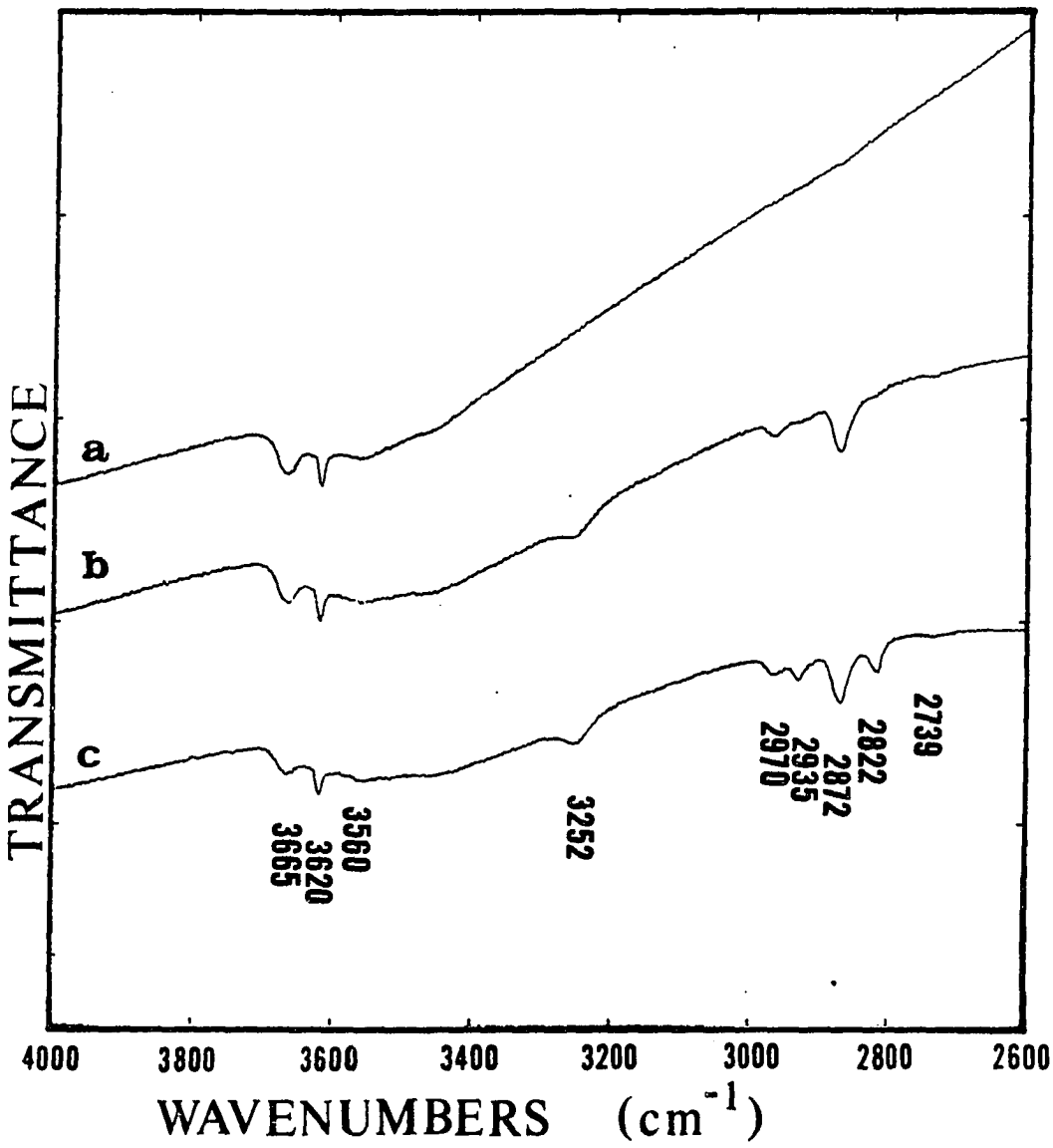
TRANSMITTANCE
a
b
c
3665
3620
3560
3252
2970
2935
2872
2822
2739
4000
3800
3600
3400
3200
3000
2800
2600
WAVENUMBERS (cm-1)

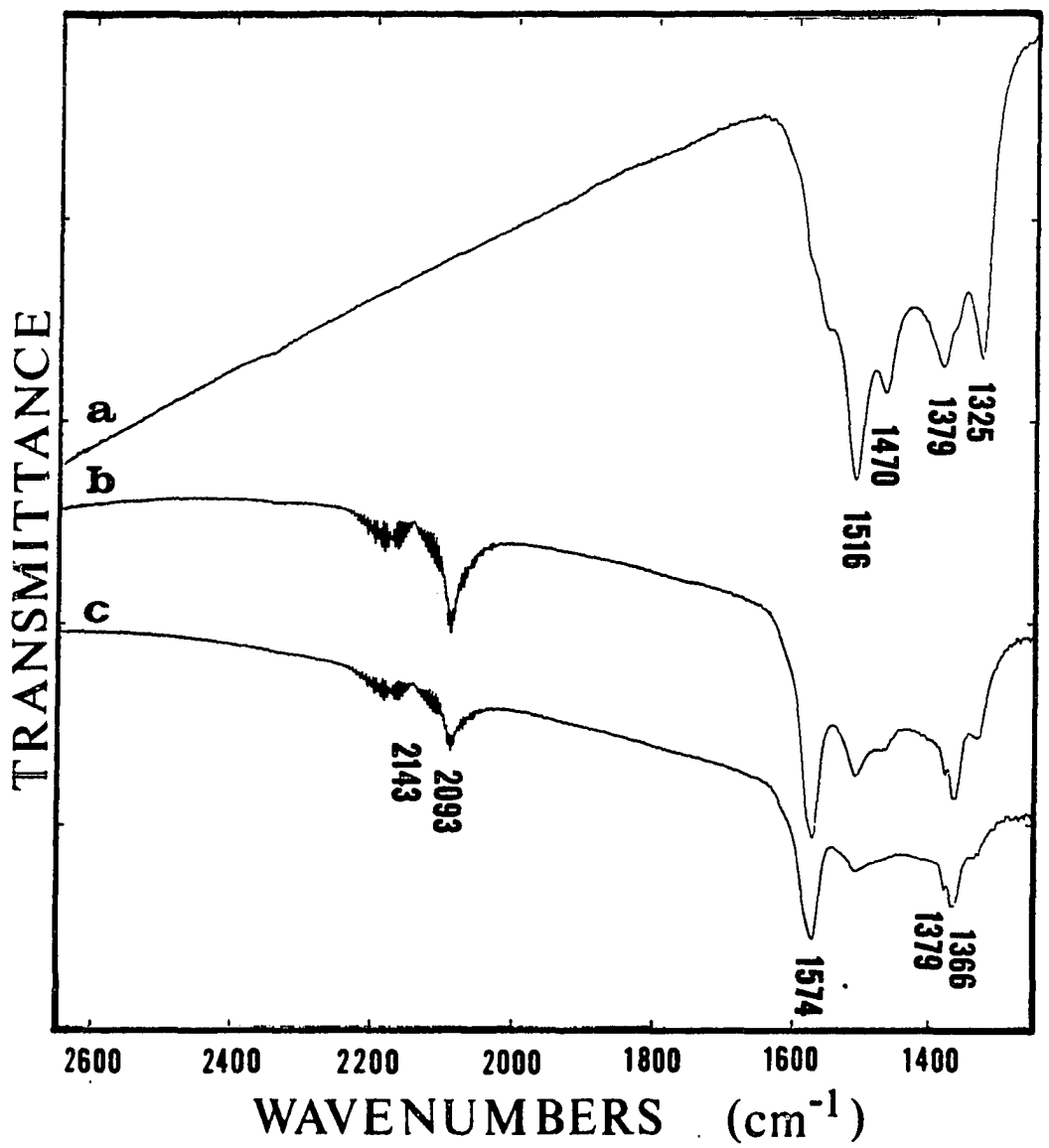

Figure 25. Continued

Figure 26. Adsorption of CO-H_2 mixture on 90/10 Zn/Cu oxide at 200°C

a) oxidized surface

b) exposure for 5 minutes

c) exposure for 1 hour

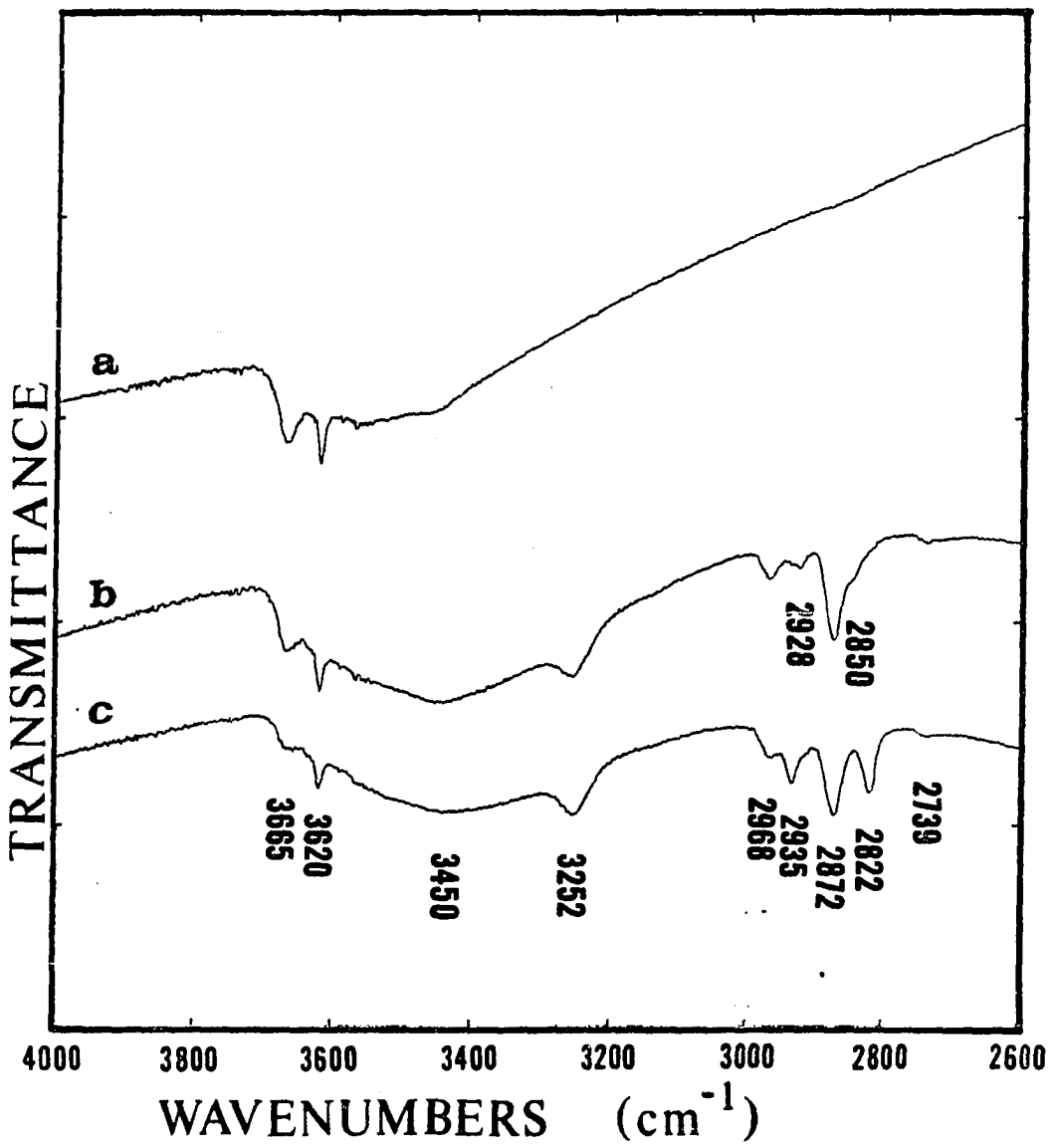
TRANSMITTANCE
a
b
c
2928
2850
3665
3620
3450
3252
2968
2935
2872
2822
2739
4000
3800
3600
3400
3200
3000
2800
2600
WAVENUMBERS (cm-1)

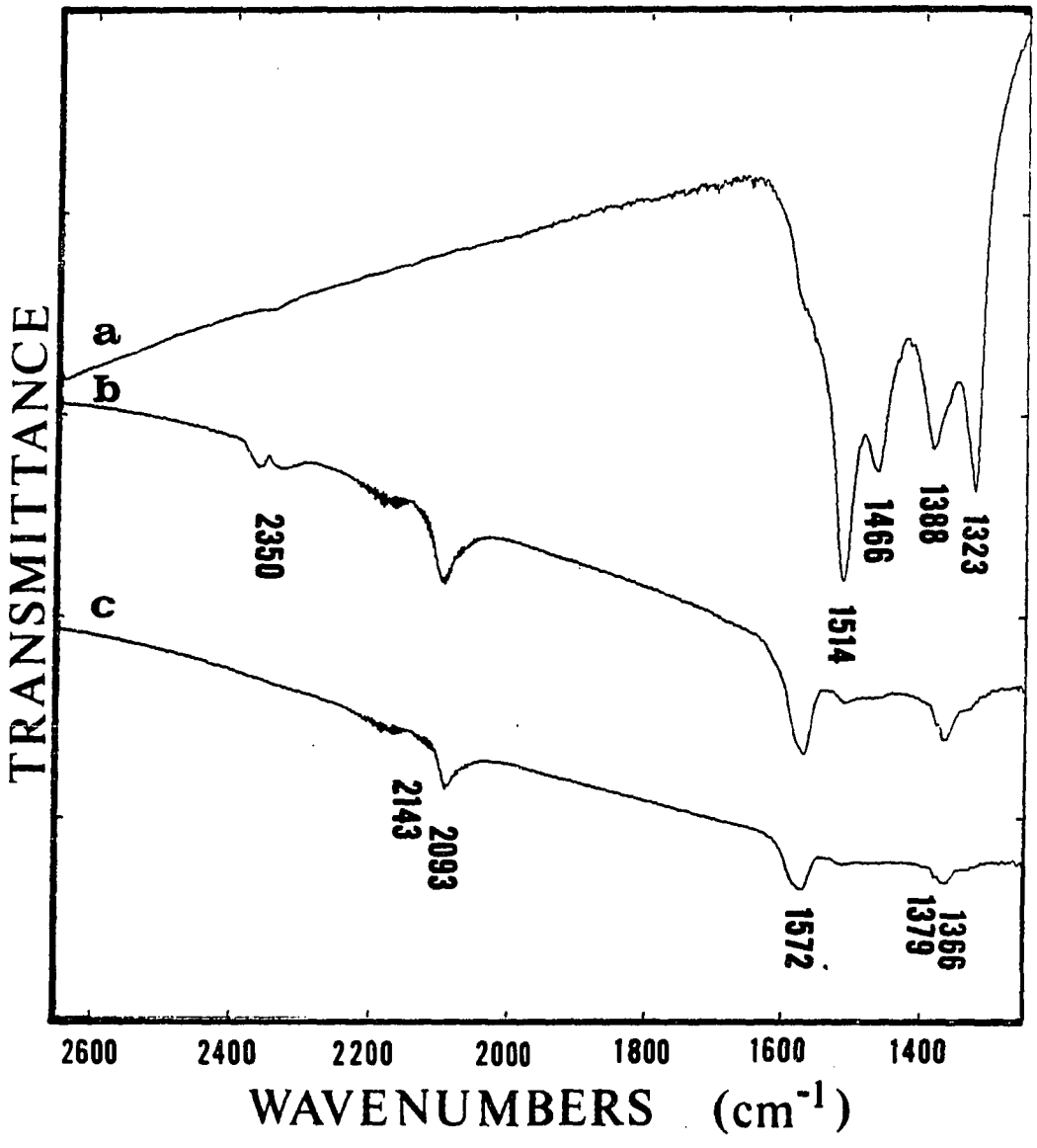

Figure 26. Continued

was rapid in each experiment, indicated by the loss of transmittance and the quick development of the hydroxyl band at 3252 cm^{-1}. The carbonyl species and formate groups were rapidly formed. Methoxy groups (bands at 2935 and 2822 cm^{-1}) gradually developed accompanied by the gradual disappearance of the hydroxyl at 3665 cm^{-1}, suggesting that these species occupied the same sites. The rate of hydrogenation of surface species on the 90/10 Zn/Cu oxide was faster than the rate on 95/5 Zn/Cu oxide. The presence of gaseous CO_2 (band at 2350 cm^{-1}) in the spectrum of 90/10 Zn/Cu oxide immediately after reduction indicated that the water-gas shift reaction was possible. Catalyst reduction by hydrogen was more rapid than reduction by carbon monoxide, forming water which quickly reacted with carbon monoxide to yield carbon dioxide and hydrogen. The carbon dioxide did dissipate within an hour, but the lack of vibrational-rotational bands suggested that the carbon dioxide interacted with the catalyst surface. The presence of CO_2 could also be responsible for the observation of a transient, unstable surface species (bands at 2928 and 2850 cm^{-1}) which was assigned to an adsorbed formaldehyde species.

Carbon monoxide and deuterium (CO/D_2 = 1/2) were adsorbed concurrently on an oxidized 95/5 Zn/Cu catalyst (pretreatment #1) at 200°C to check the band assigmments for deuterated surface species. The formation of the OD group at 2418 cm^{-1} showed reduction of the oxide. A carbonyl species (band at 2091 cm^{-1}) was formed and surface carbonate groups were deuterated to yield a formate species (bands at 2166, 1570, and 1336 cm^{-1}). The deuterated methoxy species (one band at 2055 cm^{-1}

Figure 27. Adsorption of CO-D_2 mixture on 95/5 Zn/Cu oxide

a) oxidized surface

b) exposure for 10 minutes

c) exposure for 1 hour

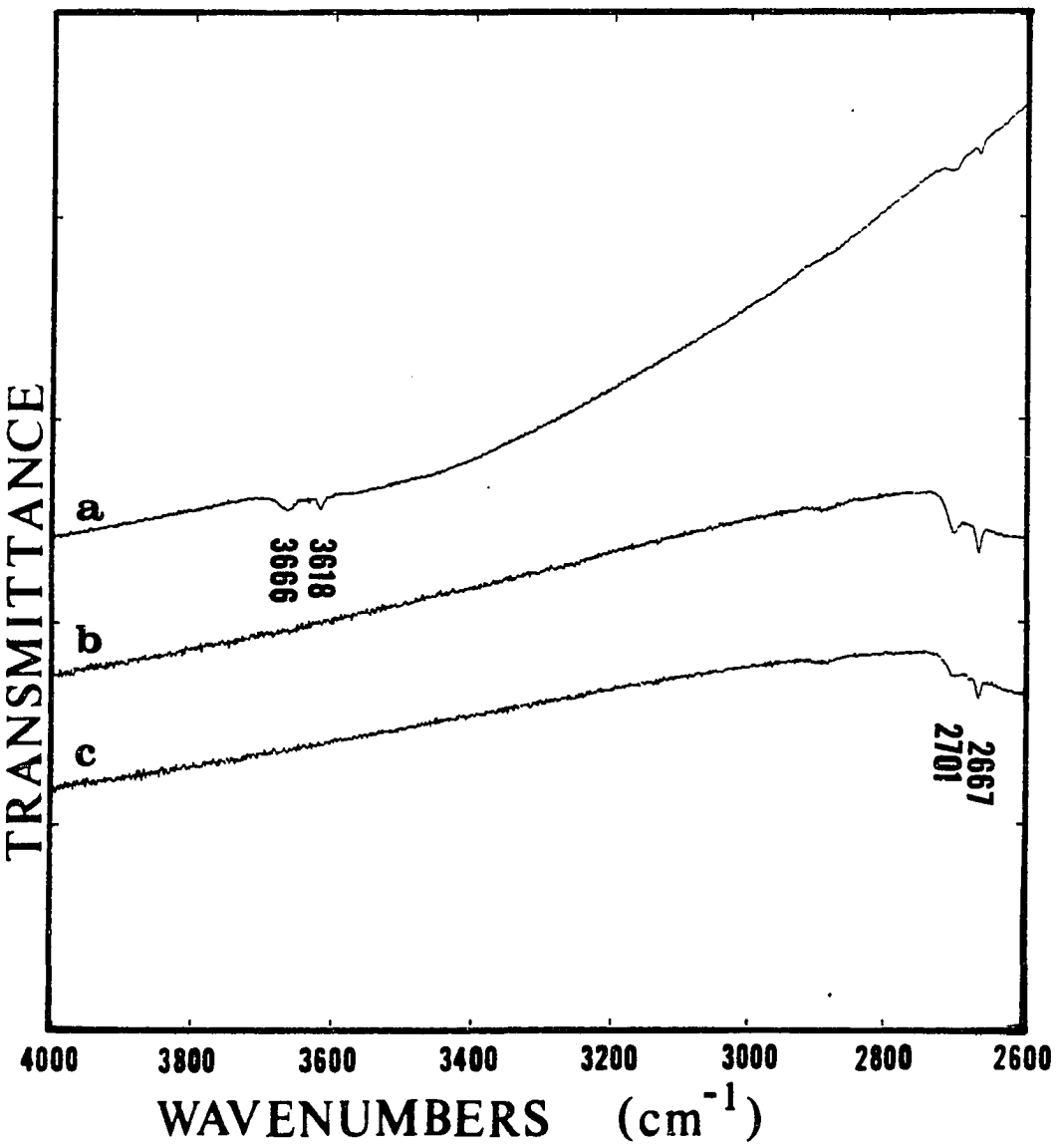
TRANSMITTANCE
a
b
c
3666
3618
2701
2667
4000
3800
3600
3400
3200
3000
2800
2600
WAVENUMBERS (cm-1)

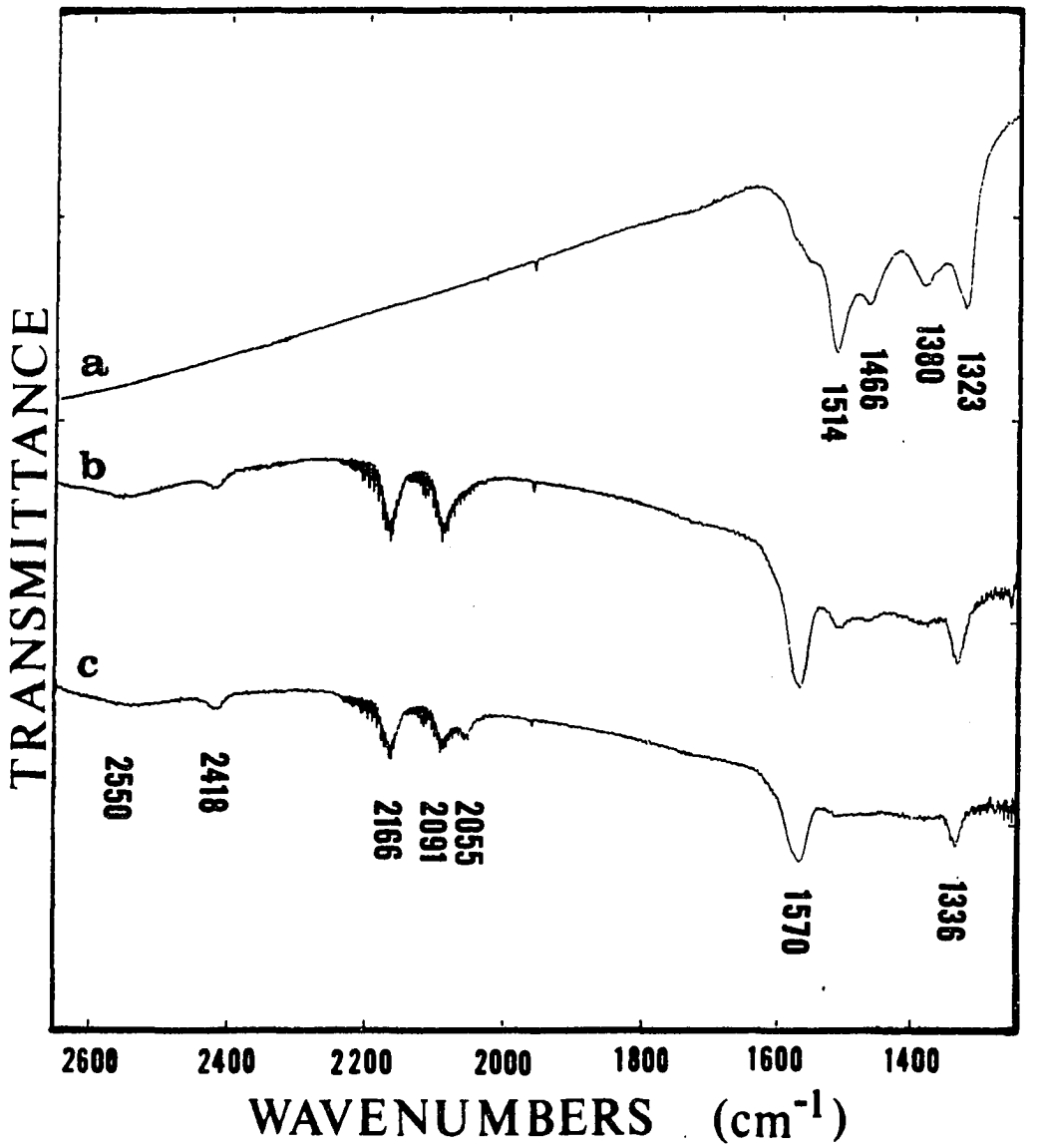

Figure 27. Continued

apparent) developed with the concurrent decrease in the OD group at 2701 cm^{-1}.

The adsorption of carbon monoxide on a reduced 90/10 Zn/Cu catalyst (pretreatment #3) at 200°C and 1 atmosphere, shown in Figure 28, was conducted to determine if the hydrogenation of surface species would be greater on a reduced rather than oxidized catalyst. A carbonyl species was formed at 2093 cm^{-1} and the unidentate carbonate (bands at 1469 and 1380 cm^{-1}) diminished. The formate (bands at 2972, 2880, 1576, 1379, and 1364 cm^{-1}) and bidentate carbonate (bands at 1516 and 1325 cm^{-1}) species were essentially unaffected by CO adsorption. The transmittance did decrease during adsorption, especially at the lower wavenumbers.

When a mixture of carbon monoxide and hydrogen (CO/H_2 = 1/2) was adsorbed on a reduced 90/10 Zn/Cu catalyst (pretreatment #3) at 200°C, the behavior of surface species was comparable to other studies with this mixture. Figure 29 shows that formate groups were hydrogenated to methoxy groups, accompanied by the decrease of the hydroxyl group at 3665 cm^{-1}.

A decrease in the temperature of CO hydrogenation to 100°C had the effect of lowering surface reaction rates and stabilizing a reaction intermediate. Adsorption of carbon monoxide and hydrogen (CO/H_2 = 1/2) on a reduced 95/5 Zn/Cu catalyst (pretreatment #3) is shown in Figure 30. Surface carbonate groups gradually decreased as formate groups increased. An adsorbed formaldehyde species (bands at 2935 and 2852 cm^{-1}) formed during an 8-hour period, possibly an intermediate between formate and methoxy species. At 100°C, the carbonyl species had a slightly

Figure 28. Carbon monoxide adsorption on reduced 90/10 Zn/Cu oxide at 200°C

a) reduced surface

b) exposure for 5 minutes

c) exposure for 1 hour

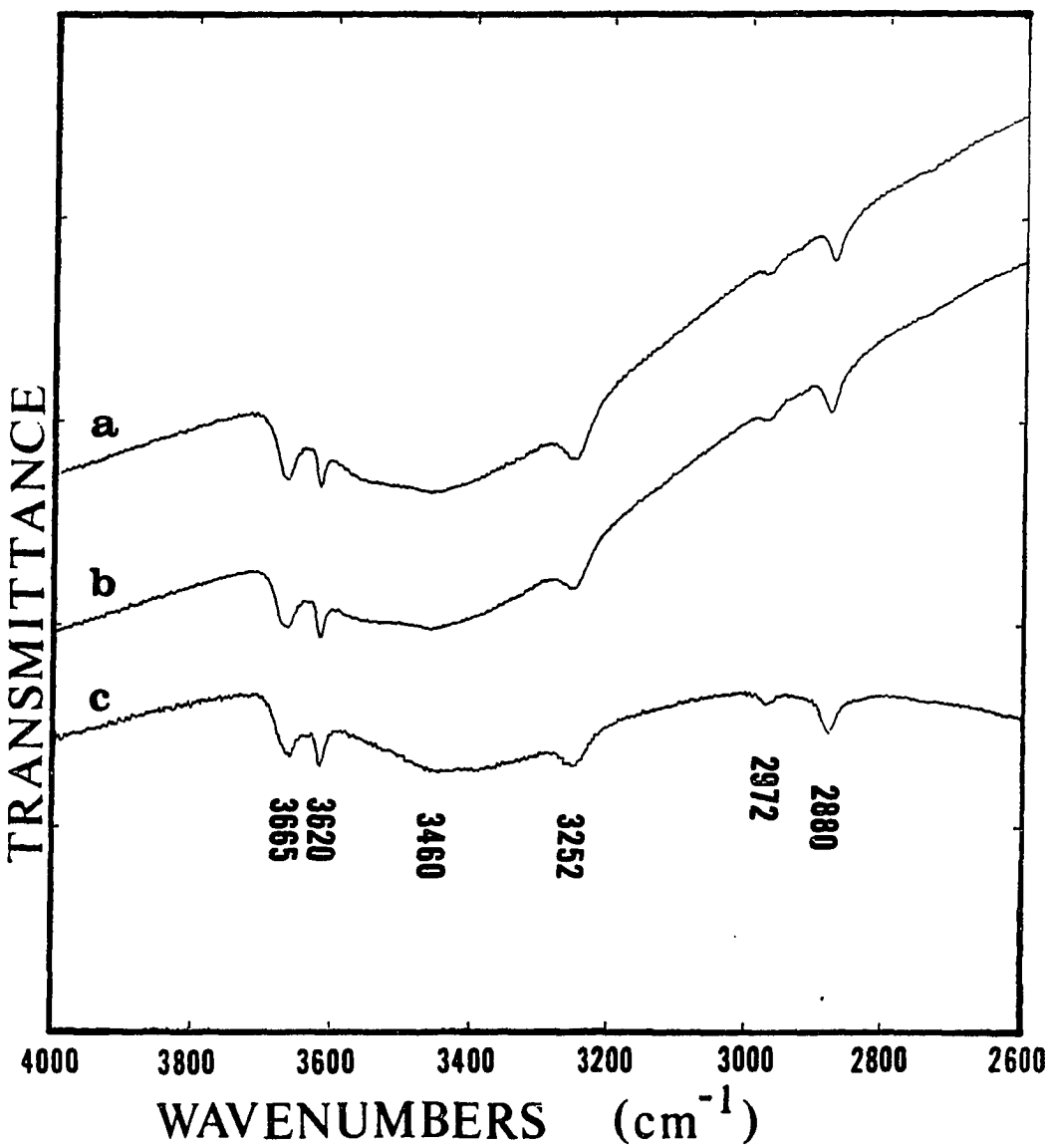
TRANSMITTANCE
a
b
c
3665
3620
3460
3252
2972
2880
4000
3800
3600
3400
3200
3000
2800
2600
WAVENUMBERS (cm-1)

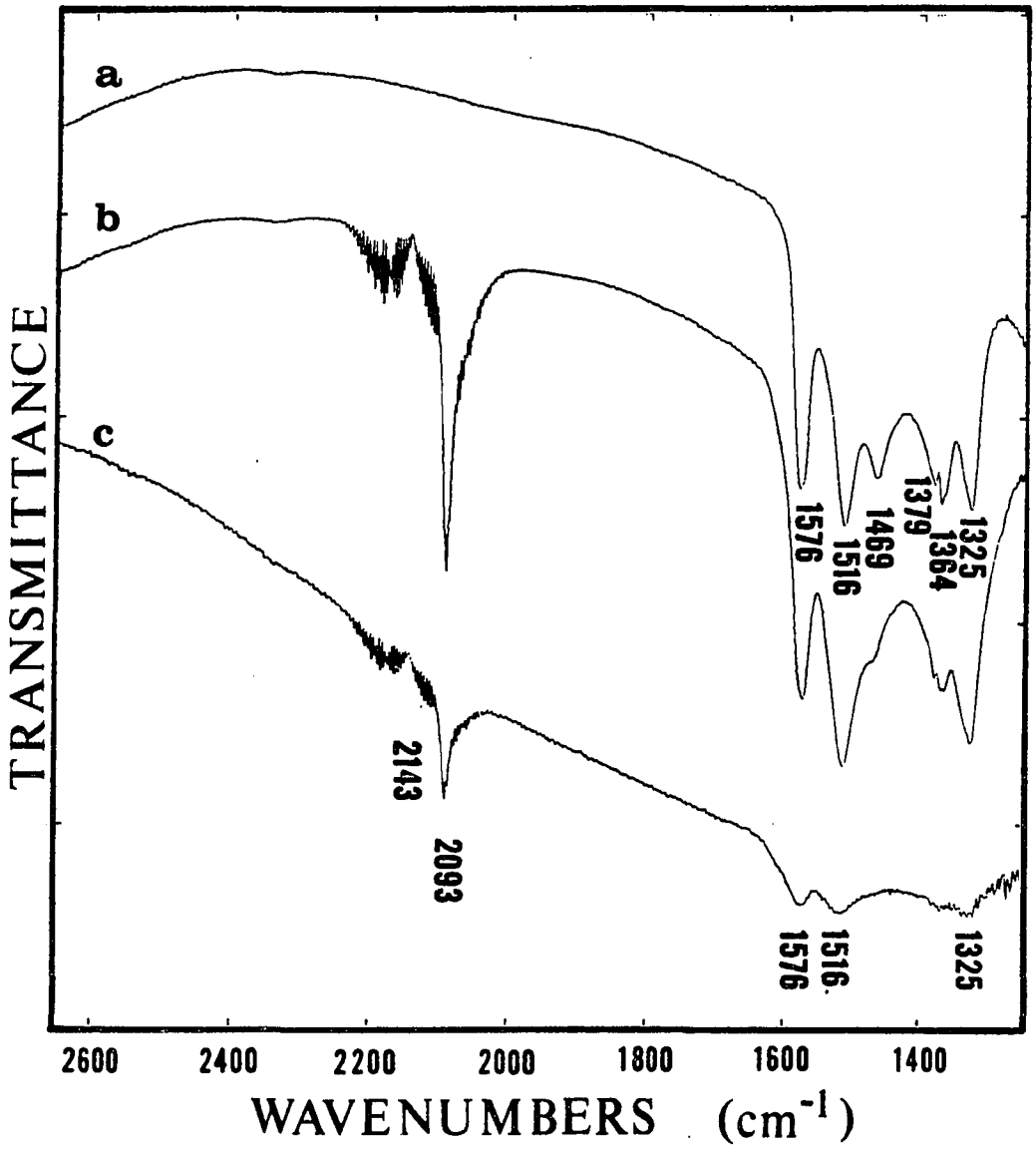

Figure 28. Continued

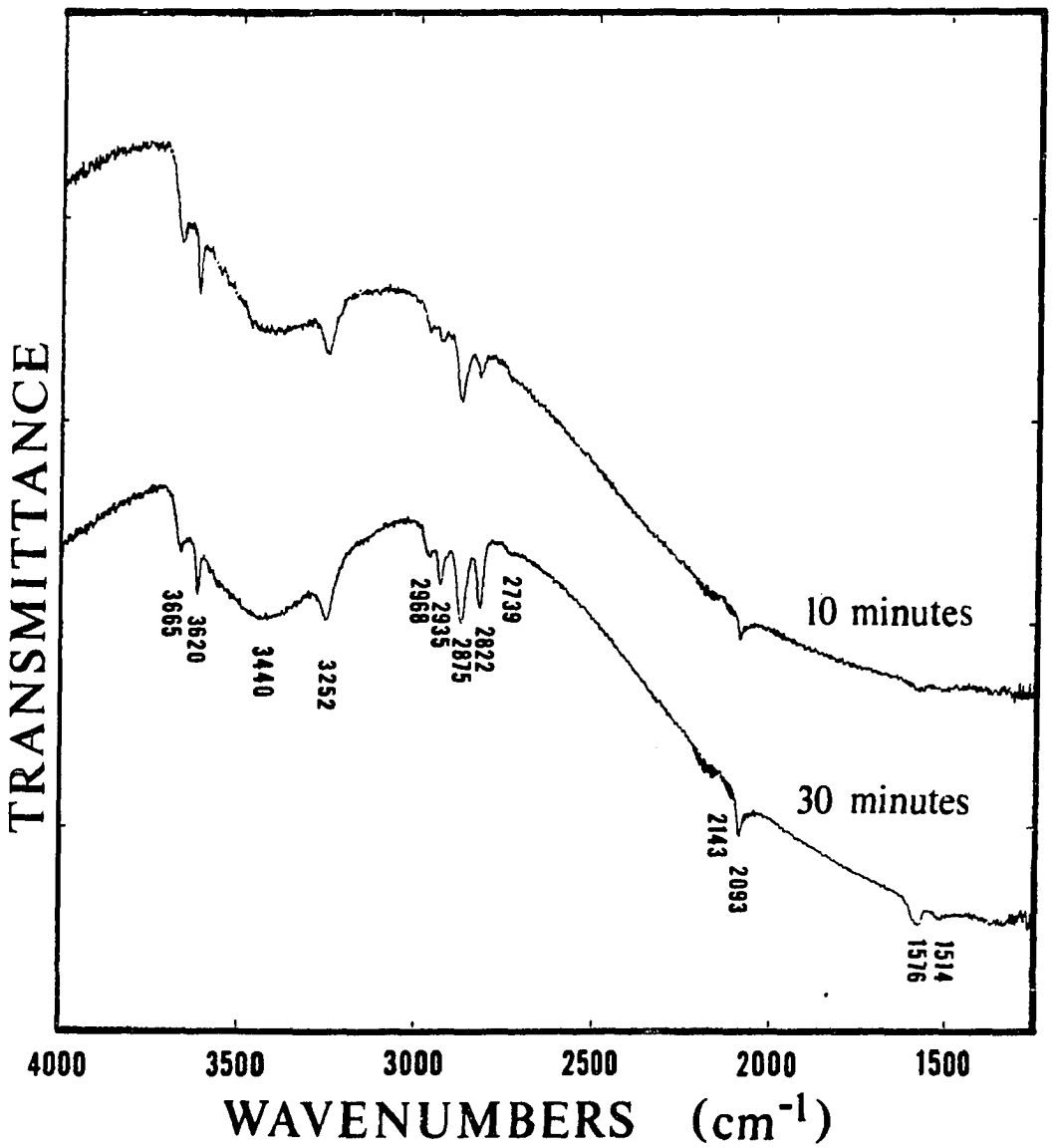

Figure 29. Adsorption of CO-H_2 mixture on reduced 90/10 Zn/Cu oxide at 200°C

Figure 30. Adsorption of CO-H_2 mixture on reduced 95/5 Zn/Cu oxide at 100°C

a) reduced surface

b) exposure for 5 minutes

c) exposure for 8 hours

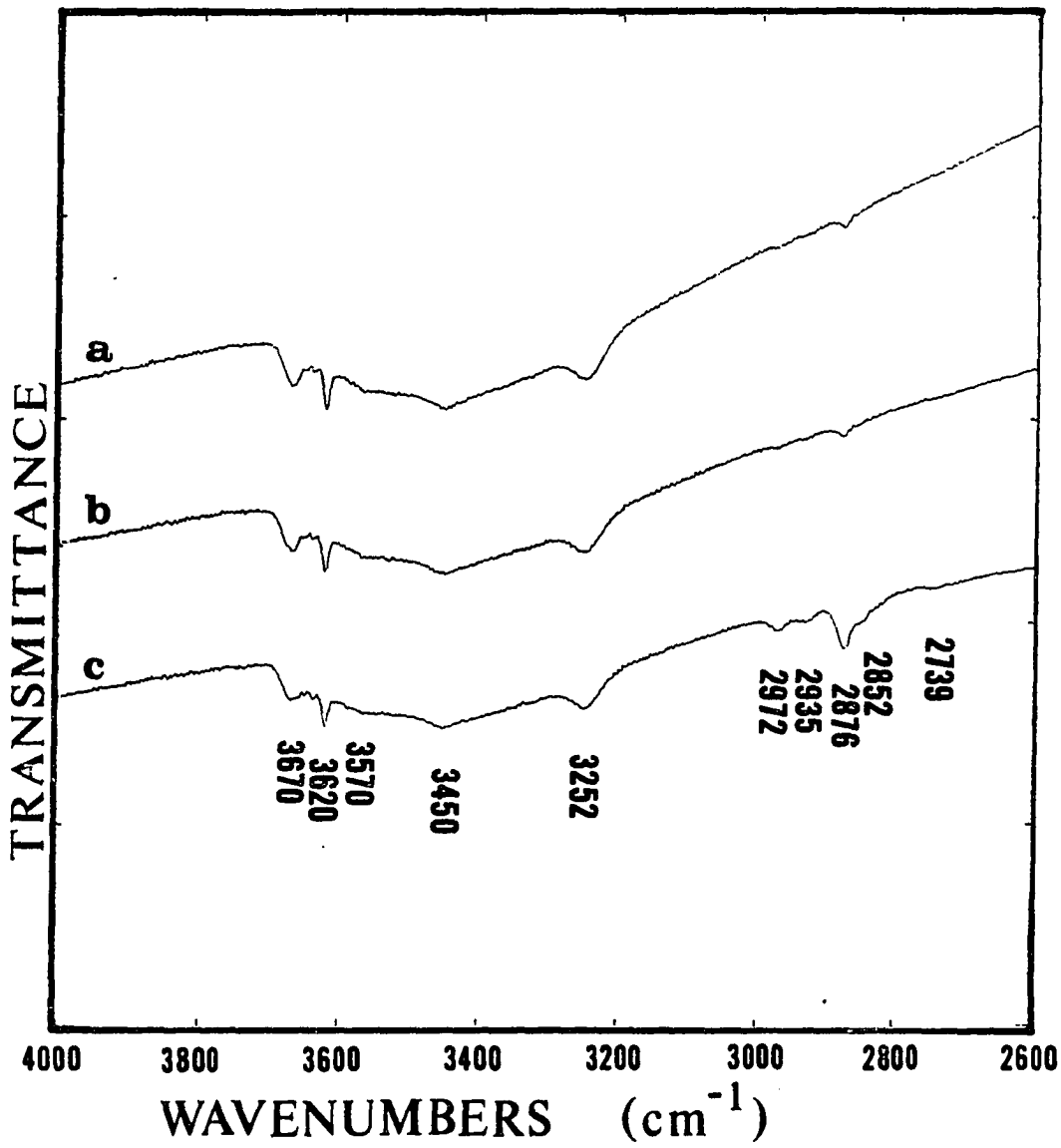
TRANSMITTANCE
a
b
c
3670
3620
3570
3450
3252
2972
2935
2876
2852
2739
4000
3800
3600
3400
3200
3000
2800
2600
WAVENUMBERS (cm-1)

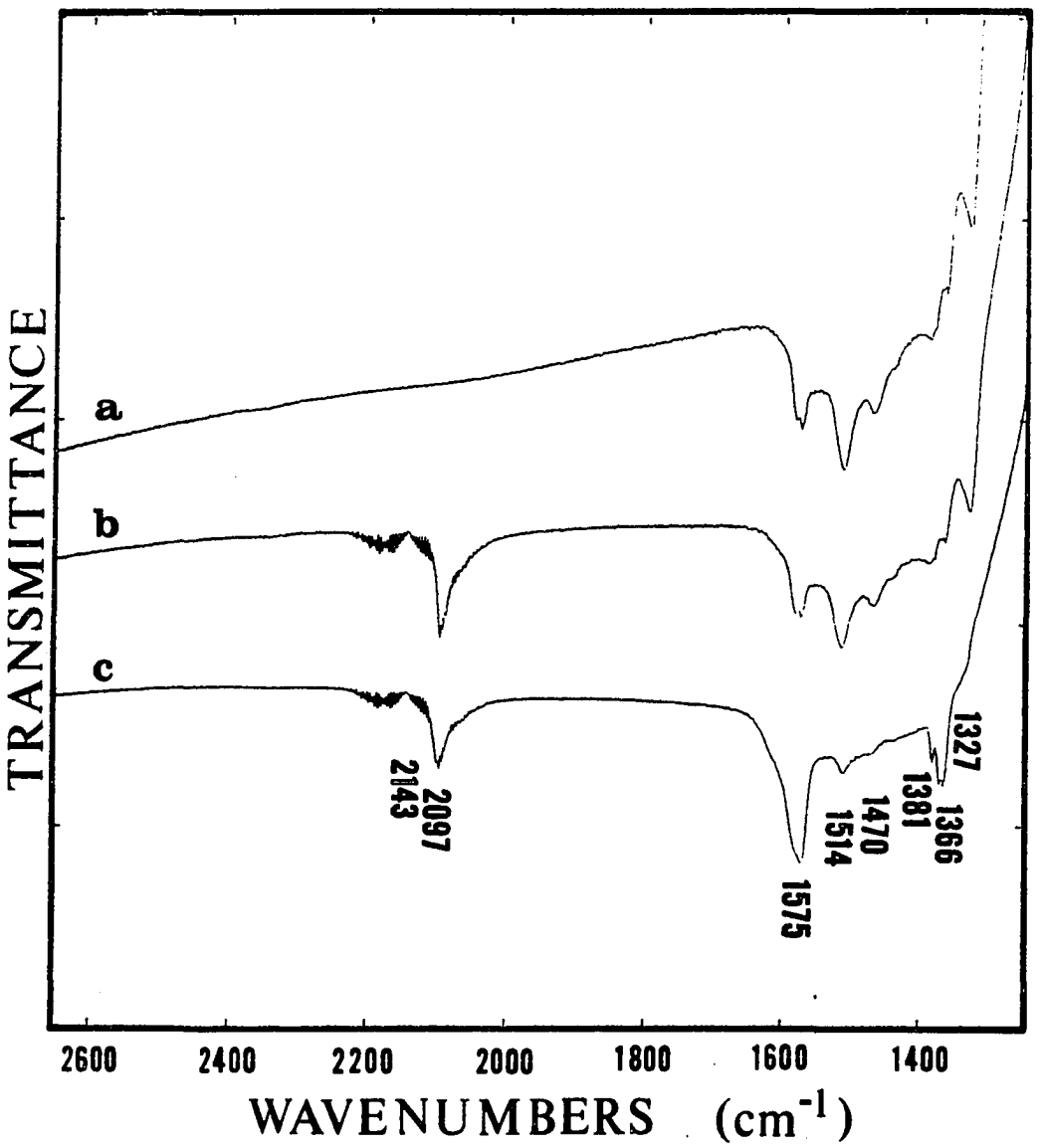

Figure 30. Continued

frequency (band at 2097 cm^{-1}), but the other bands occurred in the same positions found at 200°C.

The activity of a reduced 90/10 Zn/Cu catalyst (pretreatment #3) for the water-gas shift reaction at 200°C and 1 atmosphere was determined for a high CO/H_2O ratio (approximately 100/1). Figure 31 shows that carbonyl species and formate groups were quickly formed without any significant changes in the residual carbonate groups. The water-gas shift reaction occurred at these conditions as indicated by the presence of gaseous carbon dioxide (band at 2350 cm^{-1}) in the spectra. No methoxy groups were formed.

The hydrogenation of carbon dioxide (reverse water-gas shift reaction or methanol synthesis) would be expected to have surface species in common with both reactions. The concurrent adsorption of carbon dioxide and hydrogen (CO_2/H_2 = 1/1) on an oxidized 90/10 Zn/Cu catalyst (pretreatment #1) at 200°C and 1 atmosphere is shown in Figure 32. Formate (bands at 2970, 2872, 2737, 1572, and 1366 cm^{-1}) and adsorbed formaldehyde (bands at 2930, 2851, and 1620 cm^{-1}) groups developed quickly. The surface carbonate species diminished and the catalyst was reduced (development of 3252 cm^{-1} band). After 4 hours, the amount of methoxy groups formed was negligible. Substitution of the gas phase with pure hydrogen did not produce methoxy groups after an hour of hydrogen exposure.

Since formate groups were hydrogenated to methoxy groups in the presence of carbon monoxide but not in the presence of carbon dioxide, it appeared that the carbonyl species might enhance formate hydrogenation. To test this possibility, carbon monoxide was adsorbed on a

Figure 31. Adsorption of CO-H_2O mixture on reduced 90/10 Zn/Cu oxide at 200°C

a) reduced surface

b) exposure for 30 minutes

c) exposure for 4 hours

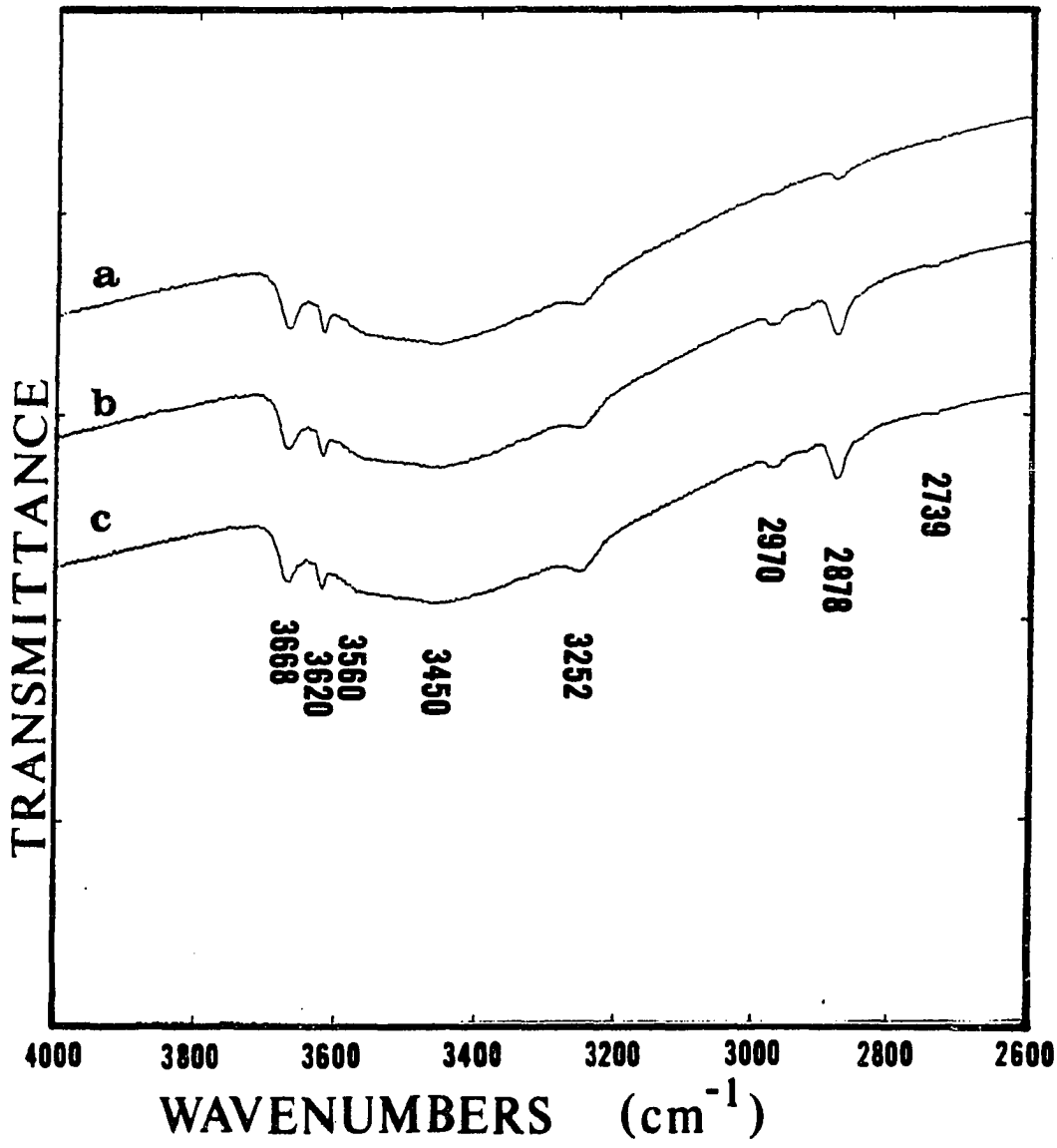
a
b
c
TRANSMITTANCE
3668
3620
3560
3450
3252
2970
2878
2739
4000
3800
3600
3400
3200
3000
2800
2600
WAVENUMBERS (cm-1)

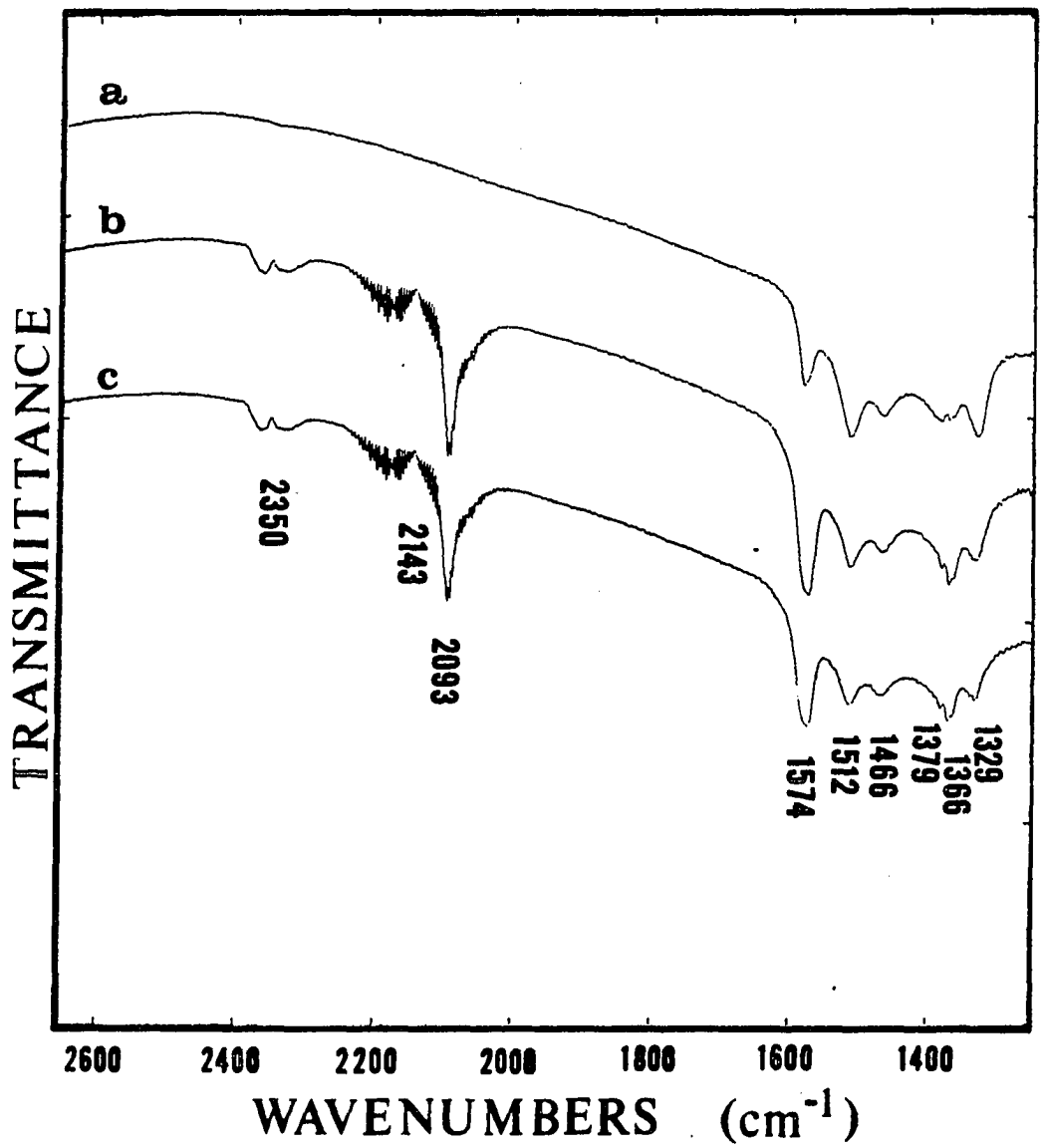

Figure 31. Continued

Figure 32. Adsorption of CO_2-H_2 mixture on 90/10 Zn/Cu oxide at 200°C

a) oxidized surface

b) exposure for 5 minutes

c) exposure for 4 hours

d) exposure to hydrogen for 1 hour

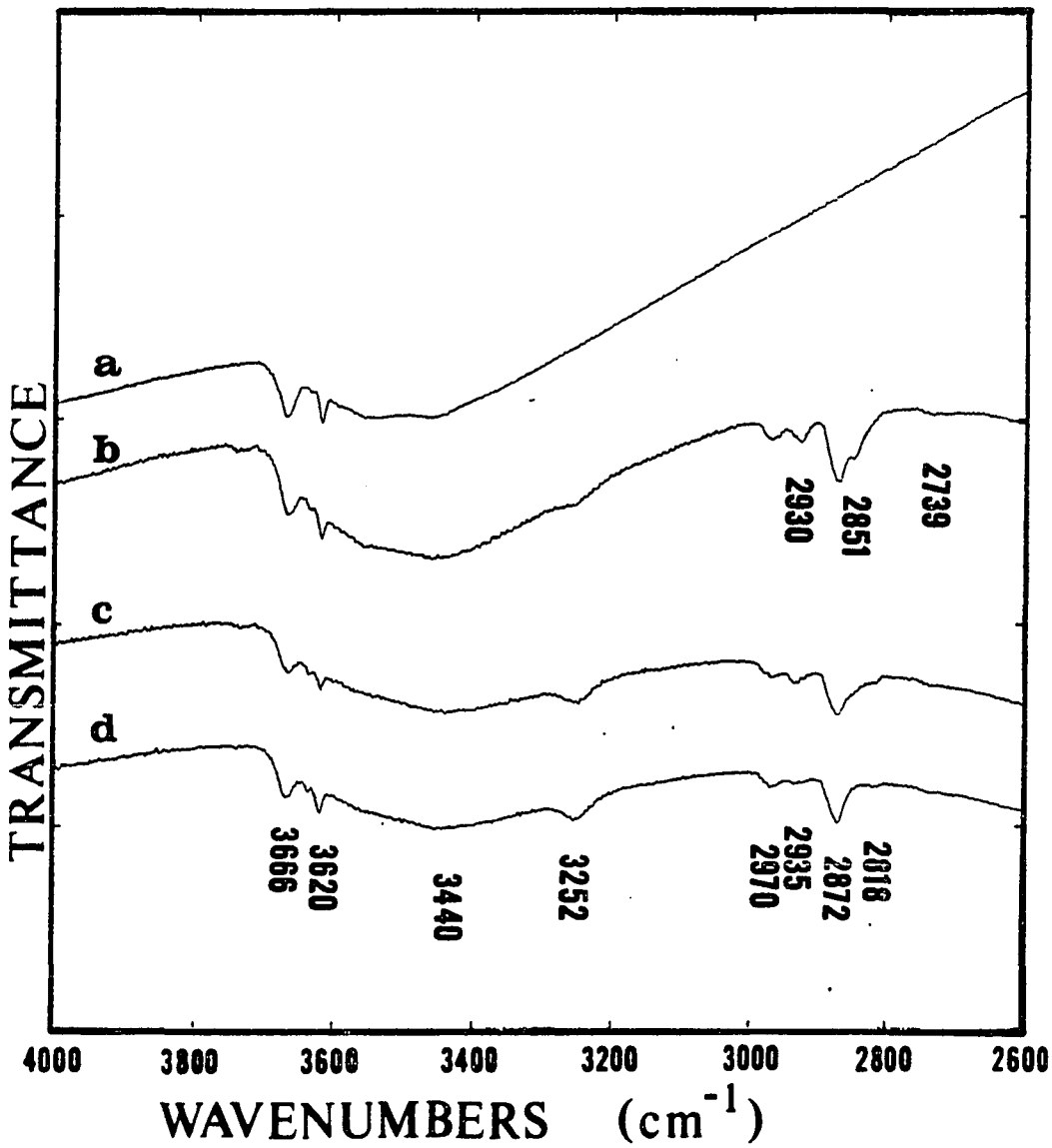
TRANSMITTANCE
a
b
c
d
2930
2851
2739
3666
3620
3440
3252
2970
2935
2872
2818
4000
3800
3600
3400
3200
3000
2800
2600
WAVENUMBERS (cm-1)

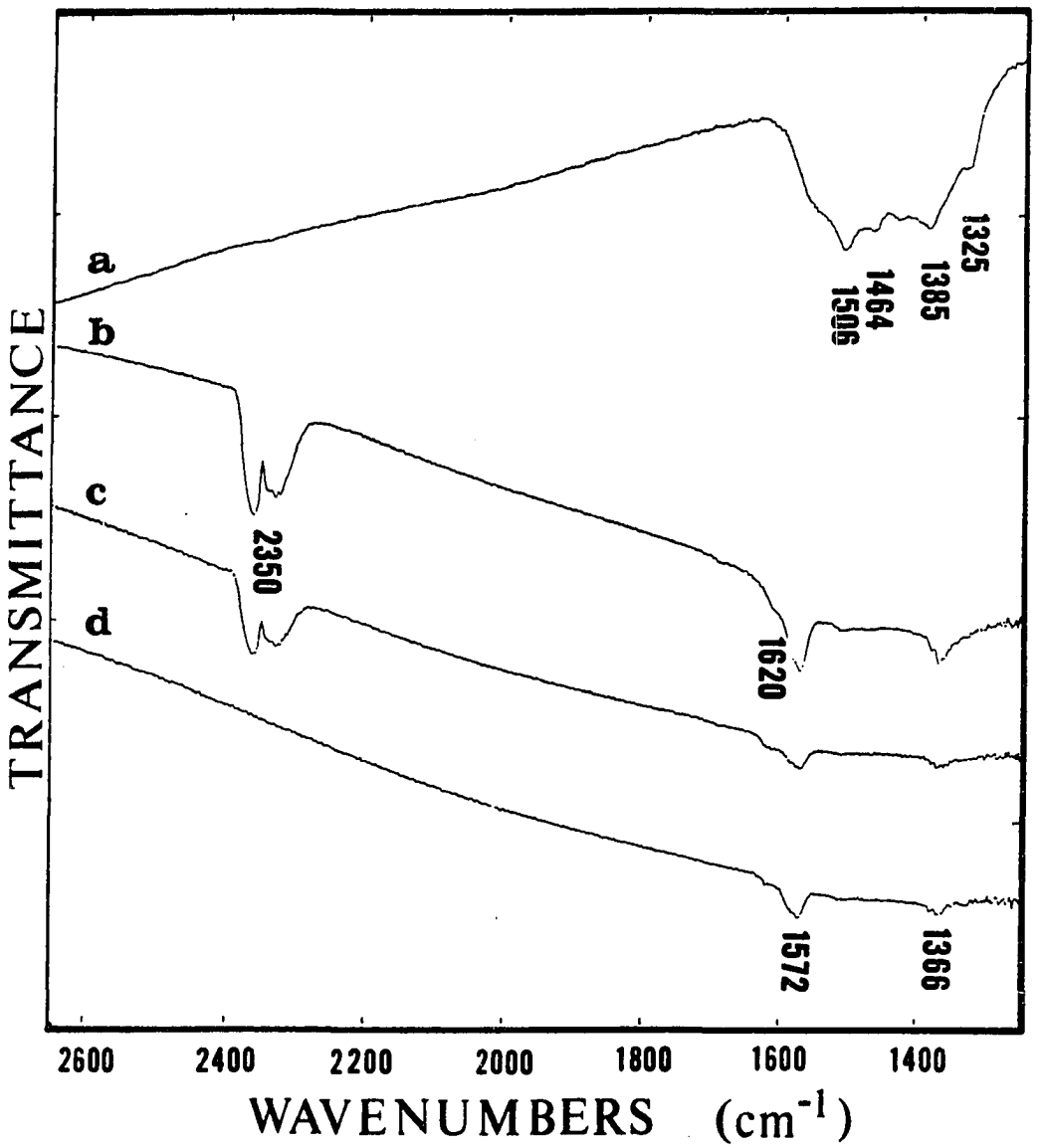

Figure 32. Continued

reduced 95/5 Zn/Cu catalyst (pretreatment #3) at 200°C and 1 atmosphere followed by carbon dioxide adsorption (Figure 33). The carbonyl species was weakly adsorbed, desorbing when the gaseous CO was flushed from the cell with nitrogen. The subsequent adsorption of carbon dioxide caused partial oxidation of the catalyst (a transmission increase and the 3252 cm^{-1} band decrease) and decreased formate groups, while the carbonate groups were increased. The addition of hydrogen to the carbon dioxide decreased carbonate groups and increased formate groups without any development of methoxy groups.

The adsorption of formic acid (88% HCOOH, 12% H_2O) on a reduced 95/5 Zn/Cu catalyst (pretreatment #3) at 165°C and 1 atmosphere is shown in Figure 34. Exposure of the acid to the catalyst was brief (5 minutes) because the acid severely decreased the transmittance through the sample. Spectra were taken in nitrogen after the transmission had increased to several percentage transmittance. Formic acid adsorption produced a formate species (bands at 2968, 2873, 2736, 1572, 1380, and 1366 cm^{-1}), methoxy groups (bands at 2935 and 2825 cm^{-1}), and a new hydroxyl group (band at 3524 cm^{-1}). This hydroxyl species disappeared as methoxy groups increased, and formate decomposition was indicated by the presence of carbon dioxide in the isolated cell. Methoxy groups formed without any gaseous hydrogen present because the cell was flushed with nitrogen after the initial exposure. Since it was possible that some hydrogen might have existed in the micropores, this experiment was repeated using a 50% nitrogen-50% hydrogen gas mixture. The development of methoxy groups occurred at essentially the same rate as that in nitrogen, indicating that gaseous hydrogen was not

Figure 33. CO_2 hydrogenation preceded by CO adsorption

a) exposure to CO

b) N_2 purge for 10 minutes

c) exposure to CO_2 and N_2

d) exposure to CO_2, H_2, and N_2

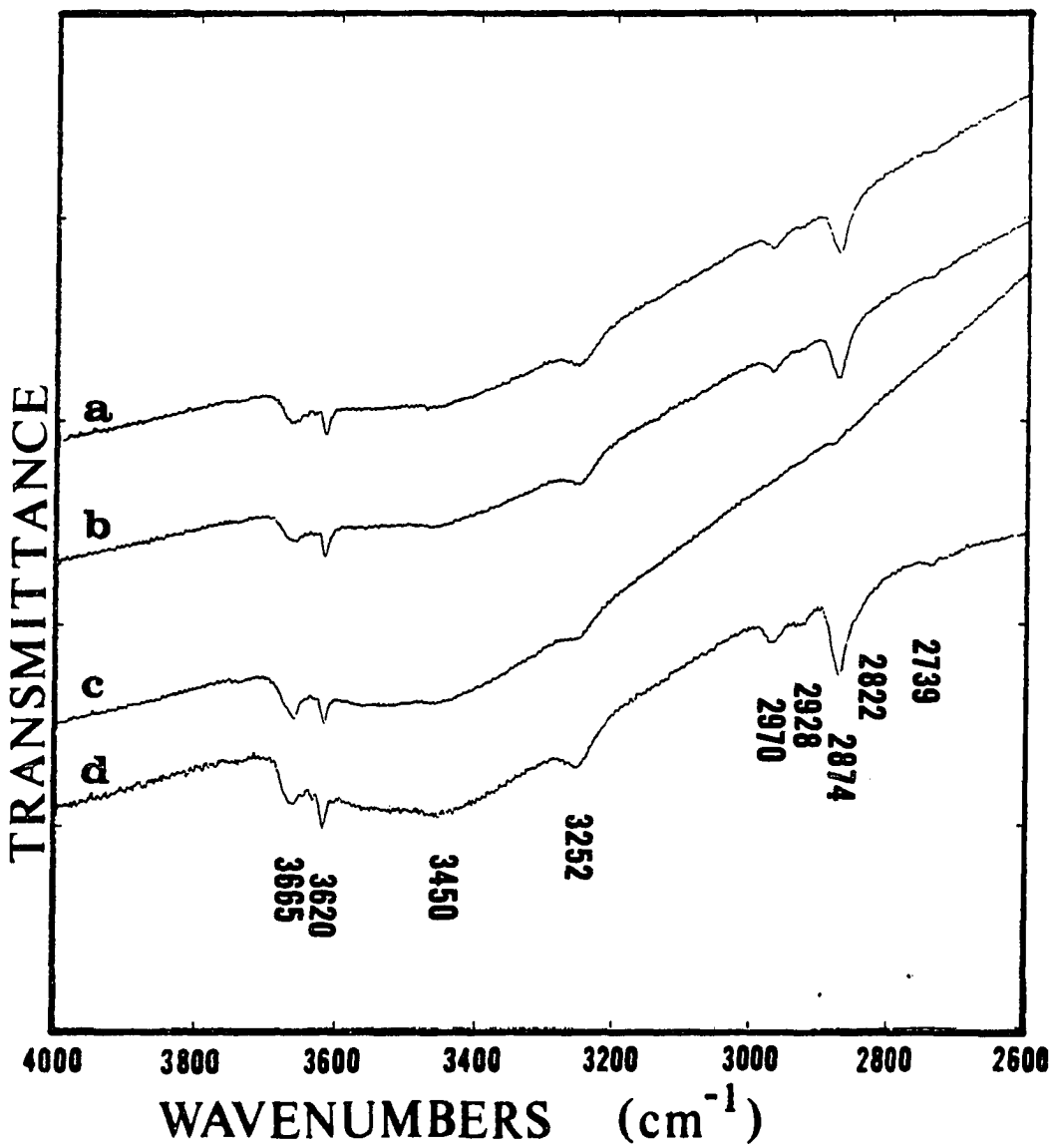
TRANSMITTANCE
a
b
c
d
3665
3620
3450
3252
2970
2928
2874
2822
2739
4000
3800
3600
3400
3200
3000
2800
2600
WAVENUMBERS (cm-1)

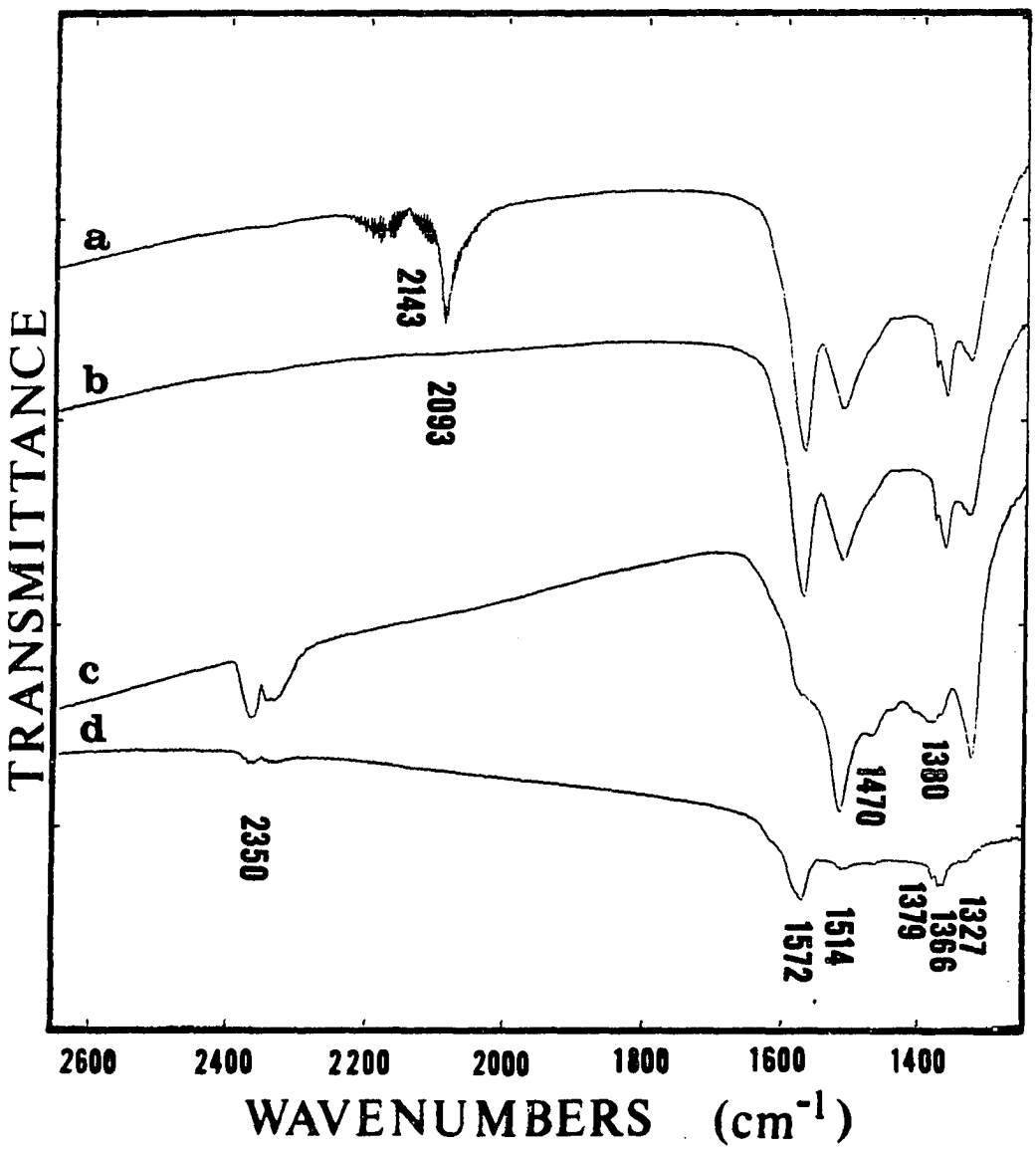

Figure 33. Continued

Figure 34. Adsorption of formic acid on 95/5 Zn/Cu oxide at 165°C

a) reduced surface

b) 30 minutes after exposure

c) 4 hours after exposure

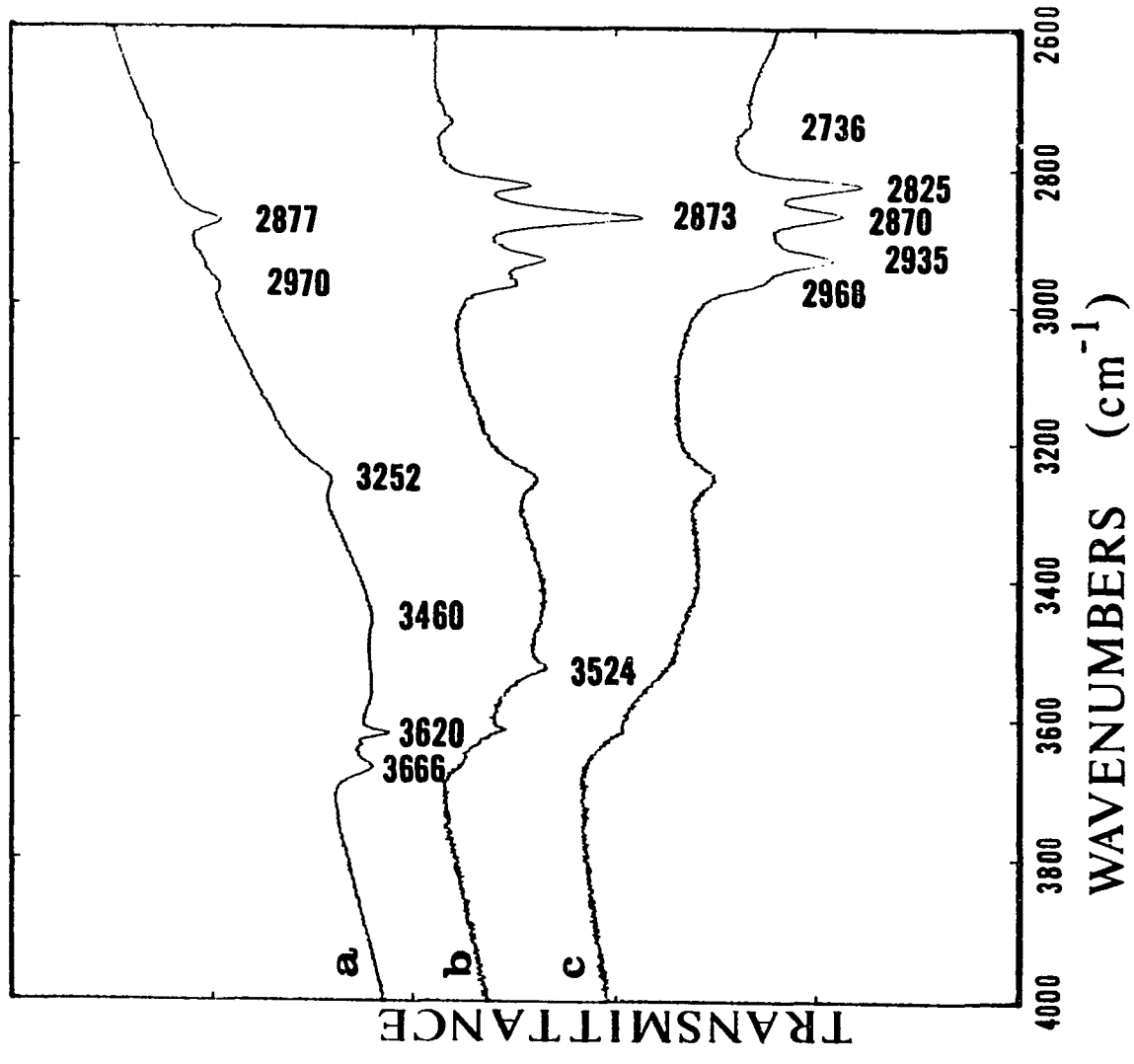
2736
2825
2877
2873
2870
2935
2970
2968
3252
3460
3524
3620
3666
a
b
c
TRANSMITTANCE
4000
3800
3600
3400
3200
3000
2800
2600
WAVENUMBERS (cm-1)

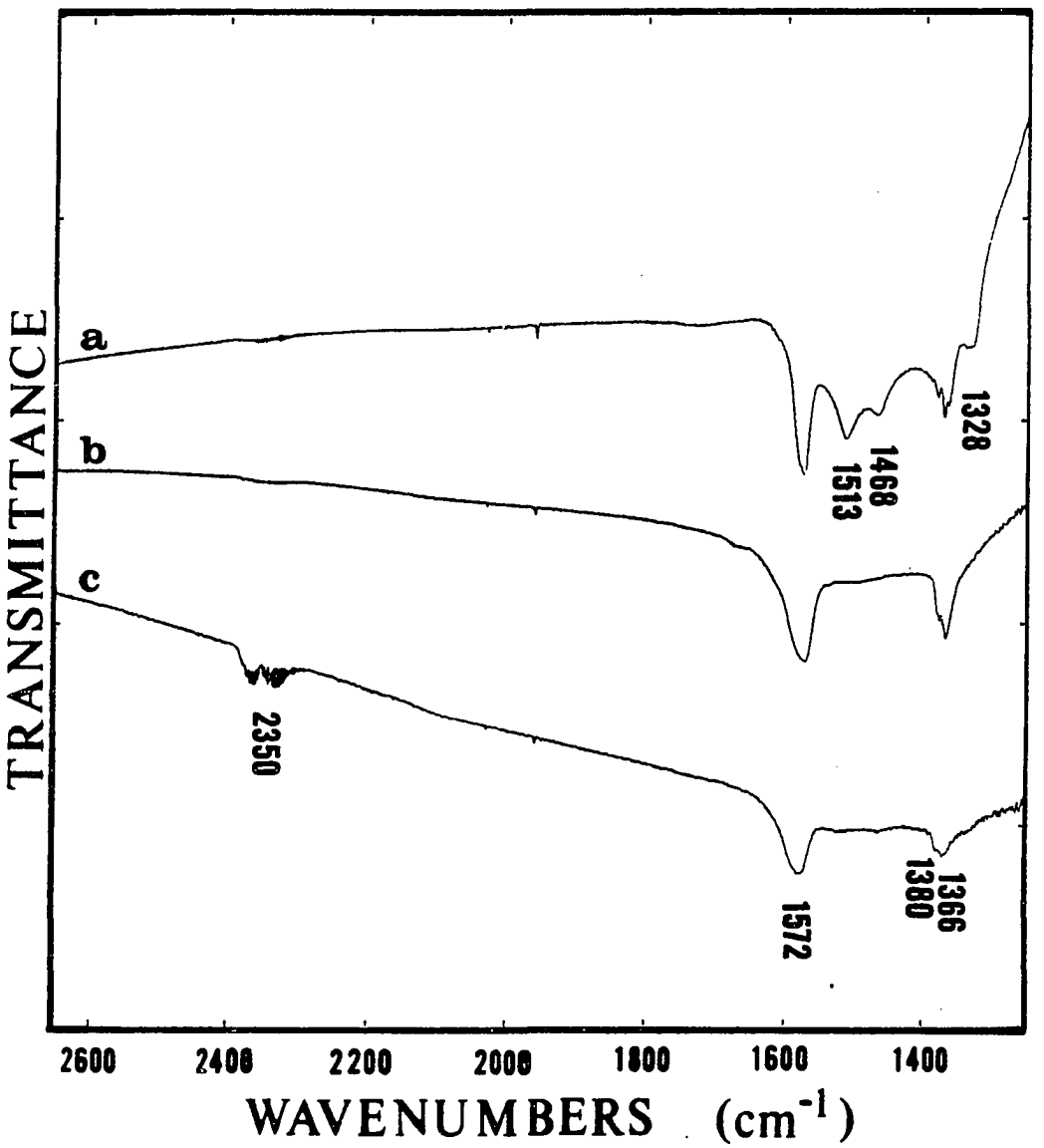

Figure 34. Continued

directly involved in methoxy formation. The development of methoxy groups led to the disappearance of the isolated hydroxyl groups at 3666 and 3620 cm^{-1}. The C-H stretching frequency of the formate species was shifted from 2877 to 2870 cm^{-1} as the amount of methoxy groups increased on the surface; the hydroxyl at 3620 cm^{-1} shifted to 3613 cm^{-1} as the band decreased.

Formaldehyde adsorption on a reduced 95/5 Zn/Cu catalyst (pretreatment #3) at 200°C and 1 atmosphere is shown in Figure 35. Formaldehyde vapor was briefly exposed to the surface (5 minutes) and the spectra were taken in nitrogen. Initially, formate (bands at 2970, 2875, 2739, 1578, 1379, and 1364 cm^{-1}) and methoxy (bands at 2934 and 2820 cm^{-1}) groups dominated the surface without any evidence of adsorbed formaldehyde. Both the methoxy and formate groups gradually decomposed, restoring the isolated hydroxyl groups (bands at 3668 and 3620 cm^{-1}) and increasing the amount of surface carbonates.

The surface of a reduced 95/5 Zn/Cu catalyst (pretreatment #3) was exposed to formaldehyde vapor at 100°C (Figure 36) to stabilize the surface formaldehyde groups. An adsorbed formaldehyde species (bands at 2935, 2860, 2739, 1700, and 1609 cm^{-1}) and formate groups (bands at 2976, 2880, 2739, 1578, 1381, and 1366 cm^{-1}) were formed, accompanied by the disappearance of the isolated hydroxyl groups (bands at 3670 and 3620 cm^{-1}). Because formate groups were known not to displace the isolated hydroxyls, it can be safely assumed that adsorbed formaldehyde occupied the same sites as isolated hydroxyls.

The adsorption of methanol on a reduced 95/5 Zn/Cu catalyst (pretreatment #3) at 190°C and 1 atmosphere is shown in Figure 37. Methanol

Figure 35. Adsorption of formaldehyde on 95/5 Zn/Cu oxide at 200°C

a) reduced surface

b) 5 minutes after exposure

c) 20 minutes after exposure

d) 1 hour after exposure

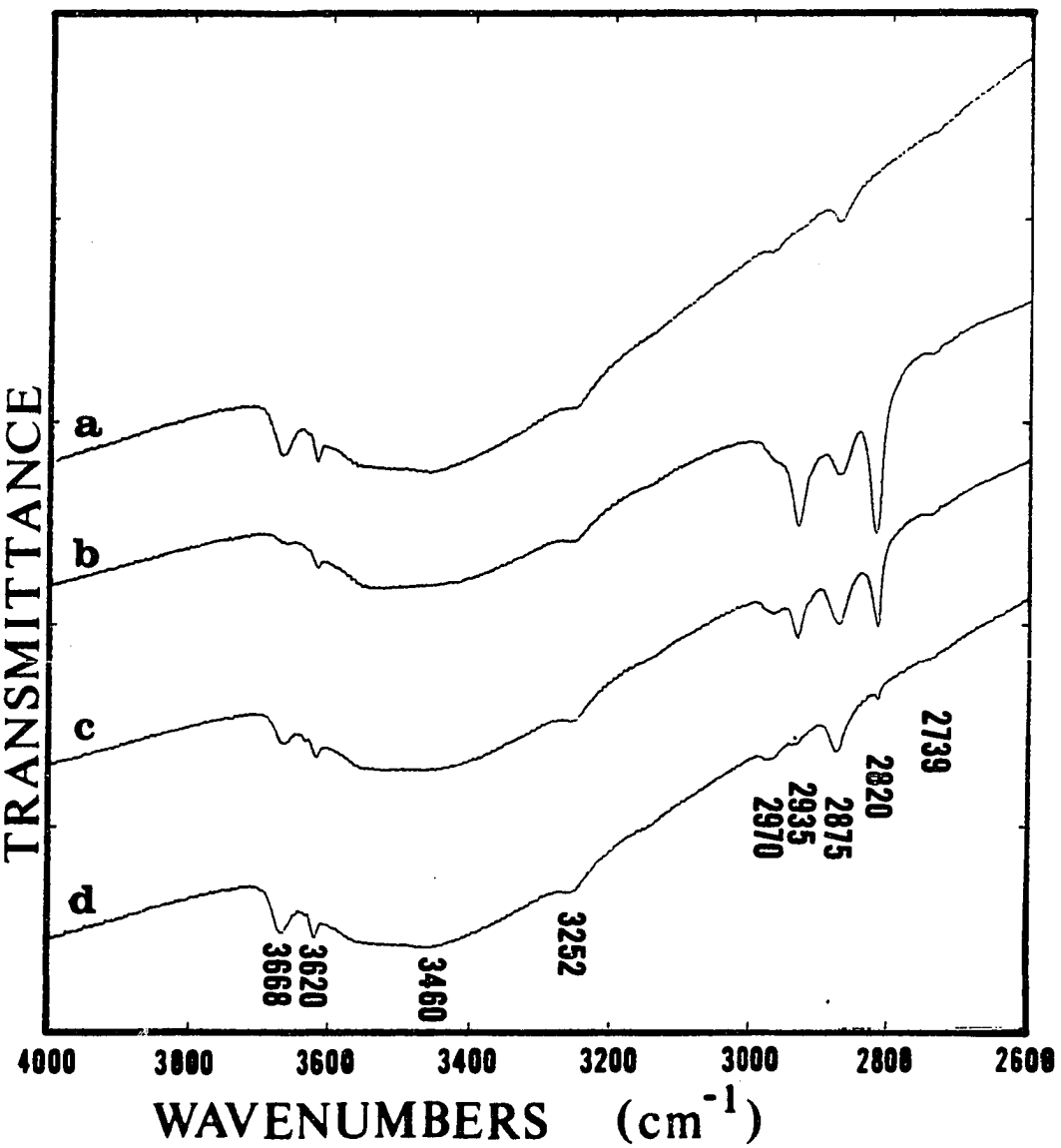
TRANSMITTANCE
a
b
c
d
3668
3620
3460
3252
2970
2935
2875
2820
2739
4000
3800
3600
3400
3200
3000
2800
2600
WAVENUMBERS (cm-1)

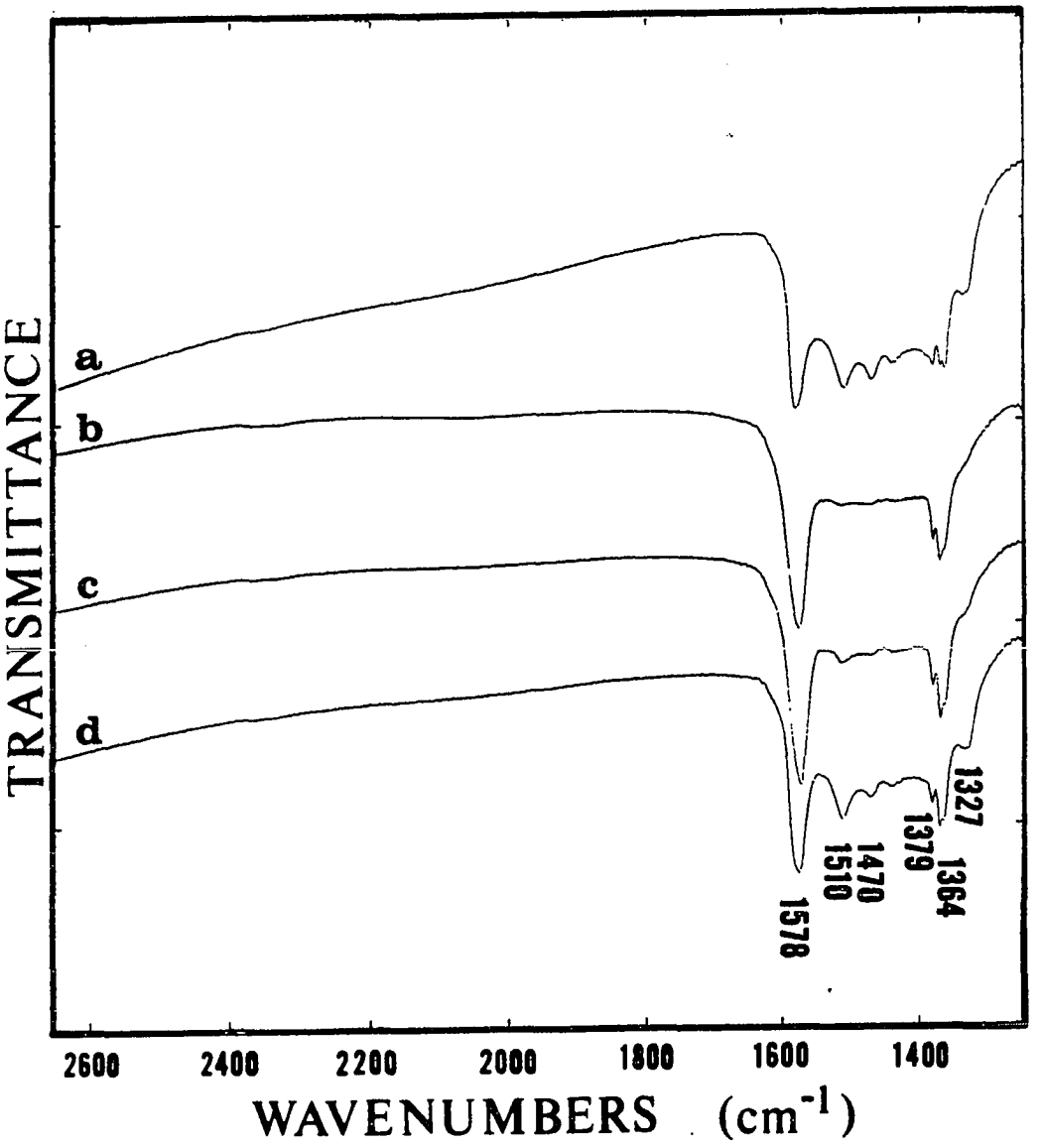

Figure 35. Continued

Figure 36. Adsorption of formaldehyde on 95/5 Zn/Cu oxide at 100°C

a) reduced surface

b) 30 minutes after exposure

c) after second H_2CO exposure

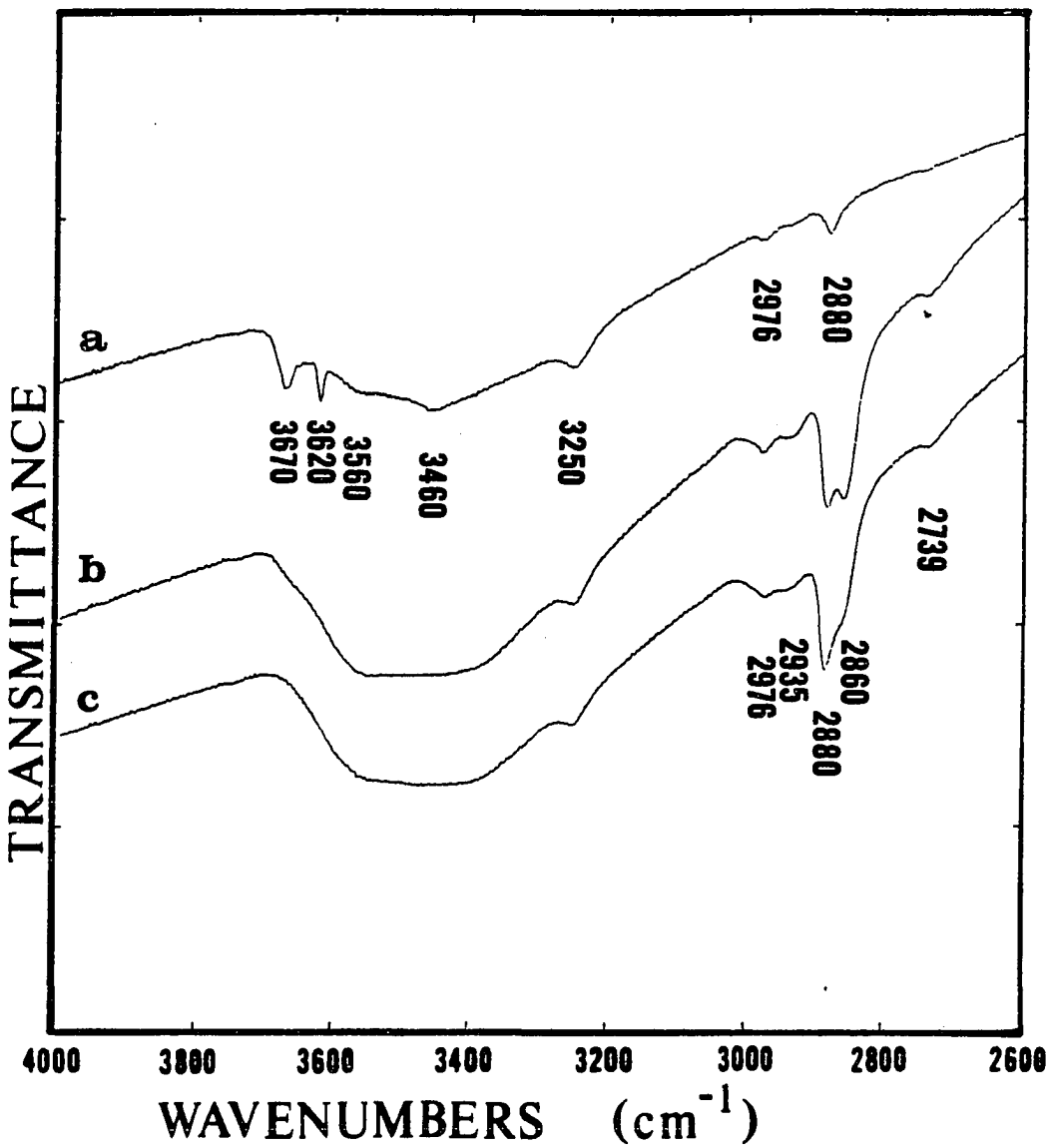
TRANSMITTANCE
a
b
c
3670
3620
3560
3460
3250
2976
2880
2739
2935
2860
4000
3800
3600
3400
3200
3000
2800
2600
WAVENUMBERS (cm-1)

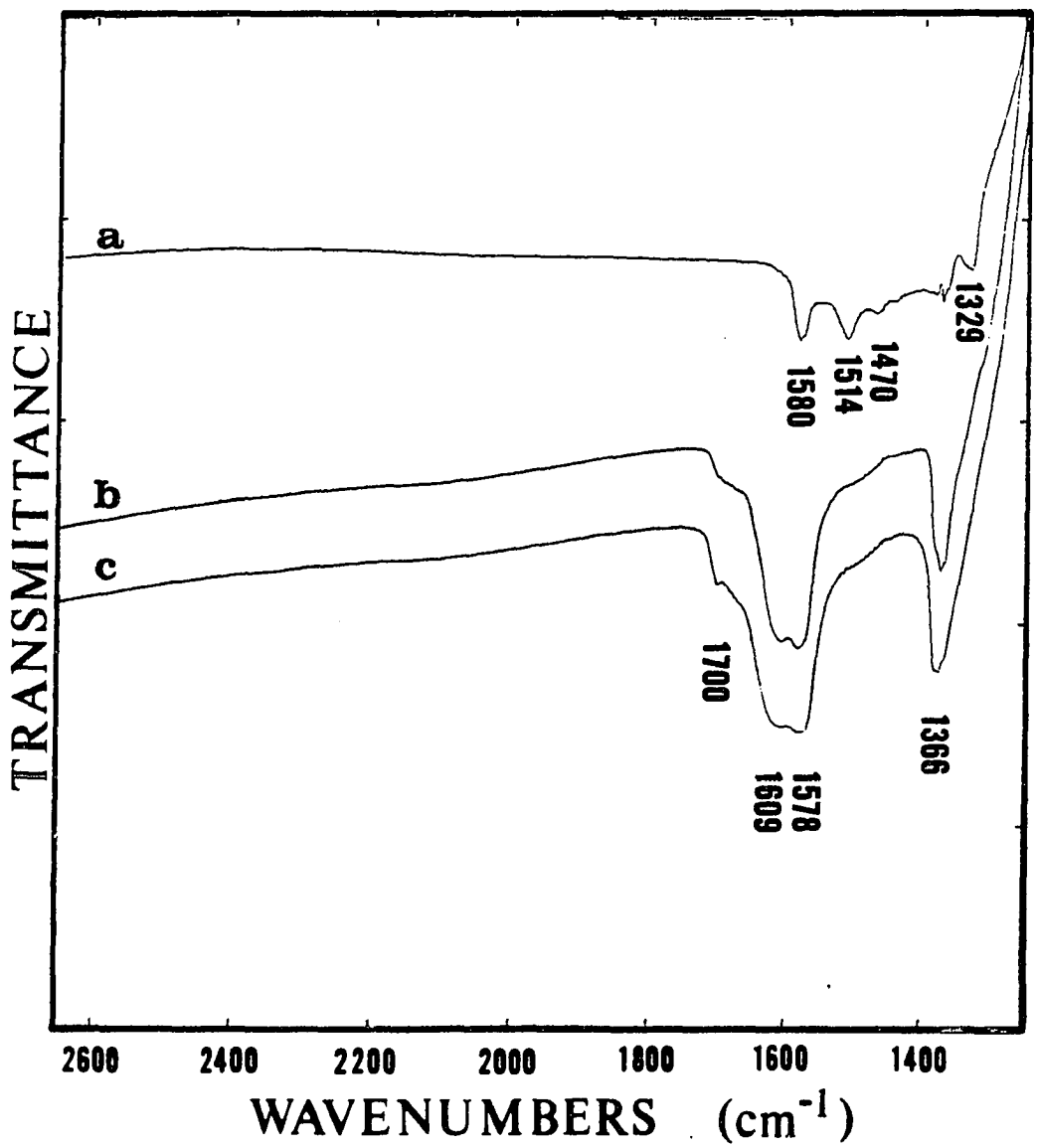

Figure 36. Continued

Figure 37. Adsorption of methanol on reduced 95/5 Zn/Cu oxide at 190°C

a) during exposure

b) 10 minutes after exposure

c) 4 hours after exposure

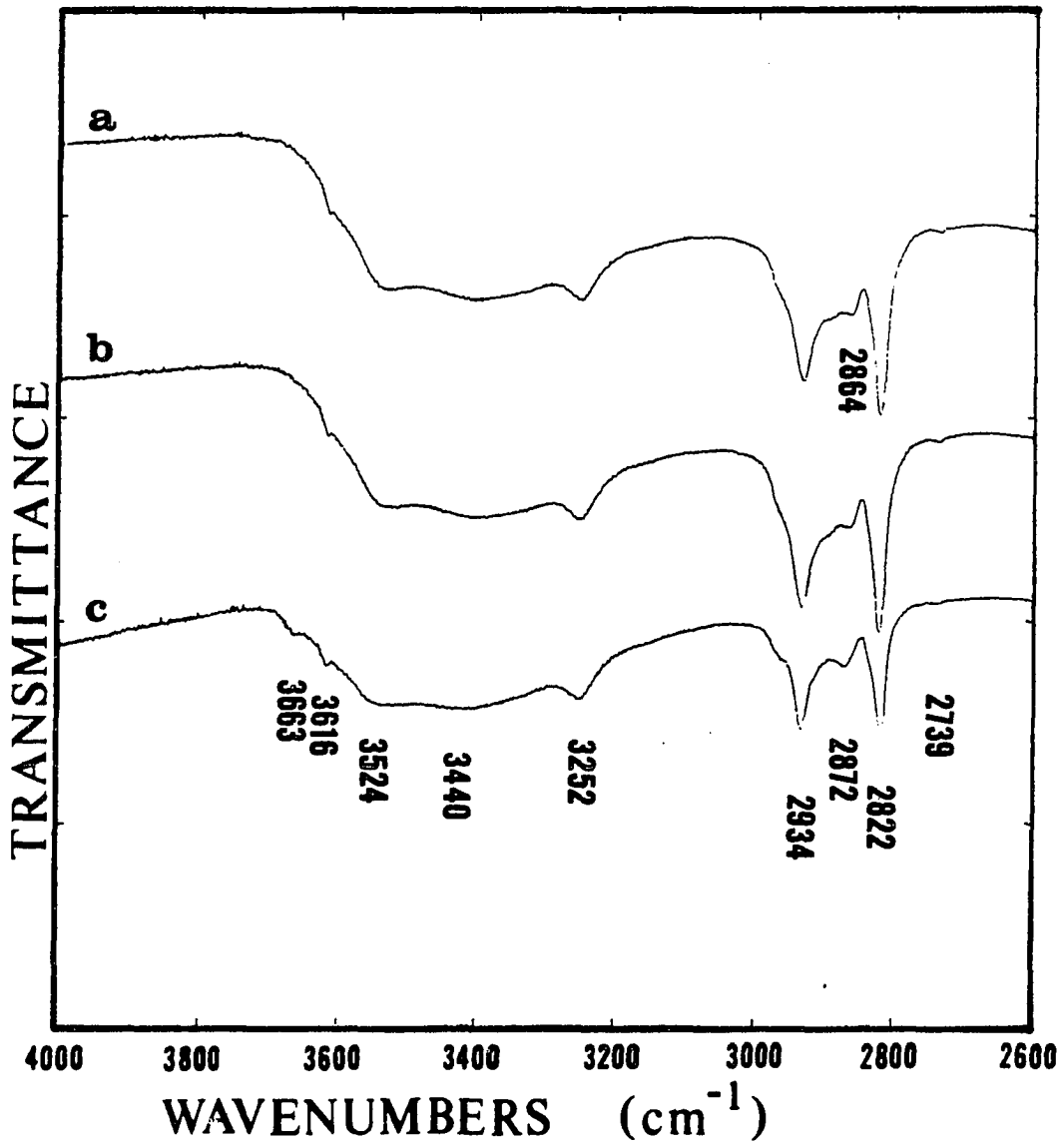
a
b
c
2864
3663
3616
3524
3440
3252
2934
2872
2822
2739
TRANSMITTANCE
4000
3800
3600
3400
3200
3000
2800
2600
WAVENUMBERS (cm-1)

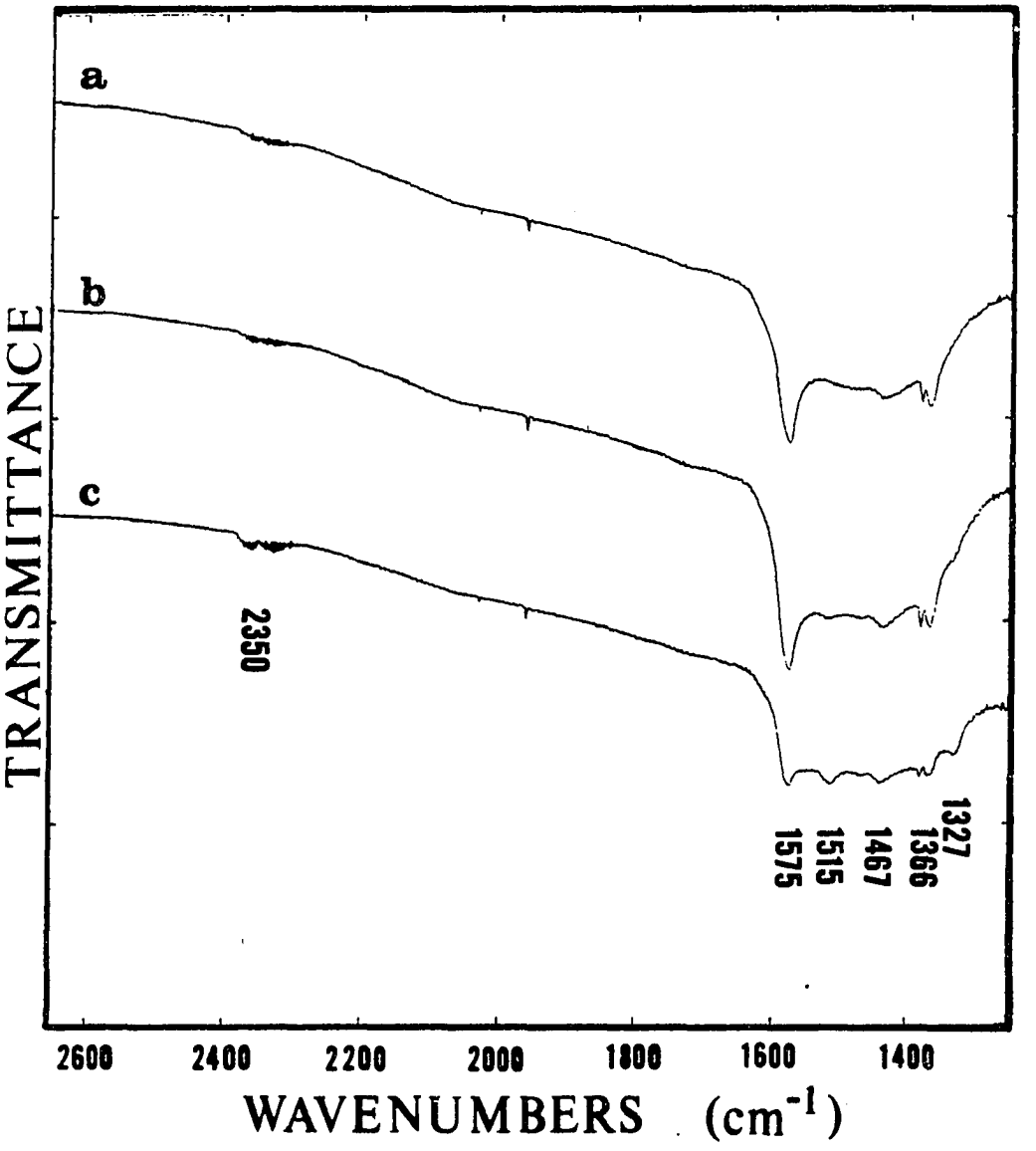

Figure 37. Continued

adsorption produced methoxy groups (bands at 2934 and 2822 cm^{-1}) and a new hydroxyl group at 3524 cm^{-1} while displacing the isolated hydroxyls (bands at 3663 and 3616 cm^{-1}). The slow decomposition of methoxy groups began to restore the isolated hydroxyl groups (bands at 3663 and 3616 cm^{-1}) while formate decomposition increased the amount of surface carbonates and produced some gaseous carbon dioxide.

Because the formation of a methoxy species from methanol would involve the dissociation of the hydroxyl hydrogen, a deuterated methanol (CH_3OD) was adsorbed on a reduced 90/10 Zn/Cu catalyst (pretreatment #3) at 130°C and 1 atmosphere to establish the adsorption sites of the dissociated hydrogen. The adsorption temperature of 130°C was used to inhibit methoxy decomposition which would increase isotopic mixing between adsorbed hydrogen and deuterium species. Figure 38 shows that methanol-d adsorption formed methoxy groups (bands at 2935 and 2824 cm^{-1}) and a new OD group (band at 2613 cm^{-1}). The residual hydroxyl groups (bands at 3670, 3620, and 3450 cm^{-1}) were displaced or shifted to OD groups whereas the hydroxyl group at 3252 cm^{-1} remained unchanged. No exchange was observed between OD groups and methoxy groups, and only a slight exchange occurred between OD groups and the formate species as indicated by the small band at 2152 cm^{-1} (the C-D stretch of deuterated formate).

The adsorption of CD_3OD on a reduced 90/10 Zn/Cu catalyst (pretreatment #3) at 130°C and 1 atmosphere is shown in Figure 39. These spectra were complex and harder to interpret because the initial surface had formate groups. Methanol-d_4 adsorption formed deuterated methoxy groups (bands at 2222, 2201, 2140, and 2058 cm^{-1}) and the new OD group (band at 2619 cm^{-1}). The hydroxyls except the band at 3252 cm^{-1}

Figure 38. Adsorption of CH_3OD on 90/10 Zn/Cu oxide at 130°C

a) reduced surface

b) exposure for 10 minutes

c) exposure for 1 hour

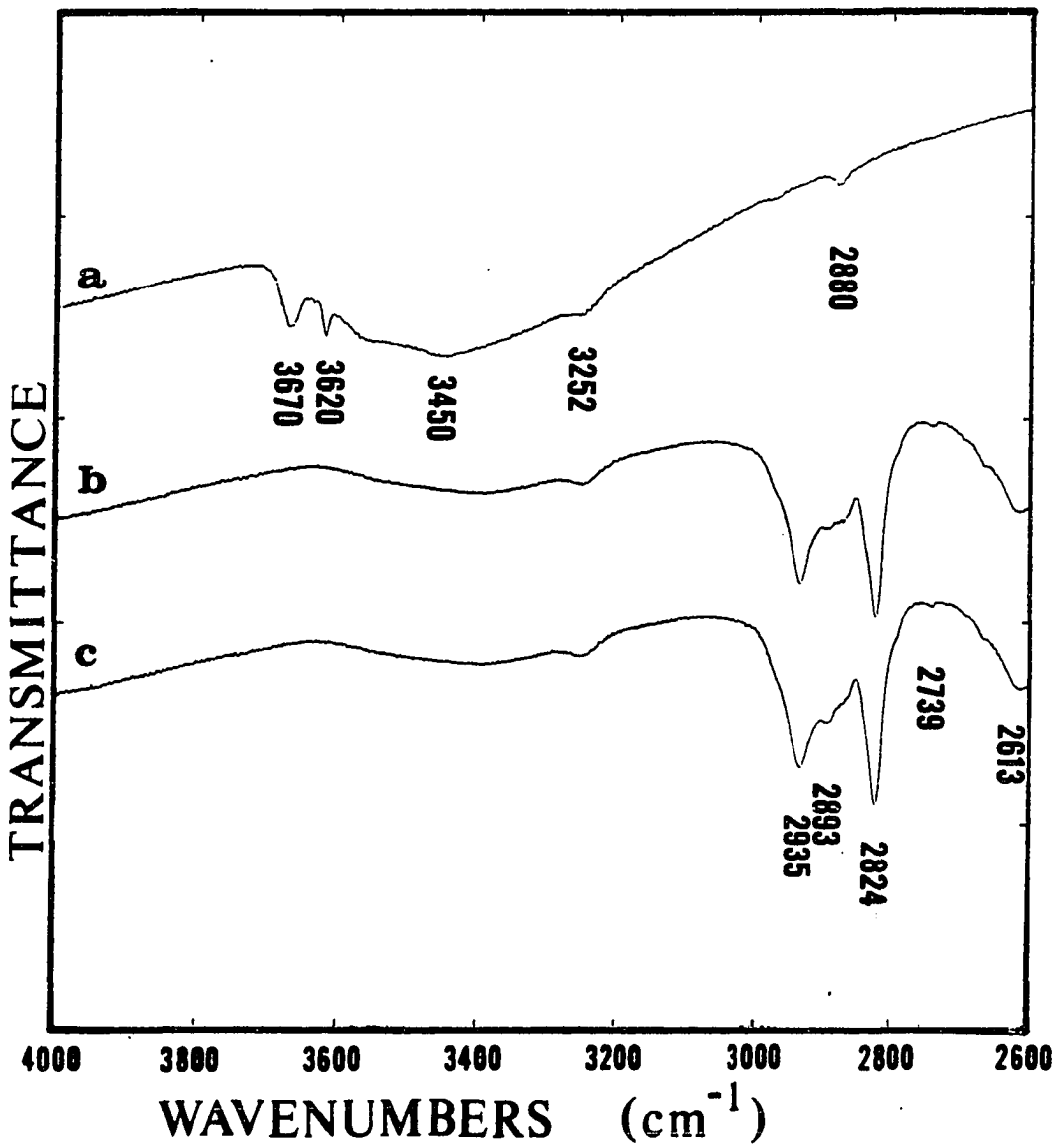
a
b
c
3670
3620
3450
3252
2880
2935
2893
2824
2739
2613
TRANSMITTANCE
4000
3800
3600
3400
3200
3000
2800
2600
WAVENUMBERS (cm-1)

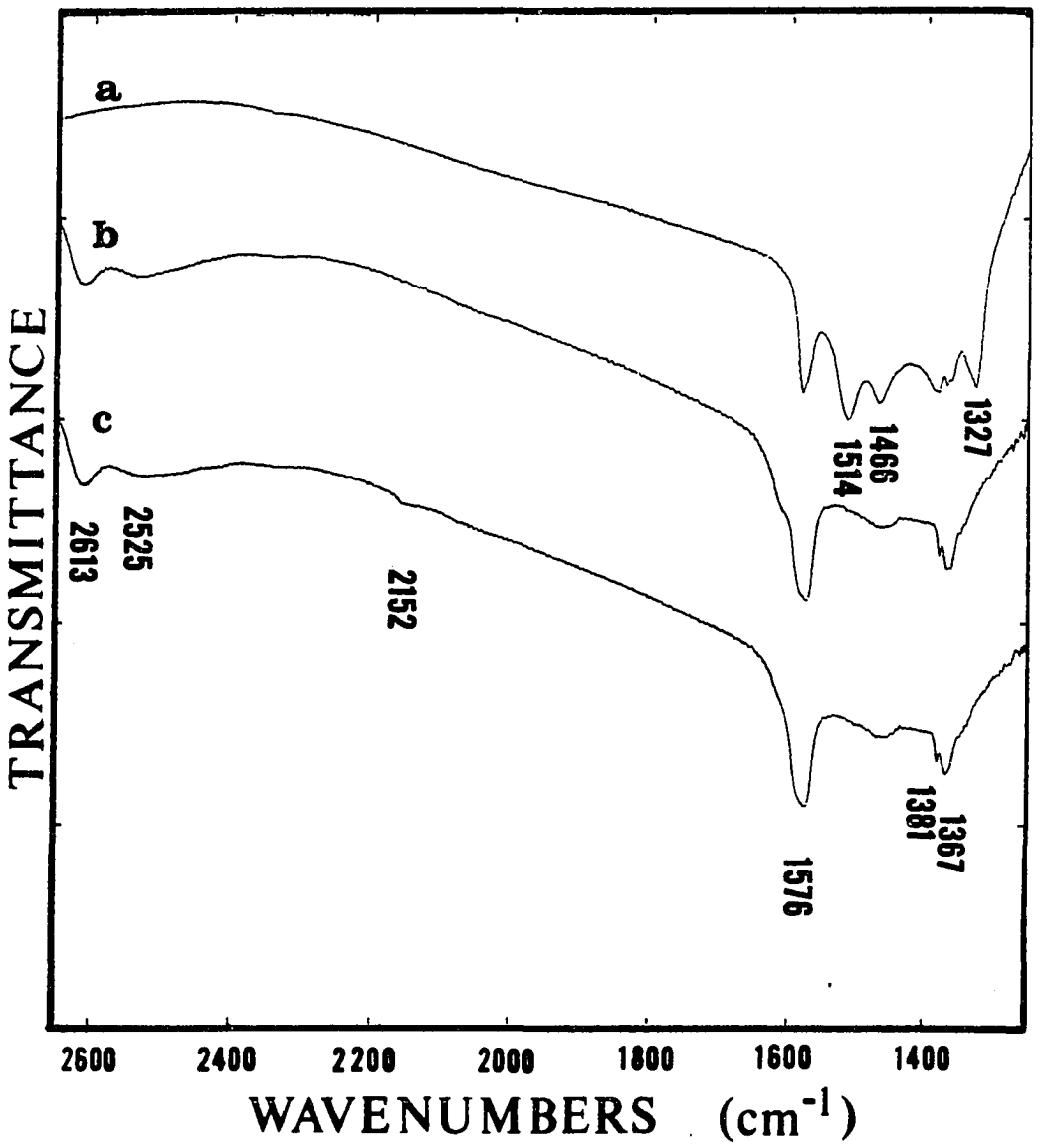

Figure 38. Continued

Figure 39. Adsorption of CD_3OD on 90/10 Zn/Cu oxide at 130°C

a) reduced surface

b) exposure for 5 minutes

c) exposure for 1 hour

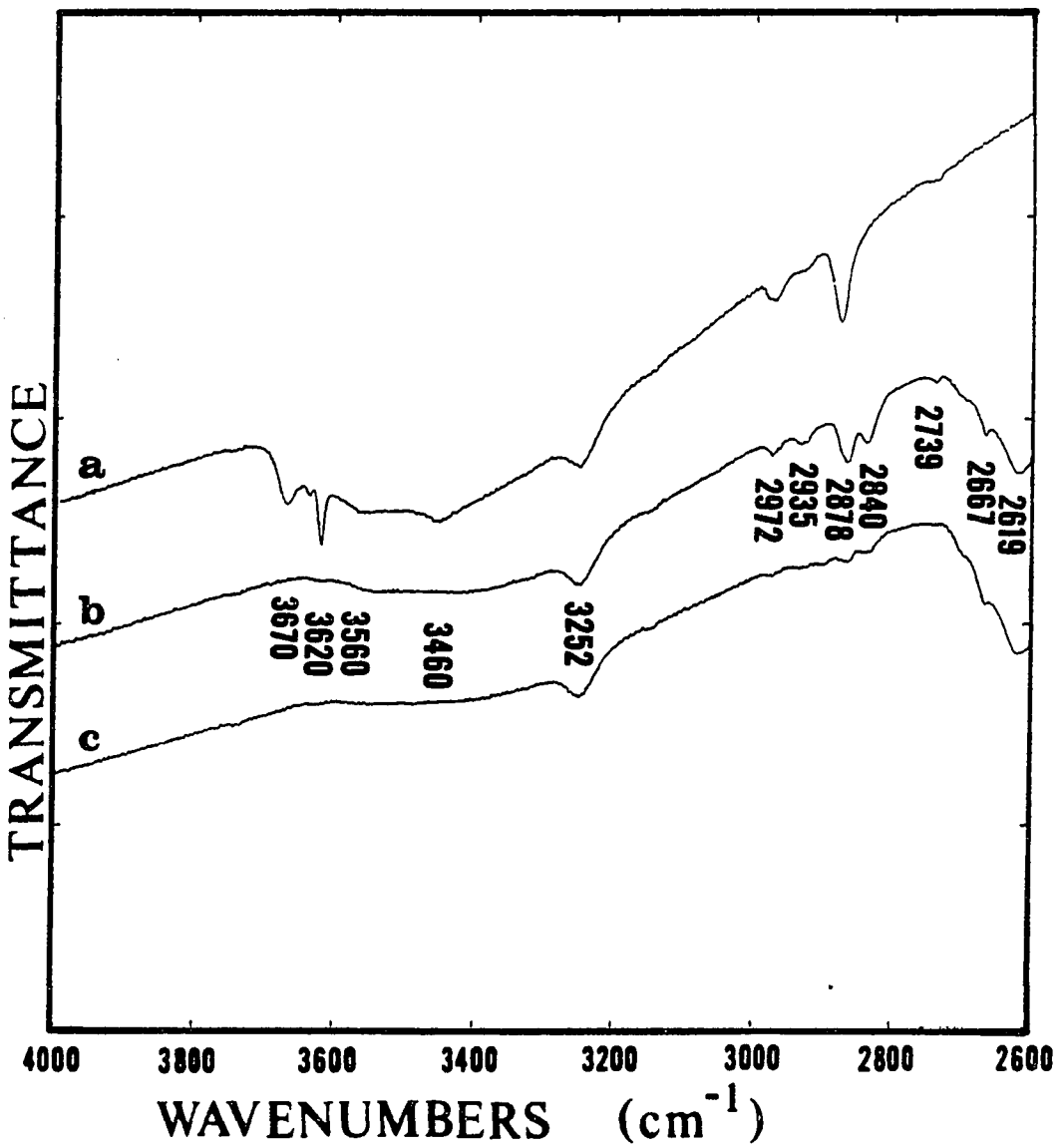
TRANSMITTANCE
a
b
c
3670
3620
3560
3460
3252
2972
2935
2878
2840
2739
2667
2619
4000
3800
3600
3400
3200
3000
2800
2600
WAVENUMBERS (cm-1)

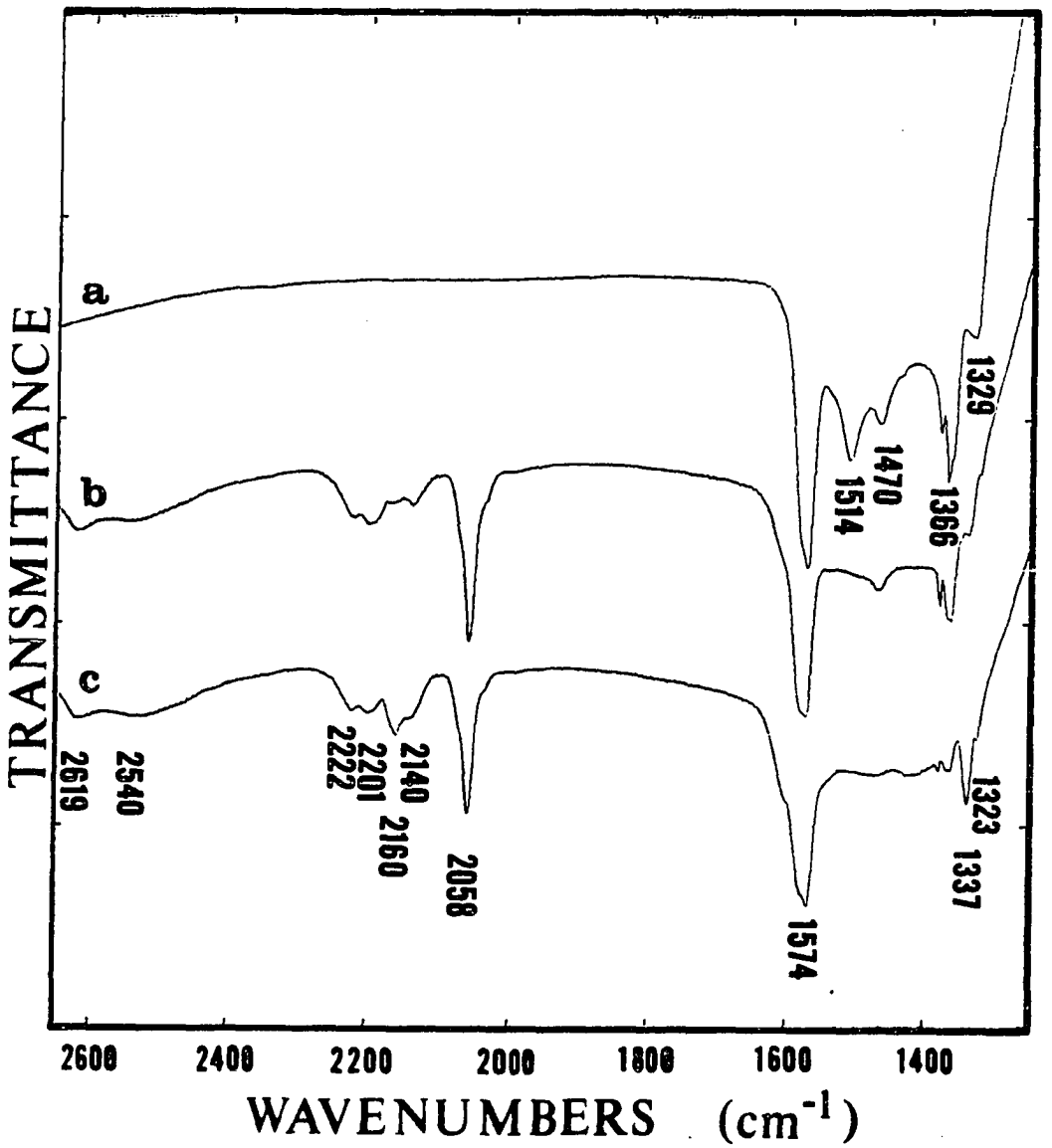

Figure 39. Continued

were shifted or displaced. The formate was diminishing while it appeared an adsorbed formaldehyde species (bands at 2935 and 2840 cm^{-1}) was temporarily formed. Both the formate and adsorbed formaldehyde species eventually disappear. Deuterated formate species (bands at 2160, 1574, and 1337 cm^{-1}) developed as the formate decreased, indicating that exchange between deuterated and hydrogenated species occurred readily.

The effect of methanol adsorption in an oxidizing environment was determined by exposing a reduced 95/5 Zn/Cu catalyst (pretreatment #3) to a methanol-water mixture (20% CH_3OH) at 150°C and 1 atmosphere (Figure 40). Initially, methoxy (bands at 2934 and 2818 cm^{-1}) and formate (bands at 2972, 2878, 1576, 1381, and 1364 cm^{-1}) groups developed with some indication of an adsorbed formaldehyde species (band at 2845 cm^{-1}) also present. The isolated hydroxyl groups (bands at 3666 and 3620 cm^{-1}) were greatly diminished but had not disappeared. After an hour, the surface species were essentially the same as the initial adsorbed species.

Adsorption on Ternary Oxides

The zinc-copper-aluminum oxide catalysts were satisfactory for transmission infrared studies in the fully oxidized state, but became nearly opaque when reduced in hydrogen. This class of catalysts could not be investigated. The zinc-copper-chromium oxide catalysts maintained good transmittance in both the oxidized and reduced states. Results obtained from this class of catalysts were better than some of

Figure 40. Adsorption of CH_3OH-H_2O mixture on 95/5 Zn/Cu oxide at 150°C

a) reduced surface

b) exposure for 5 minutes

c) exposure for 1 hour

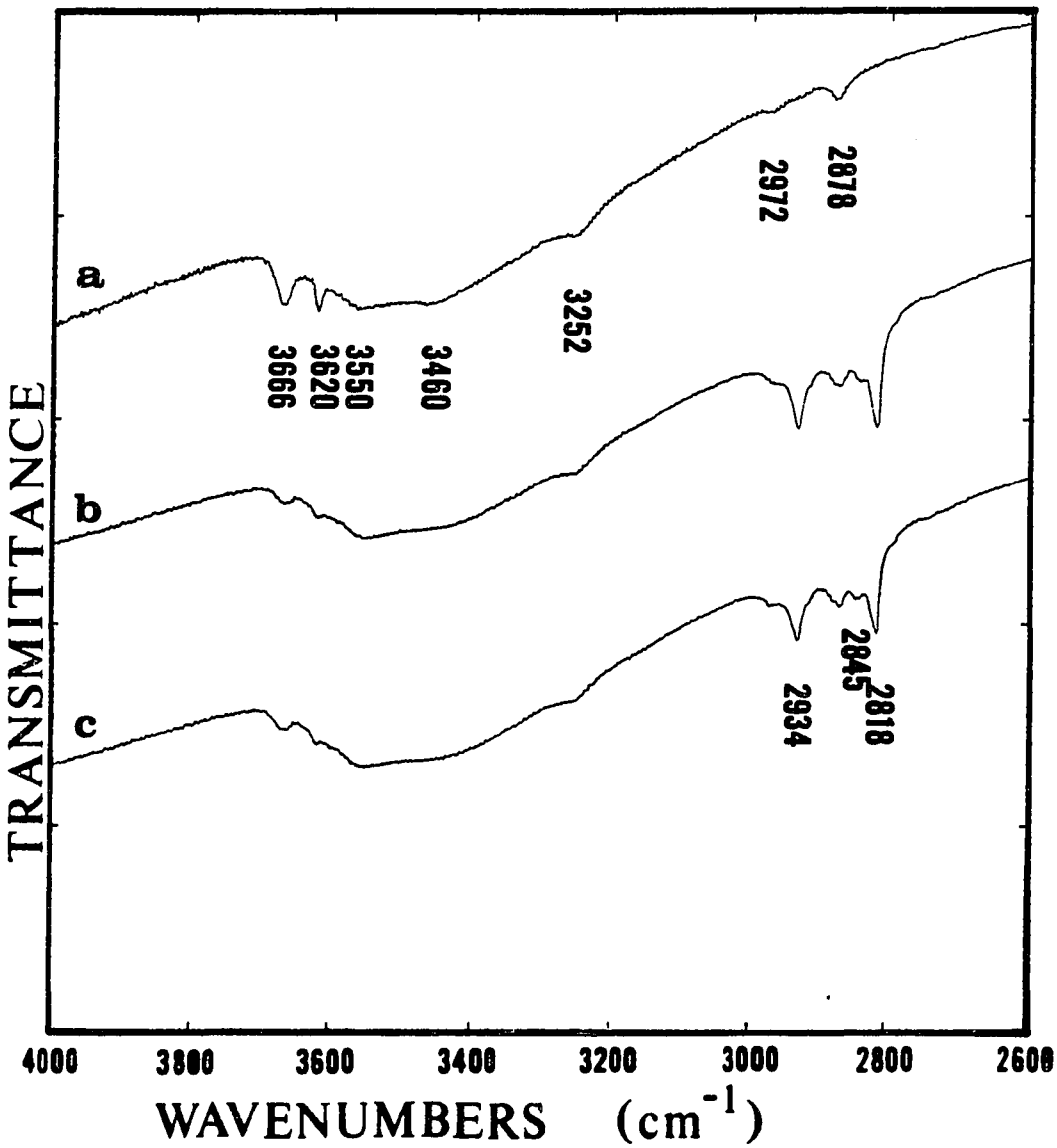
a
b
c
3666
3620
3550
3460
3252
2972
2878
2934
2845
2818
TRANSMITTANCE
4000
3800
3600
3400
3200
3000
2800
2600
WAVENUMBERS (cm-1)

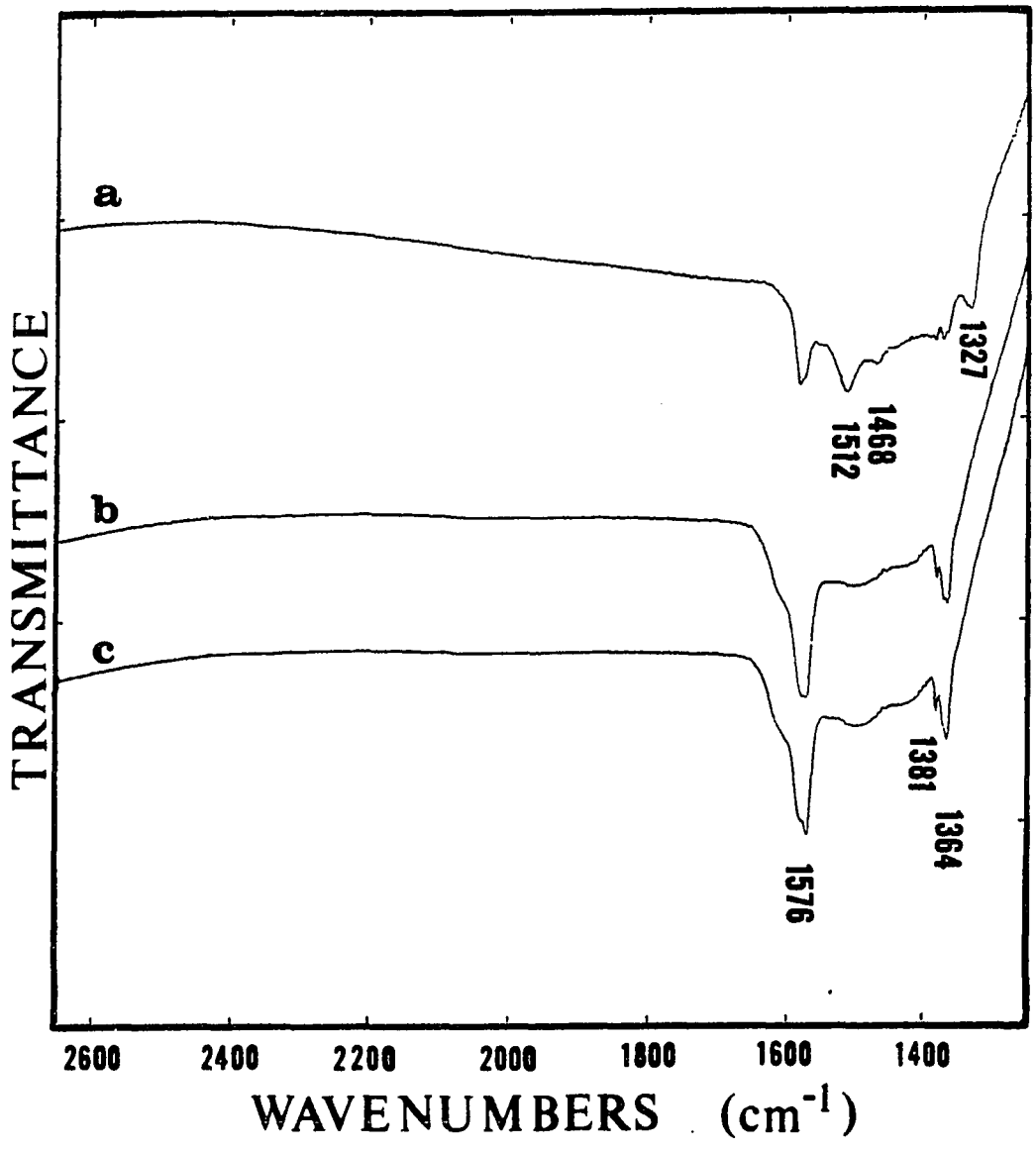

Figure 40. Continued

the information collected from the binary catalysts because the transmittance was always good over the entire wavenumber region. The catalysts used in this investigation had compositions of 90/5/5 and 80/10/10 Zn/Cu/Cr oxides which were reduced in a 5% H_2-95% N_2 mixture (pretreatment #3) prior to all adsorption studies.

The adsorption of carbon monoxide and hydrogen ($H_2/CO = 2/1$) on 90/5/5 and 80/10/10 Zn/Cu/Cr catalysts at 200°C and 1 atmosphere is shown in Figures 41 and 42, respectively. The residual hydroxyl groups (bands at 3666, 3620, and 3480 cm^{-1}) and the hydroxyl species at 3252 cm^{-1} were not very distinct on these ternary compositions; band intensity decreased with increasing chromium content. The behavior of adsorbed species on each catalyst was quite similar. The initial exposure to the mixture produced the carbonyl species (band at 2087 cm^{-1}) and a formate group (bands at 2964, 2872, 1576, 1381, and 1360 cm^{-1}). The surface carbonates (bands at 1510, 1433, and 1323 cm^{-1}) gradually disappeared. Methoxy groups (bands at 2932 and 2820 cm^{-1}) developed more quickly on the 90/5/5 Zn/Cu/Cr catalyst than the 80/10/10 Zn/Cu/Cr catalyst.

The transmittance of these ternary catalysts during the adsorption of formic acid solution (88% HCOOH, 12% H_2O) did not decrease sufficiently to prevent detection of adsorbed species, unlike the binary catalysts. Formic acid adsorption on 90/5/5 Zn/Cu/Cr and 80/10/10 Zn/Cu/Cr catalysts at 200°C and 1 atmosphere is shown in Figures 43 and 44, respectively. An adsorbed formate species (bands at 2964, 2872, 1576, 1381, and 1360 cm^{-1}) and gaseous carbon dioxide (band at 2350 cm^{-1}) can be seen in the spectra when formic acid was in the gas phase. A band in the 1985-1992 cm^{-1} region on 90/5/5 Zn/Cu/Cr oxide

Figure 41. Adsorption of CO-H_2 mixture on 90/5/5 Zn/Cu/Cr oxide at 200°C

a) reduced surface

b) exposure for 5 minutes

c) exposure for 1 hour

d) exposure for 8 hours

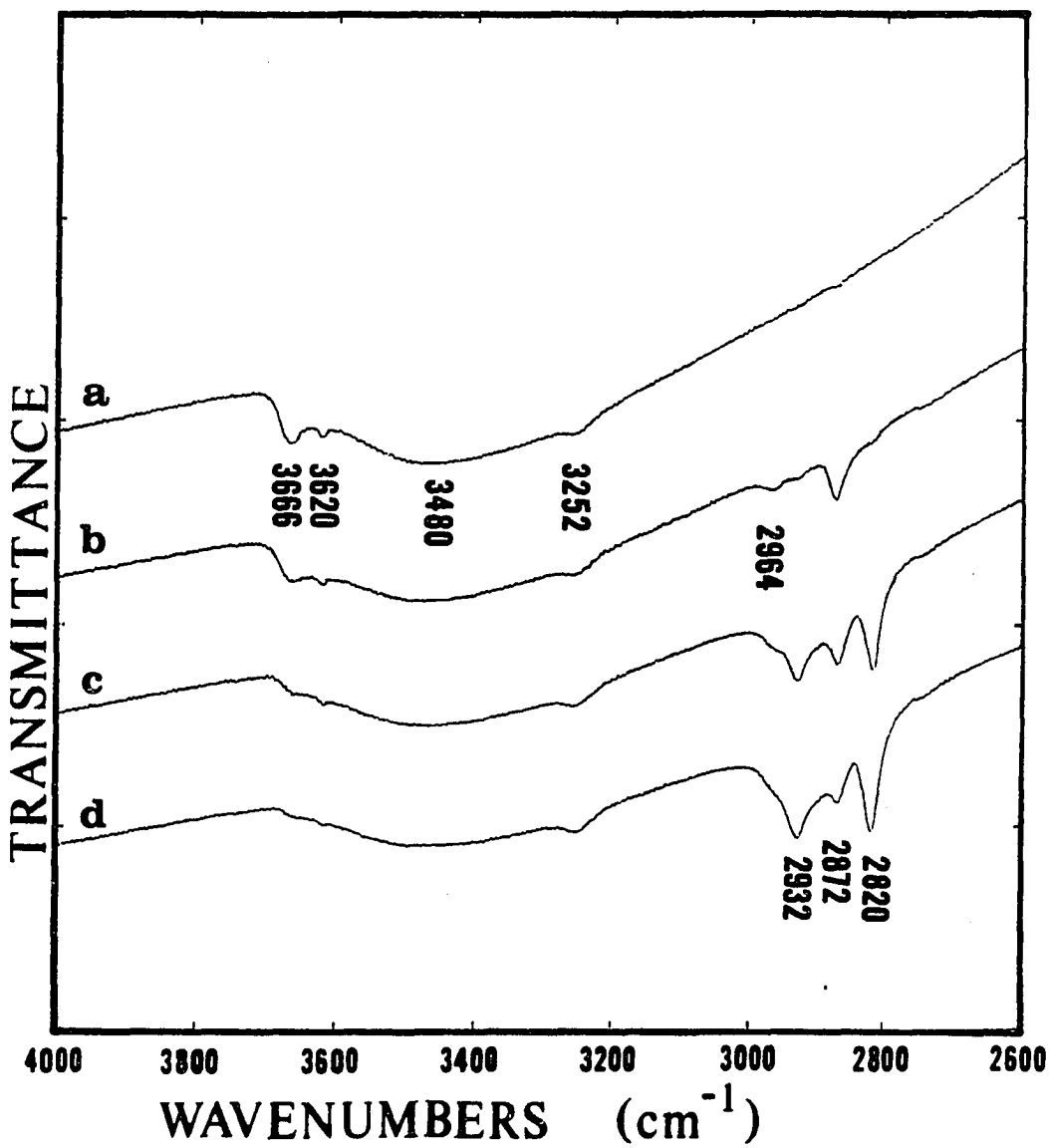
TRANSMITTANCE
a
b
c
d
3666
3620
3480
3252
2964
2932
2872
2820
4000
3800
3600
3400
3200
3000
2800
2600
WAVENUMBERS (cm-1)

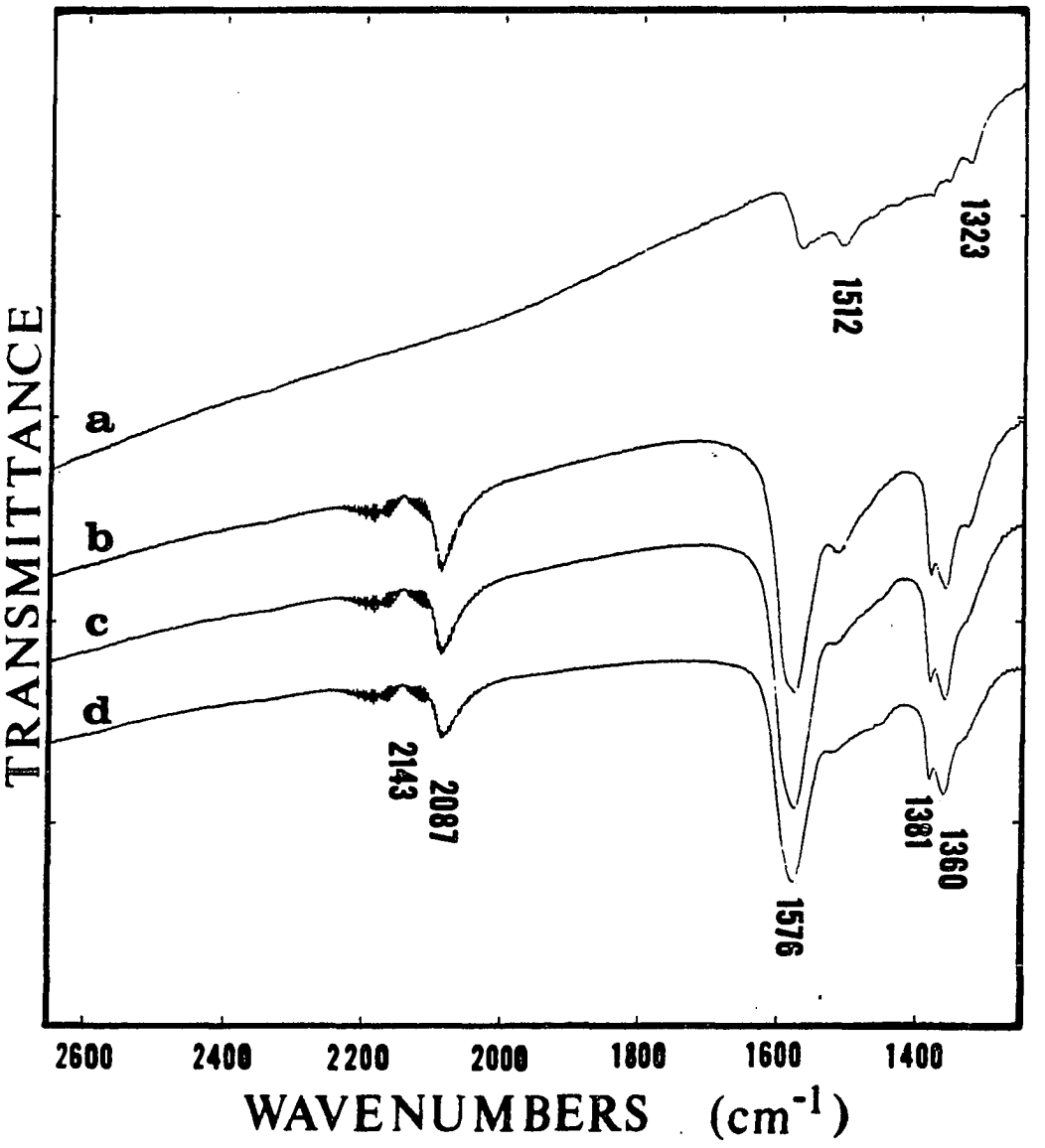

Figure 41. Continued

Figure 42. Adsorption of CO-H_2 mixture on 80/10/10 Zn/Cu/Cr oxide at 200°C

a) reduced surface

b) exposure for 5 minutes

c) exposure for 1 hour

d) exposure for 8 hours

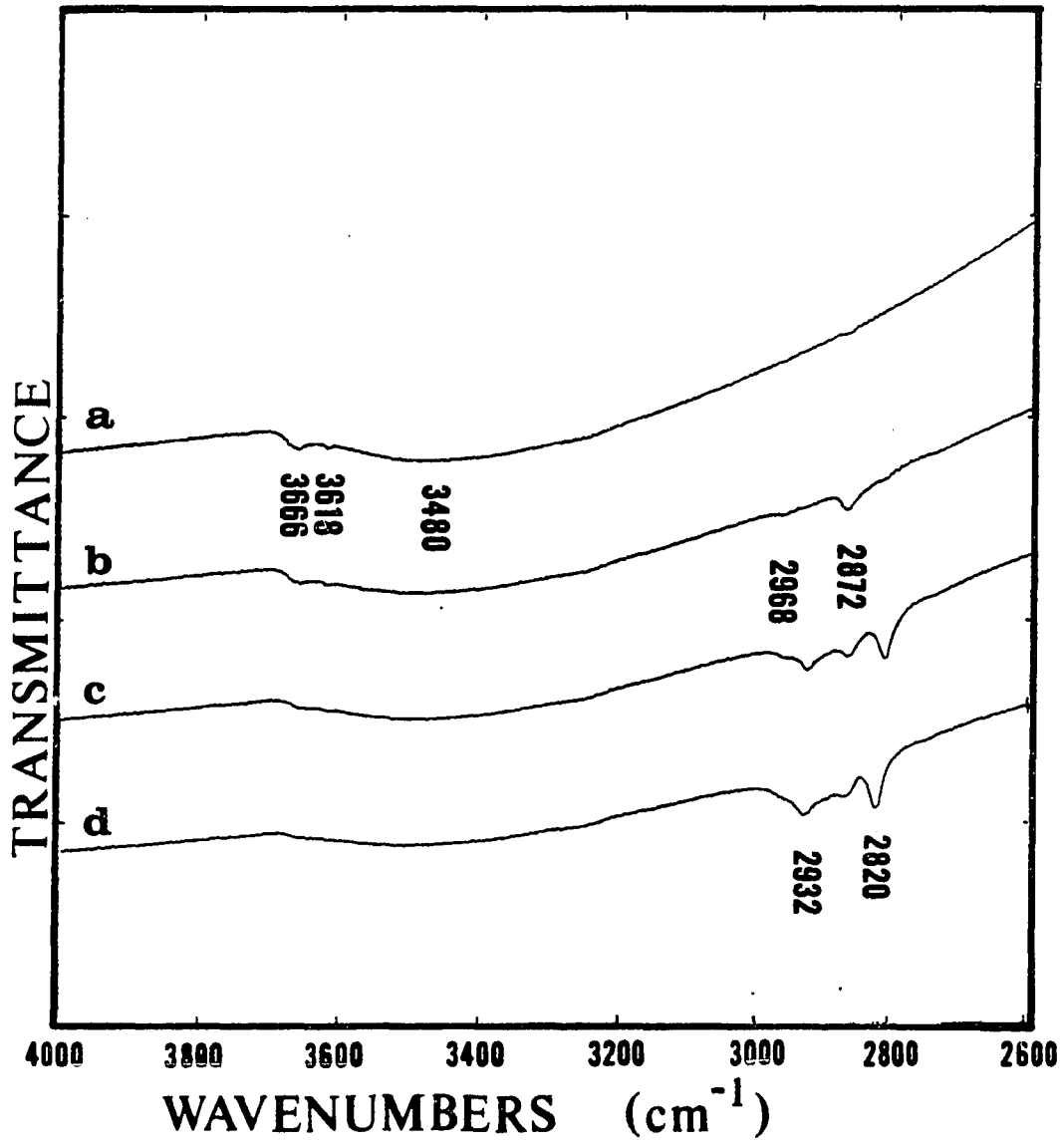
TRANSMITTANCE
a
b
c
d
3666
3618
3480
2968
2872
2932
2820
4000
3800
3600
3400
3200
3000
2800
2600
WAVENUMBERS (cm-1)

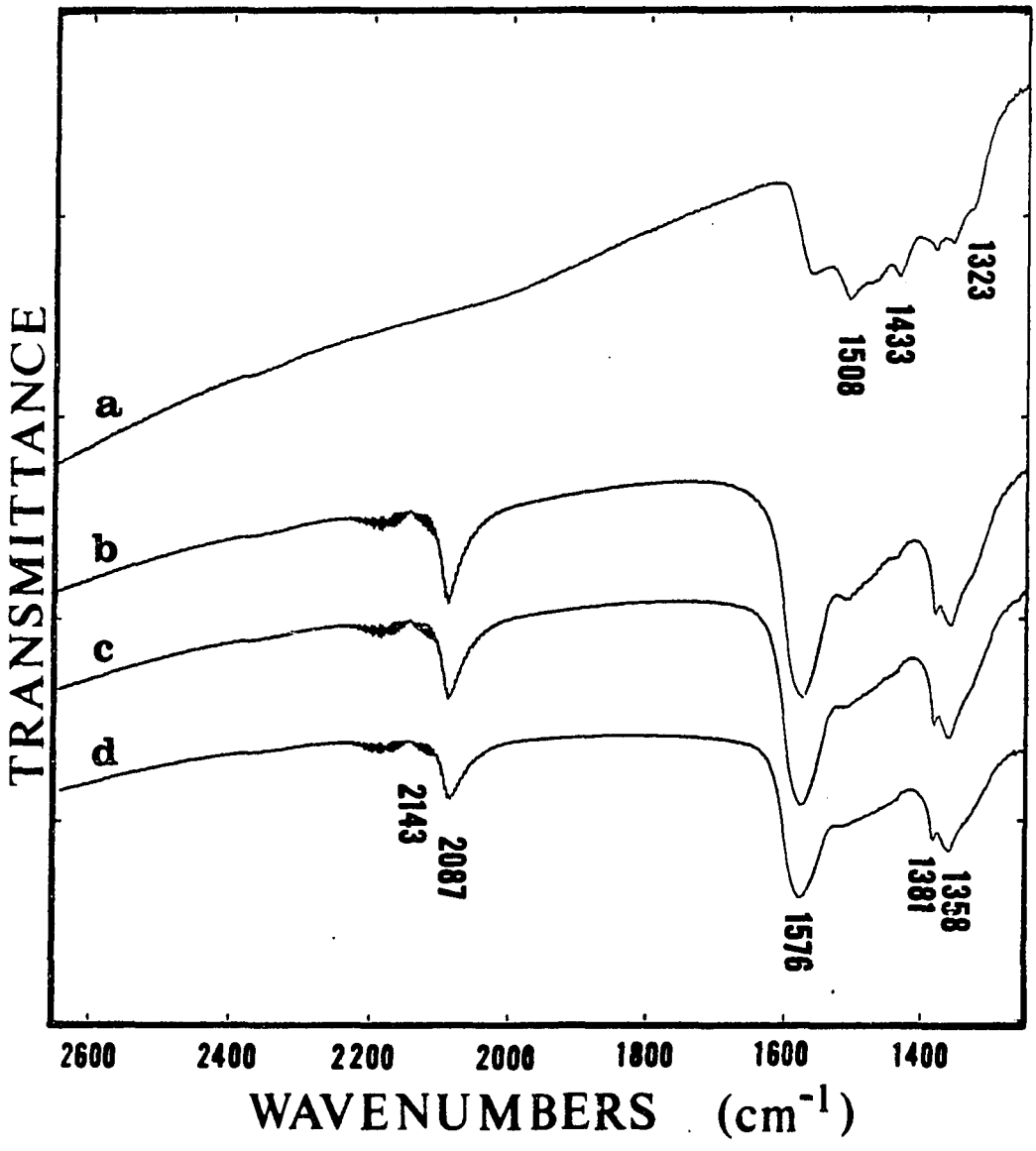

Figure 42. Continued

Figure 43. Adsorption of formic acid on 90/5/5 Zn/Cu/Cr oxide at 200°C

a) reduced surface

b) exposure for 5 minutes

c) 1 hour after exposure

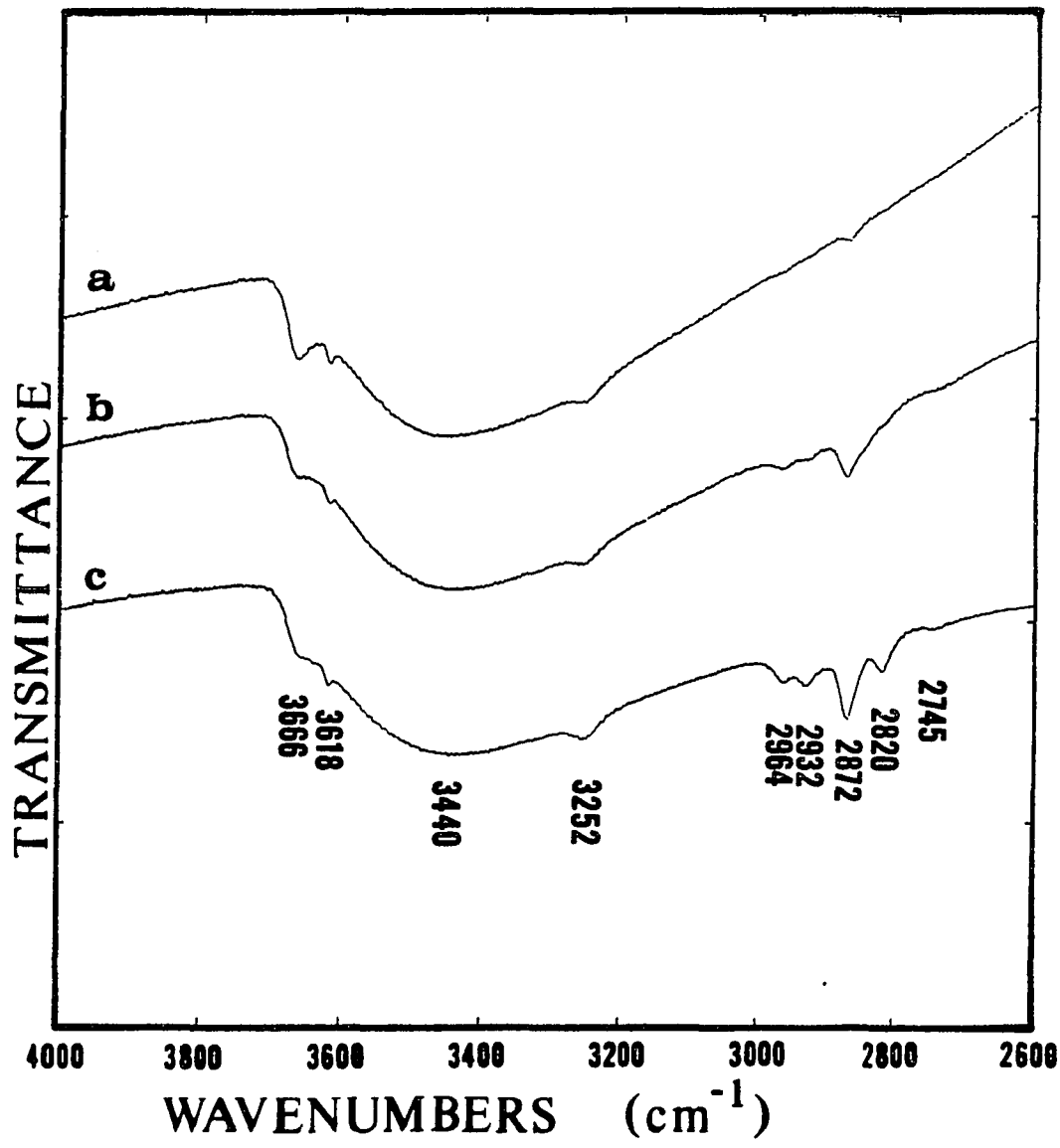
a
b
c
TRANSMITTANCE
3669
3618
3440
3252
2964
2932
2872
2820
2745
4000
3800
3600
3400
3200
3000
2800
2600
WAVENUMBERS (cm-1)

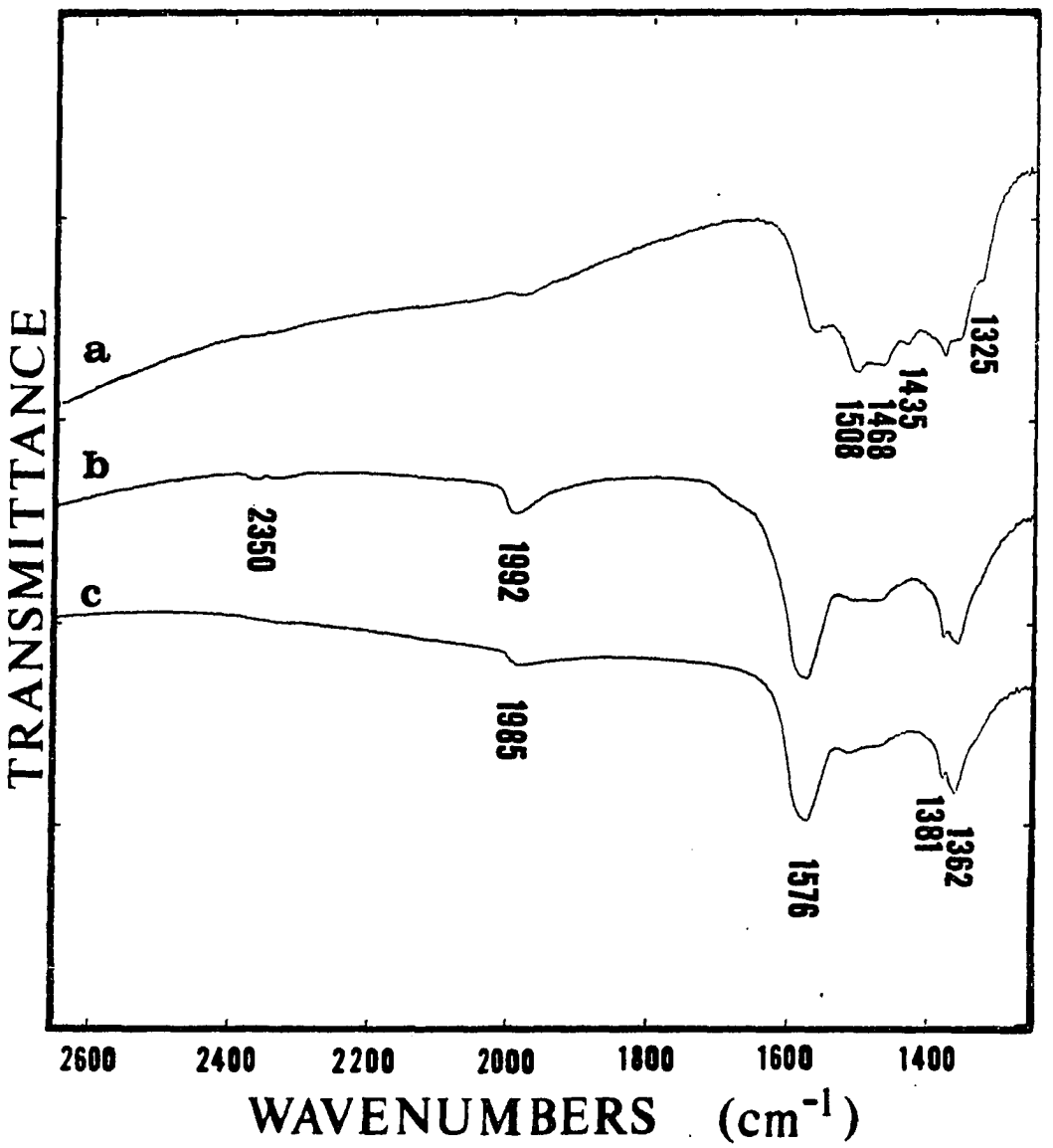

Figure 43. Continued

Figure 44. Adsorption of formic acid on 80/10/10 Zn/Cu/Cr oxide at 200°C

a) reduced surface

b) exposure for 5 minutes

c) exposure for 1 hour

d) 1 hour after exposure

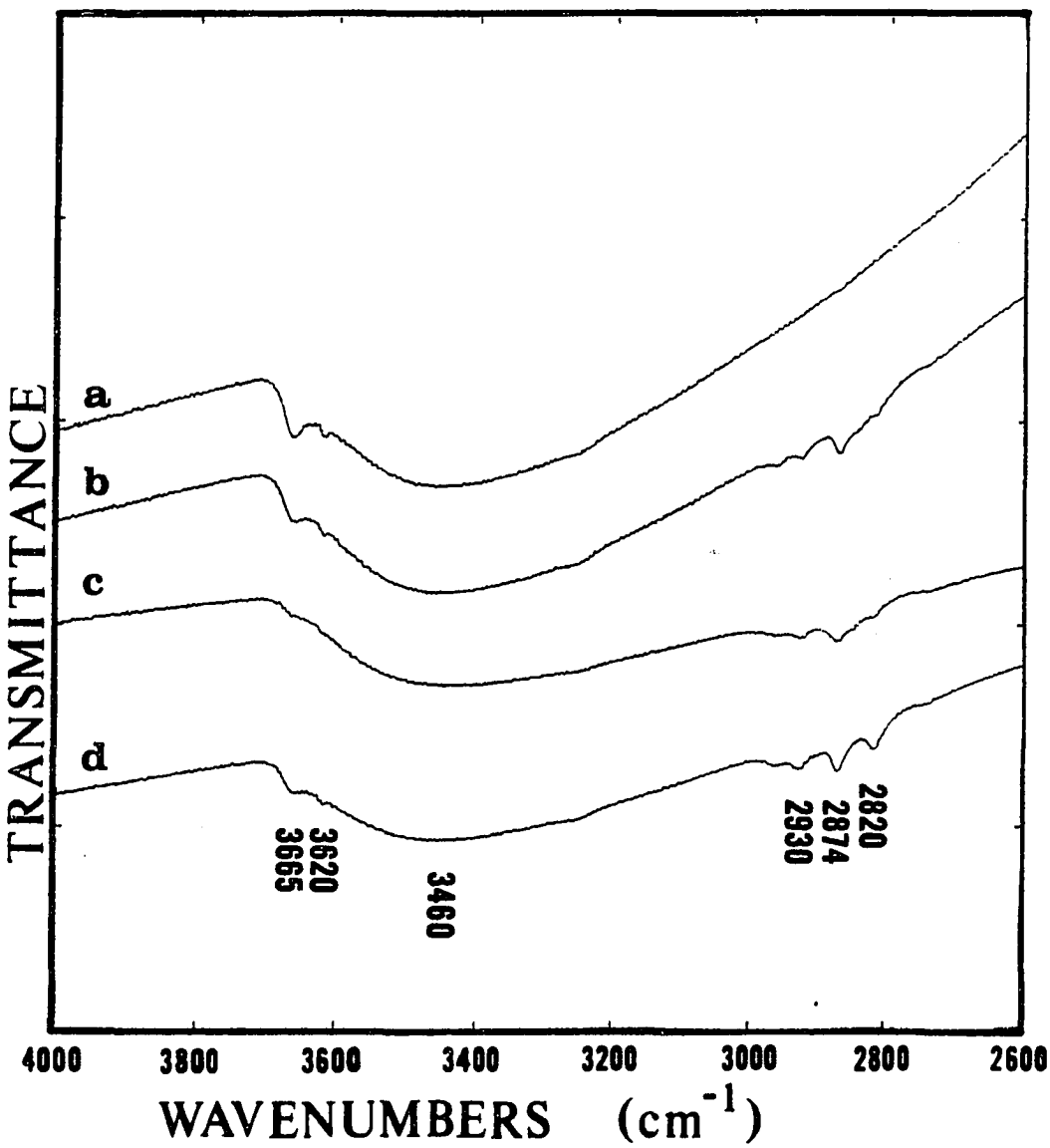
TRANSMITTANCE
a
b
c
d
3620
3665
3460
2820
2874
2930
4000
3800
3600
3400
3200
3000
2800
2600
WAVENUMBERS (cm-1)

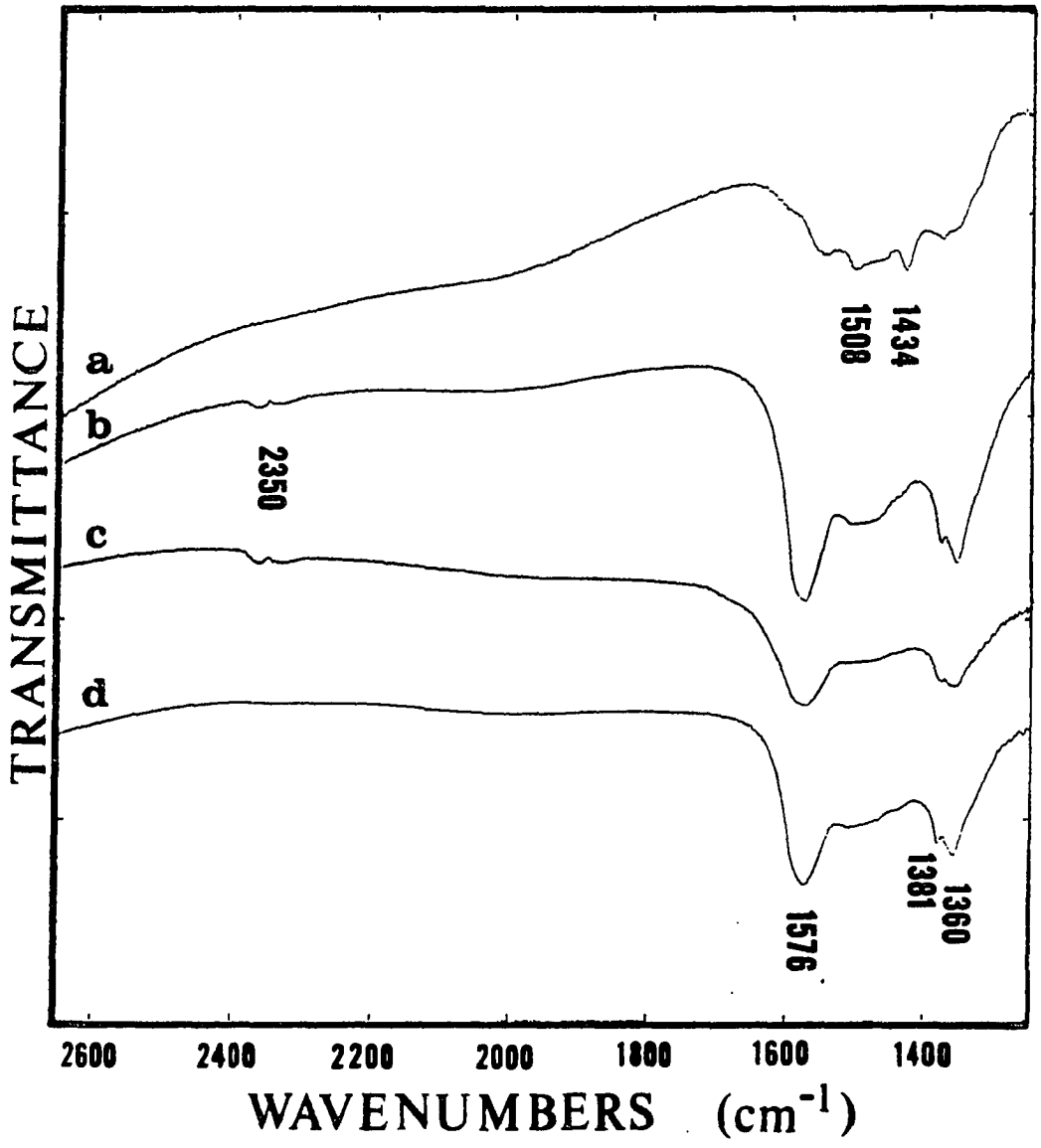

Figure 44. Continued

was assigned to an adsorbed formic acid molecule. There was negligible methoxy development until after the formic acid was flushed from the gas phase, possibly because the gas phase also contained some water (the formic acid solution has water) which inhibited methoxy formation.

A brief exposure (5 minutes) of formaldehyde to 90/5/5 and 80/10/10 Zn/Cu/Cr catalysts at 200°C and 1 atmosphere is shown in Figures 45 and 46, respectively. The formation of methoxy groups (bands at 2930 and 2822 cm^{-1}) and formate groups (bands at 2872, 1576, 1381, and 1360 cm^{-1}) occurred initially, followed by decomposition of the methoxy groups. Both catalysts had a weak band at 2087 cm^{-1} suggesting that carbon monoxide was a decomposition product during formaldehyde adsorption at 200°C. The rate of methoxy formation was more rapid on the 90/5/5 Zn/Cu/Cr catalyst than the 80/10/10 Zn/Cu/Cr catalyst. The weak band at 1670 cm^{-1} can be assigned to adsorbed water, probably another decomposition product during formaldehyde adsorption.

The adsorption of formaldehyde on 90/5/5 and 80/10/10 Zn/Cu/Cr catalysts at 100°C and 1 atmosphere is shown in Figures 47 and 48, respectively. Initially, the exposure to formaldehyde produced an adsorbed formaldehyde species (bands at 2935, 2850, and 2737 cm^{-1}), formate (bands at 2966, 2876, 1580, 1381, and 1365 cm^{-1}), and some methoxy groups (bands at 2932 and 2820 cm^{-1}). As the amount of adsorbed formaldehyde increased on the surface, the isolated hydroxyl groups (bands at 3666 and 3618 cm^{-1}) and the methoxy groups were displaced. The adsorbed formaldehyde gradually decomposed to formate species.

The adsorption and decomposition of methanol (CH_3OH) on 90/5/5 and

Figure 45. Adsorption of formaldehyde on 90/5/5 Zn/Cu/Cr oxide at 200°C

a) reduced surface

b) 10 minutes after exposure

c) 30 minutes after exposure

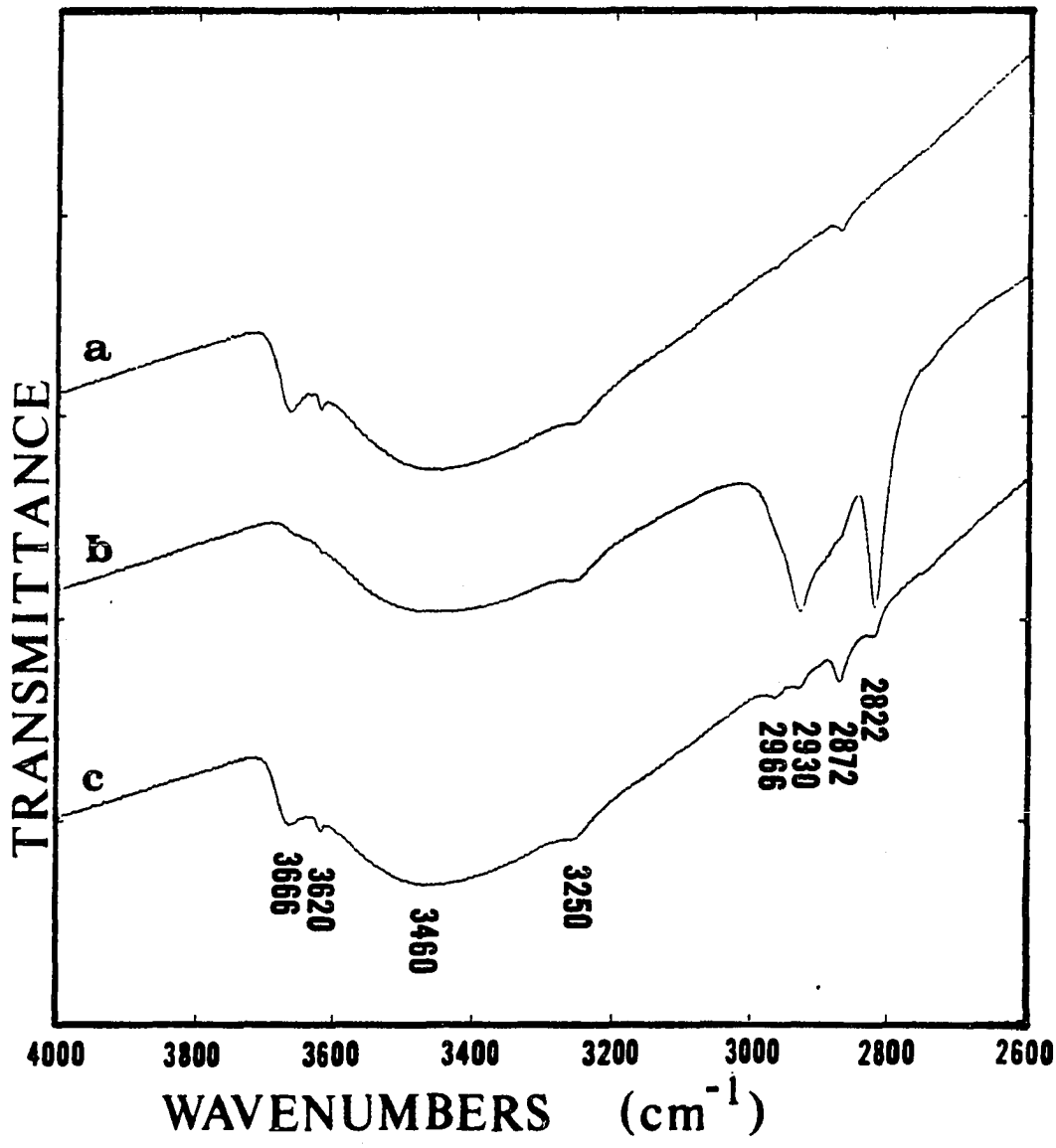
TRANSMITTANCE
a
b
c
3666
3620
3460
3250
2966
2930
2872
2822
4000
3800
3600
3400
3200
3000
2800
2600
WAVENUMBERS (cm-1)

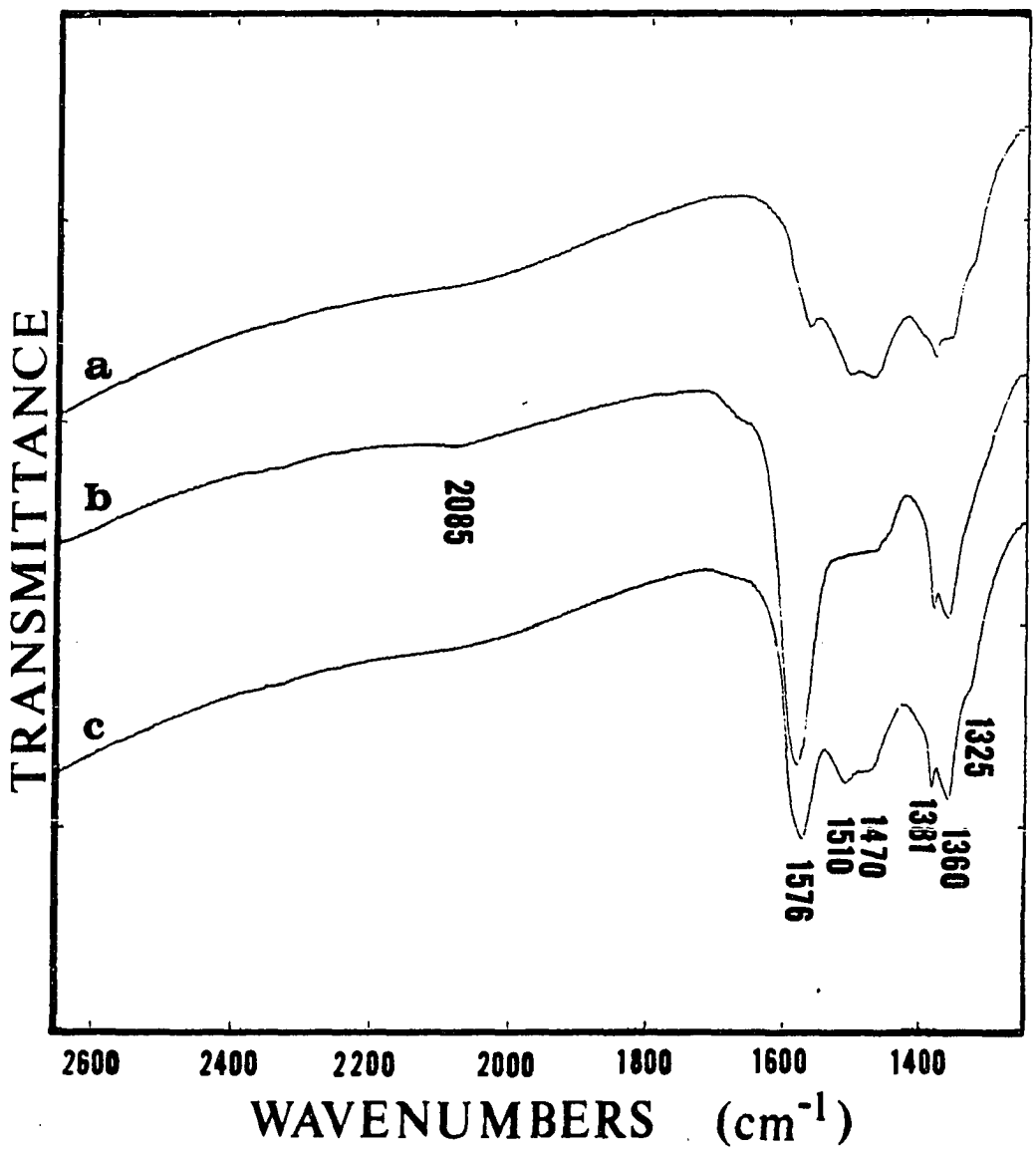

Figure 45. Continued

Figure 46. Adsorption of formaldehyde on 80/10/10 Zn/Cu/Cr oxide at 200°C

a) reduced surface

b) 10 minutes after exposure

c) 30 minutes after exposure

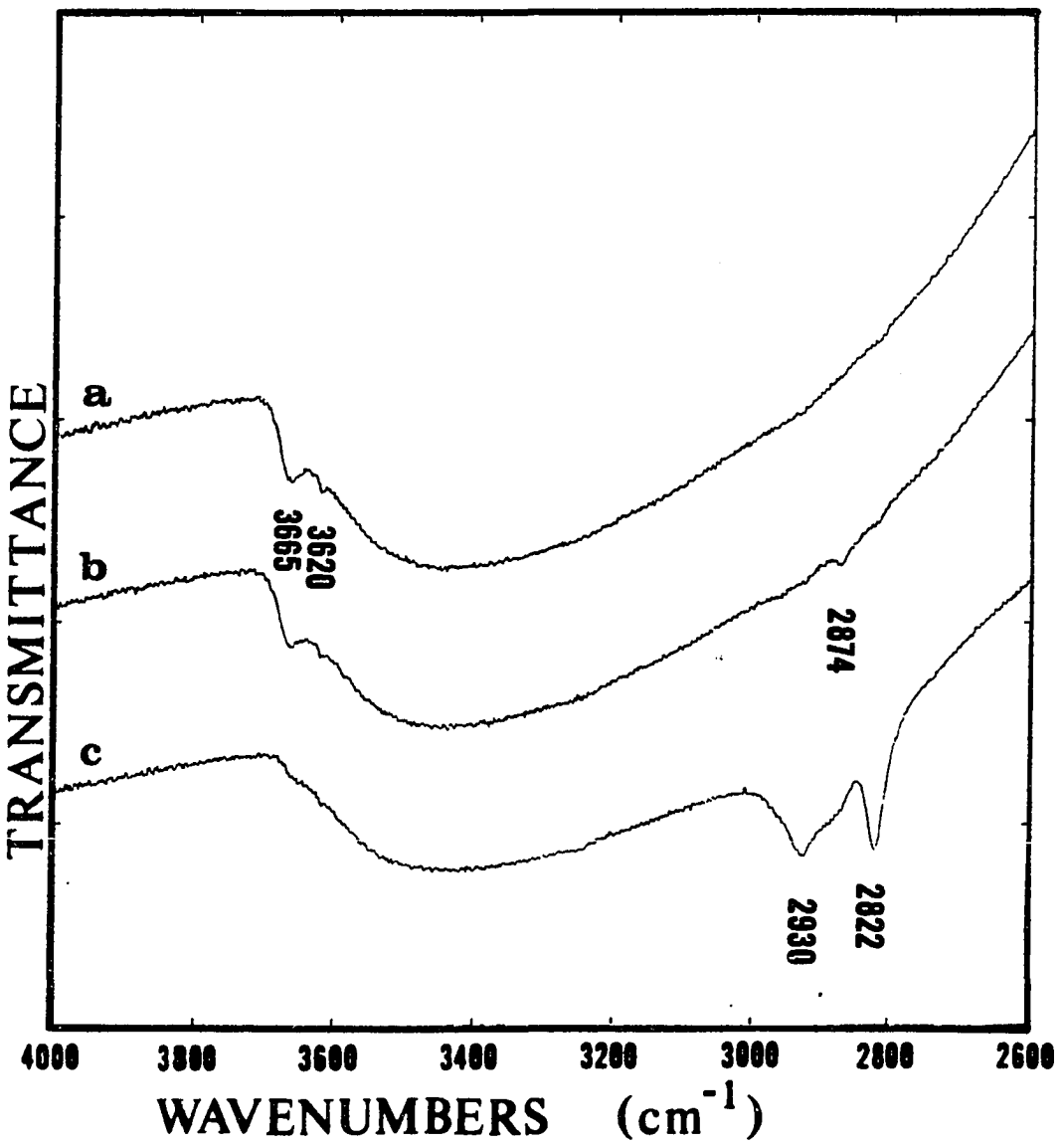
TRANSMITTANCE
a
b
c
3665
3620
2874
2930
2822
4000
3800
3600
3400
3200
3000
2800
2600
WAVENUMBERS (cm-1)

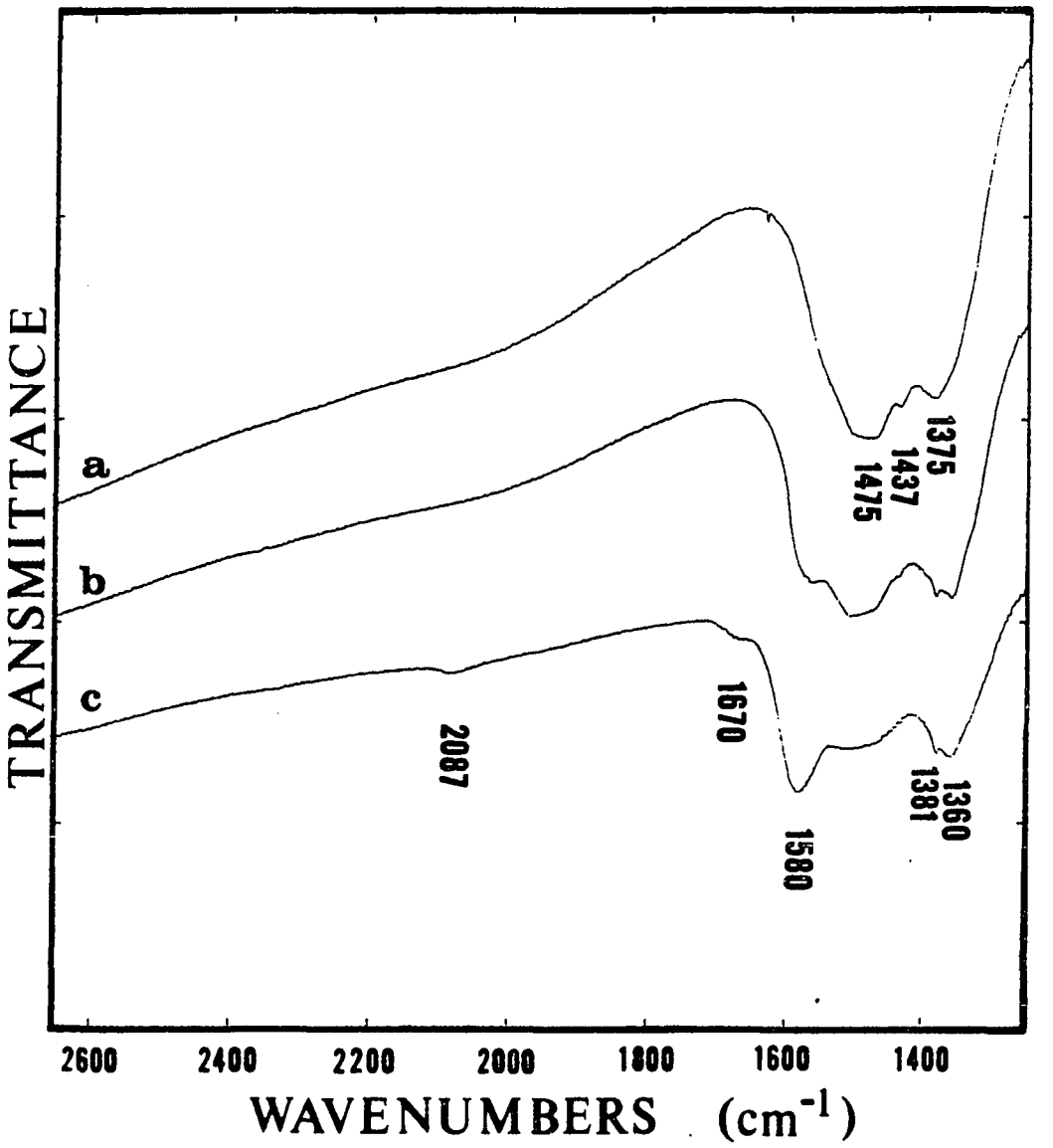

Figure 46. Continued

Figure 47. Adsorption of formaldehyde on 90/5/5 Zn/Cu/Cr oxide at 100°C

a) during exposure

b) 10 minutes after exposure

c) 30 minutes after exposure

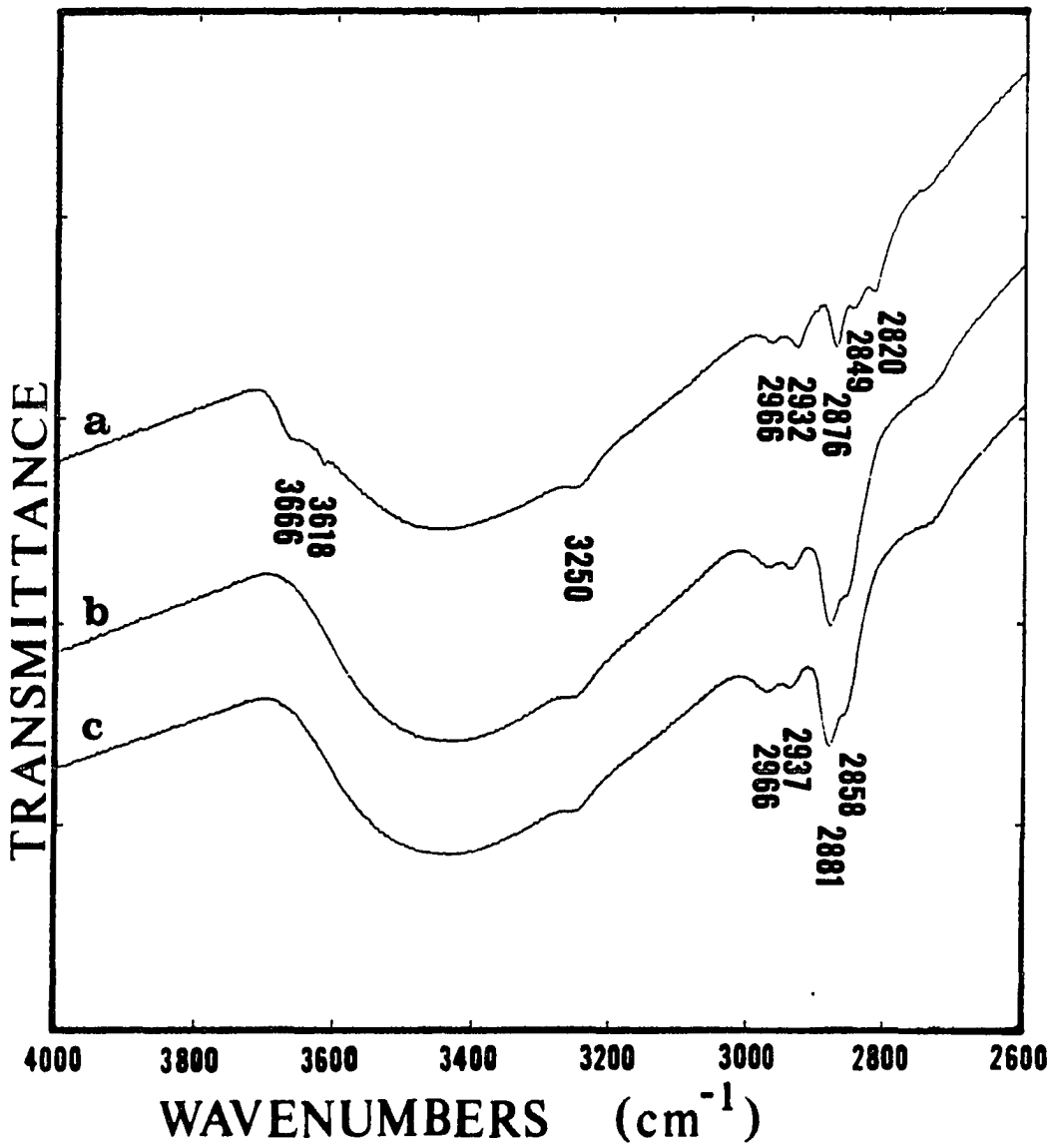
TRANSMITTANCE
a
b
c
3666
3618
3250
2966
2932
2876
2849
2820
2966
2937
2881
2858
4000
3800
3600
3400
3200
3000
2800
2600
WAVENUMBERS (cm-1)

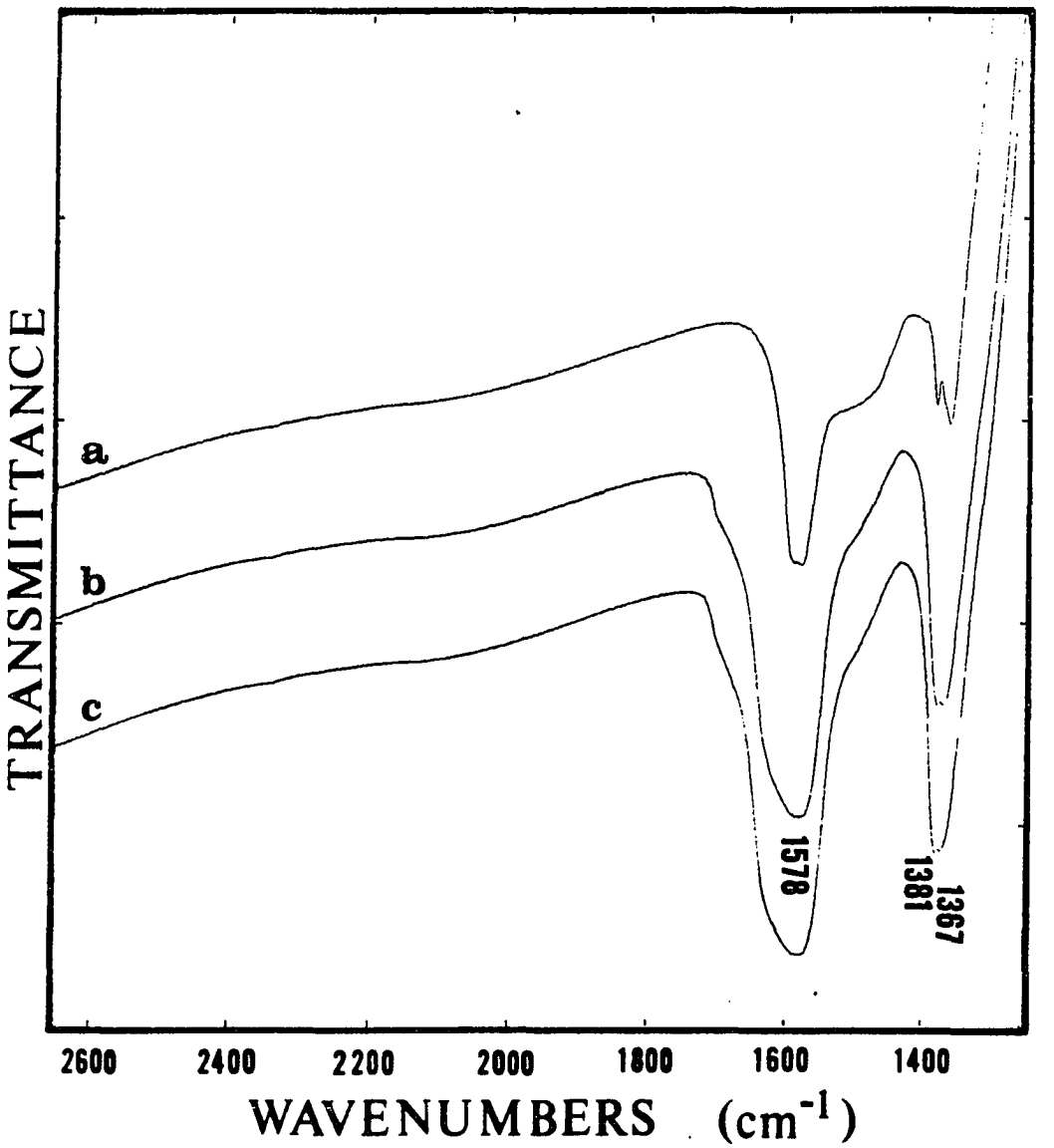

Figure 47. Continued

Figure 48. Adsorption of formaldehyde on 80/10/10 Zn/Cu/Cr oxide at 100°C

a) reduced surface

b) 10 minutes after exposure

c) 30 minutes after exposure

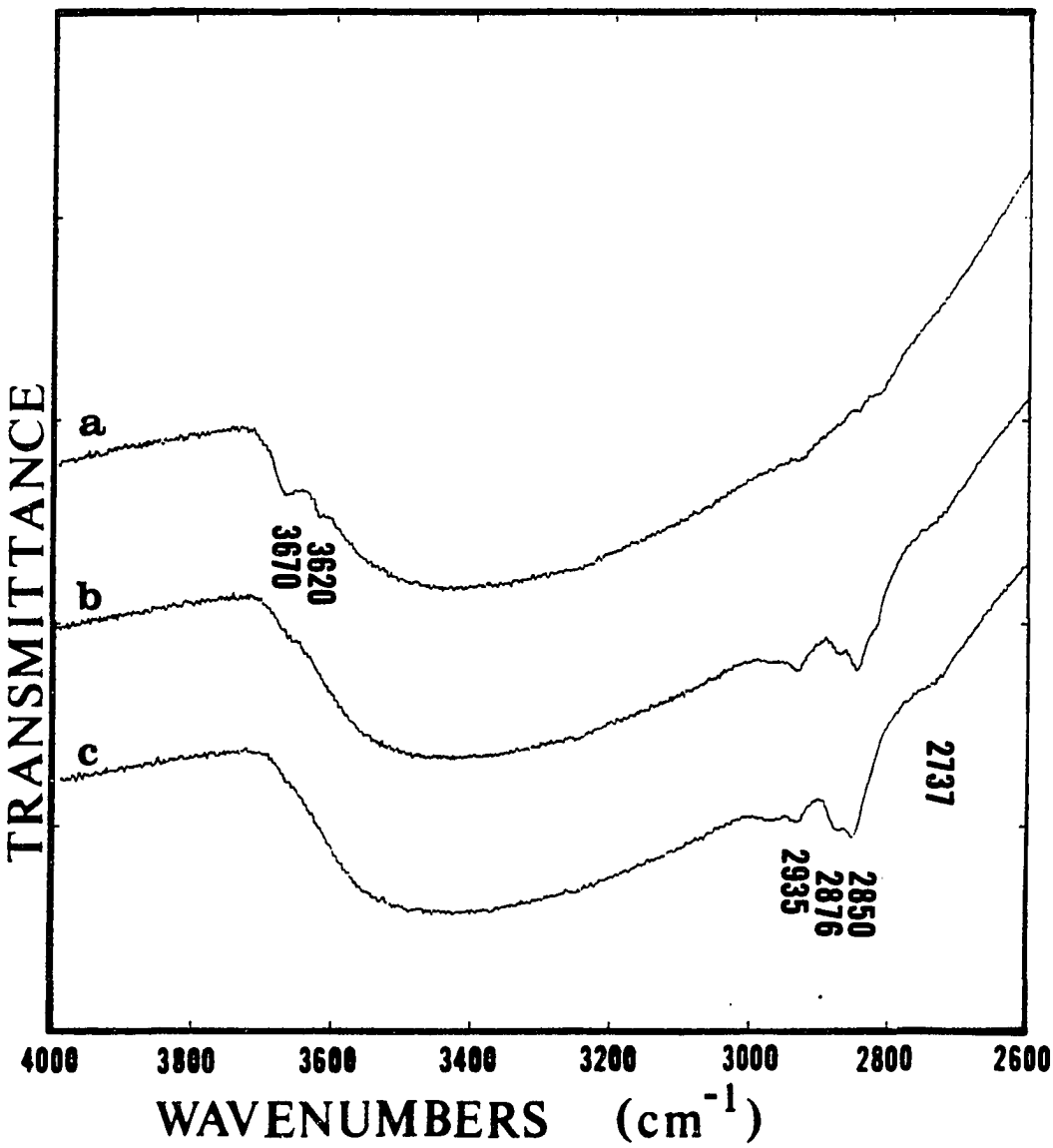
TRANSMITTANCE
a
b
c
3670
3620
2737
2935
2876
2850
4000
3800
3600
3400
3200
3000
2800
2600
WAVENUMBERS (cm-1)

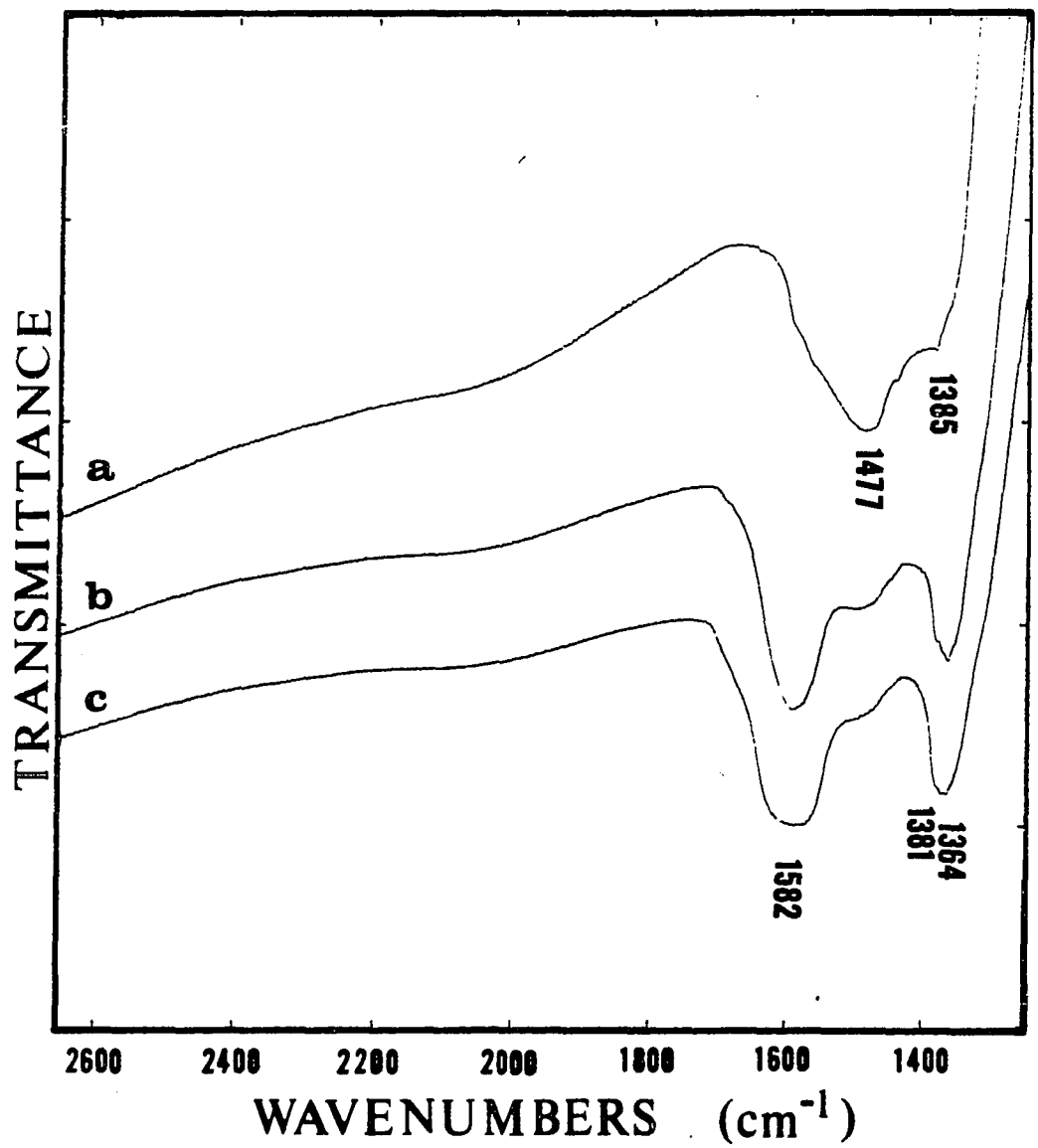

Figure 48. Continued

80/10/10 Zn/Cu/Cr catalysts were very similar at 200°C and 1 atmosphere (Figures 49 and 50). Exposure to methanol formed methoxy groups (bands at 2930 and 2820 cm^{-1}) and formate groups (bands at 2872, 1576, 1381, and 1360 cm^{-1}) with the concurrent disappearance of isolated hydroxyl groups (bands at 3666 and 3620 cm^{-1}). Some carbon dioxide was observed in the gas phase from methoxy decomposition. Removal of methanol from the gas phase caused rapid decomposition of the methoxy groups, leading to the development of formate and bidentate carbonate (bands at 1510 and 1327 cm^{-1}) groups. Methoxy groups did not decompose as readily after a second exposure to methanol.

Photoacoustic Spectra

Both oxidized and reduced methanol catalysts with Zn/Cu ratios below 85/15 were unsuitable for *in situ* infrared studies because they exhibited poor transmittance over the entire mid-infrared spectrum. Since the most active catalysts have Zn/Cu ratios near 67/33, it was desirable to compare spectra of catalysts with higher copper content to those catalysts employed in transmission infrared studies in order to determine if similar surface species exist on these various compositions. The technique of photoacoustic spectroscopy (PAS) was used to characterize several binary oxides subjected to different treatments. All spectra were taken at ambient conditions.

The spectra of several oxides that were not subjected to any pretreatment are shown in Figure 51. Each spectrum was taken with 256 scans at 8 cm^{-1} resolution. Surface carbonate bands can be seen in

Figure 49. Adsorption of methanol on 90/5/5 Zn/Cu/Cr oxide at 200°C

a) reduced surface

b) exposure for 1 hour

c) 1 hour after exposure

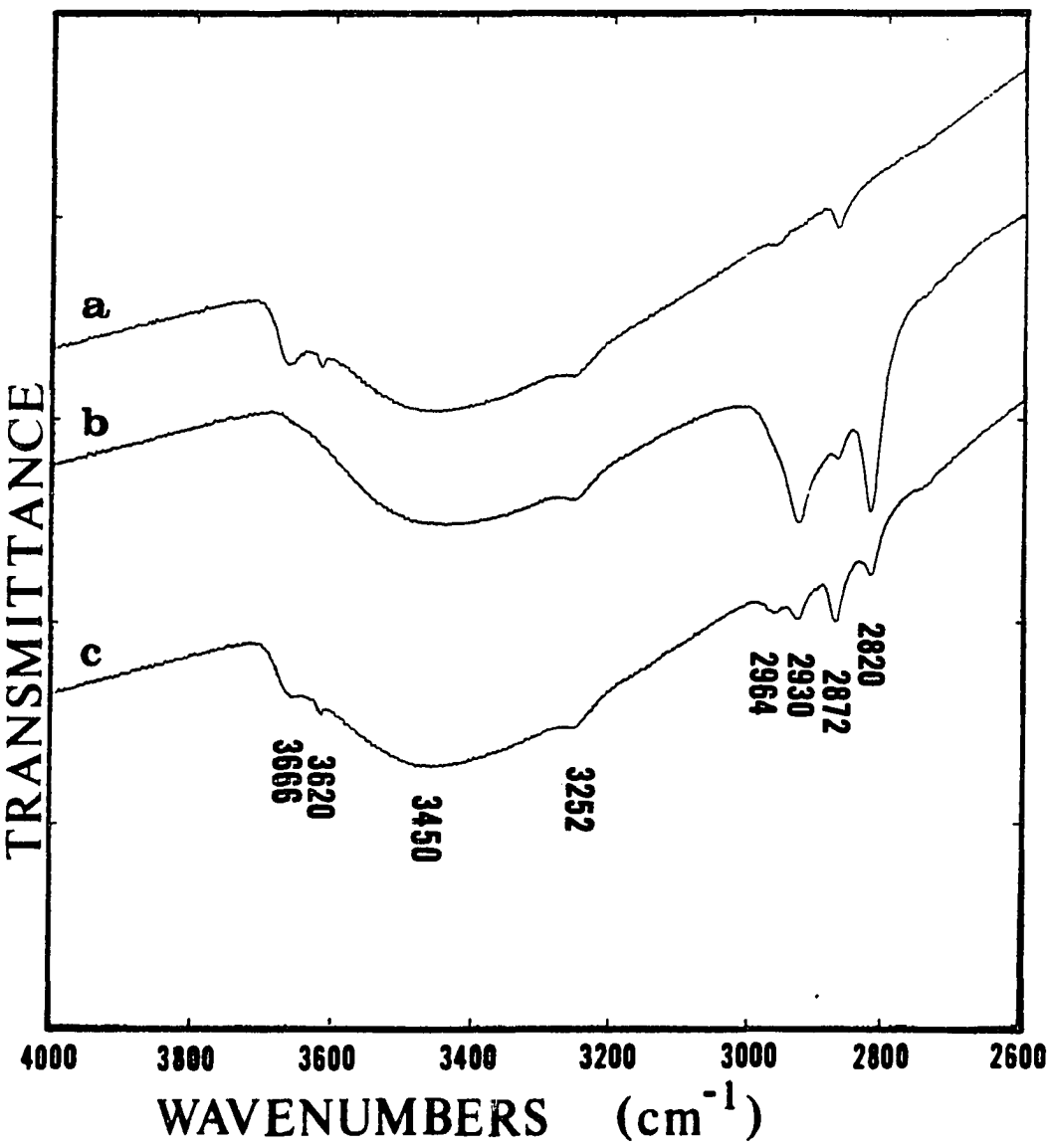
a
b
c
TRANSMITTANCE
3666
3620
3450
3252
2964
2930
2872
2820
4000
3800
3600
3400
3200
3000
2800
2600
WAVENUMBERS (cm-1)

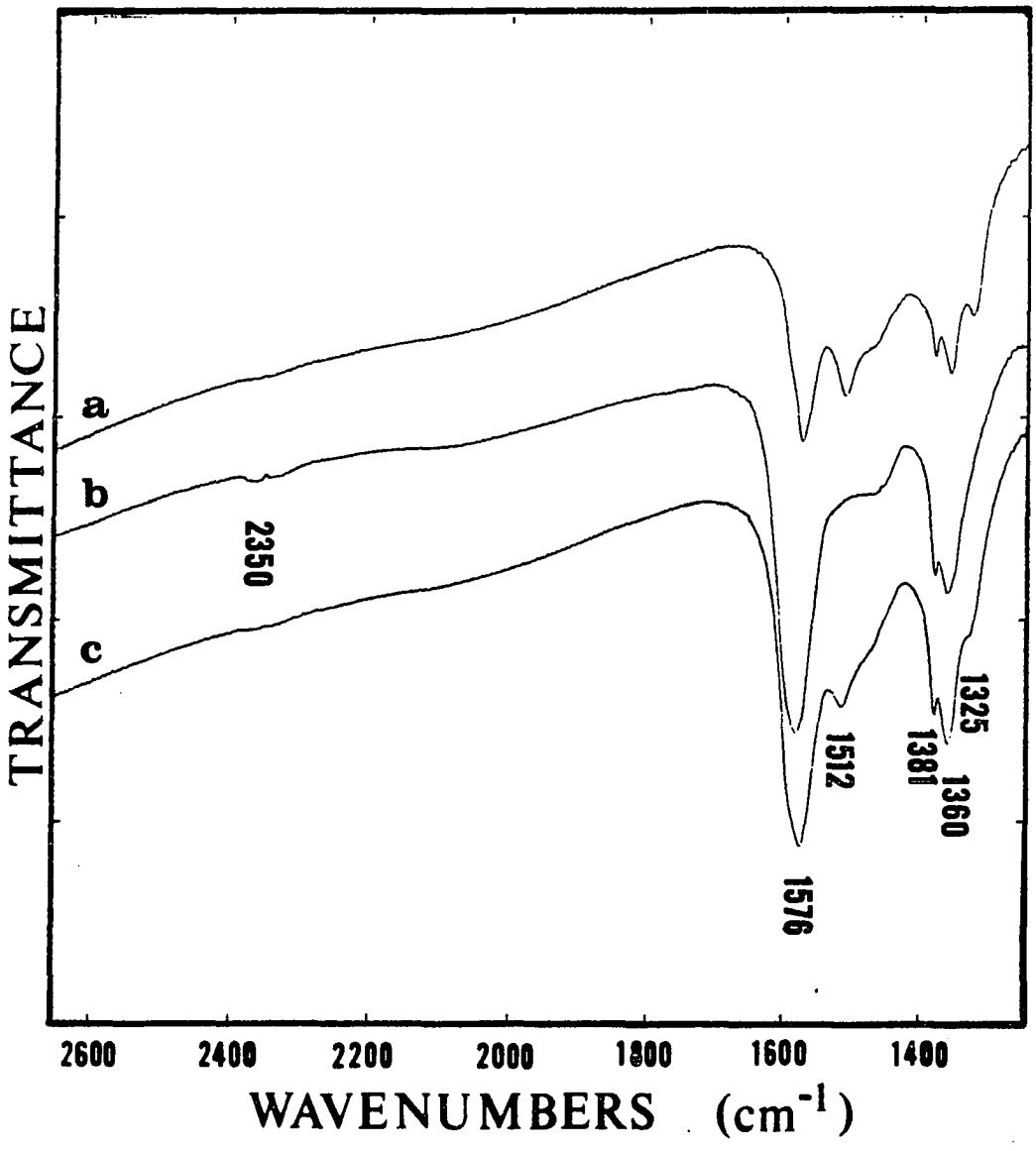

Figure 49. Continued

Figure 50. Adsorption of methanol on 80/10/10 Zn/Cu/Cr oxide at 200°C

a) reduced surface

b) exposure for 1 hour

c) 1 hour after exposure

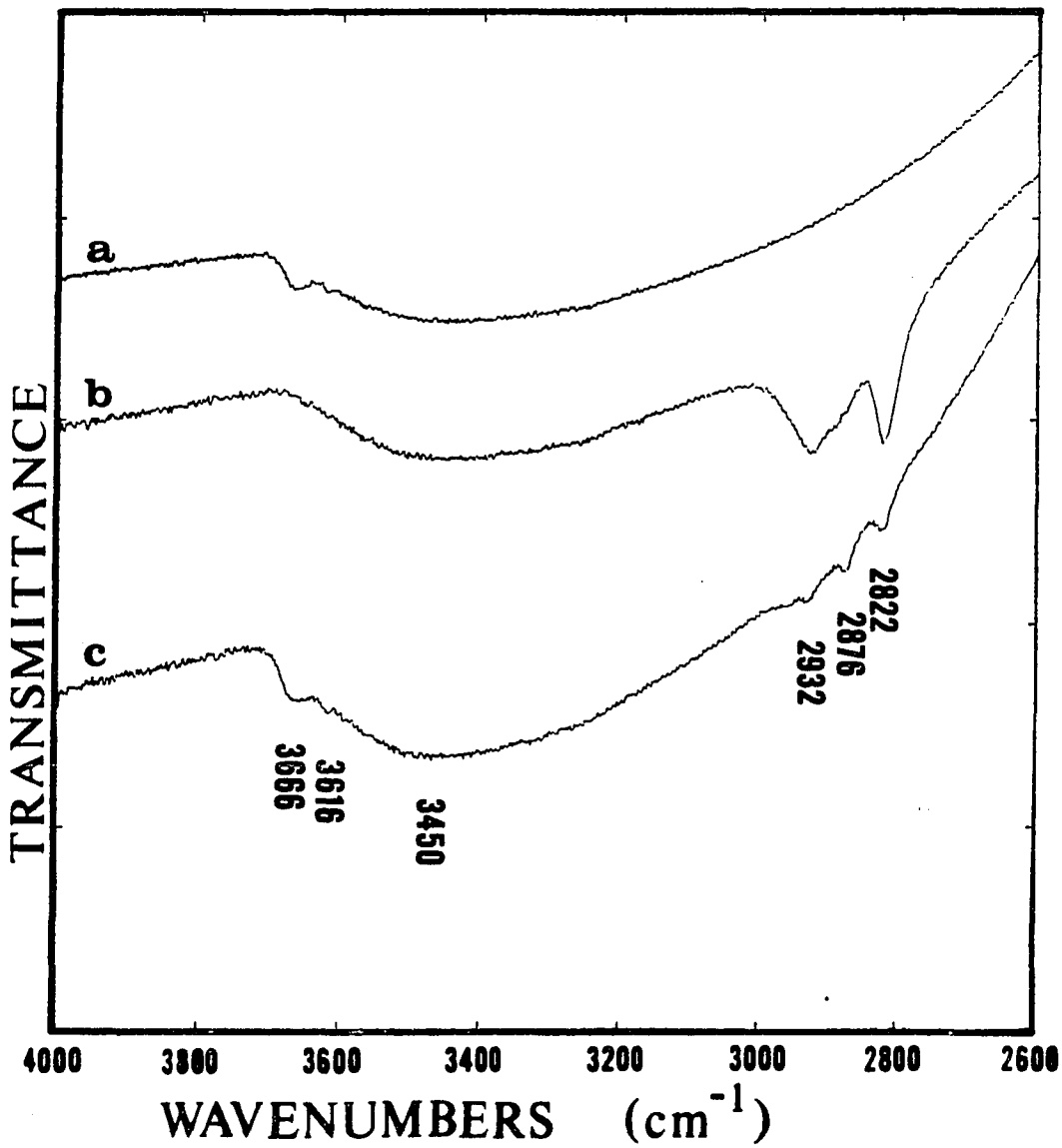
a
b
c
TRANSMITTANCE
3666
3616
3450
2932
2876
2822
4000
3800
3600
3400
3200
3000
2800
2600
WAVENUMBERS (cm-1)

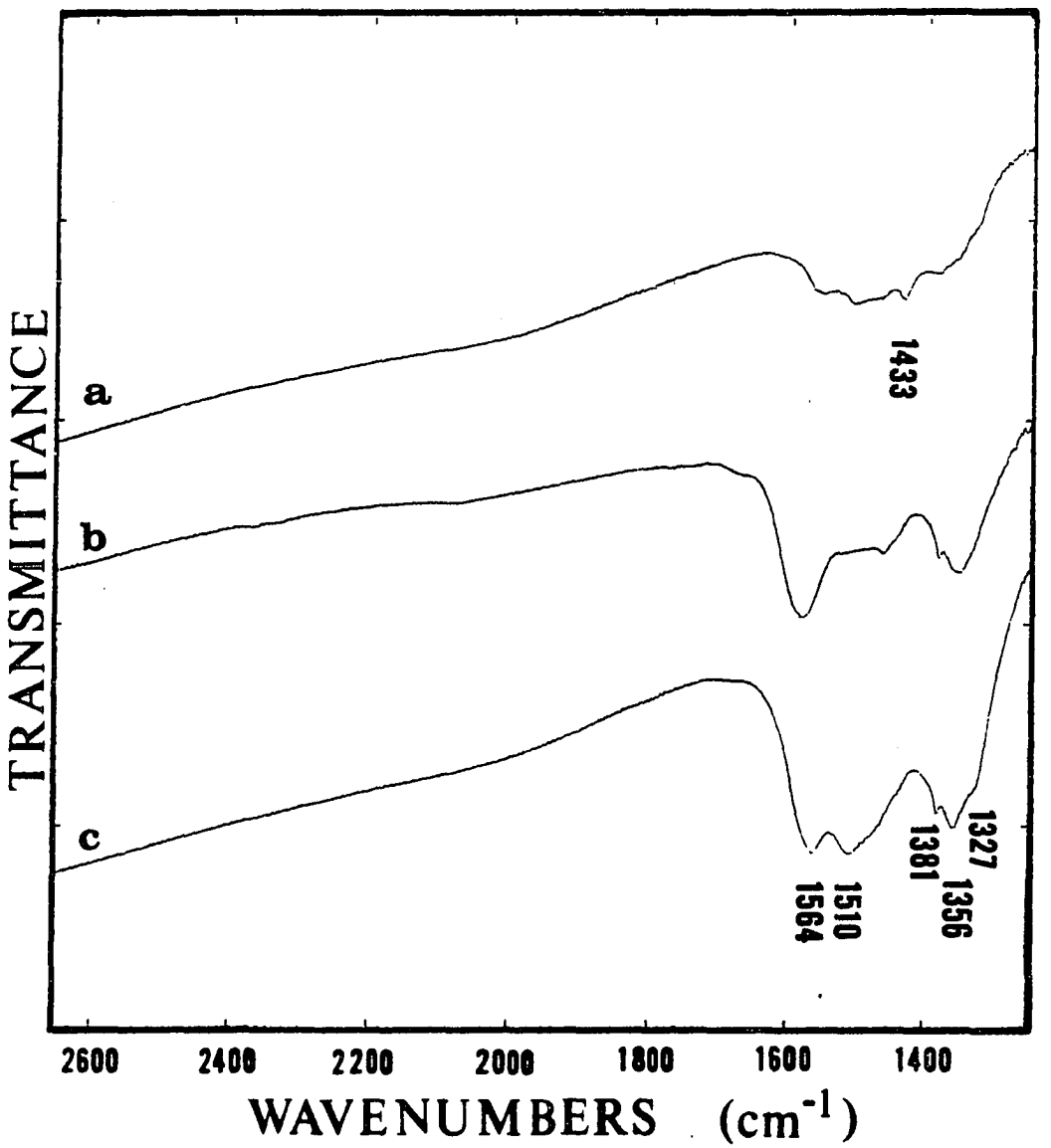

Figure 50. Continued

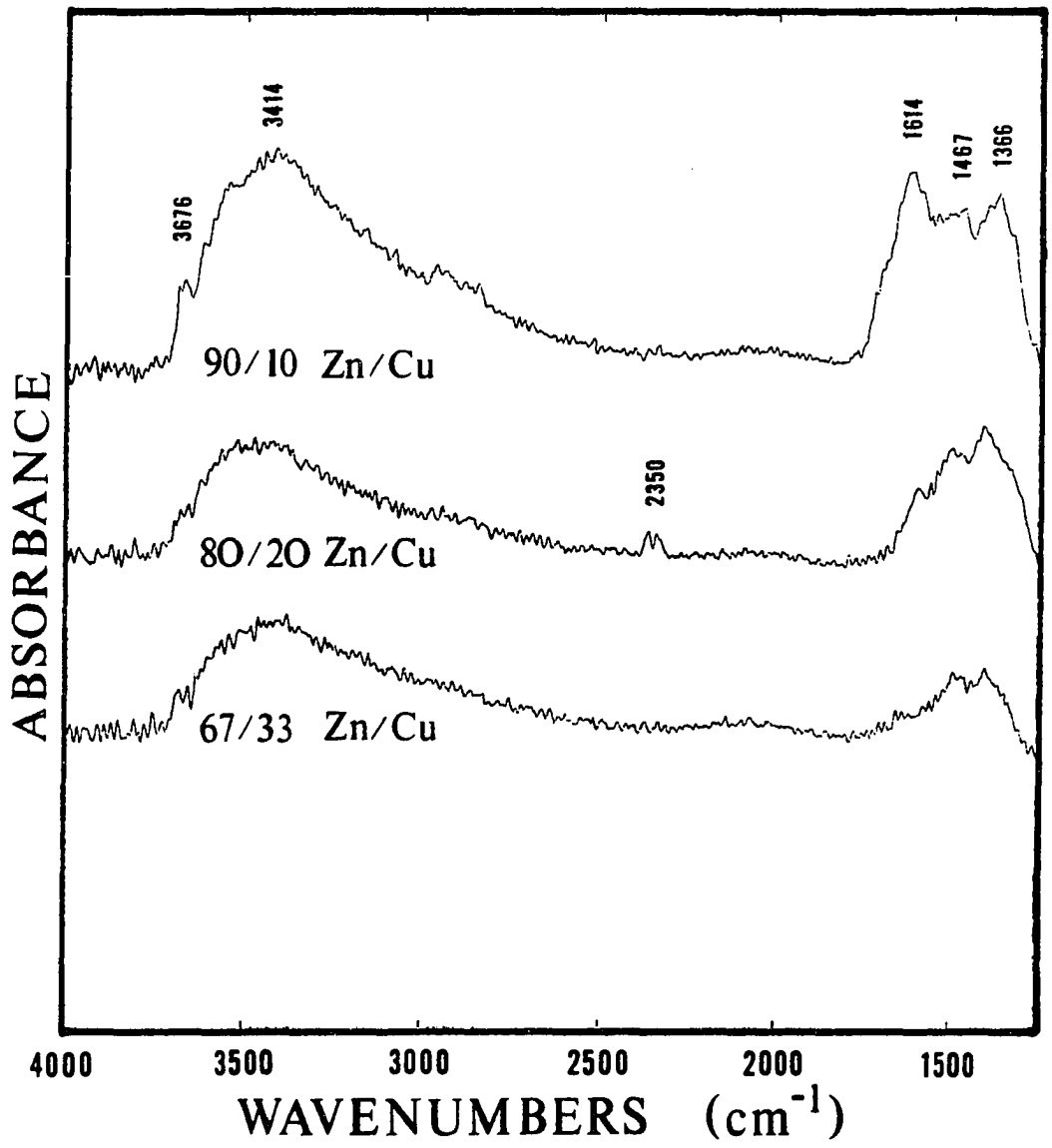

Figure 51. Binary oxides without any pretreatment

the 1700-1300 cm^{-1} region and adsorbed water near 3400 cm^{-1}. A gaseous impurity, carbon dioxide, was present in the spectrum of 80/20 Zn/Cu oxide. These oxides were pretreated at 350°C under vacuum for approximately 12 hours to remove some of the surface contaminants (adsorbed water and residual carbonates). Pretreated samples were transferred into the photoacoustic cell via a dry box to avoid contamination by atmospheric water vapor and carbon dioxide. The spectra of these oxides, shown in Figure 52, were taken with 128 scans at 8 cm^{-1} resolution. The reduction of adsorbed water revealed the isolated hydroxyl groups (bands at 3672 and 3622 cm^{-1}). The amount of residual carbonates (bands at 1535 and 1380 cm^{-1}) decreased as the zinc content of the binary oxide decreased.

The principal objective of this study was to determine if the adsorbed species formed on these binary oxides during exposure to a mixture of carbon monoxide and hydrogen (CO/H_2 = 1/2) were similar. Several binary oxides were heated at 350°C under vacuum for about 12 hours, cooled to 200°C, and exposed to the gas mixture for 4 hours. After cooling to room temperature, the samples were transferred via a dry box into the photoacoustic cell. These samples could not be subjected to a vacuum without decomposition of methoxy, formate, and carbonyl groups occurring. The spectra shown in Figure 53 were taken with 400 scans at 2 cm^{-1} resolution. The 95/5 Zn/Cu oxide had some adsorbed water (band at 3450 cm^{-1}), the hydroxyl band associated with reduced copper (band at 3230 cm^{-1}), methoxy groups (bands at 2935 and 2820 cm^{-1}), formate groups (bands at 2854, 1580, and 1370 cm^{-1}), and a carbonyl species (band at 2102 cm^{-1}). As the copper content of the

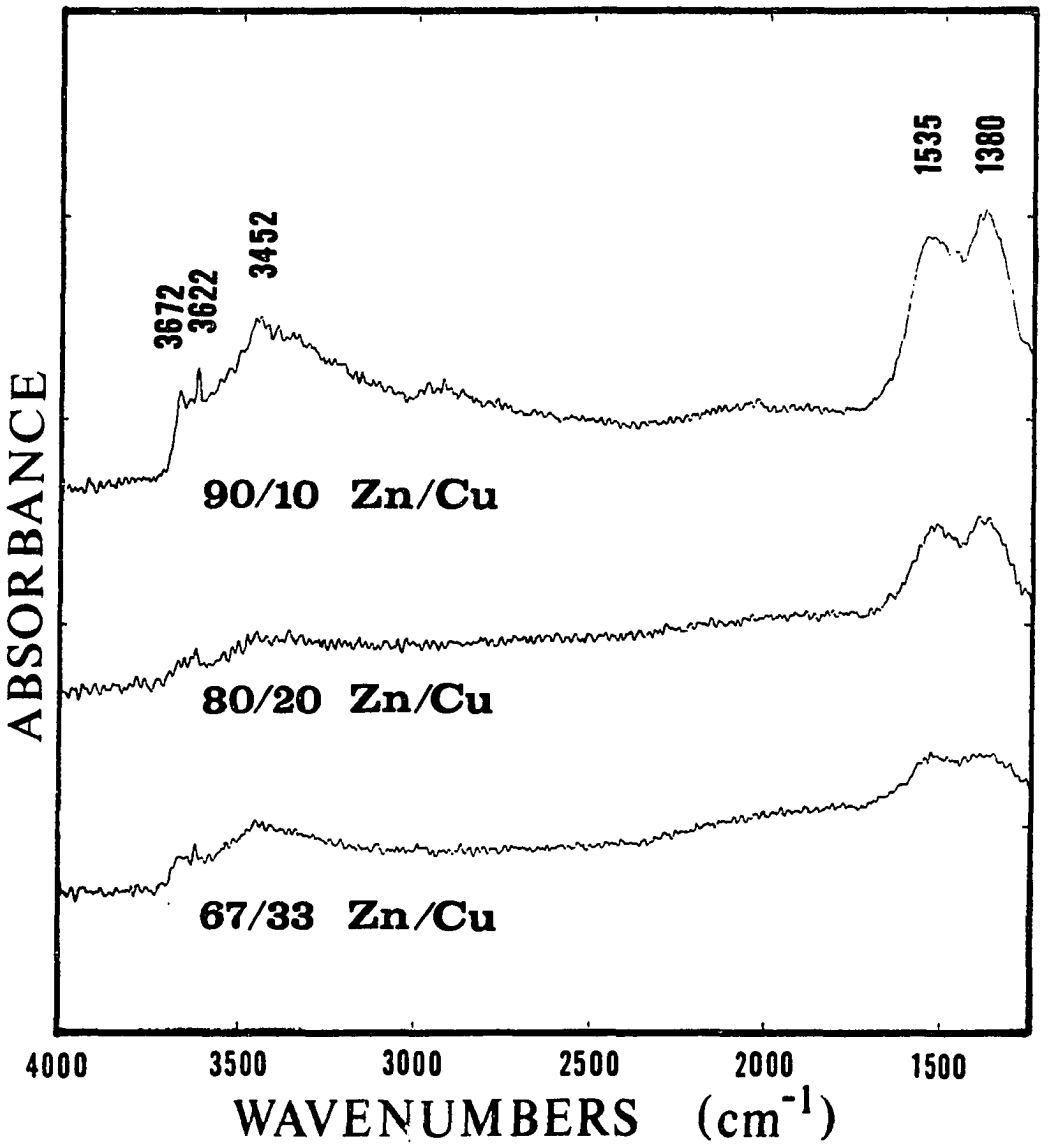

Figure 52. Binary oxides after thermal pretreatment

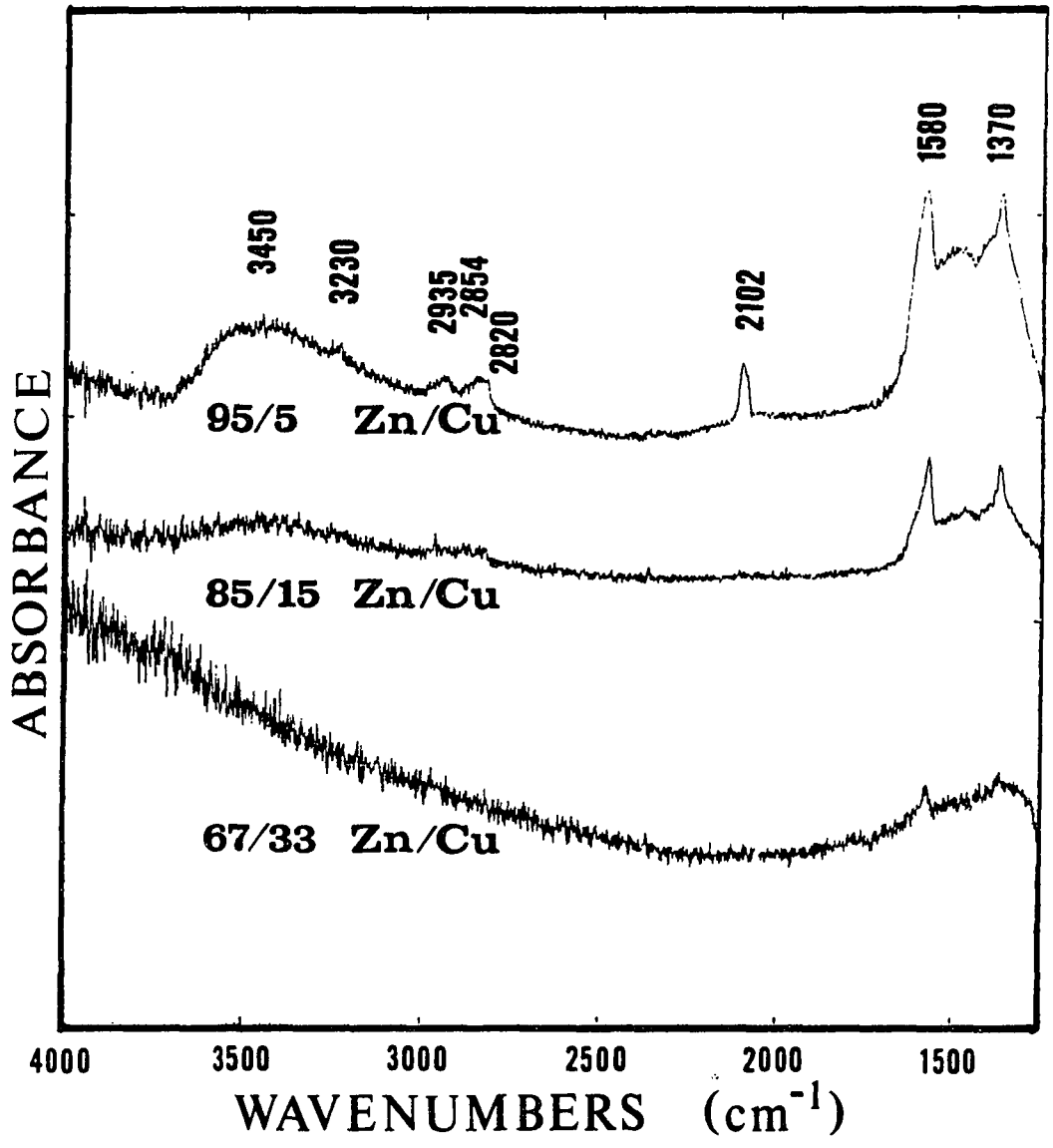

Figure 53. Adsorption of CO-H_2 mixture on binary oxides

oxide increased, the clarity of the photoacoustic spectra decreased to the extent that little information could be obtained from the spectrum of the 67/33 Zn/Cu oxide regarding surface species. The spectrum of the 85/15 Zn/Cu oxide showed a small amount of methoxy groups (bands at 2970 and 2825 cm^{-1}) and formate groups (bands at 1572 and 1370 cm^{-1}). The poor signal-to-noise ratio of these spectra and lack of detail at higher wavenumbers made the assignment of band locations quite difficult.

DISCUSSION OF RESULTS

The infrared spectra of adsorbed species on zinc oxide, binary Zn/Cu oxides, and ternary Zn/Cu/Cr oxides were sufficiently similar that infrared band assignments were applicable to all these oxides. Band positions assigned to various surface species in this discussion should be regarded as approximate because band positions can be affected by the extent of oxide reduction, temperature, surface concentration, and the presence of other species. Most results were obtained at 1 atmosphere and 200°C during flow conditions.

The infrared bands above 3000 cm^{-1} on all of these catalysts have been assigned to hydroxyl groups. Residual hydroxyl groups with bands at 3665, 3620, 3550, and 3450 cm^{-1} existed on both oxidized and reduced catalysts. A small band at 3640 cm^{-1} was also observed on some catalysts that had good transmittance. The sharp, narrow shape of the bands at 3665, 3640, and 3620 cm^{-1} were indicative of isolated hydroxyls, while the broad features of the bands at 3550 and 3450 cm^{-1} suggested that hydrogen bonding occurred among these hydroxyls. All the major hydroxyls readily exchanged with deuterium or deuterium oxide to produce OD bands at 2706, 2667, 2630, and 2560 cm^{-1}, establishing that these hydroxyls were surface species. The differences in the band positions of these hydroxyls have been attributed to the different crystal planes of zinc oxide on which these hydroxyls are located (Atherton et al., 1971).

A hydroxyl species indicated by a band at 3525 cm^{-1} developed when methanol or formic acid was adsorbed on the catalyst surface. An

exchange with deuterated compounds was not possible because this hydroxyl species was unstable at 200°C, but adsorption of deuterated methanol produced an analogous OD band at 2608 cm^{-1}. The dissociation of the hydroxyl hydrogen from the organic molecule during adsorption provided a large amount of atomic hydrogen (possibly as protons) on the surface which temporarily produced this hydroxyl species. At room temperature, this hydroxyl has been observed as a stable species on zinc oxide during hydrogen adsorption and labeled a Type I hydroxyl species (Dent and Kokes, 1969a). This hydroxyl was not formed by hydrogen adsorption at 200°C.

Binary and ternary oxides formed a hydroxyl band at 3250 cm^{-1} during reduction with hydrogen and a band at 2421 cm^{-1} during reduction with deuterium. Isotopic exchange of a hydrogen-reduced surface with deuterium shifted this hydroxyl species extremely slowly, indicating that this hydroxyl was not a surface species. During adsorption experiments, the intensity of this hydroxyl band was totally unaffected by adsorbed species as long as the catalyst remained in a reduced state. Catalyst oxidation with carbon dioxide or water caused this hydroxyl to disappear. These observations suggest that the hydroxyl at 3250 cm^{-1} is a bulk species associated with a reduced form of copper (oxidation state +1 or 0).

Fully oxidized catalysts had some residual carbonate groups on the surface which appeared as infrared bands at 1512, 1470, 1435, 1380, and 1325 cm^{-1}. The changes in band intensities during various surface conditions have indicated that the bands at 1512 and 1325 cm^{-1} belong to the same species, the bands at 1470 and 1380 cm^{-1} belong to another

species, and the band at 1435 cm^{-1} could be assigned to a third carbonate species. Infrared band assignments to specific carbonate and carboxylate complexes on surfaces reported in the literature have been dubious and sometimes contradictory because of the difficulties in making assignments based on comparisons with pure inorganic carbonates. Band frequencies can be affected by surface pretreatments and the temperature of adsorption. A choice must then be made among many different types of complexes that could be formed, e.g., bicarbonate, uncoordinated carbonate ion, unidentate carbonate, bidentate carbonate, and bridging carbonate species. The same carbonate species on zinc oxide with bands at 1530 and 1325 cm^{-1} has been assigned to a unidentate carbonate (Herd et al., 1974), bands at 1540 and 1330 cm^{-1} assigned to a carboxylate species (Bozon-Verduraz, 1970), and bands at 1560-1530 and 1342-1330 cm^{-1} assigned to a bidentate species (Hair, 1967). The single band at 1435 cm^{-1}, which was observed on ternary catalysts, was assigned to an uncoordinated carbonate ion. A carbonate ion on zinc oxide has been previously reported at 1430 cm^{-1} (Matsushita and Nakata, 1962). Based on the general assignments for unidentate and bidentate carbonate complexes given by Nakamoto (1978), the bands at 1470 and 1380 cm^{-1} were assigned to the asymmetric and symmetric O-C-O stretching frequencies of a unidentate carbonate species, while the bands at 1512 and 1325 cm^{-1} were assigned to the asymmetric and symmetric O-C-O stretching frequencies of a bidentate carbonate species, respectively.

The adsorption of carbon monoxide on zinc oxide was the same as previously reported by Taylor and Amberg (1961). A very weak band was observed at 2200 cm^{-1} after a brief flush with N_2 to remove the masking

by gaseous carbon monoxide. This band was assigned to a σ-bonded carbonyl species. A more intense band was observed near 2090 cm^{-1} on the binary and ternary oxides. This stretching frequency was in the 2080-2110 cm^{-1} region for π-bonded carbonyls on metallic copper (Pritchard and Sims, 1970; Pritchard et al., 1975; Horn and Pritchard, 1976). Although no infrared studies have been reported for carbon monoxide adsorption on cuprous oxide, carbonyl frequencies on copper(I) organometallic complexes have been characterized recently. The carbonyl frequencies, given in Table 13, fall into the 2050-2117 cm^{-1} region. Thus, the band near 2090 cm^{-1} on binary and ternary oxides was assigned to the stretching frequency of a carbonyl species adsorbed on a reduced copper site. The oxidation state of the reduced site could be either Cu(I) or copper metal.

Formate groups were formed by the hydrogenation of carbon monoxide and dioxide, the adsorption of formic acid, and the decomposition of methanol. Infrared bands at 2875, 1380, 1575, and 1365 cm^{-1} were assigned to the fundamental C-H stretching, C-H bending, asymmetric O-C-O stretching, and symmetric O-C-O stretching frequencies, respectively. Two additional bands at 2966 and 2740 cm^{-1} were assigned to combinations of fundamental frequencies; the former band was a combination of the C-H bending and asymmetric O-C-O stretching frequencies, while the latter band was a combination of the C-H bending and symmetric O-C-O stretching frequencies. These combined frequencies have been observed in the infrared spectra of inorganic formates. The infrared bands of some inorganic formates are given in Table 14. Infrared bands of a deuterated formate at 2166, 1575, and 1335 cm^{-1} were assigned to the

Table 13. Organometallic copper(I) complexes

Copper(I) complex	ν_{CO}, cm^{-1}	Reference
$[HB(C_3N_2H_3)_3]Cu(CO)$	2083	Churchill et al., 1975
$Cu(LBF_2)(CO)$	2068	Gagné et al., 1977
$[Cu(en)CO](BPh_4)$	2117	Pasquali et al., 1978
$[Cu(dien)CO](BPh_4)$	2080	Pasquali et al., 1978
$[Cu_2(tmen)_2(CO)_2Cl](BPh_4)$	2065	Pasquali et al., 1979
$[Cu_2(hm)_3(CO)_2](BPh_4)_2$	2055, 2066	Pasquali et al., 1980b
$[Cu(hm)CO](BPh_4)$	2091	Pasquali et al., 1980b
$[Cu(en)_2CO]I$	2060	Pasquali et al., 1980a
$[Cu_2(en)_3(CO)_2]I_2$	2062	Pasquali et al., 1980a
$[Cu_2(en)_3(CO)_2](BPh_4)_2$	2078	Pasquali et al., 1980a
CuCO(O-t-Bu)	2063	Geerts et al., 1983
$Cu(acac)(CO)_2$	2100	Chow and Buono-Core, 1983
$[Cu(q)CO]_4$	2050	Pasquali et al., 1983

fundamental C-D stretching, asymmetric O-C-O stretching, and symmetric O-C-O stretching frequencies, respectively.

Methoxy groups were also formed by the hydrogenation of carbon monoxide, the adsorption of formic acid, and the adsorption of methanol. Infrared bands at 2935 and 2820 cm^{-1} were assigned to the fundamental asymmetric and symmetric CH_3 stretching frequencies, respectively. Deuterated methoxy groups had infrared bands at 2220 and 2056 cm^{-1} which were assigned to asymmetric and symmetric CD_3 stretching frequencies, respectively. Infrared frequencies of methoxy groups were

Table 14. Infrared band assignments for inorganic formates

Fundamental frequencies, cm^{-1}	$NaHCO_2$ [a]	$NaHCO_2$ [b]	$NaHCO_2$ [c]	$NaHCO_2$ [d]	$Ca(HCO_2)_2$ [c]	$NaDCO_2$ [c]
$\nu_1(A_1)$ C-H stretching	2870	2841	2828	2828	2868	2130
$\nu_2(A_1)$ symmetric C-O stretching	1377	1366	1355	1364	1359	1327
$\nu_3(A_1)$ symmetric C-O bending	784	772	769	773	778	762
$\nu_4(B_1)$ asymmetric C-O stretching	1620	1567	1590	1600	1618	1580
$\nu_5(B_1)$ in-plane C-H bending	1365	1377	1385	1364	1386	1010
$\nu_6(B_2)$ out-of-plane C-H bending	1070	1073	1062	1070	1072	912
Binary frequencies, cm^{-1}						
ν_2 and ν_5	2750	2720	2715	2716	2694	–
ν_4 and ν_5	2990	2953	2950	2952	2942	–

[a] Newman, 1952.

[b] Ito and Bernstein, 1956.

[c] Harvey et al., 1963.

[d] Hammaker and Walters, 1964.

very similar to the infrared frequencies of liquid methanol. Liquid CH_3OH has asymmetric and symmetric CH_3 stretching frequencies at 2934 and 2822 cm^{-1}, respectively; liquid CD_3OD has asymmetric and symmetric CD_3 stretching frequencies at 2225 and 2082 cm^{-1}, respectively (Pinchas and Laulicht, 1971).

Infrared bands were formed at 2935, 2850, 2740, and 1600 cm^{-1} during the hydrogenation of carbon dioxide and the adsorption of formaldehyde. The assignment of these bands to a weakly adsorbed formaldehyde species was made since the CH_2 scissoring overtone, the out-of-phase CH_2 stretching, the in-phase CH_2 stretching, and the C=O stretching frequencies of gaseous formaldehyde occur at 2973, 2874, 2780, and 1745 cm^{-1}, respectively (Pinchas and Laulicht, 1971). The large shift in the C=O stretching frequency indicated that the formaldehyde species was adsorbed on the surface through the oxygen end of the molecule. The adsorption of a formaldehyde molecule on hematite (α-Fe_2O_3) produced infrared bands at 2920, 2870, 2770, and 1620 cm^{-1} (Busca and Lorenzelli, 1980). The possibility that this surface species might be a formyl group seems less likely. Infrared bands at 2770 and 2661 cm^{-1}, formed during CO hydrogenation on zinc were assigned to a formyl species (Saussey et al., 1982). The C-H and C=O stretching frequencies for various organometallic complexes containing a formyl ligand, reported in Table 15, have C-H stretching frequencies lower than those observed in this study.

Formate groups were formed during carbon monoxide adsorption on zinc oxide, binary oxides, and ternary oxides, demonstrating that surface hydrogen mobility at 200°C was increased by oxide reduction since

Table 15. Organometallic formyl complexes

Metallo-formyl complex	ν_{CO}, cm^{-1}	ν_{CH}, cm^{-1}	Reference
$(CO)_4Fe(CHO)^-N(PPh_3)_2^+$	1607	2690 2540	Collman and Winter, 1973
$Os(CHO)H(CO)_2(PPh_3)_2$	1601	2760 2680 2540	Brown et al., 1979
$[IrH(CHO)(P(CH_3)_3)_4]PF_6$	1600	2622	Thorn, 1980
RhOEP(CHO)	1700	—	Wayland and Woods, 1981
$[Ru(CHO)CO(Ph_2PCH_2PPh_2)]_2$	1600	2585	Smith and Cole-Hamilton, 1982
$[Ru(CHO)CO(Ph_2PCH_2)_2]_2$	1596	2550	Smith and Cole-Hamilton, 1982

no hydrogen was available from the gas phase. Formate formation was enhanced by the presence of gaseous hydrogen, presumably by increasing the amount of adsorbed hydrogen although no new hydroxyl or hydride species were observed. Carbon monoxide hydrogenation developed methoxy groups on binary and ternary oxides but not on zinc oxide at 200°C. Carbon dioxide hydrogenation on binary oxides at 200°C formed formate and some adsorbed formaldehyde groups but few methoxy groups, even when the gas phase was completely replaced with hydrogen. These results showed that the adsorbed carbonyl species on a reduced copper site was necessary for the formation of a methoxy group from a formate group at 200°C. Carbon monoxide hydrogenation at 100°C easily developed the copper carbonyl species but hydrogenation to formate species was very slow and no methoxy groups were formed. Thus, at 200°C, the primary function of copper in methanol synthesis catalysts was to activate carbon monoxide by forming an adsorbed carbonyl species. This carbonyl species enhanced the hydrogenation of formate groups to methoxy groups.

Formate acid decomposition on zinc oxide simply formed formate groups that decomposed to CO_2 (any H_2 formed could not be observed). Formic acid decomposition on binary and ternary oxides produced formate, methoxy, and a new hydroxyl species. Since there was no carbonyl species on these reduced surfaces, the hydrogenation of formate to methoxy groups arose from the unstable hydrogen added to the surface by the dissociative adsorption of formic acid (Type I hydrogen). At 200°C, the zinc hydride species was too unstable to be observed in the infrared spectra. The amount of gaseous hydrogen present during formic acid decomposition had no effect on the rate of methoxy formation, indicating

that an Eley-Rideal mechanism for formate hydrogenation to methoxy species was unlikely.

Methanol adsorption occurred by dissociative chemisorption to produce a methoxy and hydroxyl species and by the reaction of methanol with a surface hydroxyl to produce a methoxy species and water. The disappearance of isolated hydroxyl groups (bands at 3665 and 3620 cm^{-1}) during methanol adsorption was evidence of the reaction of methanol with surface hydroxyls. The development of the hydroxyl species at 3525 cm^{-1} (Type I hydrogen) was evidence of the dissociative chemisorption. The adsorption of isotopic methanol clearly showed that the hydrogen in the new hydroxyl species came from the hydroxyl hydrogen in the methanol molecule. Methoxy groups decomposed to formate groups, accompanied by the gradual appearance of the isolated hydroxyls.

Formaldehyde adsorption at 100°C produced an adsorbed formaldehyde species that caused the disappearance of isolated hydroxyl groups. Decomposition of adsorbed formaldehyde produced formate groups. Formaldehyde adsorption at 200°C formed methoxy and formate species. At this higher temperature, adsorbed formaldehyde was not stable under reducing conditions but the hydrogen from the decomposition of formaldehyde was readily utilized to form methoxy groups. No hydroxyl band was observed at 3525 cm^{-1}, indicating that formaldehyde adsorption was not dissociative and that hydrogenation of this unstable formaldehyde species was more favorable than the formation of a Type I hydroxyl group during decomposition.

A few concluding remarks have been addressed to the nature of surface sites for adsorbed species. The only species believed to be

adsorbed on copper sites was the carbonyl near 2090 cm^{-1}. All other species were adsorbed on zinc oxide. Isolated hydroxyl groups have been associated with polar ZnO surfaces and hydrogen-bonded hydroxyl groups associated with nonpolar ZnO surfaces using geometric arguments (Atherton et al., 1971). The band intensities of the bidentate carbonate species varied inversely with those of the formate species, suggesting that the same surface site was involved. Carbonate formation on zinc oxide has been found to occur on dehydroxylated sites (Morimoto and Morishige, 1975); these dehydroxylated sites have been associated with the sites of hydrogen-bonded hydroxyls (Atherton et al., 1971). The formation of carbonate and formate groups did not affect the isolated hydroxyls, but the formation of adsorbed formaldehyde and methoxy groups caused these isolated hydroxyls to disappear. Thus, it appears that adsorbed formaldehyde, methoxy, and isolated hydroxyls are all adsorbed on the same sites, which are zinc atoms on the polar ZnO surfaces. Formaldehyde was produced during the decomposition of methanol on a polar ZnO surface but not on any other type of surface (Cheng and Kung, 1982). The remaining species, the Type I hydroxyl at 3525 cm^{-1}, apparently adsorbs on an energetic surface or defect site. Because both formic acid and methanol adsorption produced this hydroxyl species, it will be proposed that stepped surfaces between polar and nonpolar planes are the sites for this hydroxyl group.

PART III.

IN SITU CHARACTERIZATION OF METHANOL SYNTHESIS CATALYSTS

LITERATURE REVIEW

Thermodynamics

Carbon monoxide and hydrogen can react to form a great variety of products. Some of the possible reactions are:

$$CO + H_2 = HCHO \quad (1)$$

$$CO + 2H_2 = CH_3OH \quad (2)$$

$$CO + 3H_2 + CH_4 + H_2O \quad (3)$$

$$2CO + 2H_2 = CH_4 + CO_2 \quad (4)$$

$$2CO = CO_2 + C \quad (5)$$

$$2CO + 4H_2 = (CH_3)_2O + H_2O \quad (6)$$

$$nCO + 2nH_2 = C_nH_{2n} + nH_2O \quad (7)$$

$$nCO + (2n+1)H_2 = C_nH_{(2n+2)} + nH_2O \quad (8)$$

$$nCO + 2nH_2 = C_nH_{(2n+1)}OH + (n-1)H_2O \quad (9)$$

$$(n+1)CO + 2nH_2 = C_nH_{(2n+1)}COOH + (n-1)H_2O \quad (10)$$

An important reaction involving products from previous reactions is:

$$CO_2 + 3H_2 = CH_3OH + H_2O \quad (11)$$

Because the desired product is methanol, the reaction conditions should be chosen to favor reaction 2 while minimizing the others. Free energies of reaction for several of these reactions are given in Table 16; over the range of practical temperatures, the formation of methanol from carbon monoxide and hydrogen is least favorable. Methanol synthesis can be enhanced by using high pressures since the molar reduction for reaction 2 is greater than the others with the exceptions of dimethyl

Table 16. Free energy of reaction[a]

T, °K	ΔG° (kcal/mol)				
	300°	400°	500°	600°	700°
Reaction (2)	- 6.3	- 0.8	5.0	10.8	16.7
Reaction (3)	-33.9	-28.6	-23.0	-17.3	-11.4
Reaction (4)	-40.7	-34.4	-27.9	-21.2	-14.5
Reaction (5)	-28.6	-24.3	-20.0	-15.7	-11.4
Reaction (7)	-27.2	-19.3	-11.1	- 2.7	5.9
Reaction (8)	-51.3	-40.5	-29.2	-17.6	- 5.9

[a]Natta, 1955.

ether (reaction 6) and ethanol (n = 2 in reaction 9) formation. A catalyst is required to selectively form methanol.

The methanol content at equilibrium is determined from the equilibrium constant:

$$K = f_{CH_3OH}/(f_{CO})(f_{H_2})^2 \tag{12}$$

Using the subscripts CH_3OH = 1, CO = 2, and H_2 = 3, then

$$K = p_1\gamma_1/(p_2\gamma_2)(p_3\gamma_3)^2 \tag{13}$$

$$= K_y K_\gamma \tag{14}$$

where K_y is the equilibrium constant at low pressures and K_γ is the fugacity coefficient ratio. Numerical equations for K have been developed by Cherednichenko (Strelzoff, 1970):

$$\log K = 3971T^{-1} - 7.492 \log T + 0.00177T - 3.11 \times 10^{-8}T^2 + 9.218 \quad (15)$$

and by Thomas and Portalski (1958):

$$\log K = 3921T^{-1} - 7.971 \log T + 0.00250T - 2.95 + 10^{-7}T^2 + 10.20 \quad (16)$$

Values for K_γ are shown in Figure 54, as calculated and plotted by Ewell (1940). Rearranging Equation 13 and using mole fractions, the methanol mole fraction is:

$$y_1 = Ky_2y_3^2P^2/K_\gamma \quad (17)$$

Since K decreases with increasing temperature and K_γ increases with increasing temperature, the temperature for methanol synthesis should be as low as practicable to maximize conversion.

The reaction is strongly exothermic ($\Delta H^\circ_{298^\circ K} = -21.7$ kcal/mol). A numerical expression for the heat of reaction is (Thomas and Portalski, 1958):

$$\Delta H^\circ_T = -17,920 - 15.84T + 0.01142T^2 = 2.699 \times 10^{-6}T^3 \quad (18)$$

and at elevated pressures:

$$\Delta H_{T,P} = \Delta H^\circ_T - 0.5411P - 3.255 \times 10^6 P/T^2 \quad (19)$$

Because the heat of reaction increases with increased pressure, methanol reactors must be designed for large amounts of heat removal to maintain adequate conversion and to protect the catalyst from deactivation.

A more fundamental approach for determining equilibrium concentra-

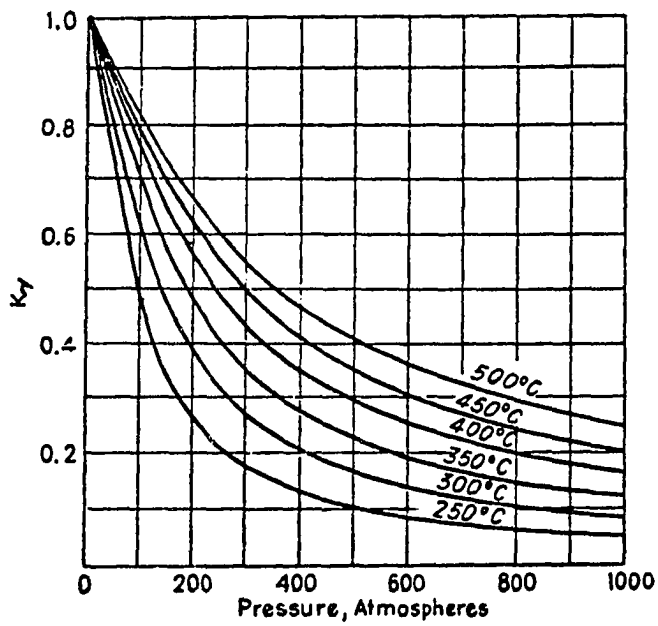

Figure 54. Values of K_γ (Ewell, 1940)

tions requires information about the free energy of formation, heat of formation, heat capacity, and fugacity coefficient of each component in the reaction. The equilibrium constant can also be expressed as:

$$K = \exp[-\Delta G/RT] = \exp[-\Sigma \nu_i \Delta G_i/RT] \tag{20}$$

For the methanol synthesis reaction at 298°K and 1 atm:

$$\Delta G^o = \Delta G^o_{CH_3OH} - \Delta G^o_{CO} - 2\Delta G^o_{H_2}$$

Values for ΔG^o_i can be obtained from Table 17, giving a value:

$$\Delta G^o = -38.6 + 32.8 = -5.8 \text{ kcal/gmol}$$

The standard-state equilibrium constant becomes:

$$K^o = \exp[5800/(1.99)(298)] = 1.8 \times 10^4$$

The effect of temperature on the equilibrium constant can be determined using the van't Hoff equation:

$$\left(\frac{\partial \ln K}{\partial T}\right)_P = \frac{\Delta H^o_T}{RT^2} \tag{21}$$

The heat of formation is calculated from the expression:

$$\Delta H^o_T = \Delta H^o + \int_{T_o}^{T} \Delta C^o_P dT \tag{22}$$

where the standard-state heat of formation, ΔH^o, can be expressed as:

$$\Delta H^o = \Sigma \nu_i \Delta H_i \tag{23}$$

and the heat capacity of the reaction mixture is:

$$\Delta C^o_P = \Sigma \nu_i C^o_{P_i} \tag{24}$$

Table 17. Heat and free energy of formation[a]

Compound	ΔH^o_{298}, kcal/mol	ΔG^o_{298}, kcal/mol
CH_3OH	-48.08	-38.62
H_2	0.0	0.0
CO	-26.416	-32.808
CO_2	-94.052	-94.260
H_2O	-57.798	-54.635
HCOOH	-86.67	-80.24
HCHO	-28.29	-26.88

[a]Chemical Engineers' Handbook, 1973.

Values for ΔH^o_i are given in Table 17. The heat capacity is temperature dependent, and may be expressed as:

$$C^o_{pi} = a + bT + cT^2 + dT^3 \tag{25}$$

where values for the constants are given in Table 18. Substituting Equations 25 and 22 into Equation 21, and integrating yields the expression:

$$\begin{aligned} \ln K = \ln K^o &+ (\Delta a/R)\ln(T/T_o) + (\Delta b/2R)(T - T_o) \\ &+ (\Delta c/6R)(T^2 - T_o^2) + (\Delta d/12R)(T^3 - T_o^3) \\ &+ \frac{1}{R}\left[-\Delta H^o + \Delta a T_o + \frac{\Delta b}{2} T_o^2 + \frac{\Delta c}{3} T_o^3 + \frac{\Delta d}{4} T_o^4\right]\left[\frac{1}{T} - \frac{1}{T_o}\right] \end{aligned} \tag{26}$$

The temperature of the reaction is T and the standard-state temperature, T_o, is 298°K. The effect of pressure on the equilibrium concentrations

Table 18. Heat capacity[a]

Compound	$c_p^o = a + bT + cT^2 + dT^3$, cal/mol-°K			
	a	b x 10^2	c x 10^5	d x 10^9
CH_3OH	5.052	1.694	0.6179	-6.811
H_2	6.483	0.2215	-0.3298	1.826
CO	7.373	-0.307	0.6662	-3.037
CO_2	4.728	1.754	-1.338	4.097
H_2O	7.701	0.04595	0.2521	-0.859
HCOOH	2.798	3.243	-2.009	4.187
HCHO	5.607	0.7540	0.7130	-5.494

[a]Reid et al., 1977.

can be determined by calculating the value of the fugacity coefficient ratio:

$$K = K_y K_\gamma = [\prod_i (y_i^{\nu_i})][\prod_i (f/p)_i^{\nu_i}](\frac{P}{1\ atm})^{\Sigma\nu_i} \qquad (27)$$

Using the critical properties given in Table 19, reduced pressures and temperatures are calculated and used with Figure 55 to estimate fugacity coefficients. The mole fraction of methanol can then be expressed as:

$$y_1 = Ky_2y_3^2P^2(f/P)_2(f/P)_3^2/(f/P)_1 \qquad (28)$$

The detailed numerical results for several reactions are given in Appendix C, using a stoichiometric mixture of reactants at 200°C and 50 atmospheres. Table 20 gives reduced pressures, reduced temperatures, and fugacity coefficients at these conditions. Methanol formation is

Table 19. Critical properties[a]

Compound	T_c, °K	P_c, atm
CH_3OH	512.6	79.9
H_2	33.2	12.8
CO	132.9	34.5
CO_2	304.2	72.8
H_2O	647.3	217.6
HCOOH	580.	(70.)[b]
HCHO	408.	65.

[a]Reid et al., 1977.

[b]Estimate, acetic acid plus 10 atm.

Table 20. Fugacity coefficients at 200°C and 50 atmospheres

Compound	T_R	P_R	f/P
CH_3OH	0.92	0.63	0.70
CO	3.56	1.45	0.98
H_2	14.2	3.91	1.03
H_2O	0.73	0.23	0.38
CO_2	1.56	0.69	0.96
HCOOH	0.82	0.70	0.30
HCHO	1.16	0.77	0.85

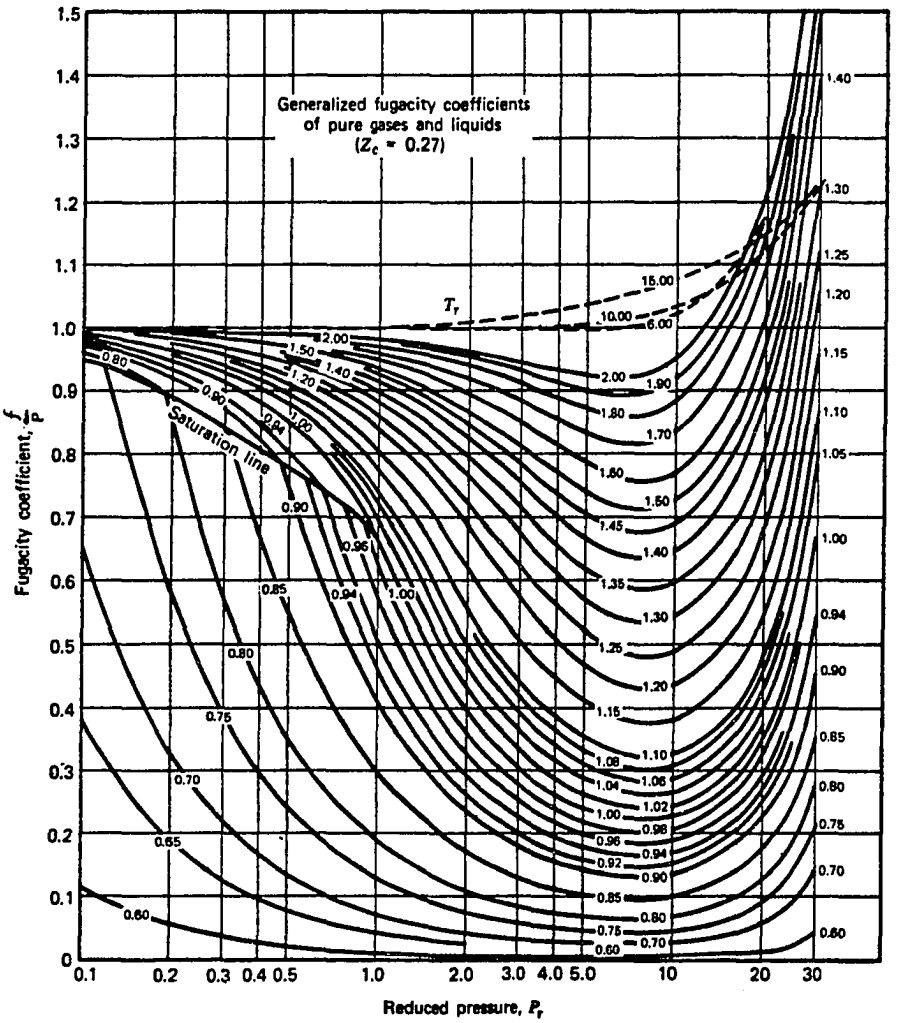

Figure 55. Generalized fugacity chart (Hougen et al., 1960)

favorable in carbon monoxide hydrogenation, carbon dioxide hydrogenation, formic acid hydrogenation, and formaldehyde hydrogenation.

Mixed metal oxides having compositions very similar to those used for methanol synthesis catalyze the water-gas shift reaction (Newsome, 1980). The methanol synthesis and water-gas shift reactions could occur at the same time on the catalyst and might involve a common intermediate. A surface formate has been determined to be an intermediate species on ZnO (Ueno et al., 1970) and on Cu/ZnO catalysts (van Herwijnen and de Jong, 1980; van Herwijnen et al., 1980) during studies of the water-gas shift reaction. The thermodynamics of the water-gas shift reaction, using a stoichiometric mixture of reactants at 200°C and 50 atmospheres, are given in Appendix D. The products were strongly favored under these conditions.

Kinetics

Although thermodynamics establishes the maximum possible conversion of carbon monoxide and hydrogen to methanol, the actual methanol yield also depends on the rate of reaction. Because the reaction is heterogeneous, the overall rate of reaction may depend on rates of adsorption of the reactants, surface reaction rates, and the rate of product desorption. Rate expressions are derived from reaction schemes involving a sequence of elementary steps with various assumptions concerning the assignment of the rate determining step. Kinetic data are applied to the rate expressions to determine rate constants for those models compatible with the data and to discard those models in which the data

will not fit.

Using the method of Hougen and Watson (1943), Natta developed an expression for the rate of methanol synthesis on a zinc oxide-chromia catalyst and a ternary $ZnO\text{-}CuO\text{-}Cr_2O_3$ catalyst assuming that a trimolecular surface reaction was rate determining (Natta, 1955):

$$r = \frac{f_{CO}f_{H_2}^2 - f_{CH_3OH}/K}{(A + Bf_{CO} + Cf_{H_2} + Df_{CH_3OH})^3} \qquad (29)$$

The values of the empirical rate constants A, B, C, and D were dependent on the catalyst and experimental conditions. During the two decades since Natta's work, experimental data have been successfully applied to other kinetic models with significantly different assumptions concerning the rate determining step. Various models have assumed that the adsorption of hydrogen, a bimolecular surface reaction, the reaction of adsorbed hydrogen with a methoxy species, a Rideal-type reaction between gaseous hydrogen and a surface formaldehyde species, or the desorption of methanol was the rate determining step (Denny and Whan, 1978). In most expressions, the rate of reaction was found to be proportional to $(P_{CO}P_{H_2}^2)^n$, where n had values between 0.5 and 1.

The industrial reaction mixture normally contains some carbon dioxide in the feed to improve the activity for methanol synthesis. The role of carbon dioxide has been described both as a primary reactant and as an oxidant to maintain the catalyst in an active state. At first glance, the extent of CO_2 hydrogenation to methanol appears to be easily determined by simply measuring the amount of water formed. However, as a result of the water-gas shift reaction, the amount of water in the gas phase would be quite small at equilibrium conditions. If the reaction

rate for the water-gas shift occurs more rapidly than methanol synthesis from carbon dioxide, it would be possible for the carbon dioxide concentration to remain constant and the water concentration to be very low even during CO_2 hydrogenation to methanol.

Experimental studies of methanol synthesis by Rozovskii and coworkers during the past decade have shown that carbon dioxide was hydrogenated to methanol under reaction conditions. Methanol was formed from a feed containing CO, CO_2, and H_2 but synthesis activity ceased when CO_2 was removed from the gas phase (Rozovskii et al., 1975). Studies of methanol synthesis from CO_2 and H_2, taking into account the CO formed by the water-gas shift reaction, showed no correlation between methanol yield and CO concentrations for various contact times; in some cases, the methanol yield exceeded the equilibrium amount for CO hydrogenation (Kagan et al., 1976; Kuznetsov et al., 1983). Using feed mixtures containing either isotopic CO or CO_2, radioactivity measurements of the reaction products established that methanol was formed by direct hydrogenation of carbon dioxide and provided estimates of reaction rates for individual steps, i.e., water-gas shift and methanol synthesis (Rozovskii et al., 1977; Rozovskii, 1980). High concentrations of CO_2 decreased the product yield by oxidative dehydrogenation of methanol (Rozovskii et al., 1976a):

$$CH_3OH + CO_2 = 2CO + H_2 + H_2O \qquad (30)$$

Klier and coworkers have also investigated the effect of carbon dioxide on methanol synthesis (Klier et al., 1982). Carbon dioxide was hydrogenated to methanol but at a lower rate than carbon monoxide hydro-

genation. The loss of methanol synthesis activity when using a feed of only CO and H_2 was attributed to deactivation of active surface sites due to strong reduction of the catalyst rather than the reactivity of feed itself. This conclusion was based on an increase in the rate of methanol synthesis by small additions of water or oxygen as well as carbon dioxide. The decrease in the rate of methanol synthesis at higher CO_2 concentrations was attributed to strong CO_2 adsorption on the same sites involved in the adsorption of carbon monoxide and hydrogen. A kinetic rate expression incorporating both the promoting and inhibiting effects of carbon dioxide had the general form

$$r = C_o L^m \frac{P_{CO}P_{H_2}^2 - P_{CH_3OH}/K}{(A + BP_{H_2} + CP_{CO} + DP_{CH_3OH} + EP_{H_2O} + FP_{CO_2})^n} + k[P_{CO_2} - K_o^{-1}(P_{CH_3OH}P_{H_2O}/P_{H_2}^3)] \quad (31)$$

where C_o and k were constants, L was the concentration of active sites, and K and K_o were equilibrium constants for methanol synthesis from CO and CO_2, respectively.

Several investigators have compared the rates of methanol synthesis by CO hydrogenation and CO_2 hydrogenation (Bardet et al., 1981; Kieffer et al., 1981; Denise et al., 1982). It was determined that carbon dioxide was hydrogenated directly to methanol at lower temperatures than CO hydrogenation. A chemical trapping technique was used to identify a stable formate species on the catalyst surface after these reactions.

Reaction Mechanisms

An understanding of how catalysts function to selectively form the desired product is an important factor in the development of improved catalysts. This requires a detailed understanding of the reaction mechanism. A methanol catalyst serves as a classic example of how a selective catalyst can be utilized to produce a product that is thermodynamically disfavored.

An indirect method for mechanistic studies involves the proposal of a mechanism from which a rate expression can be derived, then making a comparison between the proposed rate and experimental data. Invalid mechanisms may be discounted by this method, but agreement between a rate expression and experimental data does not constitute proof that the mechanism is correct. Natta used this approach to propose a mechanism for methanol synthesis (Natta, 1955). Using Hougen and Watson models and kinetic data with the assumption that a trimolecular surface reaction occurred, the following steps were proposed:

$$CO + * = CO*$$

$$H_2 + * = H_2*$$

$$CO* + 2H_2* = CH_3OH* + 2*$$

$$CH_3OH* = CH_3OH + *$$

where * was an active site on the catalyst surface. A rate expression based on the assumption that the surface reaction was controlling (Equation 29) agreed very well with experimental data. However, many other kinetic models have been found to satisfy the data, making any

conclusions concerning the reaction mechanism ambiguous (Denny and Whan, 1978).

Additional indirect mechanistic information was obtained from adsorption experiments. Measurements of the simultaneous adsorption of carbon monoxide and hydrogen at low pressures on a methanol catalyst suggested that an intermediate surface species having the formula $-OCH_3$ existed on active sites (Tsuchiya and Shiba, 1965). A critical assumption in this approach was that the $-OCH_3$ species dominated the surface, since the total amount of carbon monoxide and hydrogen adsorbed was used to predict the surface species. These investigators concluded that the rate determining step for methanol synthesis was the reaction of hydrogen with the surface species $-OCH_3$. This conclusion was supported by a high pressure study using a methanol catalyst and labeled hydrogen (Borowitz, 1969). After exposing the catalyst to a $CO-H_2$ mixture, the reactor was evacuated and a $CO-D_2$ mixture admitted. Analysis of the product methanol by nmr spectroscopy showed a predominance of deuterium in the hydroxyl groups. This finding indicated that a surface methoxy species was a stable intermediate and that the source of the hydrogen in the hydroxyl group of methanol was gaseous hydrogen. However, it was not clear whether gaseous hydrogen reacted directly with methoxy groups or if an adsorbed form of hydrogen was involved because the exchange rates of deuterium with adsorbed hydrogen (hydroxyl or hydride species) were not determined.

Several mechanisms for methanol synthesis have been proposed in recent years. The scheme in Figure 56 was suggested by Deluzarche, Kieffer, and Muth (1977) for methanol synthesis on an industrial ZnO-

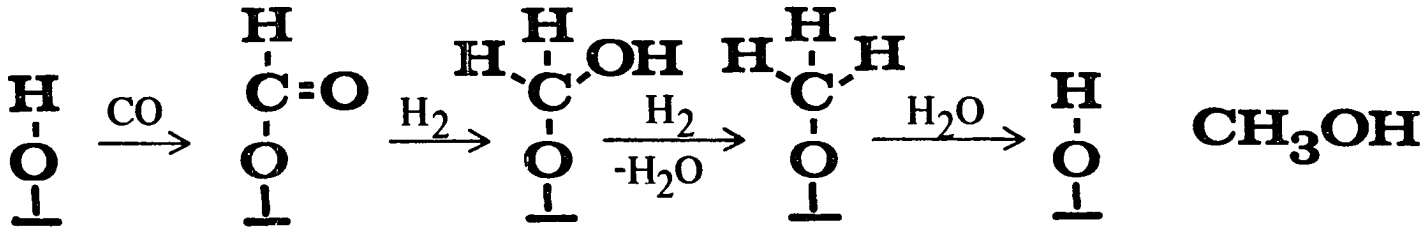

Figure 56. Methanol synthesis mechanism #1 (Deluzarche et al., 1977)

Cr_2O_3 catalyst. Carbon monoxide insertion into a surface hydroxyl group formed a formate (formyloxy) species which was hydrogenated to produce a methyloxy species. Dehydration and hydrogenation of the methyloxy species formed a methoxy group which was hydrated to produce methanol and a surface hydroxyl group. This mechanism did not involve carbon monoxide adsorption on metal ions. The proposed mechanism was based on the results of a chemical trapping technique which identified the stable intermediates on used catalysts. Only the formate and methoxy groups were detected by this method. The conclusion that the methoxy species was hydrated rather than hydrogenated to methanol was based on the observation that methanol synthesis required some CO_2 or H_2O in the CO-H_2 feed mixture (the presence of CO_2 ensures some H_2O formation via the water-gas shift reaction).

The mechanism shown in Figure 57 proposed that carbon monoxide was adsorbed on a metal ion followed by successive hydrogenation to formyl, hydroxycarbene, and hydroxymethyl species until further hydrogenation produced methanol (Herman et al., 1979). The active site for CO adsorption was proposed to be Cu(I) ions while adjacent zinc ions were the centers for hydrogen adsorption. None of these intermediate species were proven to exist on an active methanol catalyst. The presence of carbon dioxide provided an alternate pathway to methanol and methane formation via formate and methoxy intermediates (Klier et al., 1982). This concept of different routes to methanol synthesis for CO and CO_2 hydrogenation involving carbon-bonded and oxygen-bonded intermediates, respectively, was reached independently in kinetic studies (Denise et al., 1982). It was proposed that an adsorbed formate species was

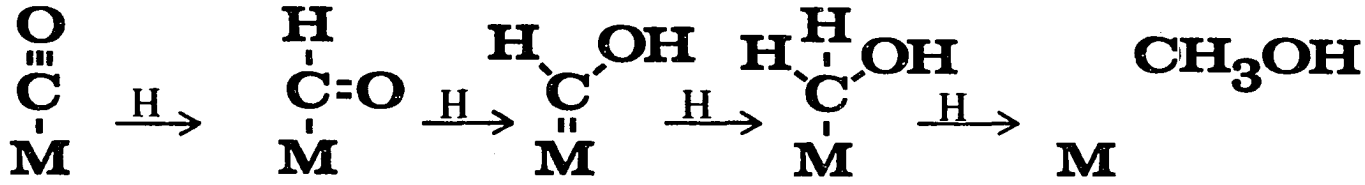

Figure 57. Methanol synthesis mechanism #2 (Herman et al., 1979)

formed both by CO insertion into an adsorbed hydroxyl group and by CO_2 insertion into a surface hydride species. The mechanism for CO_2 hydrogenation suggested by these investigators is presented in Figure 58.

The studies of Rozovskii and coworkers concluded that methanol was formed by direct hydrogenation of carbon dioxide; carbon monoxide was hydrogenated indirectly via the water-gas shift reaction. The general form of the mechanism for methanol synthesis was proposed to be

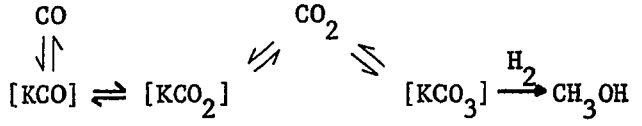

where [KCO], [KCO_2], and [KCO_3] were intermediate surface complexes (Rozovskii et al., 1976b). The intermediates in the water-gas shift reaction were believed to be different from the intermediates in methanol synthesis.

A methanol synthesis mechanism incorporating both carbon-bonded and oxygen-bonded intermediates was recently proposed by reviewing the literature up to 1981 (Henrici-Olivé and Olivé, 1982). This reaction scheme, shown in Figure 59, proposed that carbon monoxide was adsorbed on Cu(I) active sites within the zinc oxide lattice. Hydrogen was dissociatively adsorbed to form Cu(I) hydride and zinc hydroxide. Carbonyl insertion into the Cu-H bond produced a formyl species which was hydrogenated to form a side-bonded formaldehyde species. Further hydrogenation yielded a methoxy species and ultimately methanol. This type of mechanism has also been suggested for methanol synthesis by CO hydrogenation in homogeneous catalysis using ruthenium complexes (Dombek, 1980) and cobalt or rhodium complexes (Fahey, 1981).

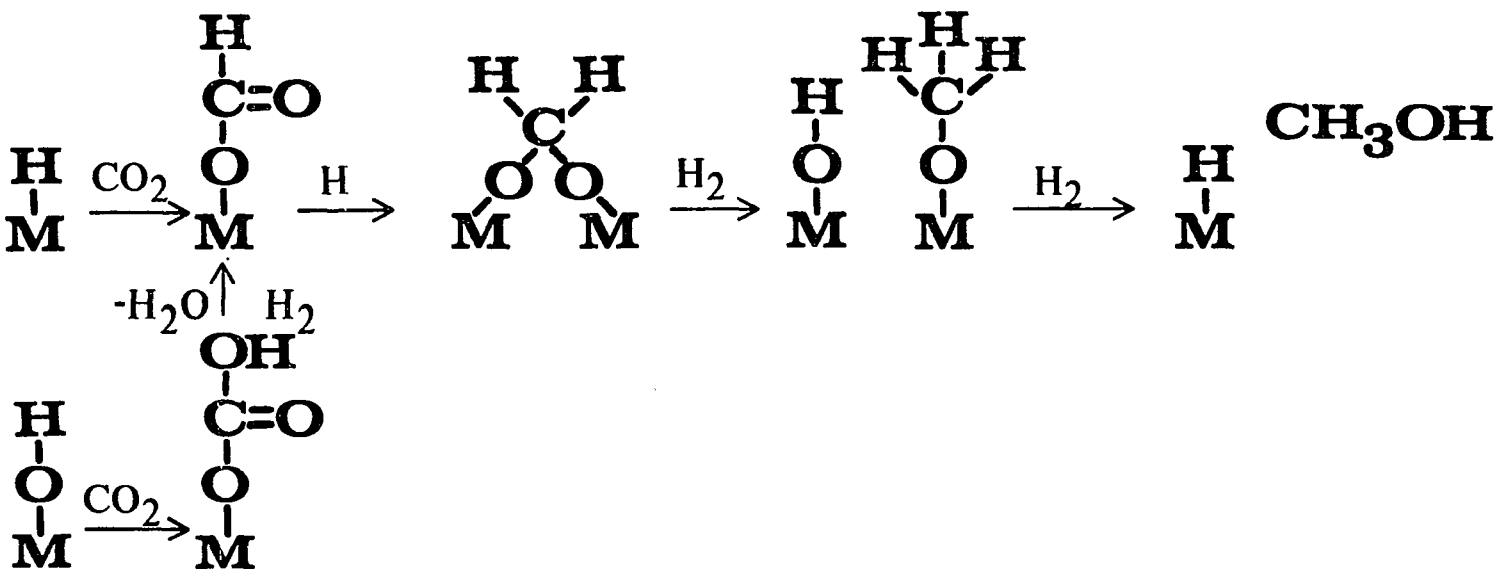

Figure 58. Methanol synthesis mechanism #3 (Denise et al., 1982)

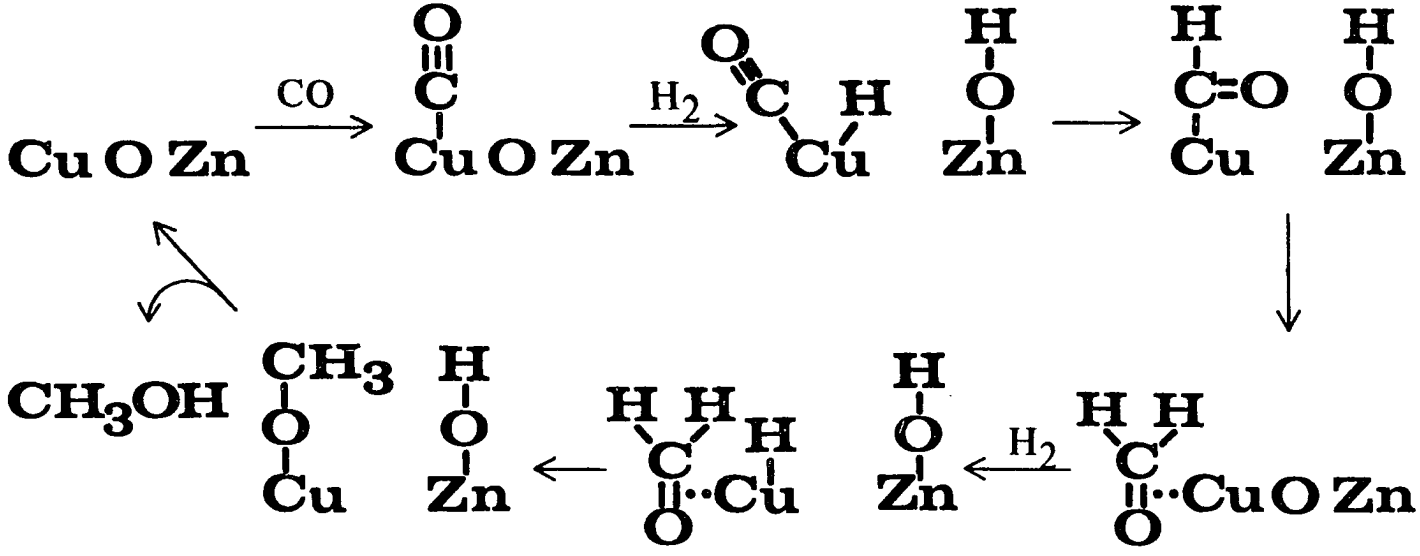

Figure 59. Methanol synthesis mechanism #4 (Henrici-Olivé and Olivé, 1982)

Some studies have investigated the adsorption of various organic molecules, their decomposition, and desorption from the surface of zinc oxide to obtain an insight on methanol synthesis. The temperature programmed desorption of adsorbed species on zinc oxide powder using the adsorbates H_2, CO, CO_2, HCHO, CH_3OH, CO + H_2, and CO_2 + H_2 indicated that an adsorbed formate intermediate was involved in the decomposition of methanol and formaldehyde as well as the hydrogenation of carbon dioxide (Bowker et al., 1981). The decomposition of methanol and formaldehyde also produced a surface methoxy species. The mixture of hydrogen and carbon monoxide did not yield an adsorbed formate species. This same technique has been applied to specific crystal faces of zinc oxide (Cheng and Kung, 1982; Cheng et al., 1983). It was established that the type of crystal face and the presence of defects affected the nature of adsorbed species. In particular, the decomposition of deuterated methanol yielded DCDO, D_2O, CO, CO_2, and D_2 on the polar (0001) surface whereas CD_4, CO, CO_2, and D_2 were the products from the stepped and nonpolar surfaces. Nonpolar surfaces with steps or anion vacancies, as well as polar surfaces, were believed to be active for methanol synthesis. The reaction mechanism depicted in Figure 60 demonstrates the role of an anion vacancy in CO hydrogenation to methanol (Kung, 1980). The active site was proposed to be an oxygen vacancy surrounded by metal ions. Carbon monoxide adsorbed on a metal ion, carbon end down, and was hydrogenated by a neighboring adsorbed hydrogen atom to form a formyl species. The oxygen on the formyl species then interacted with the electron-deficient vacancy as further hydrogenation occurred, eventually forming a methoxy species as the bonding between the oxygen

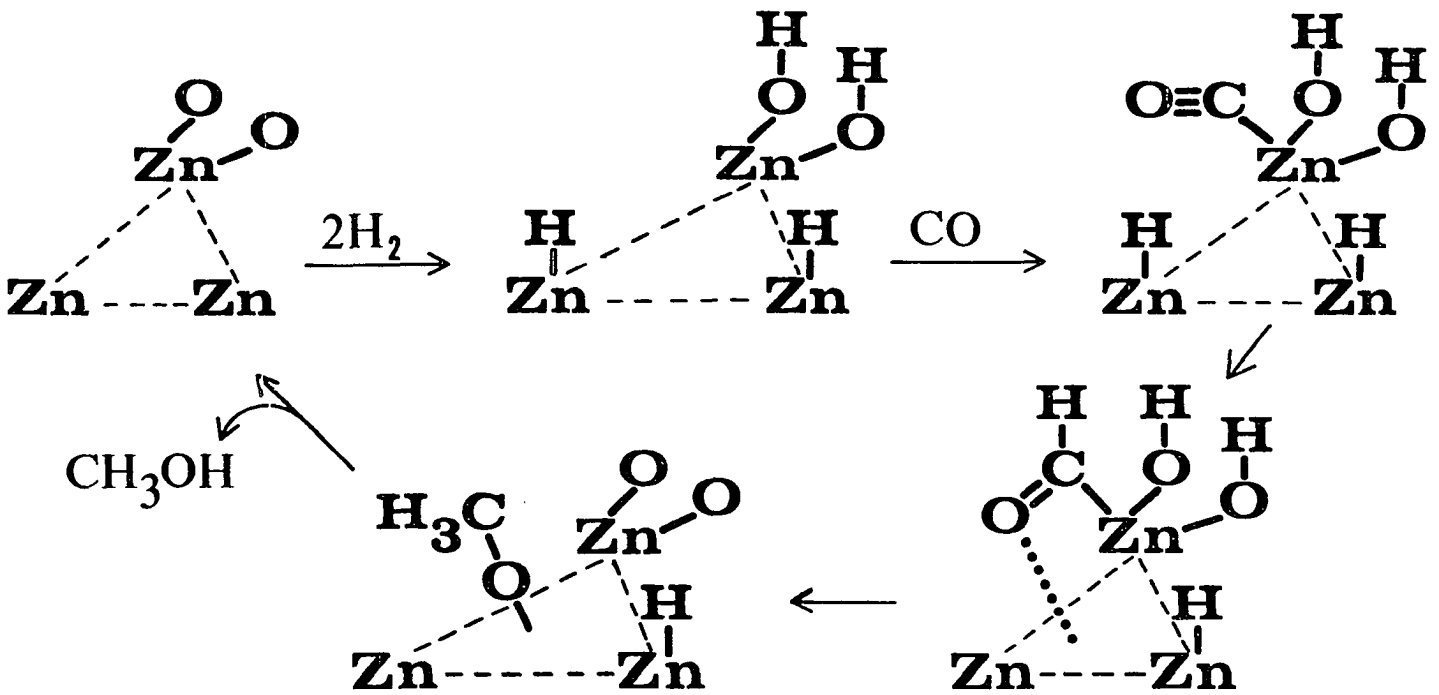

Figure 60. Methanol synthesis mechanism #5 (Kung, 1980)

and the vacancy strengthened while the bonding between the carbon and the metal ion weakened. Additional hydrogenation produced methanol.

High Pressure Spectroscopic Cells

Several infrared cells have been made for studying catalytic reactions at elevated pressures and temperatures, primarily for gas-liquid systems (Tinker and Morris, 1972; Gallei and Schadow, 1974; King et al., 1978; Ballintine and Schmulbach, 1979; Penninger, 1979). A common feature of these cells has been the use of thick calcium fluoride, magnesium fluoride, or quartz windows which have relatively large optical diameters. Short, variable path length designs have been used. High pressure studies of gas-solid systems involving gases which strongly absorb infrared radiation, such as CO, require a cell with a short path length. These cells generally have been designed for a maximum pressure of several hundred atmospheres, limited by the strength of the windows. The maximum temperature of the cell is limited by the seal material employed. Temperatures up to 600°C could be achieved with the cell of Gallei and Schadow because the windows were water-cooled; this cell also had high vacuum capability.

A high pressure cell has been developed for studying gas-solid reactions on a catalyst wafer (Hicks et al., 1981). Temperatures up to 317°C and pressures up to 76 atmospheres can be achieved with this cell. The design allows infrared windows and catalyst wafers to be removed and replaced easily.

EXPERIMENTAL APPARATUS AND METHODS

Reactor System

The flow system shown in Figure 61 was designed for catalytic studies at pressures in the range from 10^{-4} torr to 100 atm. There are three major sections in this system: 1) a high pressure section constructed with stainless steel components for optimum safety, 2) an atmospheric section to handle the effluent from the system for venting or sampling, and 3) a vacuum section composed of glass and stainless steel to desorb impurities in the system or on catalyst surfaces. The entire system was built on a mobile frame permitting the system to be connected with various other analytical instruments (i.e., gas chromatograph or infrared spectrometer) at different locations.

High pressure section

Gas streams for nitrogen, carbon monoxide, hydrogen, and oxygen were included in the system. The oxygen line provided additional flexibility which was not utilized in the studies of methanol catalysts. Gas cylinders were used as the pressure source for the system. A full cylinder of carbon monoxide (99.5% min. purity) provided 1650 psig (113 atm), a full cylinder of nitrogen (99.9% min. purity) provided 2490 psig (170 atm), and a full cylinder of hydrogen (99.9% min. purity) provided 2200 psig (150 atm). Cylinders were replaced when the tank's pressure dropped to 50 atm since most experiments were conducted at this pressure. The size of the CO cylinder (#2, 1.87 m^3) was smaller than the others because of the toxicity of the gas (to minimize the amount of gas lost in the case of an accidental release). Because these

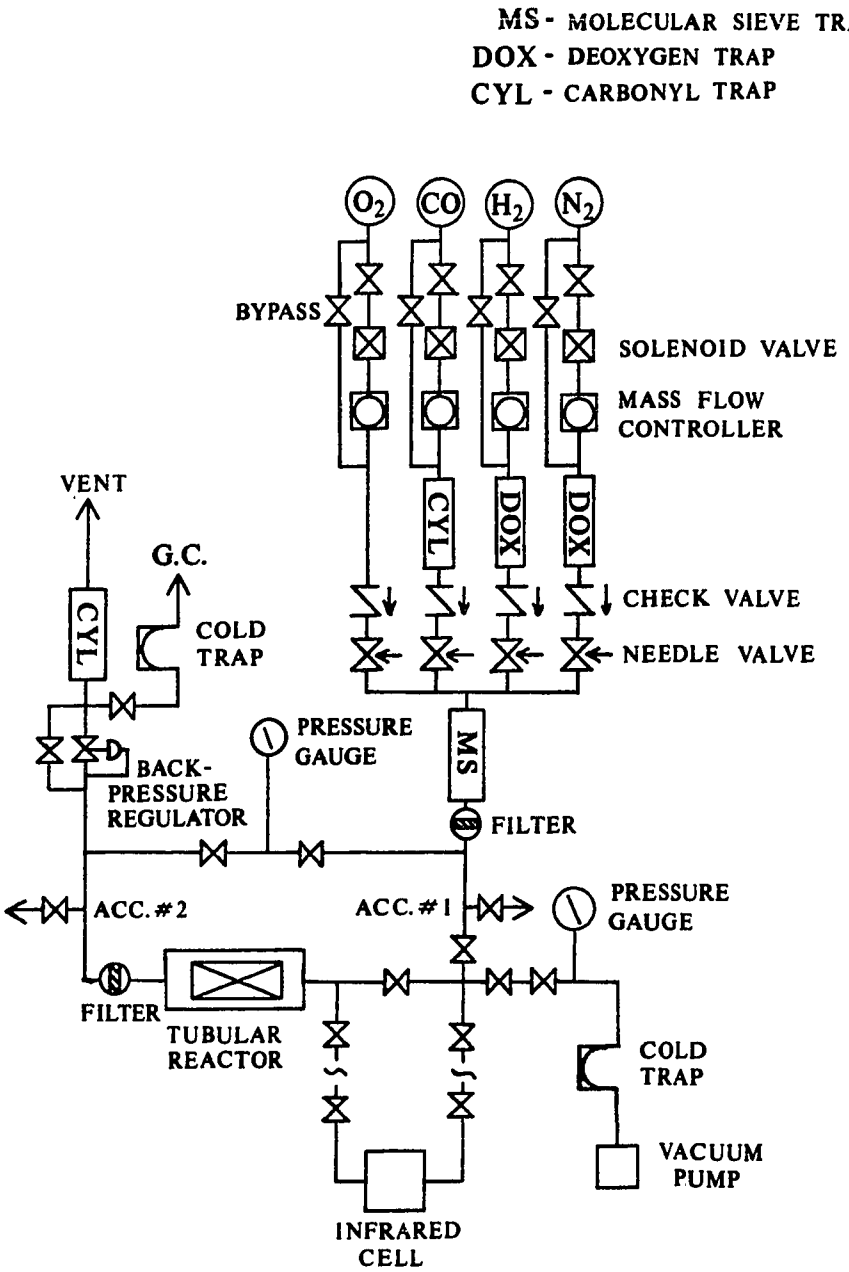

Figure 61. High pressure system

cylinder pressures were above the safe operating pressure of some components in the system (1500 psig), each cylinder had a high pressure regulator (Matheson, Model 3064) capable of delivering any pressure in the safe operating range (0-100 atm).

The gas lines were 1/8" 316SS tubing (0.062" ID) connected to various fittings (Autoclave Engineers, Speedbite) specifically made for high pressures. Three types of hand-operated valves were used: 1) a vee stem for on-off use having a metal-to-metal seal, 2) a soft-seating stem for bubble-tight on-off use, and 3) a regulating stem for control as well as shut-off use. Figure 61 indicates where each type of valve has been used in the system. Each gas has a flow line with a solenoid valve (Atkomatic, Type SBTD) and a thermal mass flow controller (Brooks, Model 5810/5835A). All the solenoid valves have been wired via the alarm relay of a CO detector system (Mine Safety Appliances, Model 571) to provide an automatic shut-down feature if a major gas leak (CO or H_2) develops downstream. The solenoid valves close when the CO level exceeds 200 ppm (or about 2000 ppm H_2) as measured by the electrochemical sensor. The mass flow controllers measure and regulate the flow over a range of 0-500 sccm with an accuracy of 1% full scale. These controllers are rated for 1500 psig maximum operating pressure. The flow sensors are attached to the secondary electronics and digital indicators (Brooks, Models 5871/5872) where the flowrates are set. Calibration curves for flowrate vs. digital indicator reading over a range of pressures for each of the gases are given in Appendix E. A bypass line in each gas stream allows quick gas bleedoff from the cylinders and, if necessary, can be used with the regulating valve downstream to set flowrates (e.g.,

if a flowrate greater than 500 sccm were desired).

Each gas passed through a trap to remove impurities. All high pressure traps were comprised of a 12" length of tubing (9/16" OD x 0.312" ID) wrapped with heating tape and insulation. The trap in the nitrogen line contained a copper-supported catalyst (BASF, R3-11) which removed trace amounts of oxygen at room temperature by the oxidation of copper to copper oxide. The trap in the hydrogen line also contained the same copper-supported catalyst which removed trace amounts of oxygen at 70°C by reacting hydrogen with oxygen to form water. Both traps were activated by reducing the 10-20 mesh particles in hydrogen at 180°C. The trap in the carbon monoxide line contained activated alumina (Alcoa, F-1) as 28-48 mesh particles. During operation of the CO flow line, this trap was heated at about 300°C to decompose any metal carbonyls that might be present in the feed. All gases passed through a trap containing a molecular sieve (Linde, 13X) to remove any water in the feed stream. This final trap in the feed system was followed by a dual-disc filter to remove particles larger than 35 μm. Each gas line had a check valve to prevent backflow and a regulating valve.

Pressures from atmospheric to 2000 psig can be measured with the pressure gauge (Heise, Model CMM) to an accuracy of $\pm$ 2 psi. This tubing configuration permitted both the upstream (pre-reactor) and downstream (post-reactor) pressures to be recorded, from which the pressure drop through the reactor could be determined. Several ports were installed in the high pressure section which could be connected to external equipment. The ports labeled IR #1 and IR #2 were normally utilized as inlet and outlet connections to a high pressure infrared cell. This

design made it possible to conduct simultaneously infrared and catalyst activity studies. The ports labeled Accessory #1 and Accessory #2, which provided additional flexibility to the system, were used in infrared studies involving a saturator. In these studies, the reactor was removed and the connections plugged, the Accessory #1 and IR #2 ports connected to the saturator, and the IR #1 and Accessory #2 ports connected to the infrared cell.

The reactor, shown in Figure 62, was a 12-inch length of 316SS tubing (9/16 inch OD by 0.312 inch ID) fitted with a 316SS sheathed thermocouple (Omega, Sub-Miniature) that passed axially through the reactor inlet to the catalyst bed. An 8-inch section of the outer reactor wall was wrapped with 12 feet of alumel wire (Leeds & Northrup, 22 gauge) insulated electrically by fish-spine porcelain beads (Leeds & Northrup, #034365) for the purpose of heating the reactor; the total resistance of the wire was 4 Ω. The beads were held in place with electric resistor cement (Sauereisen, #78) having good thermal conductivity. The entire heating section was wrapped with refractory fiber insulation (Manville, Cerafelt) and aluminum foil. The reactor preheater was packed with silicon carbide particles (Norton, 10 grit); the catalyst bed followed and then additional silicon carbide particles were used to fill the remaining volume in the reactor. The contents were kept in place with 316SS screens ($\sim$ 100 mesh) at each end of the reactor. The reactor was followed by a dual-disc filter to remove particles larger than 35 μm from the flow stream.

The reactor thermocouple was used to operate a proportional controller (Omega, Model 49) and a high limit controller (Omega, Model

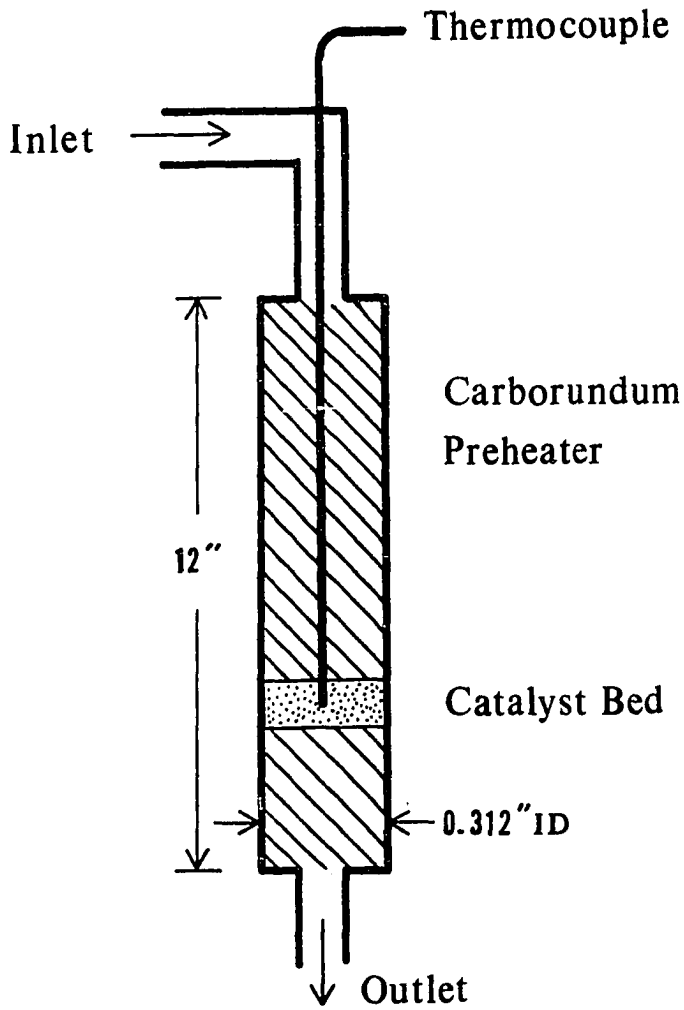

Figure 62. Methanol synthesis reactor

50) which supplied power to the reactor heating jacket. The electrical circuit, depicted in Figure 63, is composed of the limit controller and proportional controller in series with a Variac transformer. The high limit controller was set 50°C above the reactor operating temperature to protect the catalyst from an abnormal temperature increase that could arise if the catalyst reduction takes place too rapidly or an electrical malfunction occurs. The proportional controller was very responsive to the thermocouple measurement, providing temperature control better than ± 1°C (the temperature indicator, Omega Model 199, was only accurate to ± 1°C). Power from the proportional controller was passed through a transformer set at 15% of full voltage, limiting the rate of the reactor temperature rise and providing additional protection against a temperature overshoot.

At the downstream end of the high pressure section was a back pressure regulator (Tescom, #26-1724) providing pressure relief over the range 15-2500 psig with an accuracy of ± 25 psi. Generally, the back pressure regulator was kept at a setting corresponding to 50 atm (720 psig) because of the difficulty in reproducing the same pressure (setting the back pressure is a trial-and-error procedure and the accuracy is poor); both pressure increases and decreases were made by closing and opening, respectively, the valve in the bypass line. The bypass line was also used for studies at atmospheric pressure.

Atmospheric section

The gas lines downstream from the back pressure regulator were 304SS tubing (1/4 inch OD by 0.18 inch ID) connected with Swagelok

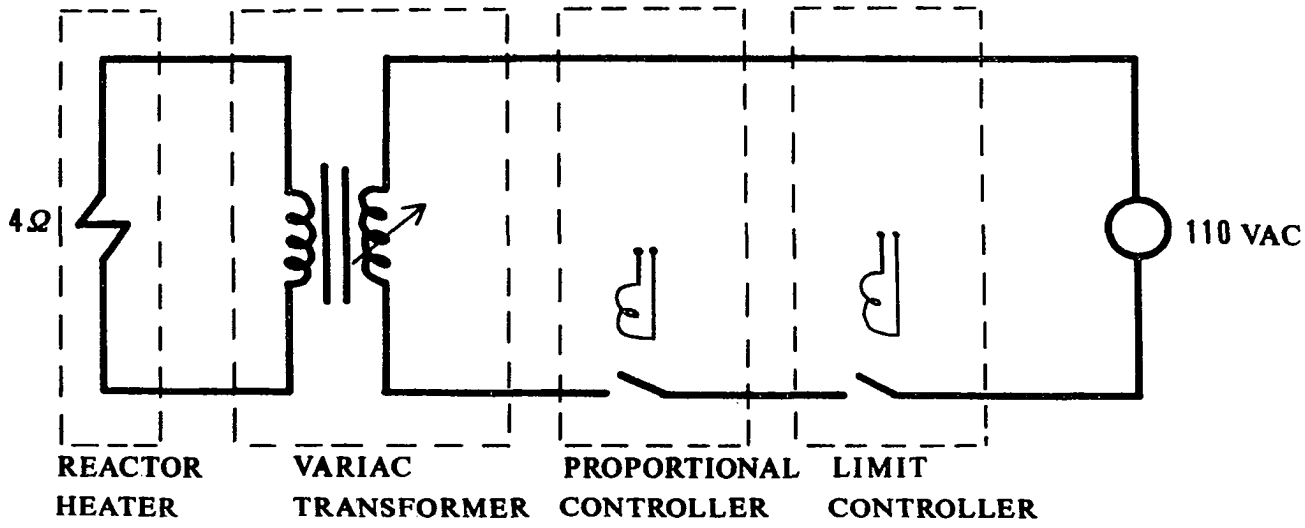

Figure 63. Reactor electrical circuit

fittings. The vent line contained a 12-inch section filled with activated alumina (Alcoa, F-1) heated at approximately 300°C to decompose any carbonyls formed in the reactor system. The gas-sampling line could be attached to a gas chromatograph for analysis of the reactor effluent. This line contained a cold trap which could be used to condense the heavier components in the effluent stream for subsequent gas chromatographic analysis to detect trace products. The regulating valve (Whitey, SS-1RS4) allowed a part of the flow to pass through the sampling line and the remaining flow to pass through the vent line. In practice, no carbonyl formation was detected, so for convenience, the sampling line was also used for venting.

Vacuum section

A vacuum section was incorporated into the design primarily to provide pretreatment of infrared samples for removing surface contaminants prior to analysis. The line from the high pressure section led to a vacuum valve (Veeco, 1/2 inch brass) which would allow the vacuum section to operate isolated from the rest of the system. This valve was connected to a flexible piece of 321SS tubing with a metal-to-glass seal for making the transition to the Pyrex components; the flexible tubing compensated for vibration and stresses to protect the glassware. The pressure was measured with an ionization gauge controller, using a Pirani gauge over the 1000 to 10^{-3} torr range. Both gauges were attached to the vacuum line near a liquid nitrogen trap. The pumping system consisted of a two-stage vacuum pump (Welch, Model 1402) and an air-cooled diffusion pump (Edwards, Model E02) producing an ultimate

vacuum of 10^{-6} torr with silicon oil (Dow Corning, Silicon 704). Most of the glass portion of the system could be easily detached when the vacuum system was not in use, making it easier to clean the glassware and avoiding damage when transferring the system to a new location.

High Pressure Infrared Cell

The infrared cell used in these studies was a modification of the design by Tinker and Morris (1972). The cell was constructed to examine catalysts at pressures ranging from 10^{-6} torr to 240 atmospheres and temperatures from ambient to 300°C. The cross section of a partially disassembled cell is shown in Figure 64. The cell body (A) was constructed of 304 stainless steel. The inner surface of the cell body was copper plated and copper tubing was inserted into the inlet and outlet ports to prevent metal carbonyl formation at elevated CO pressures. Four equally spaced holes were drilled around one end of the body for the insertion of 150 watt heating cartridges. The outer circumference of the cell body was insulated, and a thermocouple well was positioned directly between the inlet ports.

A copper-plated 304 stainless steel spacer (C) held the windows in place and distributed the gas around the sample wafer (G). Gases entering from the inlet ports (H) contacted the sample and exited through eight 1.6 mm holes drilled around the circumference of the spacer. A pair of grooves around the outer circumference was used to channel the exiting gases to the outlet port (I). This type of configuration, which admitted gases to both sides of the sample, decreased the chance for

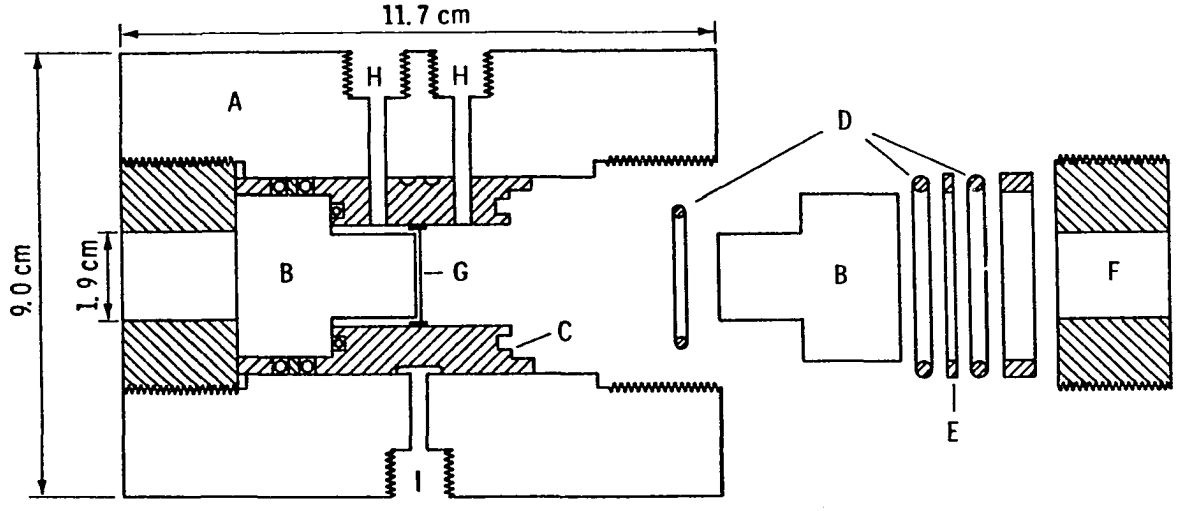

A CELL BODY
B CALCIUM FLUORIDE STEP WINDOWS
C SPACER
D VITON OR KALREZ O-RINGS
E ALUMINUM GASKET
F SCREW PLUG
G WAFER SAMPLE
H INLET PORTS
I OUTLET PORT

Figure 64. High pressure infrared cell

sample breakage due to pressure differences. Samples were pressed into the form of a wafer, generally between 0.05 and 0.20 mm thick. A thin aluminum ring could be used to hold the wafer in the center of the spacer.

Calcium fluoride step windows (B), manufactured by Harshaw Chemical Co., were used which have an outer diameter of 3.34 cm, an inner diameter of 1.80 cm, and an overall length of 3.66 cm. The small-diameter end of the window displaced most of the gaseous volume in the spacer. The maximum operating pressure for these windows, using a safety factor of 4, was calculated from the formula (Eastman Kodak Company, 1971):

$$P = M(t/2.1\ r)^2$$

where M is the modulus of rupture, t is the window thickness, and r is the radius of the unsupported window area. For these windows at room temperature, M = 5300 psi, t = 1.9 cm, and r = 1.1 cm; the maximum pressure was calculated to be 3530 psi (240 atm). The cell had separate seals (D) for vacuum or elevated pressure conditions. The innermost o-ring provided the vacuum seal, and a pair of o-rings separated by a thin aluminum ring (E) encircling the larger diameter of the window provided the seal at high pressures. The use of two o-rings around each window at high pressures distributed the radial stress caused by compression better than a single o-ring, avoiding one cause of window failure. A single o-ring can be utilized successfully if the o-ring is not compressed too much. Screw plugs (F) at each end of the cell were used to compress the o-rings. Because the windows could be chipped or cracked fairly easily during compression, the polished ends

of the windows were protected from the plugs and spacer with thin-gaskets (1 mil) of Mylar film in applications at 200°C and less. Viton o-rings were used at temperatures below 230°C; Kalrez o-rings may be used at temperatures up to 300°C.

Gas Chromatography

A gas chromatograph (Antek, Model 310/40-ALP) with dual column thermal conductivity detectors coupled with a reporting integrator (Hewlett-Packard, Model 3390A) was used for the analysis of gaseous mixtures. Samples of the reactor effluent were taken with a 6-port sampling valve and analyzed with the column arrangement depicted in Figure 65. A Porapak N column (6 ft by 1/8 inch SS) in series with a Porapak T column (6 ft by 1/8 inch SS) separated all species normally found in the effluent; a typical chromatogram is shown in Figure 66. If nitrogen was added to the feed as an internal standard, a Carbosieve S column (6 ft by 1/8 inch SS) provided the separation of nitrogen and carbon monoxide. These two light gases eluted together from the Porapak columns and passed into the Carbosieve column. A stand-off 4-port switching valve allowed the heavier species to bypass the Carbosieve column while trapping the light gases. After all the heavier species had eluted, the switching valve was turned back to pass the carrier through the Carbosieve column and separate the N_2-CO mixture. The operating conditions for all analyses have been given in Table 21.

In order to measure quantitatively the amount of each component in the sample, it was necessary to determine the response factor of each

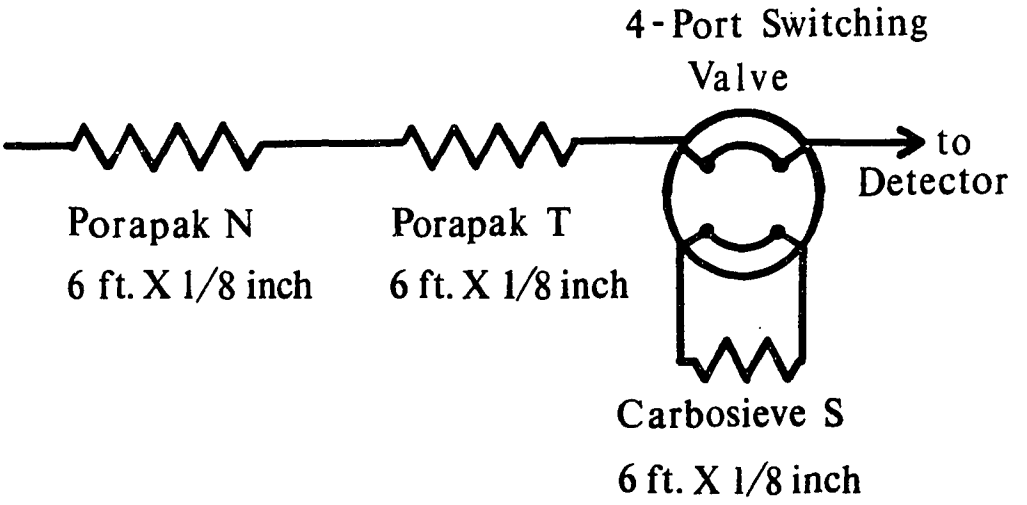

Figure 65. Gas chromatograph analysis system

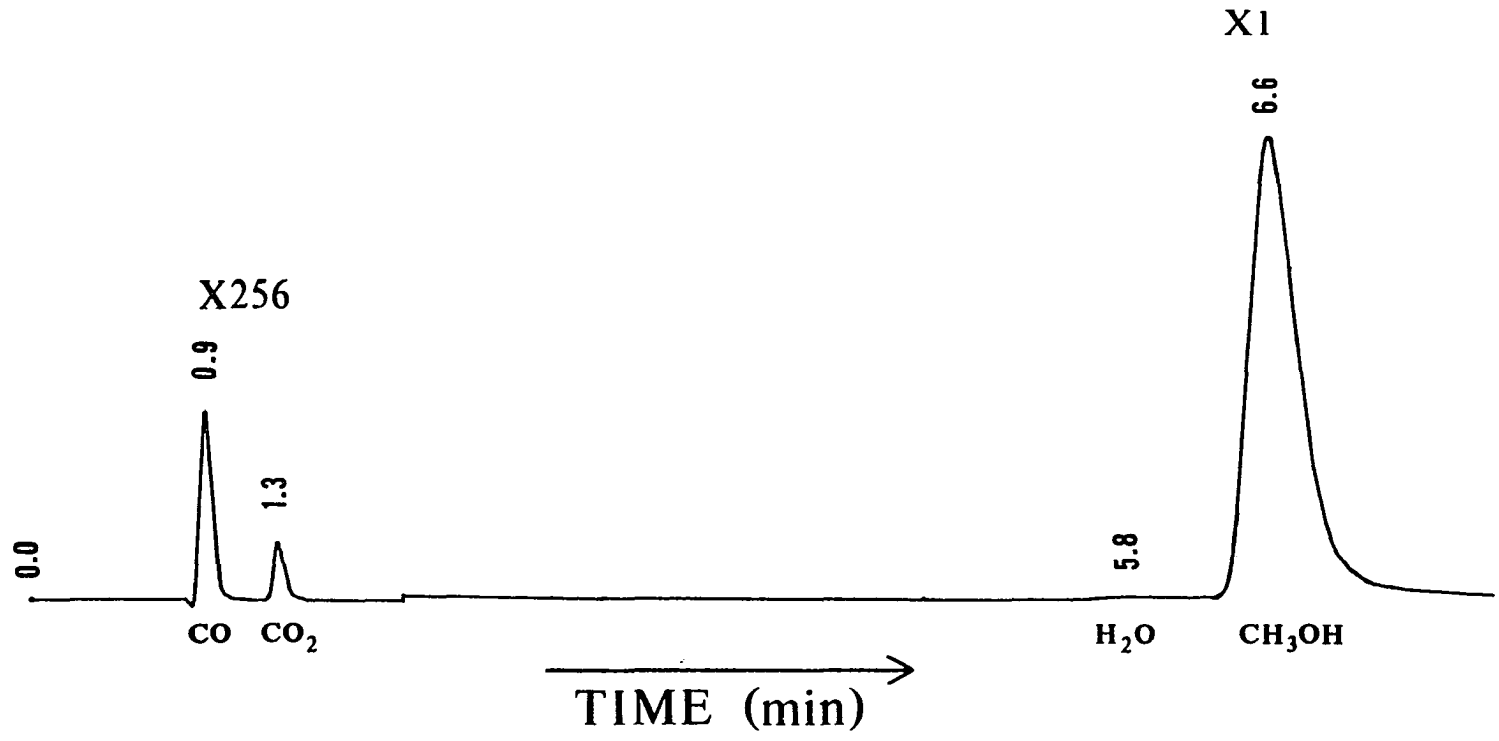

Figure 66. Chromatogram of methanol synthesis effluent

Table 21. Chromatographic operating conditions

Detector: thermal conductivity
Filament current: 180 mA
Detector temperature: 250°C
Carrier gas: helium
Carrier flowrate: 30 cc/min
Oven temperature: 150°C

species. Relative molar response factors were determined using prepared mixtures in a gas sampling bulb from which 0.5 cc samples were injected into the gas chromatograph. The response factor for CO was defined as having the value 1.00, and all other response factors were established relative to this value. A known mixture was injected into the gas chromatograph and peak areas measured, repeating the injections enough times to ensure the reproducibility and accuracy of the results. Because carbon monoxide was a component in each mixture, the relative molar response factor for any species could be determined using the relationship:

$$RF_i = (moles_i/moles_{CO})(area_{CO}/area_i)RF_{CO}$$

The exact amount injected did not need to be known since the relative area and relative composition would be independent of sample size. The use of relative response factors avoided problems that arise from variations in operating conditions over a period of time. The details for mixture preparations and chromatographic results have been given in

Appendix F. The relative molar response factors were determined to be 1.15 for CH_3OH, 0.91 for H_2O, 0.98 for CO_2, and 1.10 for N_2.

Safety Considerations

There were several major safety concerns in this study. Both hydrogen and carbon monoxide are hazardous gases; hydrogen is highly flammable and carbon monoxide is toxic and flammable. A continuous carbon monoxide detection system (MSA, Model 571) was incorporated into the high pressure system to close the solenoid valves in all flow lines if the concentration of carbon monoxide exceeded 200 ppm or the concentration of hydrogen exceeded 2000 ppm. The electrochemical sensor was placed at head level on the front side of the rack to provide maximum protection to the operator. In addition, a hand-held carbon monoxide indicator (MSA, MiniCO) provided the flexibility for spot checks and for locating gas leaks.

Carbon monoxide in contact with stainless steel at the pressures and temperatures used in this study can form metal carbonyls which are extremely toxic (Ludlum and Eischens, 1973; Brynestad, 1976). Carbonyl traps consisting of activated alumina at 300°C were placed in the CO feed line and in the exit line before venting to decompose any carbonyls present. The vented gases were sent to an exhaust hood.

The main concern to personnel when using high pressure gases is the danger of flying projectiles in the event of failure of some part of the system. The high pressure section of the system was enclosed on five sides by 1/8-inch thick steel sheet, leaving the top open for maintenance

(mostly to install and remove the reactor) and for gas expansion in the unlikely event of an explosion. The pressure gauge had a blowout back within this section and valves were mounted with only the stems protruding through the steel sheet. The valve stems were anchored to the steel sheet. The pressures in the system were obtained directly from the gas cylinders, requiring that all cylinder pressures had to be above 50 atmospheres. The weakest part of the system was the flow controllers whose maximum operating pressure was rated at 100 atmospheres. Because it was desirable to minimize the amount of CO in the cylinder owing to its toxicity to personnel in the event of a major leak yet also provide a sufficient amount for extended flow experiments at high pressure, a size #2 CO cylinder was chosen. Additional protection was provided to the system by using this cylinder size because the maximum cylinder pressure was 110 atmospheres; if the pressure regulator should fail, exposing the flow controller to the cylinder pressure, the system would still be safe (the 10% overpressure would not be dangerous). Failure of the CO pressure regulator should not be regarded as an unlikely event because it has occurred twice during a two-year period. Most components of the high pressure system have been rated for 200 atmospheres or better.

RESULTS OF IN SITU CHARACTERIZATION

Catalytic Reactivity

Because the catalysts developed for infrared studies had copper contents considerably lower than those in an industrial methanol synthesis catalyst, it was important to determine the activity and selectivity of these various catalysts to verify that they functioned as methanol synthesis catalysts. Activities and selectivities were measured under the same conditions as those used in the high-pressure infrared studies, i.e., a pressure of 50 atm and a temperature of 200°C. Additional studies were made at higher temperatures. Catalyst evaluations were conducted in a fixed-bed tubular reactor containing a bed of broken catalyst wafers surrounded by SiC particles. Silicon carbide was found to have no activity for CO hydrogenation at 50 atm of 2/1 H_2/CO up to a temperature of 250°C. The binary oxides were evaluated with a flow rate of 1800 GHSV and the ternary oxides evaluated with a flow rate of 3600 GHSV, to compensate for the difference in surface areas between the two types of oxides.

The standard procedure for catalyst testing involved heating the catalyst at 200°C overnight in 60 cc/min STP of N_2. The N_2 flow was replaced with a 5% H_2-in-N_2 flow for 1 hr to reduce the oxide. Then the reducing feed was replaced with the reaction feed mixture and the pressure gradually increased to 50 atm. Reaction runs were generally conducted over a period of 8 hrs, taking samples of the reactor effluent periodically to observe changes in activity and selectivity. The effluent was analyzed by gas chromatography using Porapak T and N columns in

series at 150°C and a thermal conductivity detector. The gc output was quantitatively analyzed by a HP 3390A reporting integrator.

Binary catalysts

The selectivity for CO hydrogenation to methanol was 100% for all binary catalysts under the experimental conditions used in these reactions. The effects of catalyst composition, reactor temperature, and feed composition on CO conversion were examined and the results are summarized in Table 22. Pure zinc oxide, either as a precipitated oxide (wet process) or Kadox 25 (dry process), has no measurable activity at 200°C but some activity at 250°C. The reactor system was carefully checked to verify that this low activity was due to the zinc oxide and did not arise from impurities or components of the reactor. The precipitated binary catalysts had comparable activities, which were an order of magnitude higher than pure zinc oxide at 250°C. The impregnated binary catalyst was prepared by adding a copper nitrate solution to Kadox 25, followed by drying and calcination. Unlike the precipitated oxide of some composition, the impregnated catalyst possessed no activity at 200°C. The addition of an oxidizing agent to the feed mixture produced little change in activities at 200°C but significantly improved conversions at 250°C for the precipitated binary catalysts. Carbon dioxide was added as a gas premixed with hydrogen (10% CO_2 in H_2), while water was added by bubbling the H_2/CO mixture through liquid water at high pressure. The reactor effluent from experiments using water in the feed had no water but some carbon dioxide,

Table 22. Reactivity of binary catalysts at 50 atmospheres

Composition ZnO/CuO[a]	CO conversion to CH_3OH (%) 200°C	250°C	Methanol yield (x 10^{-5} moles/m^2/hr) 200°C	250°C
With feed composition H_2/CO = 67/33 vol %				
Kadox 25	0.0	0.6	0.0	0.6
100/0	0.0	0.6	0.0	0.5
95/5	1.6	6.3	1.1	4.5
Imp. 95/5	0.0	–	0.0	–
90/10	1.3	5.2	0.9	3.7
With feed composition $H_2/CO/CO_2$ = 66/28/6.6 vol %				
95/5	0.7	11.4	0.5	8.2
90/10	1.1	15.6	0.8	11.2
With feed composition $H_2/CO/H_2O$ = 67/33/0.5 vol %				
95/5	1.9	8.8	1.4	6.3
90/10	1.1	12.6	0.8	9.0

[a]Mole percent.

indicating that the catalysts had good activity for the water-gas shift reaction:

$$CO + H_2O \rightleftharpoons CO_2 + H_2$$

Methanol yields have been based on BET surface areas; values of 9.1, 20, and 27 m^2/g were used for Kadox 25, precipitated ZnO, and the precipitated binary oxides, respectively.

The initial yield of methanol was generally higher than the steady-state yield (value after 8 hr), usually in the range of 20 to 50% higher. This loss of activity could arise from several causes, and has been examined by taking the transient behavior of 90/10 Zn/Cu

catalyst as an example. The concentrations of CO_2, CH_3OH, and H_2O were measured periodically during the first 8 hr of a reaction run for each of the feed mixtures utilized in these studies; these transients are shown in Figure 67. When a feed of H_2 and CO was used, the initial methanol yield was 50% higher than the steady-state yield. The activity of the catalyst gradually decreased during the transient. At the reaction temperature of 200°C, however, this deactivation is quite slow and thus the activity after 8 hr is relatively good. The small amount of CO_2 in the initial effluent sample most likely arose from the water-gas shift reaction berween CO and some residual water formed previously from the reduction of CuO by H_2. The transient behavior of the effluent components from a reaction run using a feed of CO, H_2, and CO_2 had some significant differences compared to the previous run using a feed of CO and H_2. The initial methanol yield was twice the amount obtained without any CO_2 present, while the amount of CO_2 was approximately one-tenth the feed concentration. The CO_2 concentration returned to the value in the feed and a steady-state methanol yield was established in under 4 hours at a level less than the steady-state value of the reaction with CO and H_2. Water was also a product in the effluent stream. The initial low level of CO_2 arose from absorption by the catalyst; relatively high CO_2 concentrations were found in the effluent from the reactor system following the pressure drop at the end of a reaction run. At steady state, the methanol yield could result from CO hydrogenation and CO_2 hydrogenation; the water could be formed by CO_2 hydrogenation or the water-gas shift reaction. Because the methanol yield was less with a feed containing CO_2 at 200°C, the diffusive

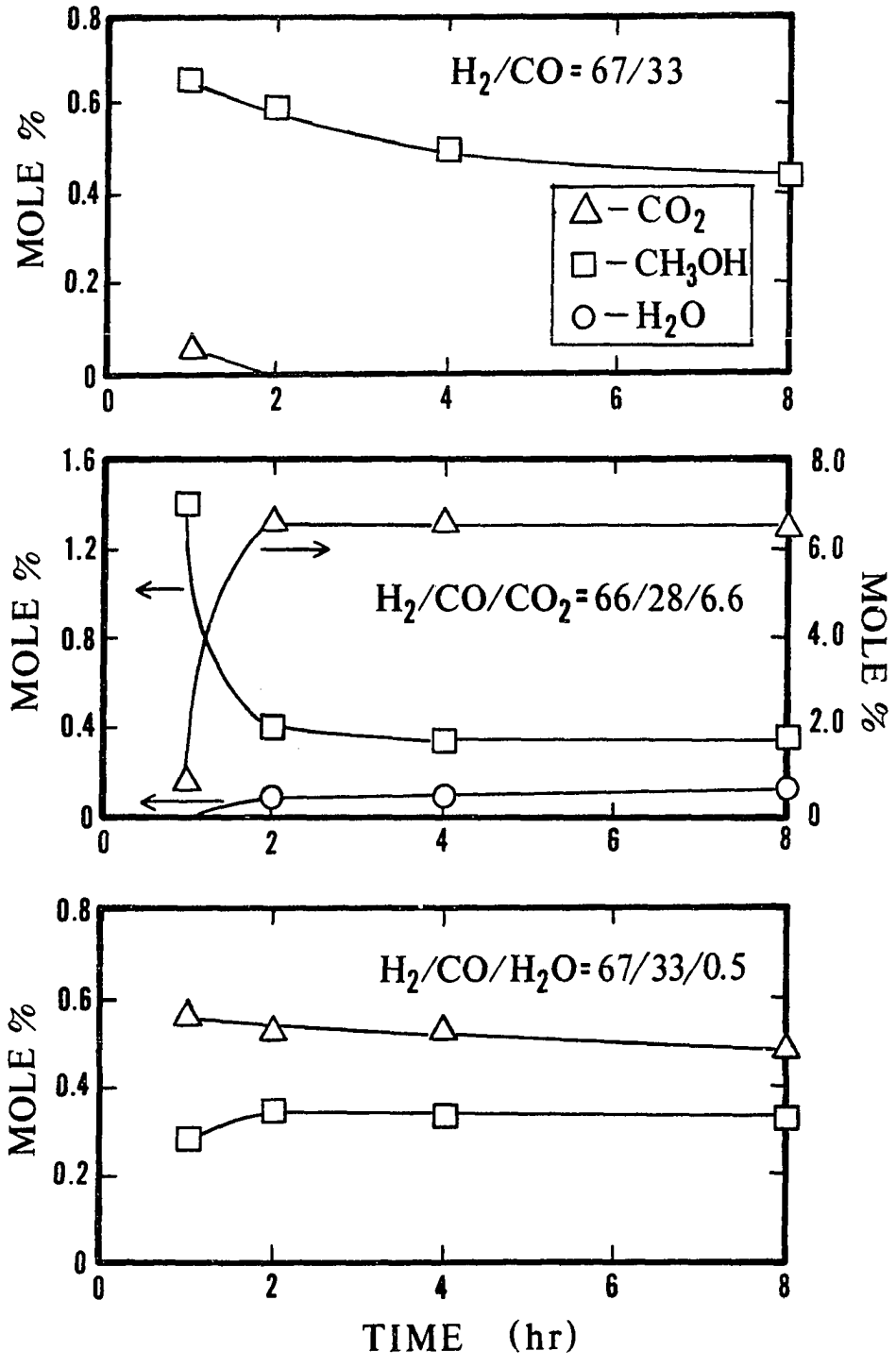

Figure 67. Transient behavior

restrictions caused by CO_2 in the catalyst pores overrode any advantage that CO_2 may provide as a reactant or in preventing deactivation (strong reduction) of active sites.

At 250°C, however, these conditions were reversed; CO_2 had a positive effect on the methanol yield. The feed mixture with water produced effluent concentrations essentially constant over the entire 8-hour period. The methanol yield was approximately the same as the yield obtained from the feed mixture containing CO_2, which is logical since the water in this feed mixture was converted to CO_2 by the water-gas shift reaction. A pressure drop at the end of the reaction run resulted in relatively high levels of CO_2 and H_2O in the effluent, indicating some absorption of these two species. These pressure drops were also used to detect for condensation of methanol, since a pressure decrease would increase the amount of CH_3OH in the gas phase if any condensation had occurred.

Because a formate intermediate has been proposed in methanol synthesis from H_2 and CO, a reaction run was conducted with some 95/5 ZnO/CuO catalyst using a gas feed of H_2/N_2 = 50/50 bubbling through a formic acid solution (73% HCOOH, 27% H_2O) at 50 atm. The reaction,

$$HCOOH + 2H_2 \rightarrow CH_3OH + H_2O$$

went to completion at 200°C. No other reaction products other than methanol were observed.

Ternary catalysts

The selectivity for CO hydrogenation to methanol was 100% for the ternary catalysts at 200°C and > 98% (dimethyl ether was the other product) at 250°C. Because the surface areas of ternary oxides were approximately double the values of binary oxides, the amount of ternary catalyst (by weight) used in reactor tests was half the amount of binary catalysts. The effects of catalyst composition, reaction temperature, and feed composition on conversion to methanol have been summarized in Table 23. In general, the methanol yield per unit surface area was comparable between binary and ternary catalysts. BET surface areas of 49, 58, and 65 m^2/g were used for 90/5/2.5 $ZnO/CuO/Cr_2O_3$, 80/10/5 $ZnO/CuO/Cr_2O_3$, and 80/10/5 $ZnO/CuO/Al_2O_3$, respectively. These results support the observation (Herman et al., 1979) that the primary effect of the addition of Cr_2O_3 or Al_2O_3 to the composition of a binary oxide was to increase activity by increasing the surface area. An exception was the 80/10/5 $ZnO/CuO/Cr_2O_3$ catalyst which exhibited high activity at 200°C (approximately an order of magnitude higher yield per unit surface area than the binary catalyst). Thus, the role of the promoters Cr_2O_3 and Al_2O_3 appears to be electronic as well as physical. The activities of ternary catalysts showed better stability (less deactivation occurred) than binary catalysts. The addition of an oxidizing agent (CO_2 or H_2O) to the H_2/CO feed mixture had little effect on yields at 200°C but increased yields significantly at 250°C, using the yields for 80/10/5 $ZnO/CuO/Al_2O_3$ as the benchmark. Carbon dioxide was also absorbed by the ternary catalysts, as indicated by initially low levels of CO_2 in the reactor effluent and high levels after the pressure drop. These catalysts

Table 23. Reactivity of ternary catalysts at 50 atmospheres

Catalyst composition (mol %) $ZnO/CuO/Cr_2O_3$	Feed composition (vol %) $H_2/CO/CO_2/H_2O$	CO conversion to CH_3OH (%) 200°C	250°C	Methanol yield[a] (x 10^{-5} mol/m^2/hr) 200°C	250°C
90/5/2.5	66/28/6.6/0	0.9	10.7	0.5	6.4
80/10/5	65/33/0/0	7.8	13.8	4.8	8.4
80/10/5	67/33/0/0.1	1.8	11.0	1.1	6.7
$ZnO/CuO/Al_2O_3$					
80/10/5	67/33/0/0	0.8	3.7	0.4	2.0

[a] $$\text{Yield} = \frac{(\text{molar flowrate})(\text{fraction CO in feed})(\text{fraction CO to } CH_3OH)}{(\text{weight catalyst})(\text{surface area catalyst})}$$

were also active for the water-gas shift reaction, converting small amounts of water to carbon dioxide (the conversion has been expressed in this manner because the amounts of water and carbon dioxide can be measured more accurately than hydrogen or carbon monoxide).

The activity of the 80/10/5 $ZnO/CuO/Cr_2O_3$ catalyst was evaluated for converting formic acid to methanol. At 200°C and 250°C, no activity for methanol synthesis was observed using a gaseous mixture of 50/50 H_2/N_2 bubbling through a solution of formic acid (73% HCOOH, 27% H_2O) at 50 atm.

Infrared Spectra at High Pressure

Gaseous carbon monoxide

The high pressure cell was used initially to determine the extent to which gaseous carbon monoxide adsorbed infrared radiation in the wavelength region near 2143 cm^{-1} and to determine the effect of pressure on the spectra. The contribution by gaseous carbon monoxide to the spectrum can be subtracted to reveal the presence of adsorbed carbon monoxide on a catalyst surface only if the transmittance is nonzero. The effect of increasing pressure on the spectrum of gaseous carbon monoxide is shown in Figure 68. Each spectrum was produced by taking 500 scans at 0.24 cm^{-1} resolution. The results demonstrated that a very short pathlength was required to avoid total absorption by gaseous carbon monoxide. The transmittance in the region of 2180 cm^{-1} at a pressure of 70 atm. was close to 10% for a pathlength of 0.4 mm. These spectra demonstrated the need for an accurate reference spectrum in order to correct for

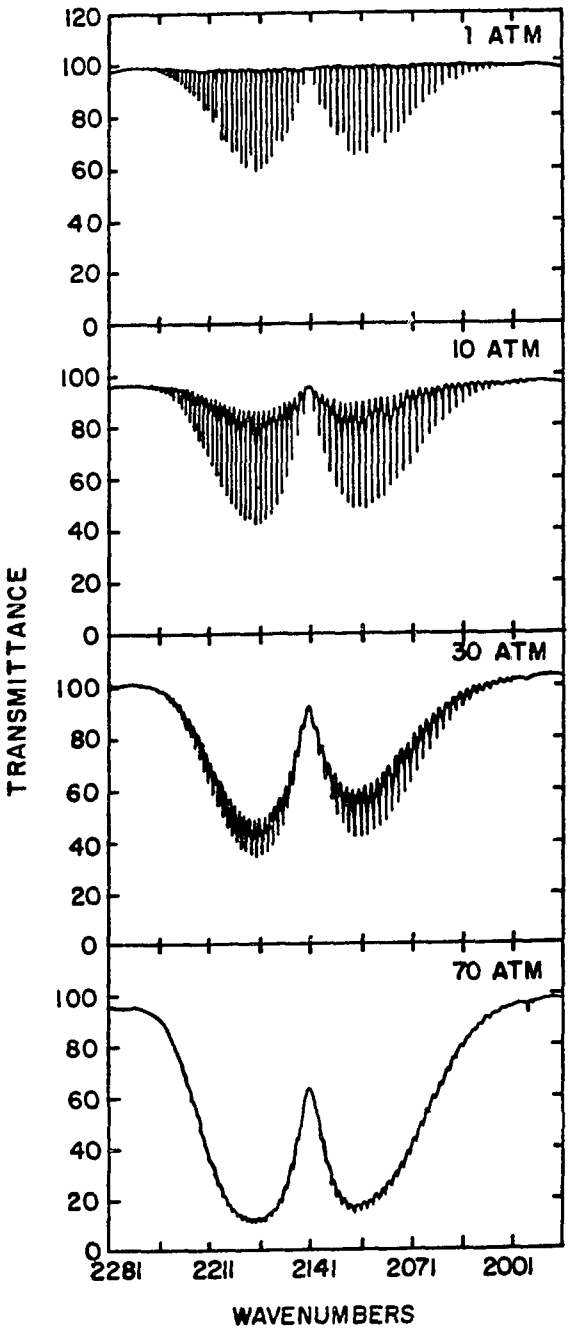

Figure 68. Infrared spectra of gaseous CO

absorption by gaseous carbon monoxide since the shape of the rotational-vibrational bands was a strong function of the pressure. The additional complications arising from the variability in sample background absorptions and the various wafer thicknesses made it impractical to subtract the effect of gaseous carbon monoxide from the spectra of metal oxides during in situ studies.

Species on zinc oxide

Although zinc oxide was inactive for methanol synthesis at 200°C, spectra of adsorbed species can be helpful for identifying which intermediates on mixed metal oxides would be adsorbed on zinc sites. The effect of pressure on the nature of surface species on zinc oxide (Kadox 25, New Jersey Zinc Company) at 200°C was established for pressures from 1 to 50 atmospheres of carbon monoxide. Each spectrum has had the background (zinc oxide) subtracted and was produced by taking 100 scans at 1.0 cm^{-1} resolution. The spectra of adsorbed species on zinc oxide are shown in Figure 69. Bands at 1580 and 1363 cm^{-1} (1 atm) were assigned to the asymmetric and symmetric C-O stretching bands, respectively, of a surface formate species. As the pressure was raised to 50 atmospheres, the asymmetric band shifted toward lower wavenumbers and the symmetric band shifted to 1366 cm^{-1}. The band at 1377 cm^{-1} has been assigned to the C-H bending frequency of a surface formate species. The band appearing at 1688 cm^{-1} and shifting to 1678 cm^{-1} at 50 atmospheres has been assigned to zinc hydride species which Boccuzzi (1978b) had designated as Band III; no additional bands were observed in this region of the spectra. A strong band at 2867 cm^{-1}, shifting to

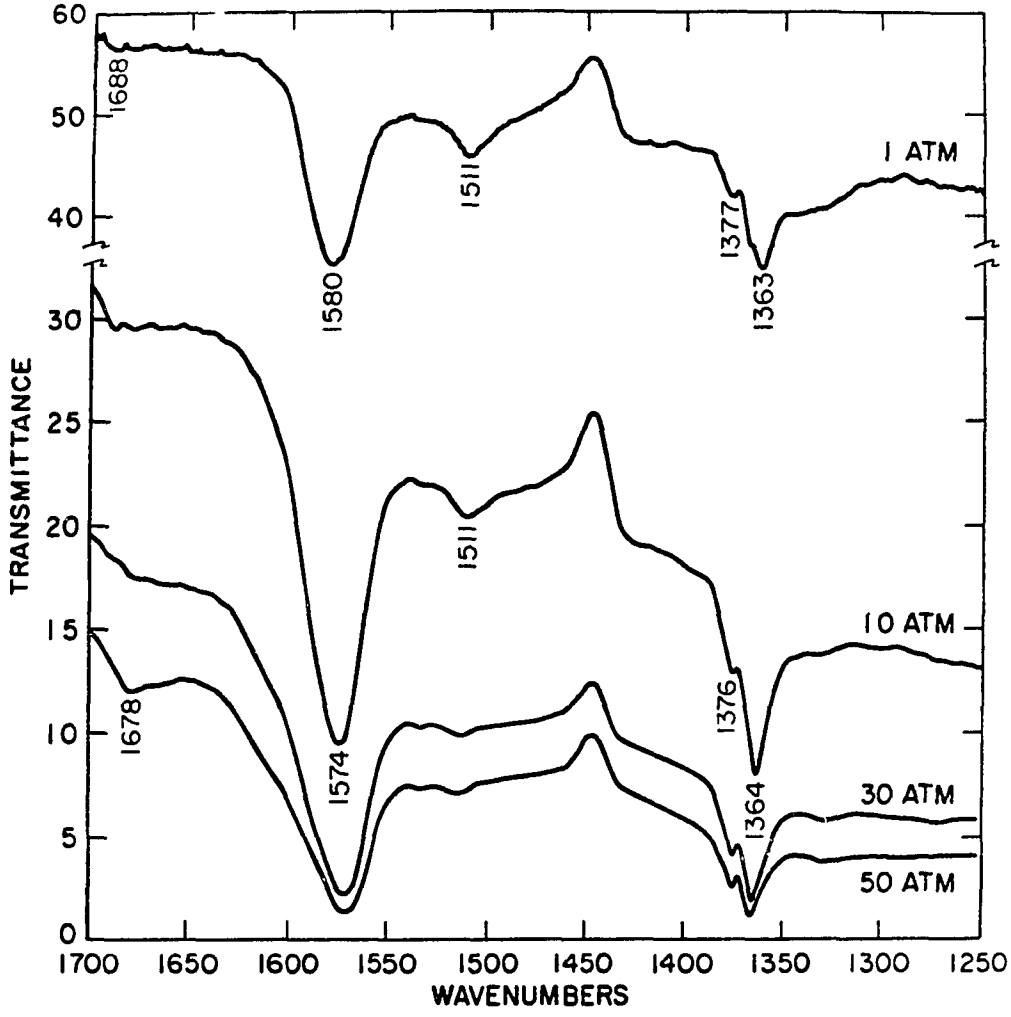

Figure 69. Infrared spectra of adsorbed CO on ZnO

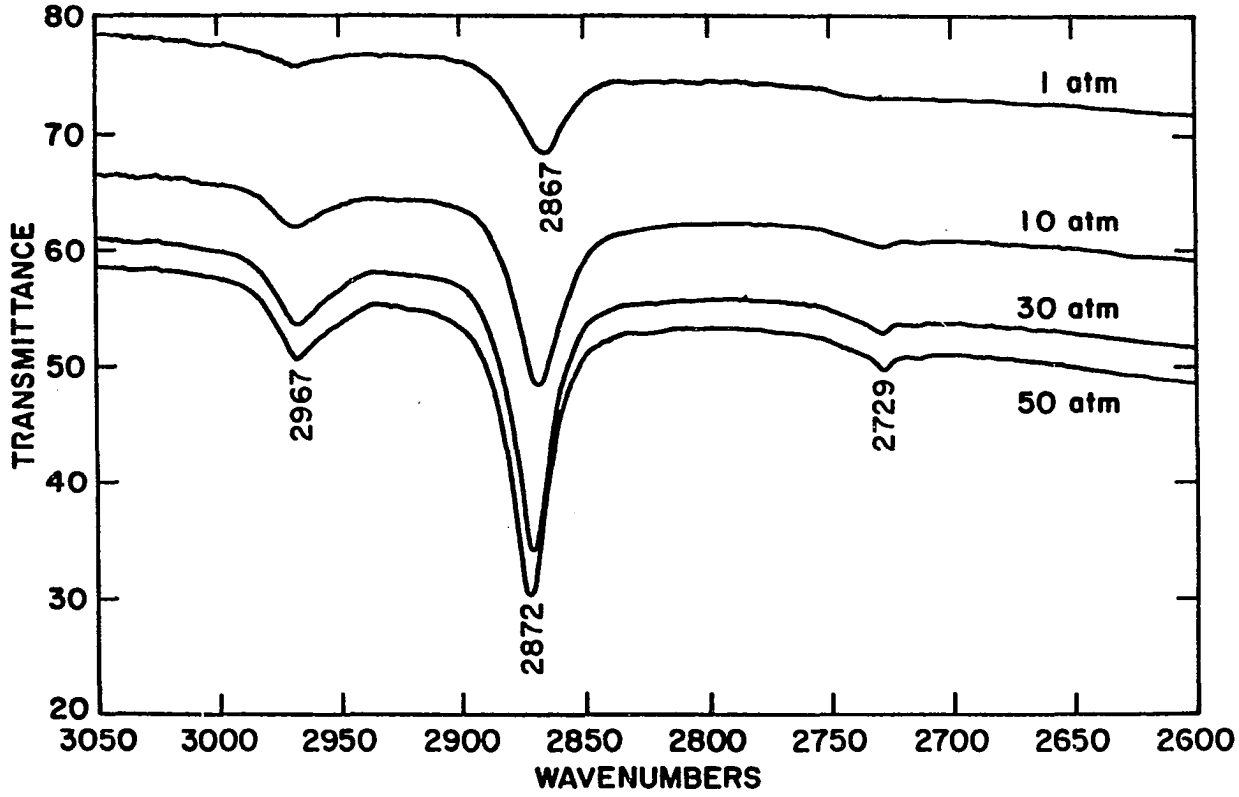

Figure 69. Continued

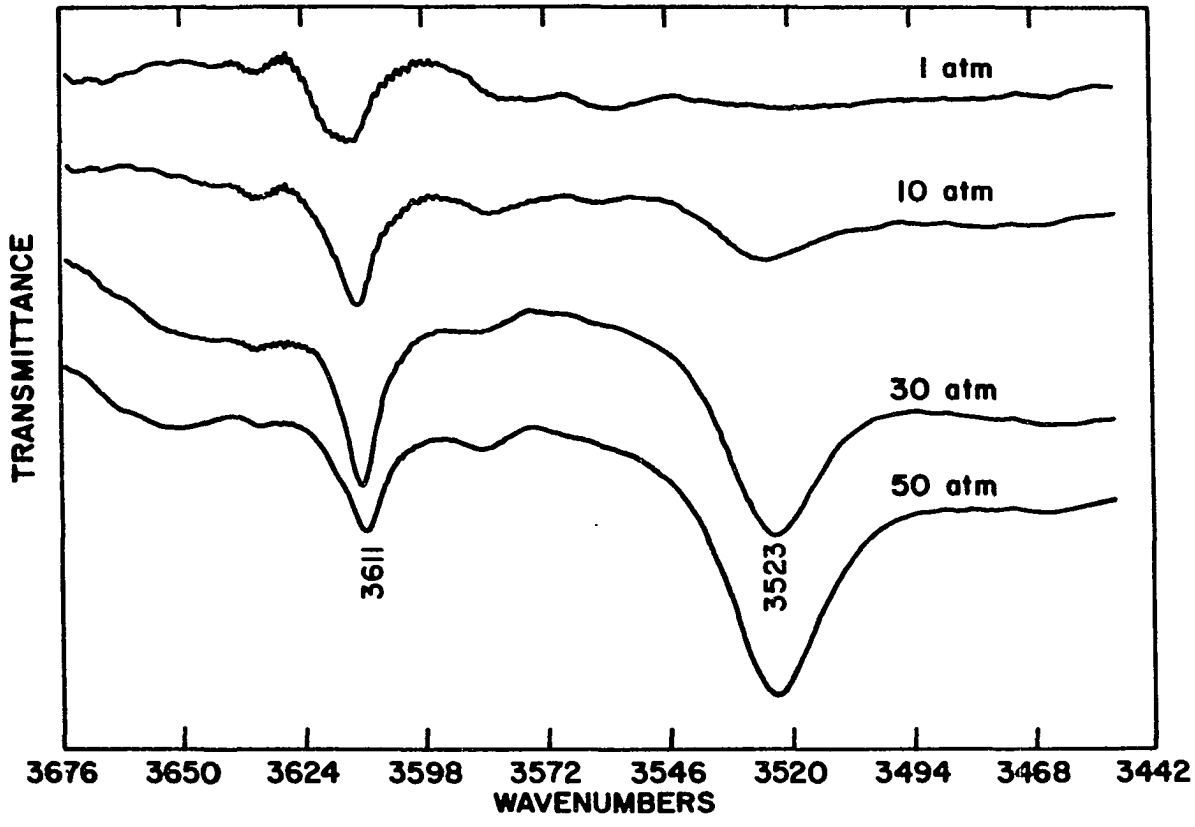

Figure 69. Continued

higher wavenumbers with increasing pressure, which was assigned to the C-H stretching frequency of the formate species. The bands appearing at 2967 and 2729 cm^{-1} have been assigned to combinations of fundamental frequencies; the 2967 cm^{-1} band is a combination of the 1570 and 1377 cm^{-1} bands of the formate species while the 2729 cm^{-1} band is a combination of the 1366 and 1377 cm^{-1} bands of the formate species. A strong band at 3523 cm^{-1} was attributed to a surface hydroxyl group having greater stability at higher pressures. Because the spectrum of zinc oxide was subtracted from each adsorption spectrum, the normal residual hydroxyl groups on zinc oxide have been removed. However, there was a shift in the residual hydroxyl species at 3620 cm^{-1} toward lower wavenumbers as the pressure increased, resulting in the appearance of the hydroxyl band seen at 3611 cm^{-1}.

Species on binary catalysts

The binary catalysts with Zn/Cu ratios of 95/5 and 90/10 were satisfactory for infrared investigations. Although the transmittance was very poor, some information was also obtained from a 85/15 Zn/Cu catalyst. Binary catalysts with copper contents above the 15/85 Cu/Zn ratio were unsatisfactory for transmission infrared studies in both oxidized and reduced states. All of these catalysts had a significant transmittance loss at lower wavenumbers during in situ studies. The experimental results for all binary compositions were not presented because the infrared spectra of adsorbed species on these catalysts were qualitatively quite similar under equal experimental conditions.

The adsorption of carbon monoxide on a 95/5 Zn/Cu catalyst (pre-

treatment #1) at 200°C and 50 atmospheres is shown in Figure 70. Prolonged exposure reduced the catalyst, indicated by the formation of the hydroxyl band at 3252 cm^{-1}. Formate groups (bands at 2969, 2878, 2731, and 1573 cm^{-1}) developed first, then an adsorbed formaldehyde species (bands at 2935, 2834, 2731, and 1660 cm^{-1}) was formed. At high pressure, the Type I hydroxyl species (band at 3520 cm^{-1}) gradually emerged as a stable surface species. The residual hydroxyl group originally at 3620 cm^{-1} shifted to 3611 cm^{-1} and the carbonyl band shifted to 1975 cm^{-1}.

The hydrogenation of surface species was accelerated by incorporating hydrogen with the carbon monoxide feed. Figure 71 shows the adsorption of a mixture of carbon monoxide and hydrogen (CO/H_2 = 9/1) on a 95/5 Zn/Cu catalyst (pretreatment #1) at 200°C and 50 atmospheres. Initially formate groups (band at 2879 cm^{-1}) and the hydroxyl of reduction (band at 3252 cm^{-1}) were formed. The development of methoxy groups (bands at 2934 and 2822 cm^{-1}) was accompanied by the disappearance of the isolated hydroxyl groups (bands at 3660 and 3612 cm^{-1}). The formate band shifted significantly from 2879 to 2868 cm^{-1}, owing to the presence of methoxy groups.

The adsorption of a 2/1 H_2/CO mixture on 95/5, 90/10, and 85/15 Zn/Cu catalysts at 200°C and 50 atmospheres after an hour of exposure is shown in Figure 72. At these conditions, very little detail could be observed at lower wavenumbers because of low transmittance. The surface condition was representative of the surface species during methanol synthesis. These spectra showed the hydroxyl of reduction (band at 3252 cm^{-1}), methoxy groups (bands at 2933 and 2822 cm^{-1}), and the formate species (bands at 2865 and 1575 cm^{-1}) in addition to

Figure 70. Carbon monoxide adsorption on 95/5 Zn/Cu oxide at 50 atm

a) oxidized surface

b) exposure for 8 hours

c) exposure for 24 hours

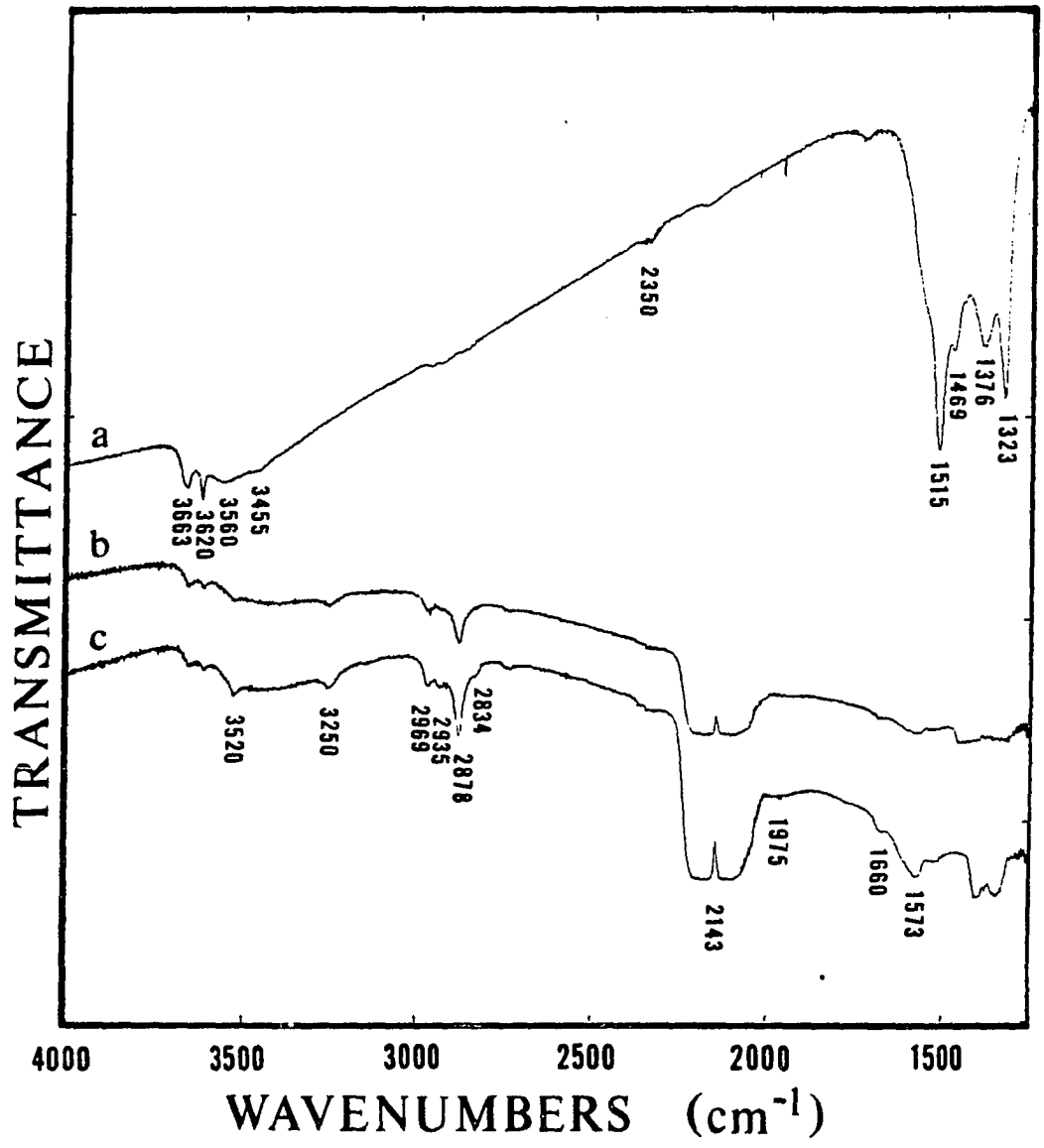
TRANSMITTANCE
a
b
c
3663
3620
3560
3455
2350
1515
1469
1376
1323
3520
3250
2969
2935
2878
2834
2143
1975
1660
1573
4000
3500
3000
2500
2000
1500
WAVENUMBERS (cm-1)

Figure 71. Adsorption of CO-H_2 mixture on 95/5 Zn/Cu oxide at 50 atm

a) oxidized surface

b) exposure for 15 minutes

c) exposure for 1 hour

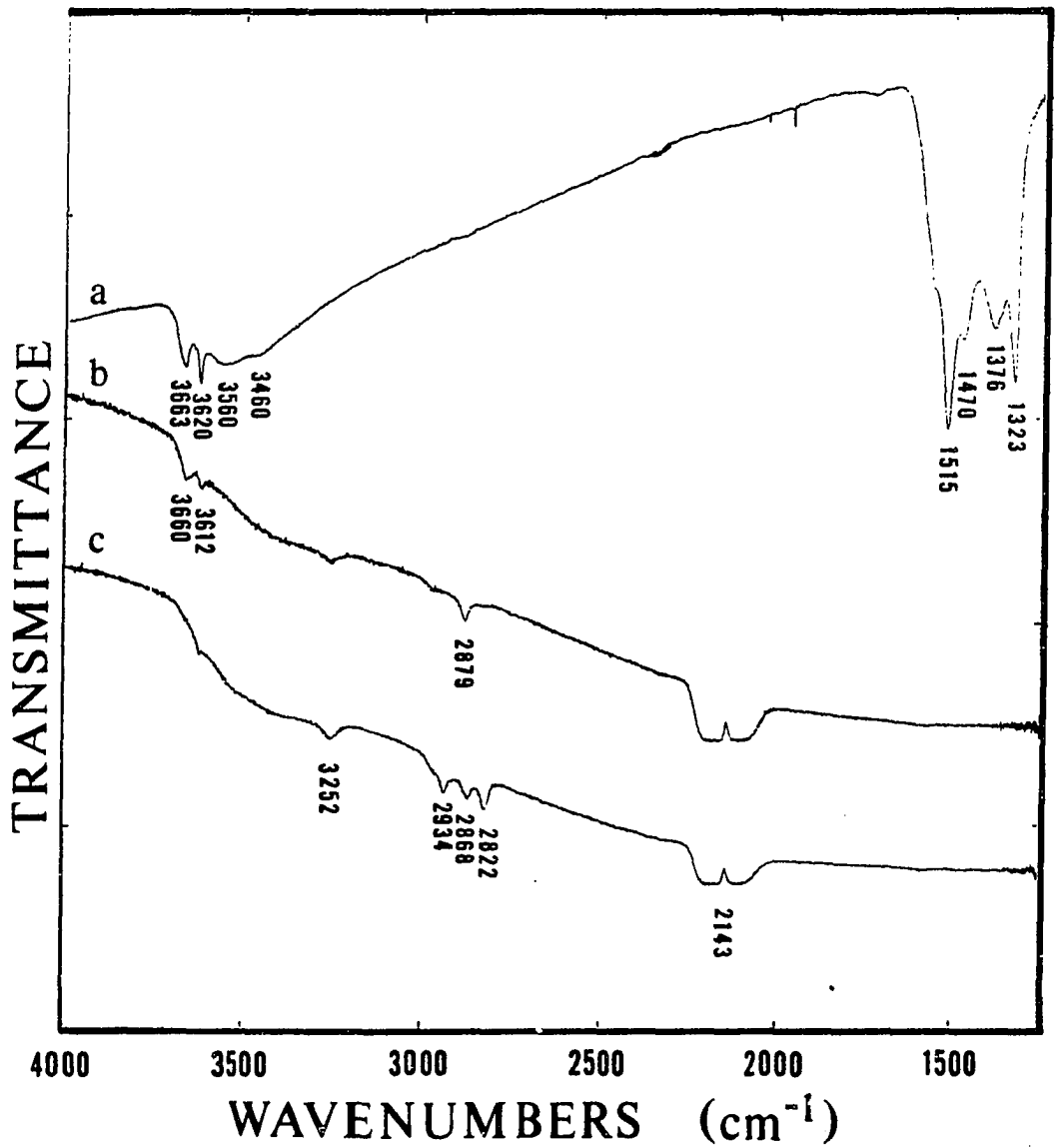
a
b
c
3663
3620
3560
3460
3660
3612
2879
3252
2934
2868
2822
2143
1515
1470
1376
1323
TRANSMITTANCE
4000
3500
3000
2500
2000
1500
WAVENUMBERS (cm-1)

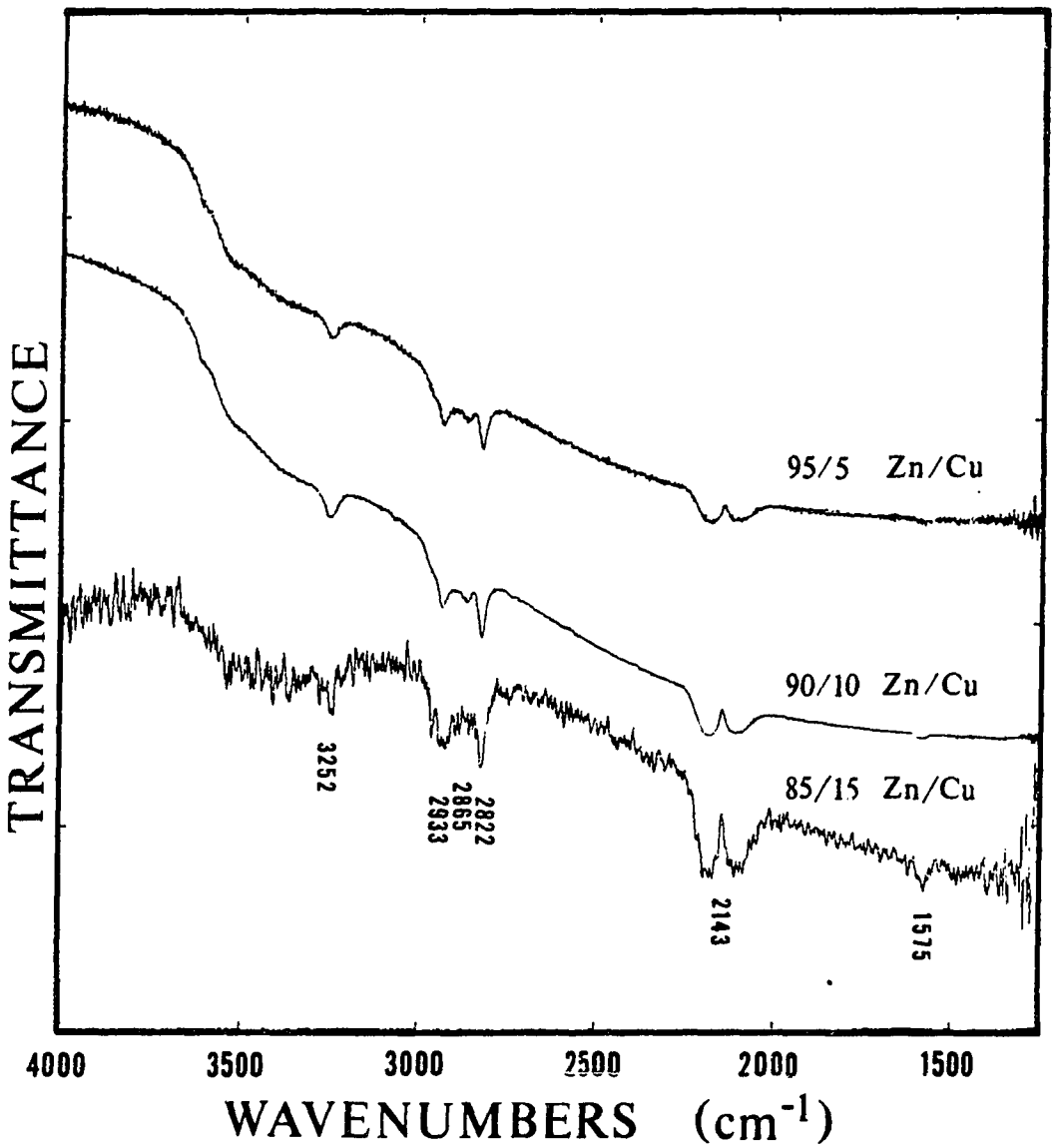

Figure 72. Adsorption of CO-H_2 mixture on binary oxides at 50 atm

the bands for gaseous carbon monoxide (band at 2143 cm^{-1}).

Because methanol synthesis normally includes some carbon dioxide in the feed mixture, the adsorption of a 27/7/66 $CO/CO_2/H_2$ mixture on 95/5 Zn/Cu catalyst (pretreatment #3) at 200°C and 50 atmospheres was examined. Surface species at high pressure were identical with those using only hydrogen and carbon monoxide in the feed. Figure 73 shows that after the pressure was dropped to 1 atmosphere, some decomposition of methoxy groups (bands at 2934 and 2826 cm^{-1}) occurred. After the cell had been thoroughly flushed with nitrogen, greater detail of surface groups was revealed. Further decomposition of methoxy groups restored the isolated hydroxyl groups (bands at 3663 and 3614 cm^{-1}), revealed a Type I hydroxyl species (band at 3524 cm^{-1}), a carbonyl group (band at 2010 cm^{-1}), an adsorbed formaldehyde species (bands at 2938, 2830, 2737, and 1616 cm^{-1}), and bidentate carbonate groups (bands at 1516 and 1327 cm^{-1}). The presence of some carbon dioxide (band at 2350 cm^{-1}) in the spectrum without the vibrational-rotational lines indicated that the carbon dioxide was trapped in the catalyst pores.

Methanol synthesis also occurred when formic acid solution was used in a hydrogenating feed stream. Figure 74 shows the spectrum of the adsorption of formic acid solution (73% HCOOH, 27% H_2O) in a carrier gas of 50% H_2-50% N_2 on a 95/5 Zn/Cu catalyst at 200°C and 47 atmospheres. The surface species during formic acid hydrogenation were very similar to those during carbon monoxide hydrogenation except for the lack of gaseous CO or any surface carbonyl species. The surface had some methoxy groups (bands at 2934 and 2820 cm^{-1}), formate groups (bands at 2868 and

Figure 73. Adsorption of $CO-CO_2-H_2$ mixture on 95/5 Zn/Cu oxide at 50 atm

a) exposure for 4 hours and pressure drop

b) 15-minute flush with nitrogen

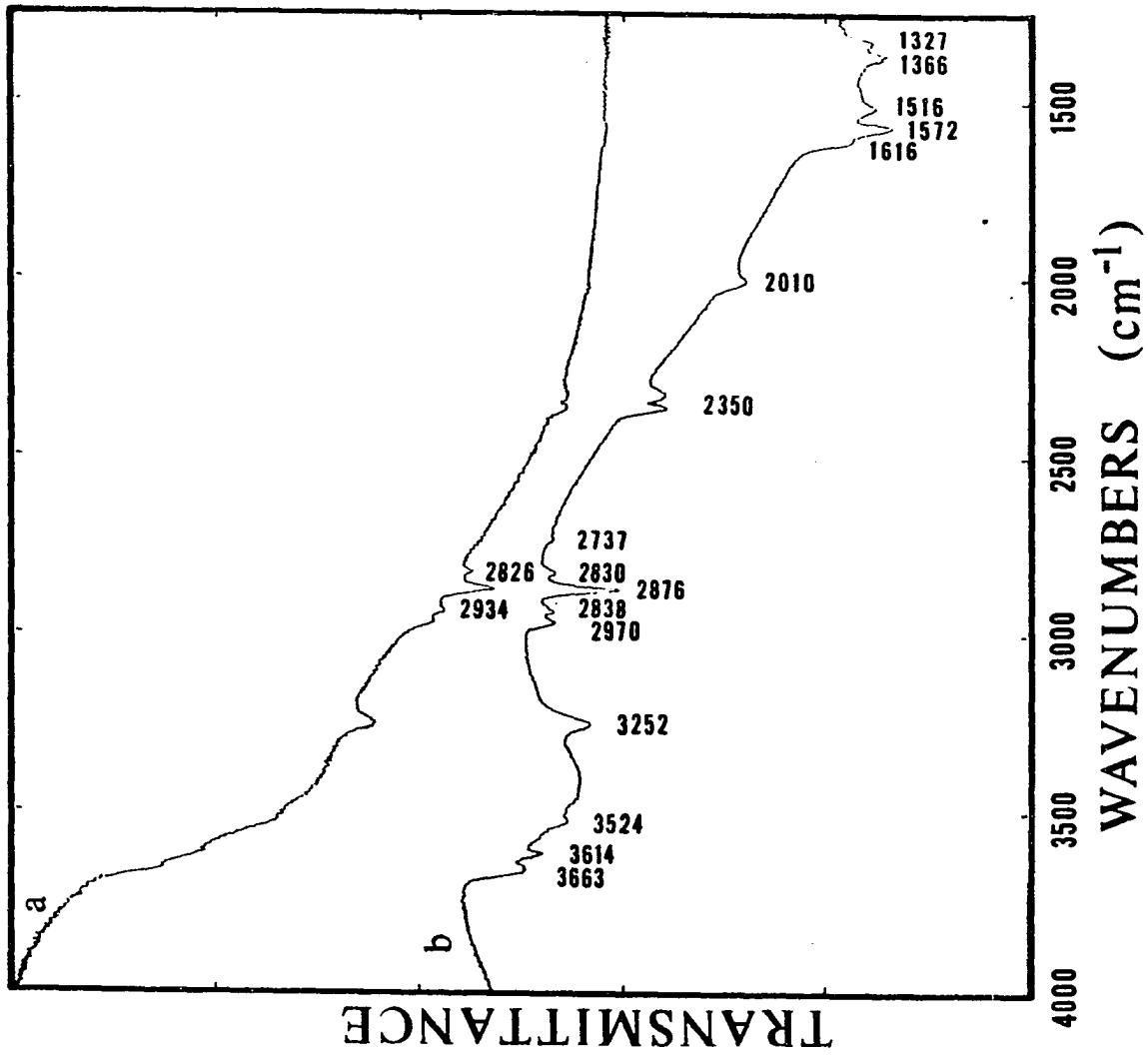
1327
1366
1516
1572
1616
2010
2350
2737
2826
2830
2876
2934
2838
2970
3252
3524
3614
3663
a
b
TRANSMITTANCE
4000
3500
3000
2500
2000
1500
WAVENUMBERS (cm-1)

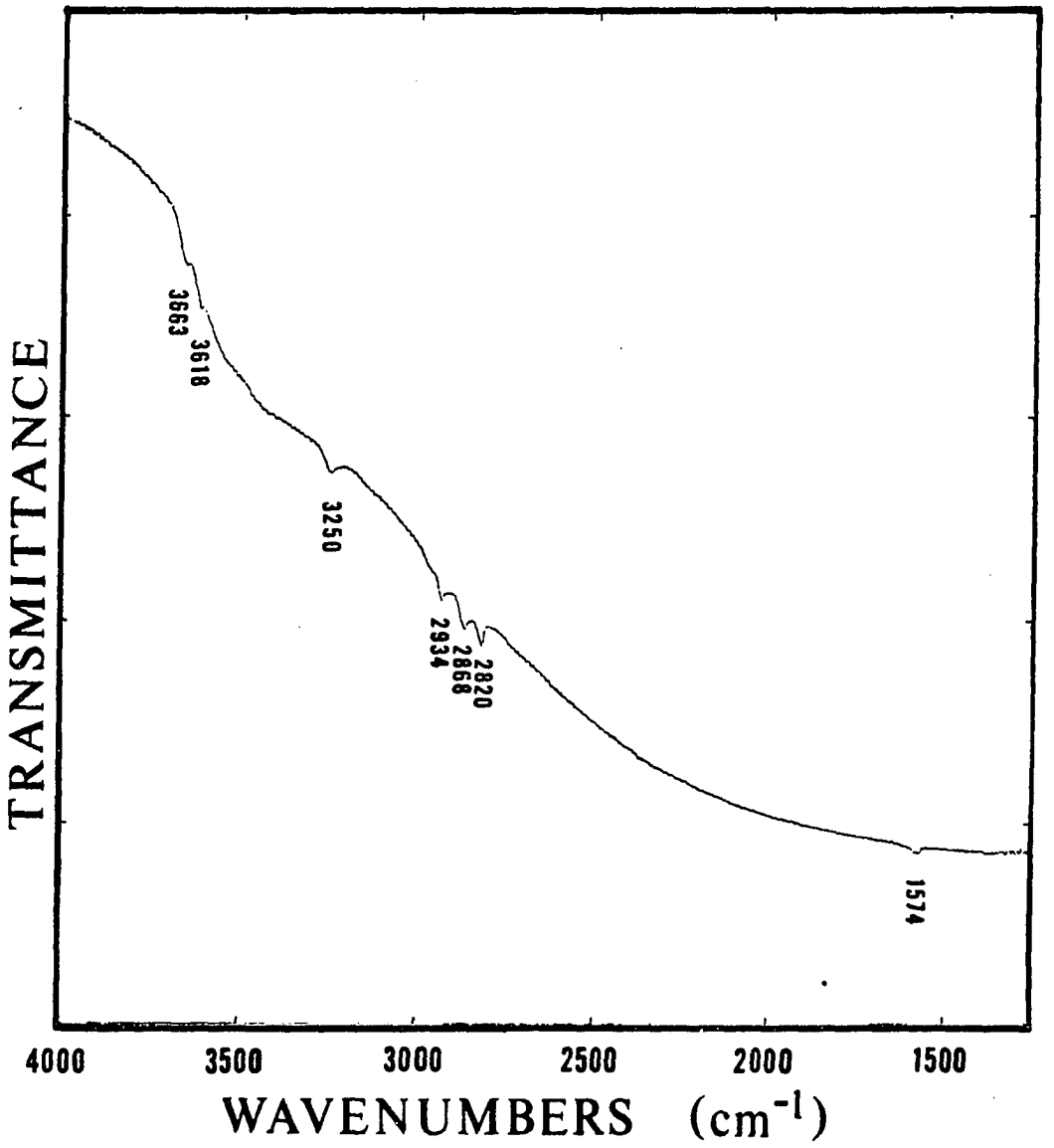

Figure 74. Adsorption of formic acid on 95/5 Zn/Cu oxide at 47 atm

1574 cm^{-1}), the hydroxyl of reduction (band at 3250 cm^{-1}), and isolated hydroxyl groups (bands at 3663 and 3618 cm^{-1}).

Species on ternary catalysts

The zinc-copper-chromium oxide catalysts were superior to binary catalysts in high-pressure infrared experiments because the transmittance remained high throughout the mid-infrared range. Better surface detail provided more information for identifying adsorbed species during methanol synthesis conditions.

The reaction of carbon monoxide and hydrogen on a 90/5/5 Zn/Cu/Cr catalyst at 200°C and 50 atmospheres is shown in Figure 75. The initial surface species on the reduced catalyst (pretreatment #3) after exposure to a 2/1 H_2/CO mixture were formate groups (bands at 2963, 2872, 1582, 1381, and 1360 cm^{-1}), adsorbed formaldehyde species (bands at 2934 and 2843 cm^{-1}), and methoxy groups (bands at 2934 and 2824 cm^{-1}). The adsorbed formaldehyde species disappeared and the amount of methoxy groups had maximized in an hour, followed by a gradual decrease in methoxy groups. A pressure drop to 1 atmosphere revealed an adsorbed carbonyl species at 2010 cm^{-1}.

Because the decrease over time of methoxy groups might have occurred owing to severe reduction of the catalyst, a similar experiment was conducted at the same conditions except that the 2/1 H_2/CO mixture was passed through the high-pressure saturator containing distilled water. Figure 76 shows the same general behavior of adsorbed species as the previous experiment without any water in the feed. The initial spectrum did not have any adsorbed formaldehyde and the final spectrum

Figure 75. Adsorption of CO-H_2 mixture on 90/5/5 Zn/Cu/Cr oxide at 50 atm

a) exposure for 15 minutes

b) exposure for 30 minutes

c) exposure for 8 hours

d) after pressure drop

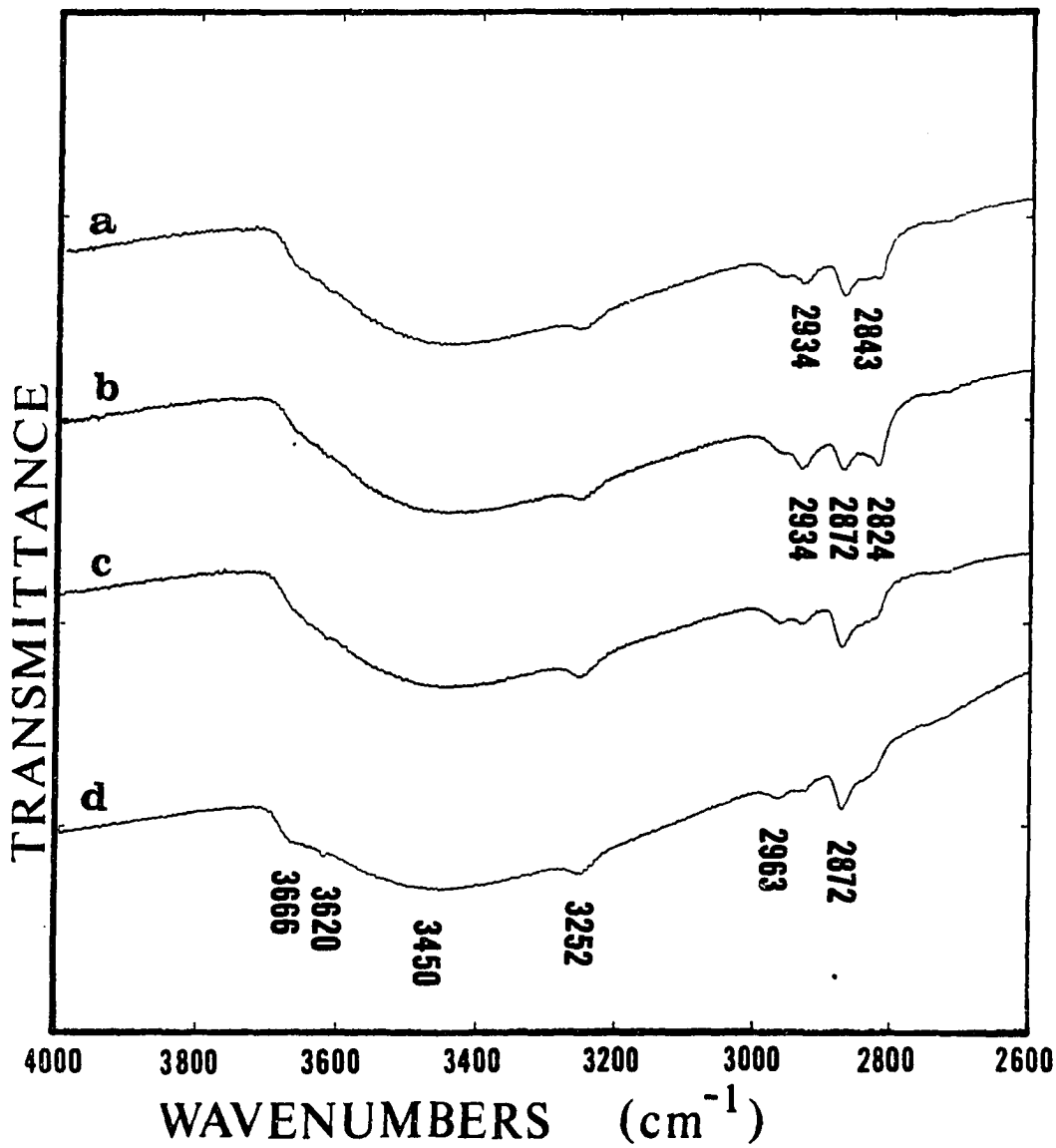
a
b
c
d
2934
2843
2934
2872
2824
3666
3620
3450
3252
2963
2872
TRANSMITTANCE
4000
3800
3600
3400
3200
3000
2800
2600
WAVENUMBERS (cm-1)

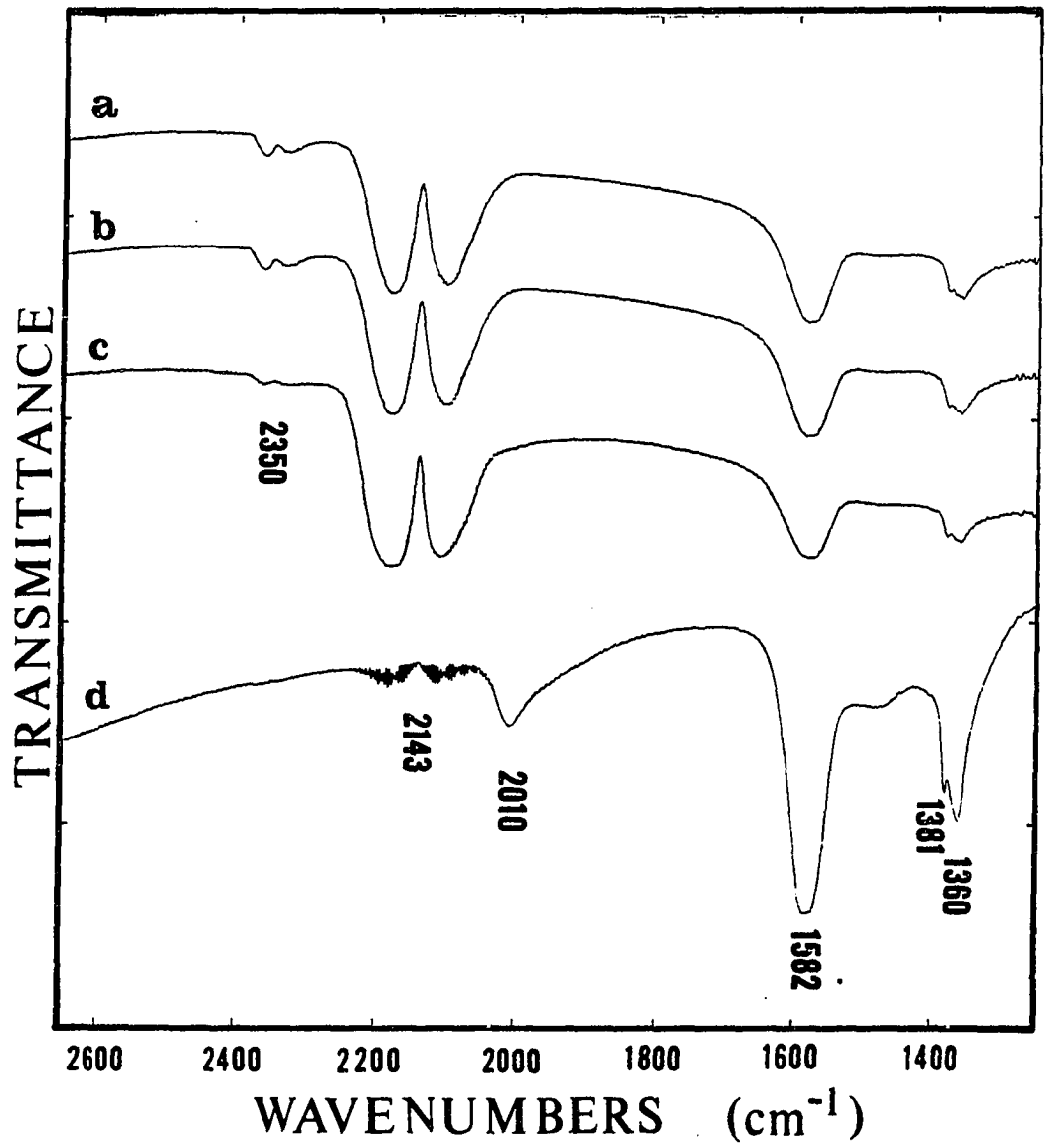

Figure 75. Continued

Figure 76. Adsorption of $CO-H_2-H_2O$ on 90/5/5 Zn/Cu/Cr oxide at 50 atm

a) exposure for 15 minutes

b) exposure for 1 hour

c) exposure for 8 hours

d) after pressure drop

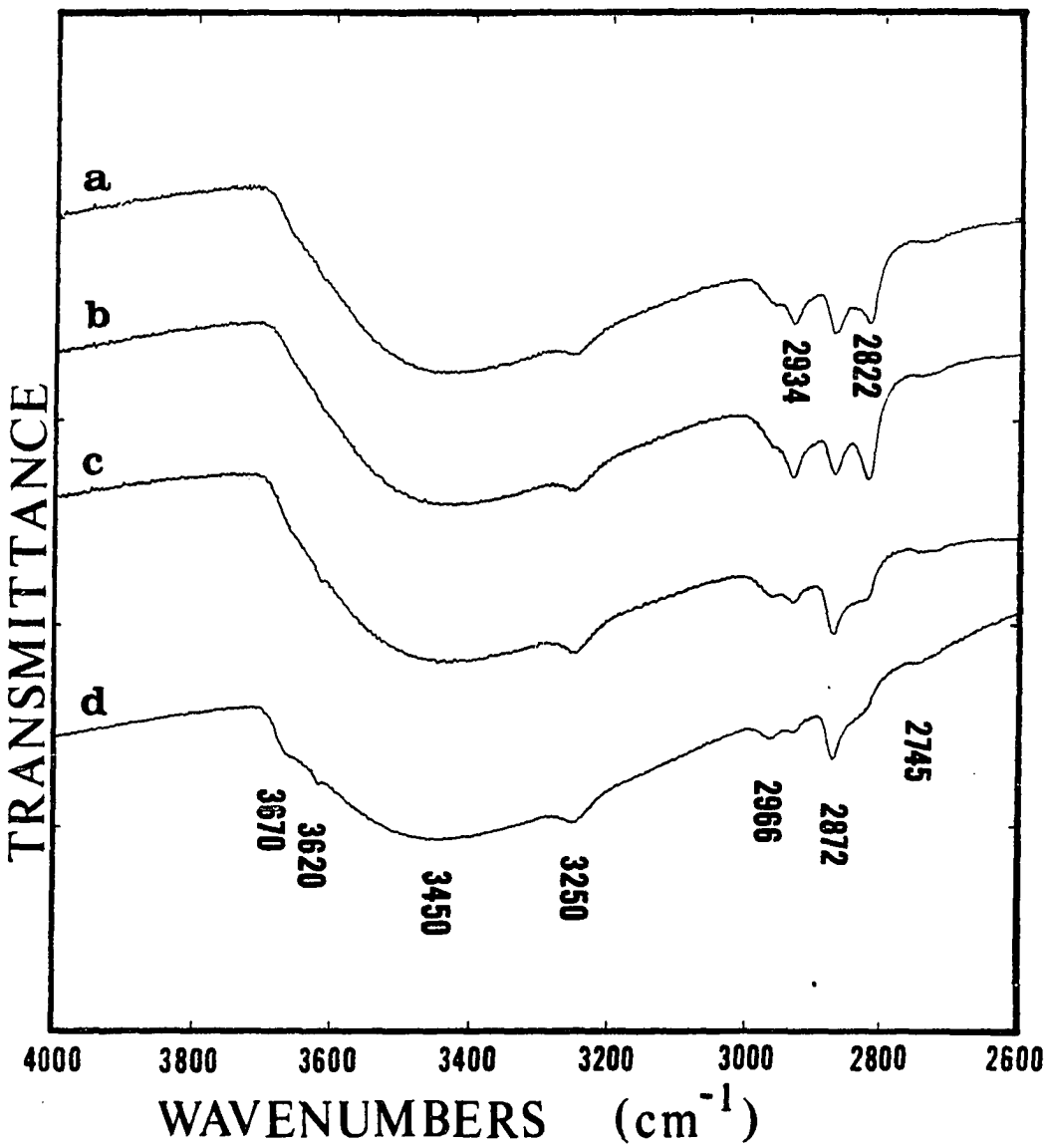
a
b
c
d
2934
2822
3670
3620
3450
3250
2966
2872
2745
TRANSMITTANCE
4000
3800
3600
3400
3200
3000
2800
2600
WAVENUMBERS (cm-1)

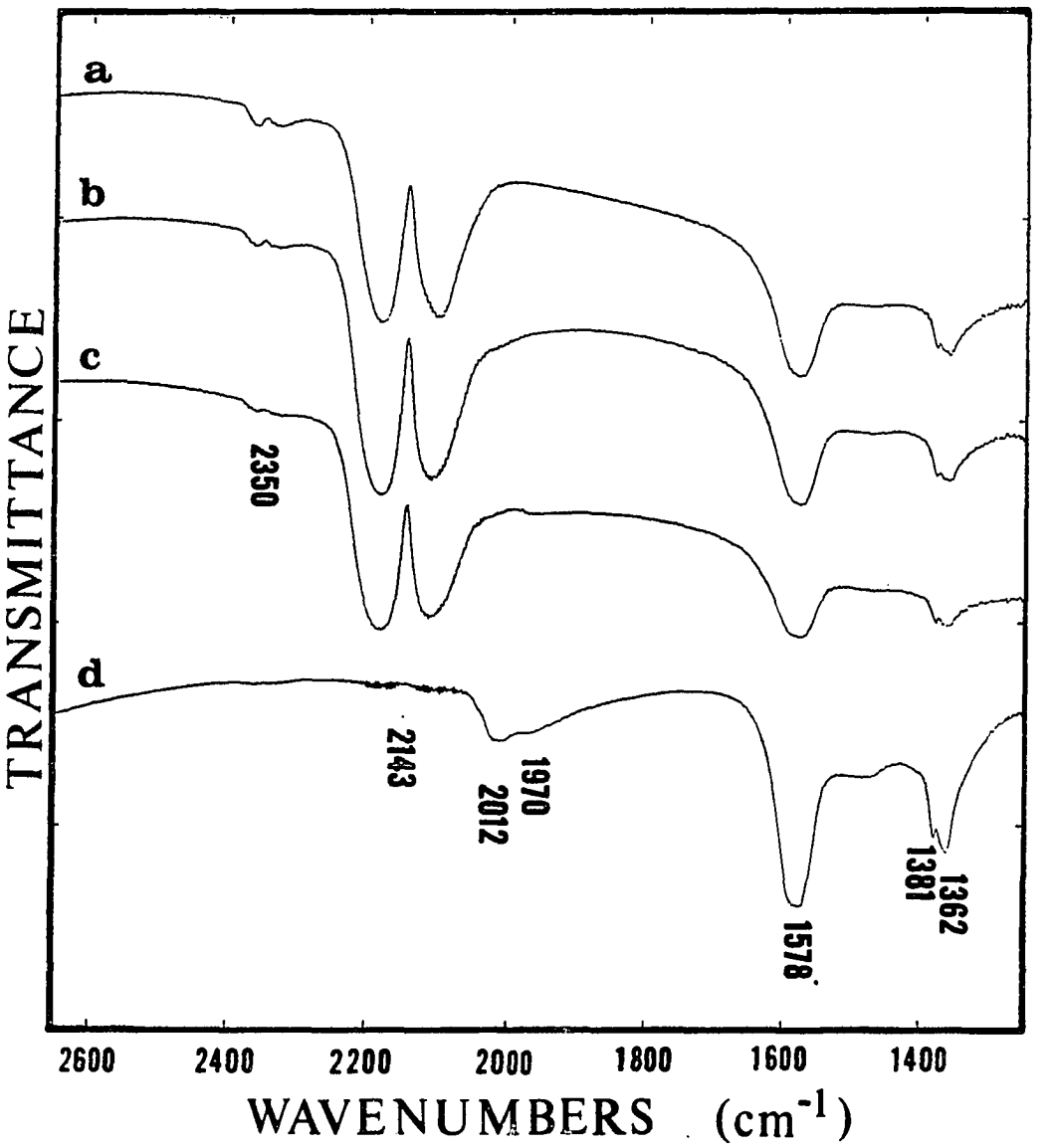

Figure 76. Continued

revealed carbonyl groups at 2012 and 1970 cm^{-1}.

The reaction of carbon monoxide and hydrogen (H_2/CO = 2/1) on a 80/10/10 Zn/Cu/Cr catalyst (pretreatment #3) at 200°C and 50 atmospheres is shown in Figure 77. The initial spectrum showed formate groups (bands at 2870, 1576, 1381, and 1360 cm^{-1}), methoxy groups (bands at 2932 and 2822 cm^{-1}), and a carbonyl species at 2089 cm^{-1}. The methoxy groups increased and reached a stable concentration as steady-state conditions were approached. The carbonyl species shifted from 2089 to 2021 cm^{-1}. A pressure drop to 1 atmosphere revealed in sharper detail the carbonyl species (band at 2010 cm^{-1}).

The reactor tests established that although a binary catalyst was active for formic acid hydrogenation to methanol, the 80/10/10 Zn/Cu/Cr catalyst was inactive for this reaction during the same operating conditions. The adsorption of formic acid solution (73% HCOOH, 27% H_2O) in a carrier gas of 50% H_2-50% N_2 on a 80/10/10 Zn/Cu/Cr catalyst (pretreatment #3) at 200°C and 50 atmospheres is shown in Figure 78. Initially, the surface species were a carbonyl species (band at 1983 cm^{-1}) with minor amounts of formate groups (bands at 2872, 1580, 1381, and 1360 cm^{-1}). Prolonged exposure began to produce some methoxy groups (bands at 2934 and 2818 cm^{-1}), but not much since the isolated hydroxyl groups (bands at 3668 and 3618 cm^{-1}) were not completely displaced. At high pressure, the decomposition of formic acid into formate and methoxy groups on zinc-copper-chromium oxides was unfavorable, hence, the poor methanol synthesis activity.

Figure 77. Adsorption of CO-H_2 mixture on 80/10/10 Zn/Cu/Cr oxide at 50 atm

a) exposure for 15 minutes

b) exposure for 1 hour

c) exposure for 4 hours

d) after pressure drop

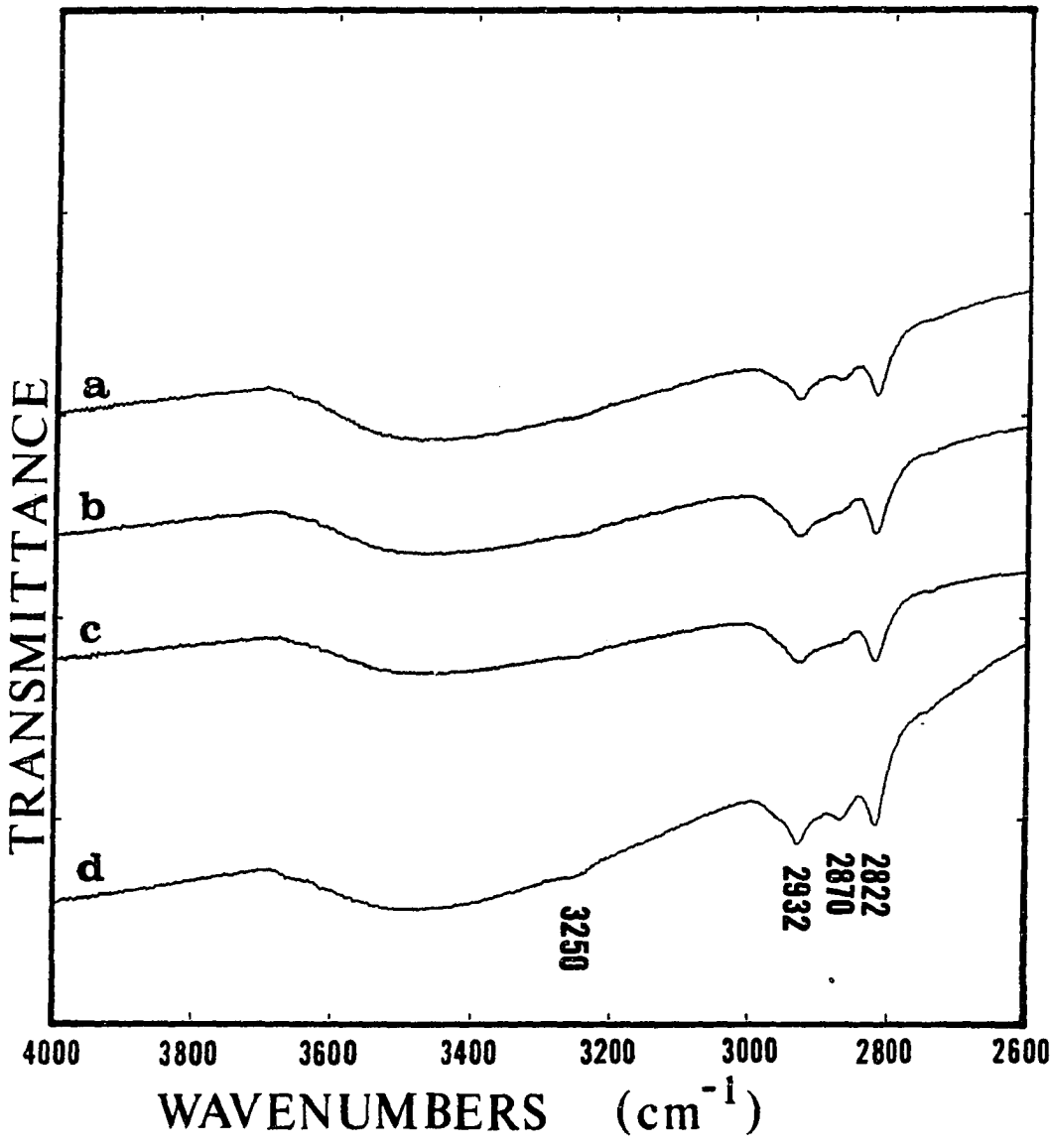
TRANSMITTANCE
a
b
c
d
3250
2932
2870
2822
4000
3800
3600
3400
3200
3000
2800
2600
WAVENUMBERS (cm-1)

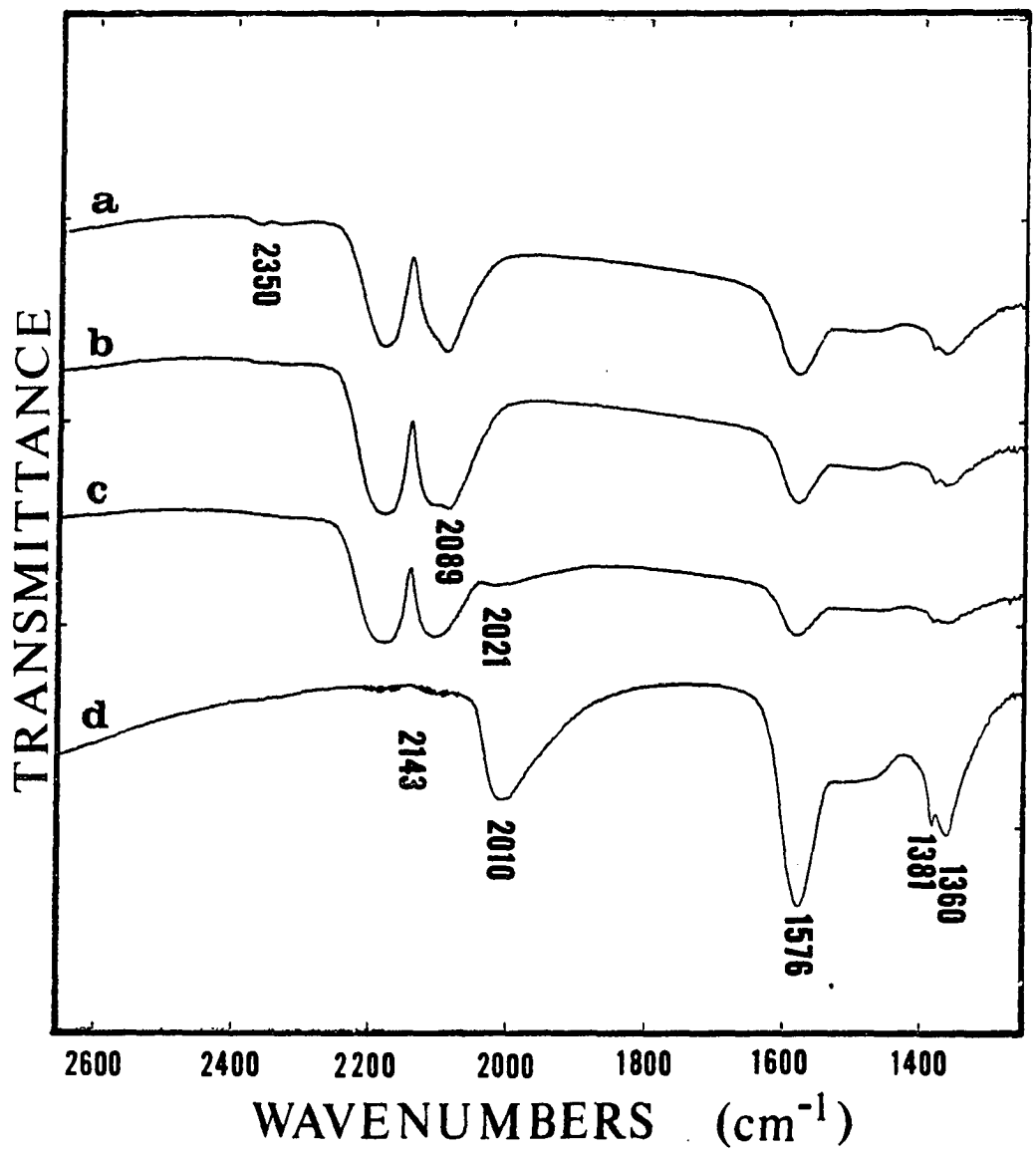

Figure 77. Continued

Figure 78. Adsorption of formic acid on 80/10/10 Zn/Cu/Cr oxide at 50 atm

a) reduced surface

b) exposure for 1 hour

c) exposure for 3 hours

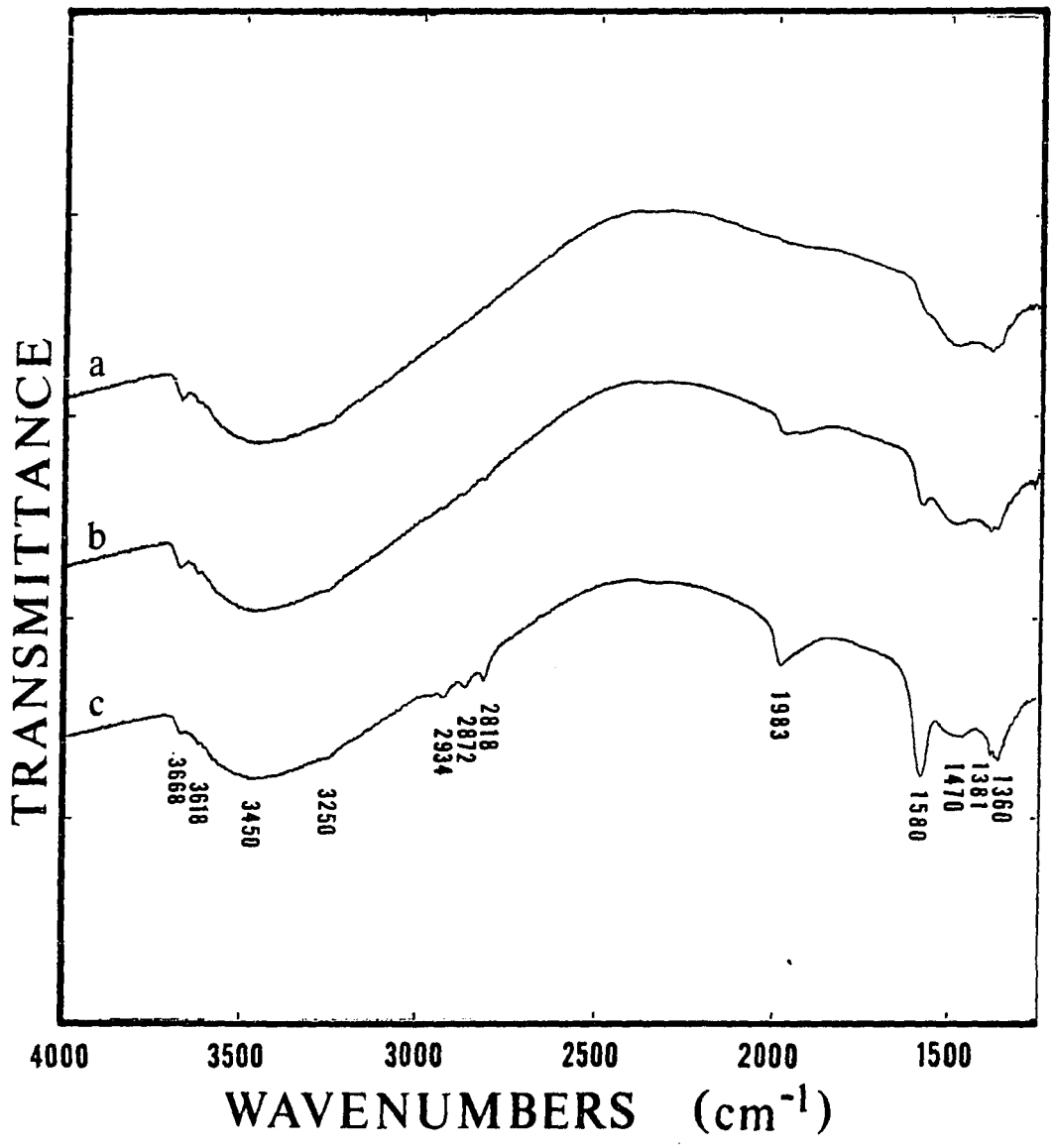
TRANSMITTANCE
a
b
c
3668
3618
3450
3250
2818
2872
2934
1983
1580
1470
1381
1360
4000
3500
3000
2500
2000
1500
WAVENUMBERS (cm-1)

DISCUSSION OF RESULTS

The reactor tests established that coprecipitated binary and ternary catalysts were active and highly selective for methanol synthesis at 50 atmospheres and 200-250°C, even though the copper contents in these compositions were much lower than those used in industrial catalysts. The methanol synthesis reaction was far from equilibrium in all the reaction experiments. At equilibrium, the conversion of carbon monoxide to methanol using a stoichiometric mixture of CO and H_2 would be 82% and 60% at 200°C and 250°C, respectively. The experimental conversions, including values from feeds containing an oxidizing promoter, were generally under 15%. A small addition of water into a CO-H_2 feed stream produced an effluent with carbon dioxide rather than water, indicating that the water-gas shift reaction was near equilibrium.

At 200°C, zinc oxide and impregnated CuO/ZnO were inactive for methanol synthesis, whereas the coprecipitated binary and ternary oxides possessed some activity. A feed stream of CO and H_2 would usually be expected to deactivate these catalysts, but some carbon dioxide was formed during the initial stage of reaction (some CO_2 was detected initially in the reactor effluent and CO_2 was observed in the infrared spectra). This carbon dioxide could be formed either from further reduction of the catalyst by carbon monoxide or via the water-gas shift reaction as carbon monoxide reacts with water in catalyst pores (the water would be the product of the prior reduction using hydrogen). The activity was maintained over an 8-hour period because some carbon dioxide persisted in the catalyst pores. The gradual decrease in

activity coincided with a gradual decrease in the CO_2 band intensity in infrared spectra. The addition of carbon dioxide or water to the CO-H_2 feed stream generally decreased the yield of methanol at 200°C. The initial decrease of the oxidant concentration in the reactor effluent and the release of relatively large amounts of the oxidant when the pressure was reduced suggested that the oxidant was adsorbed by the catalyst. Reaction rates were inhibited by relatively high concentrations of the oxidant in the catalyst pores.

At 250°C, the effect of an oxidizing additive was positive on the reaction rate. The increased temperature improved the yields on all catalysts, but catalyst deactivation was also increased as evident by the promotional effect of oxidant additions to the CO-H_2 feed stream. Assuming that Cu(I) sites are necessary for methanol synthesis (Herman et al., 1979), the function of small amounts of CO_2 or H_2O was to prevent the reduction of Cu(I) sites to copper in the zero valent state. Even pure zinc oxide showed some activity for methanol synthesis at 250°C, although the yield was an order of magnitude less than the binary and ternary catalysts.

The infrared spectra taken at 50 atmospheres in CO/H_2 mixtures had much less transmission than previous spectra taken at atmospheric pressure, especially the binary catalyst results. However, despite some lack of detail in the high pressure spectra, it was apparent that the surface species were essentially the same at the various pressures. Thus, band assignments that were given to adsorbed species on these metal oxides at atmospheric pressure have been applied to surface species at 50 atmospheres. The primary effects of elevated pressure were to

stabilize the surface hydroxyls at 3520 cm^{-1} and to weaken the carbon-oxygen bond of the surface carbonyl (band shift to lower frequency).

Information about the sequence of reaction steps and adsorption sites was obtained from transient experiments. Despite the low activity of these catalysts at 200°C, the infrared spectra showed that steady-state surface conditions were quickly reached when a stoichiometric CO/H_2 feed mixture was used. The surface reactions could be slowed by decreasing the amount of hydrogen in the feed mixture. Even in the extreme case of having only carbon monoxide in the gas phase, gradual hydrogenation of surface groups occurred because the residual hydroxyls were a source of hydrogen. The adsorption of carbon monoxide at 50 atm on zinc oxide produced formate groups, whereas on a binary catalyst formate, formaldehyde, and methoxy groups were formed. The greater extent of surface hydrogenation on a binary catalyst as compared to zinc oxide indicated that the copper component of the binary catalyst enhanced hydrogenation as well as carbon monoxide adsorption. Formate groups were clearly formed before formaldehyde and methoxy groups. The order of formaldehyde and methoxy formation at high pressure was difficult to establish because the intensity of the formaldehyde bands was low, but results from the atmospheric studies suggested that the formaldehyde species was the precursor of the methoxy species.

At 200°C, the adsorption of hydrogen caused a reduction in transmittance without forming any new species of adsorbed hydrogen observable in the infrared spectra, except the hydroxyl at 3250 cm^{-1} on mixed metal oxides. This new hydroxyl species, however, was determined in Part II to be a bulk species which was unaffected by surface reactions.

Hydrogenation of surface species during CO adsorption in the absence of gaseous hydrogen demonstrated that hydrogen was mobile on the surface at 200°C.

The spectra of Zn/Cu/Cr ternary catalysts during methanol synthesis conditions provided the most detailed information on surface species. The adsorbed carbonyl gradually shifted from 2090 to 2020 cm^{-1}, indicating a weakening of the carbon-oxygen bond without changing the nature of the carbonyl (linear bonded). Formate, formaldehyde, and methoxy species were produced during the experiment; the best methanol catalyst (80/10/10 Zn/Cu/Cr oxide) had mainly methoxy groups on the surface at steady state and no observable formaldehyde groups. The hydroxyl region was too indistinct to detect any band at 3520 cm^{-1}.

The steady-state spectrum of surface species on a binary catalyst during methanol synthesis using a feed with formic acid was the same as the spectra for feed mixtures of CO/H_2 or $CO/CO_2/H_2$. Because the spectrum from the formic acid experiment showed no surface carbonyl or gaseous carbon monoxide, the evidence for a reaction sequence involving formate and methoxy intermediates was strengthened. The ternary catalysts were unsatisfactory for methanol synthesis using a feed with formic acid. The infrared spectrum showed very little formate and methoxy groups on this catalyst, apparently because formic acid decomposition at these conditions was difficult. This study provided additional proof of the importance of formate and methoxy groups in methanol synthesis because these species were lacking on the surface of ternary catalysts.

A mechanism for methanol synthesis based on the results from this study is shown in Figure 79. Carbon monoxide was adsorbed on Cu(I)

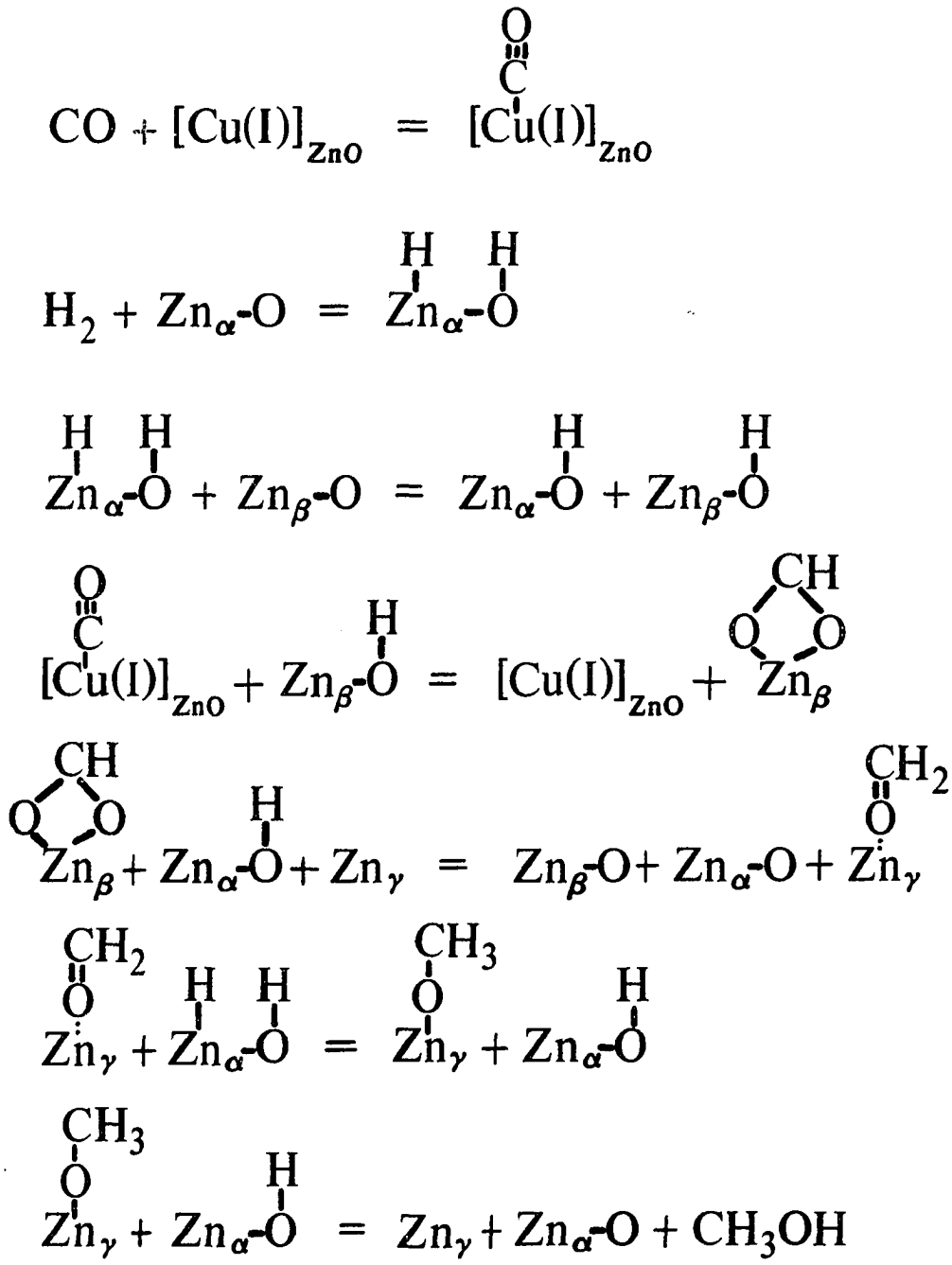

Figure 79. Methanol synthesis mechanism from infrared studies

sites in the zinc oxide lattice to form a linear carbonyl species (band at 2020 cm^{-1}). Hydrogen was adsorbed dissociatively on adjacent zinc-oxygen sites to form a hydroxyl and hydride species (Type I adsorption), but only the hydroxyl species (band at 3520 cm^{-1}) was stable enough to be seen in the infrared spectra. Hydrogen migrated to other sites to form other types of hydroxyl species (bands at 3550 and 3450 cm^{-1}) which were stable at these conditions. The surface carbonyl can insert itself into a hydroxyl group to form a bidentate formate species (bands at 2875, 1575, 1381, and 1365 cm^{-1}). Hydrogenation of the formate species produced an adsorbed formaldehyde species (bands at 2935, 2850, 2740, and 1600 cm^{-1}) which was adsorbed to a different surface site than the formate species. The formaldehyde species was quickly hydrogenated to form a methoxy species (bands at 2935 and 2820 cm^{-1}). The rate determining step was the hydrogenation of the methoxy species to methanol.

The various zinc sites proposed to be involved in this mechanism can be associated with specific hydroxyl groups. The hydroxyl band at 3520 cm^{-1} is the site of hydrogen adsorption. This band was very prominent during methanol or formic acid adsorption. The hydroxyl bands at 3550 and 3450 cm^{-1} are the sites where the formate species was adsorbed. The formate groups occupy only part of these hydroxyl sites since the formation of formate groups has little effect on the intensity of the hydrogen-bonded hydroxyl groups. The isolated hydroxyl bands at 3665 and 3620 cm^{-1} are the sites where the formaldehyde and methoxy species were adsorbed. These hydroxyl groups are completely displaced during methanol synthesis.

SUMMARY AND FUTURE RECOMMENDATIONS

This study has contributed significantly to an understanding of methanol synthesis on the type of mixed metal oxide known as the industrial low-pressure catalyst. This experimental work has placed emphasis on the characterization of binary catalysts with 95/5 and 90/10 Zn/Cu compositions, and ternary catalysts with 90/5/5 and 80/10/10 Zn/Cu/Cr compositions. Carbonyl, formate, and methoxy groups were identified by transmission infrared spectroscopy as stable surface species during methanol synthesis conditions (200°C and 50 atmospheres). The adsorption site of the carbonyl species was established to be a Cu(I) site because 1) only catalysts containing copper had this carbonyl species, 2) Auger spectra showed the presence of copper in the first valence state in reduced catalysts, and 3) the carbonyl stretching frequency in organometallic copper(I) complexes was very close to this carbonyl stretching frequency at atmospheric pressure. The carbonyl species was the only surface species to shift significantly when the pressure was increased from 1 to 50 atmospheres; the carbonyl stretching frequency shifted from 2085 to 2020 cm^{-1}. The formate species was adsorbed to a zinc site (Zn_β) which did not affect the isolated hydroxyls (bands at 3665 and 3620 cm^{-1}). The methoxy species, however, displaced the isolated hydroxyl groups, indicating that the methoxy species was adsorbed on a different zinc site (Zn_γ). A formaldehyde species, also adsorbed on a Zn_γ site, was unstable at 200°C. Some evidence suggested that a hydroxyl species adsorbed on a Zn_α site (Type I hydrogen adsorption) was stable at high pressure and 200°C, and was the source of the hydrogen

for methoxy hydrogenation to methanol. The rate-determining step in methanol synthesis was determined to be the hydrogenation of methoxy groups.

The formate species was identified as a reaction intermediate in methanol synthesis by using a feed stream containing formic acid and hydrogen. Adsorbed formate and methoxy groups were formed on a binary catalyst which produced methanol as the only product. The addition of carbon dioxide to a feed of carbon monoxide and hydrogen had little effect on the methanol yield at 200°C but substantially improved the yield at 250°C. Carbon dioxide apparently prevented the reduction of some Cu(I) active sites at the higher temperature. Carbon dioxide was absorbed in the catalyst pores at high pressure. At reaction conditions, any water in the feed or in the catalyst pores rapidly reacted with carbon monoxide to form carbon dioxide and hydrogen at thermodynamic equilibrium (water-gas shift reaction). The methanol synthesis reaction was always far from equilibrium with these catalysts.

At atmospheric pressure and 200°C, the surface species produced by a feed of carbon monoxide and hydrogen were carbonyl, formate, and methoxy groups. A feed of carbon dioxide and hydrogen only produced formate groups. It was determined that the adsorbed copper carbonyl species promoted the hydrogenation of formate groups to methoxy groups. Methanol adsorption produced methoxy groups and hydroxyls adsorbed on Zn_α sites while displacing the isolated hydroxyls adsorbed on Zn_γ sites. Adsorption with deuterated methanol established that the hydrogen in the Zn_α hydroxyl had come from the hydroxyl group of methanol. Formic acid adsorption produced formate groups and hydroxyls adsorbed on Zn_α sites without displacing the isolated hydroxyls. Formaldehyde adsorption at

200°C produced formate and methoxy groups, whereas at 100°C, an adsorbed formaldehyde species bonded to the surface through the oxygen end of the molecule to a Zn_γ site was formed. A summary of surface species, band assignments, and adsorption sites is given in Table 24. Information for deuterated species is presented in Table 25.

This work has raised many new questions about these catalysts and the behavior of adsorbed species which may be addressed with techniques that were not used in this study. It is currently thought that some copper exists as a solid solution within the zinc oxide crystallites (Herman et al., 1979). The Guinier results in Part I showed no change in the zinc oxide lattice parameters for catalysts with copper contents up to 10 atomic % in both oxidized and reduced states. These results can be explained as either 1) no copper is in the zinc oxide crystallites, or 2) the coordination of the copper in the reduced catalyst is different than the coordination in the oxidized catalyst. This problem could be resolved by conducting an EXAFS study of both oxidized and reduced binary catalysts to determine the local geometry around copper atoms,

Solid-state NMR spectroscopy may be able to provide additional information about the nature and behavior of adsorbed species. At 200°C, the adsorption of carbon monoxide on a coprecipitated binary catalyst produced both formate and methoxy groups. There is no question but that this hydrogenation involves an adsorbed form of hydrogen, but only surface hydroxyl groups are observed in the infrared spectra. Hydrogen adsorption at room temperature forms new bands at 3490 and 1710 cm^{-1} corresponding to ZnOH and ZnH species, but at 200°C, hydrogen adsorption does not affect any residual hydroxyls nor are any new bands formed.

Table 24. Infrared band assignments for surface species

Band (cm^{-1})	Assignment	Adsorbed site
Bidentate formate		Zn_{β}
ν_1 2875 ± 5	CH stretching	
ν_4 1575 ± 5	Asym. OCO stretching	
ν_5 1380 ± 2	CH bending	
ν_2 1365 ± 5	Sym. OCO stretching	
2966 ± 4	$\nu_4 + \nu_5$	
2740 ± 4	$\nu_2 + \nu_5$	
Methoxy		Zn_{γ}
2935 ± 2	Asym. CH_3 stretching	
2820 ± 2	Sym. CH_3 stretching	
Formaldehyde		Zn_{γ}
2935 ± 5	CH_2 scissoring overtone	
2850 ± 10	Asym. CH_2 stretching	
2740 ± 5	Sym. CH_2 stretching	
1600 ± 10	C=O stretching	
Carbonyls		
2200 ± 20	C≡O stretching	Zn
2085 ± 5	C≡O stretching (1 atm)	Cu
2020 ± 10	C≡O stretching (50 atm)	Cu
Hydroxyls		
3665 ± 5	OH stretching	Zn
3640 ± 4	OH stretching	Zn_{γ}
3620 ± 2	OH stretching	Zn_{γ}
3550 ± 20	OH stretching	Zn_{β}
3525 ± 5	OH stretching	Zn_{β}
3450 ± 20	OH stretching	Zn^{α}_{β}
Unidentate carbonate		Zn_{β}
1470 ± 5	Asym. OCO stretching	
1380 ± 5	Sym. OCO stretching	

Table 24. Continued

Band (cm^{-1})	Assignment	Adsorbed site
Bidentate carbonate		Zn_{β}
1512 ± 5	Asym. OCO stretching	
1325 ± 5	Sym. OCO stretching	

Table 25. Infrared band assignments for deuterated species

Band (cm^{-1})	Assignment	Adsorbed site
Bidentate formate		Zn_{β}
2166 ± 5	CD stretching	
1575 ± 5	Asym. OCO stretching	
1335 ± 5	Sym. OCO stretching	
Methoxy		Zn_{γ}
2220 ± 2	Asym. CD_3 stretching	
2088 ± 2	Sym. CD_3 stretching	
Hydroxyls		
2706 ± 5	OD stretching	Zn
2667 ± 2	OD stretching	Zn^{γ}
2630 ± 20	OD stretching	Zn^{γ}_{β}
2608 ± 5	OD stretching	Zn^{β}
2560 ± 20	OD stretching	Zn^{α}_{β}

The questions to be resolved are 1) the forms of adsorbed hydrogen which may be infrared inactive, and 2) the surface mobility of the species that are identified. Reduced binary catalysts also have a band at 3250 cm^{-1} which has been assigned to a bulk copper hydroxide. Because deuterium readily shifts all surface hydroxyl groups but not the band

at 3250 cm^{-1}, this species can be isolated and characterized by solid-state NMR.

The technique of mass spectrometry can be utilized in many types of experiments. The most powerful application of this method involves the use of isotopic reactants to elucidate the reaction mechanism. If a formate species is a reaction intermediate, then the carbon and oxygen atoms in methanol could be different from the carbon and oxygen atoms in the carbon monoxide molecule. A mixture containing $^{12}C^{18}O$ and $^{13}C^{16}O$ would establish whether or not any mixing occurs in methanol formation. The role of carbon dioxide in methanol synthesis can be determined by using an isotopic compound. Mass spectrometry can be very useful in adsorption and desorption studies. The adsorption of methanol forms methoxy groups on sites containing isolated hydroxyl groups. By using deuterated methanol as the adsorbate, the detection of HOD would establish that the hydroxyl hydrogen from methanol combines with a surface hydroxyl to form water. Infrared studies could easily be coupled with temperature programmed desorption to correlate changes in surface species with the gaseous products evolved.

REFERENCES

Abbati, I.; Braicovich, L.; De Michelis, B.; Fasana, A. Zn(0001) water interaction: An ultraviolet photoelectron spectroscopy investigation. Solid State Commun. 26: 515-517; 1978.

Amberg, C. H.; Seanor, D. A. An infrared study of CO adsorbed on surfaces of zinc oxide. Influence of pre-oxidation and doping. Sachtler, W. M. H.; Schuit, G. C. A.; Zwietering, P., eds. Proceedings of the 3rd International Congress on Catalysis. New York: Interscience; 1965; 450-460.

Atherton, K.; Newbold, G.; Hockey, J. A. Infra-red spectroscopic studies of zinc oxide surfaces. Disc. Faraday Soc. (52): 33-43; 1971.

Au, C. T.; Roberts, M. W.; Zhu, A. R. Surface hydroxylation at a Zn(0001)-O surface. Surface Sci. 115: L117-L123; 1982.

Badische Anilin und Soda Fabrik (BASF), assignee. D. R. patents 415,686; 441,433; 462,837. U.S. patents 1,558,559; 1,569,775. 1923.

Ballintine, Thomas A.; Schmulbach, C. David. High pressure reactor and cell for electronic and infrared spectral studies. J. Organometal. Chem. 164: 381-390; 1979.

Bardet, Robert; Thivolle-Cazat, Jean; Trambouze, Yves. Méthanolation des oxydes de carbone sur des catalyseurs Cu-Zn, à la pression atmosphérique. J. Chim. Phys. 78 (2): 135-138; 1981.

Bell, Alexis T. Applications of Fourier transform infrared spectroscopy to studies of adsorbed species. Bell, Alexis T.; Hair, Michael L. eds. Vibrational spectroscpies for adsorbed species. Washington, D.C.: American Chemical Society; 1980; 13-35.

Bell, Robert John. Introductory Fourier transform spectroscopy. New York: Academic Press; 1972.

Berry, Reginald I. Gasoline or olefins from an alcohol feed. Chem. Eng. 87 (Apr. 21): 86-88; 1980.

Boccuzzi, F.; Borello, E.; Zecchina, A.; Bossi, A.; Camia, M. Infrared study of ZnO surface properties I. Hydrogen and deuterium chemisorption at room temperature. J. Catal. 51: 150-159; 1978a.

Boccuzzi, F.; Garrone, E.; Zecchina, A.; Bossi, A.; Camia, M. Infrared study of ZnO surface properties II. H_2-CO interaction at room temperature. J. Catal. 51: 160-168; 1978b.

Borowitz, J. L. On the mechanism of the synthesis CO + $2H_2 \rightarrow CH_3OH$. J. Catal. 13: 106-108; 1969.

Bowker, M.; Madix, R. J. XPS, UPS and thermal desorption studies of alcohol adsorption on Cu(110) I. Methanol. Surface Sci. 95: 190-206; 1980.

Bowker, Michael; Houghton, Hilary; Waugh, Kenneth C. Mechanism and kinetics of methanol synthesis on zinc oxide. Chem. Soc., Faraday Trans. I 77: 3023-3036; 1981.

Bozon-Verduraz, F. Difficulties concerning the infrared identification of surface species on metal oxides. J. Catal. 18: 12-18; 1970.

Brown, Kevin L.; Clark, George R.; Headford, Christine E. L.; Marsden, Karen; Roper, Warren R. Organometallic models for possible Fischer-Tropsch intermediates. Synthesis, structure, and reactions of a formaldehyde complex of osmium. J. Am. Chem. Soc. 101: 503-505; 1979.

Brynestad, J. Iron and nickel carbonyl formation in steel pipes and its prevention — Literature survey. Oak Ridge National Laboratory TM-5499; 1976; 16 p.

Budneva, A. A.; Davydov, A. A.; Mikhal'chenko, V. G. IR spectroscopic study of hydrocarbon adsorption on oxide catalysts III. Adsorption of propylene on chromium oxide. Kinet. Catal. 16: 409-412; 1975. Translated from Kinet. Katal. 16: 468-490; 1975.

Bulko, John B.; Herman, Richard G.; Klier, Kamil; Simmons, Gary W. Optical properties and electronic interactions of microcrystalline Cu/ZnO catalysts. J. Phys. Chem. 83: 3118-3122; 1979.

Busca, Guido; Lorenzelli, Vincenzo. Infrared study of methanol, formaldehyde, and formic acid adsorbed on hematite. J. Catal. 66: 155-161; 1980.

Chang, C. C.; Dixon, L. T.; Kokes, R. J. The nature of molecular hydrogen adsorbed on zinc oxide. J. Phys. Chem. 77: 2634-2640; 1973.

Chemical engineers' handbook. 5th ed. Perry, Robert H.; Chilton, Cecil H. eds. New York: McGraw-Hill Book Co.; 1973; 3.137-3.144.

Cheng, W. H.; Kung, H. H. Interaction of CO, CO_2, and O_2 with nonpolar, stepped and polar Zn surfaces of ZnO. Surface Sci. 122: 21-39; 1982.

Cheng, W. H.; Akhter, S.; Kung, H. H. Structure sensitivity in methanol decomposition on ZnO single-crystal surfaces. J. Catal. 82: 341-350; 1983.

Chow, Yuan L.; Buono-Core, Gonzalo E. Triplet-state benzophenone-sensitized photoreduction of bis(acetylacetonato)copper(II): The generation and stability of copper(I) complexes. Can. J. Chem. 61: 795-800; 1983.

Churchill, Melvyn Rowen; DeBoer, Barry G.; Rotella, Frank J.; Abu Salah, Omar M.; Bruce, Michael I. Determination of the crystal structure and molecular geometry of (hydrotris(1-pyrazolyl)borato)-copper(I) carbonyl. A unique structural investigation of a copper-carbonyl linkage. Inorg. Chem. 14: 2051-2056; 1975.

Cimino, A.; Molinari, E.; Cramarossa, F.; Ghersini, G. Hydrogen chemisorption and electrical conductivity of zinc oxide semiconductors. J. Catal. 1: 275-292; 1962.

Collman, J. P.; Winter, S. R. Isolation and characterization of a kinetically stable transition metal formyl complex. J. Am. Chem. Soc. 95: 4089-4090; 1973.

Davydov, A. A.; Shchekochikhin, V. M.; Zaitsev, P. M.; Shchekochikhin, Yu. M.; Keier, N. P. Investigation of the reactivity of forms of adsorbed oxygen on chromic oxide. Kinet. Catal. 12: 611-615; 1971. Translated from Kinet. Katal. 12: 694-699; 1971.

Deluzarche, A.; Kieffer, R.; Muth, A. Réactions CO, H_2 – Synthèse du méthanol sur chromite de zinc. Étude d'espèces chimisorbées à la surface du catalyseur. Schémas réactionnels possibles. Tetrahedron Lett. 38: 3357-3360; 1977.

Denise, B.; Sneeden, R. P. A.; Hamon, C. Hydrocondensation of carbon dioxide: IV. J. Mol. Catal. 17: 359-366; 1982.

Denny, P. J.; Whan, D. A. The heterogeneously catalysed hydrogenation of carbon monoxide. Catalysis 2: 46-86; 1978.

Dent, A. L.; Kokes, R. J. Hydrogenation of ethylene by zinc oxide I. Role of slow hydrogen chemisorption. J. Phys. Chem. 73: 3772-3780; 1969a.

Dent, A. L.; Kokes, R. J. Hydrogenation of ethylene by zinc oxide II. Mechanism and active sites. J. Phys. Chem. 73: 3781-3790; 1969b.

Dodge, Barnett F., inventor. Catalyst for methanol manufacture and method of producing same. U.S. patent 1,908,696. 1933 May 16.

Dolgov, B. N.; Karpinskii, M. H. Khim. Tverdogo Topliva 3: 559; 1932.

Dombek, D. Duane. Hydrogenation of carbon monoxide to methanol and ethylene glycol by homogeneous ruthenium catalysts. J. Am. Chem. Soc. 102: 6855-6857; 1980.

Eastman Kodak Company. Kodak Irtran infrared optical materials. Kodak publication U-72. Rochester, NY: Eastman Kodak Co., 1971; 51 p.

Eischens, R. P.; Pliskin, W. A.; Low, M. J. D. The infrared spectrum of hydrogen chemisorbed on zinc oxide. J. Catal. 1: 180-191; 1962.

Ewell, Raymond H. Calculation of chemical equilibrium at high pressures. Ind. Eng. Chem. 32: 147-153; 1940.

Fahey, Darryl R. Rational mechanism for homogeneous hydrogenation of carbon monoxide to alcohols, polyols, and esters. J. Am. Chem. Soc. 103: 136-141; 1981.

Fenske, M. R.; Frolich, P. K. Catalysts for the formation of alcohols from carbon monoxide and hydrogen. V. Decomposition and synthesis of methanol with a zinc-copper-chromium oxide catalyst. Ind. Eng. Chem. 21: 1052-1055; 1929.

Fink, Peter. Über die CO_2-chemisorption auf γ-aluminiumoxid. Z. Chem. 7: 324; 1967.

Friedrich, J. B.; Wainwright, M. S.; Young, D. J. Methanol synthesis over Raney copper-zinc catalysts I. Activities and surface properties of fully extracted catalysts. J. Catal. 80: 1-13; 1983a.

Friedrich, J. B.; Young, D. J.; Wainwright, M. S. Methanol synthesis over Raney copper-zinc catalysts II. Activities and surface properties of a partially leached alloy. J. Catal. 80: 14-24; 1983b.

Frolich, P. K.; Lewis, W. K. Synthesis of methanol from carbon monoxide and hydrogen. Ind. Eng. Chem. 20: 285-290; 1928.

Gagné, Robert R.; Allison, Judith L.; Gall, Robert S.; Koval, Carl A. Models for copper-containing proteins: Structure and properties of novel five-coordinate copper(I) complexes. J. Am. Chem. Soc. 99: 7170-7178; 1977.

Gallei, E.; Schadow, E. Ultrahigh-vacuum, high pressure and temperature infrared-ultraviolet-visible spectrophotometer cell. Rev. Sci. Instrum. 45: 1504-1506; 1974.

Gay, Robert R.; Nodine, Mark H.; Henrich, Victor E.; Zeiger, H. J.; Solomon, Edward I. Photoelectron study of the interaction of CO with ZnO. J. Am. Chem. Soc. 102: 6752-6761; 1980.

Geerts, Rolf L.; Huffman, John C.; Folting, Kirsten; Lemmen, Timothy H.; Caulton, Kenneth G. Concerning the structure and stability of a copper(I) alkoxy carbonyl. J. Am. Chem. Soc. 105: 3503-3506; 1983.

Gerasimova, G. F.; Keier, N. P.; Isaenko, L. I. Nature of the hydrogen adsorption centers on zinc oxide. Kinet. Catal. 14: 1087-1092; 1973. Translated from Kinet. Katal. 14: 1239-1245; 1973.

Giamello, E.; Fubini, B. Characterization of the interaction of CO and H_2 at the ZnO surface by adsorption microcalorimetry. React. Kinet. Catal. Lett. 16: 355-358; 1981.

Green, David W.; Reedy, Gerald T. Matrix-isolation studies. Ferraro, John R.; Basile, Louis J. eds. Fourier transform infrared spectroscopy. Vol. 1. New York: Academic Press; 1978; 18-37.

Greenler, Robert G. Infrared study of the adsorption of methanol and ethanol on aluminum oxide. J. Chem. Phys. 37: 2094-2100; 1962.

Gregg, S. J.; Ramsay, J. D. F. A study of the adsorption of carbon dioxide by alumina using infrared and isotherm measurements. J. Phys. Chem. 73: 1243-1247; 1969.

Griffiths, Peter R. Chemical infrared Fourier transform spectroscopy. New York: John Wiley & Sons, 1975.

Hair, M. L. Infrared spectroscopy in surface chemistry. New York: Marcel Dekker; 1967.

Hammaker, R. M.; Walters, J. P. The infrared spectra of C-13 enriched sodium formate. Spectrochim. Acta 20: 1311-1317; 1964.

Harvey, K. B.; Morrow, B. A.; Shurvell, H. F. The infrared absorption of some crystalline inorganic formates. Can. J. Chem. 41: 1181-1187; 1963.

Hata, Kazuo; Kawasaki, Shoji; Kubokawa, Yutaka; Miyata, Hisashi. Infrared studies of oxidation of olefins adsorbed on zinc oxide. Bond, G. C.; Wells, P. B.; Tompkins, F. C. eds. Proceedings of the 6th International Congress on Catalysis. Vol. 2. London: Chemical Society; 1977; 1102-1110.

Henrici-Olivé, G.; Olivé, S. Mechanistic reflections on the methanol synthesis with Cu/Zn catalysts. J. Mol. Catal. 17: 89-92; 1982.

Herd, A. C.; Onishi, Takaharu; Tamaru, Kenzi. Studies on the mechanism of methanol oxidation on zinc oxide by dynamic treatments of chemisorbed species under the reaction conditions. Bull. Chem. Soc. Japan 47: 575-578; 1974.

Herman, R. G.; Klier, K.; Simmons, G. W.; Finn, B. P.; Bulko, J. B.; Kobylinski, T. P. Catalytic synthesis of methanol from CO/H_2 I. Phase composition, electronic properties, and activities of the $Cu/ZnO/M_2O_3$ catalysts. J. Catal. 56: 407-429; 1979.

Herman, R. G.; Simmons, G. W.; Klier, K. Catalytic synthesis of methanol from CO/H_2 III. The role of alumina and ceria in the Cu/ZnO system. Seiyama, T.; Tanabe, K. eds. New horizons in catalysis: Proceedings of the 7th International Congress on Catalysis. New York: Elsevier Scientific; 1981; 475-484.

Hertl, William; Cuenca, Angela Maria. Infrared kinetic study of reactions of alcohols on the surface of alumina. J. Phys. Chem. 77: 1120-1126; 1973.

Hicks, R. F.; Kellner, C. S.; Savatsky, B. J.; Hecker, W. C.; Bell, A. T. Design and construction of a reactor for in situ infrared studies of catalytic reactions. J. Catal. 71: 216-217; 1981.

Himelfarb, P. B.; Wawner, F. E., Jr.; Bieser, A., Jr.; Vines, S. N. Oxidation states of copper during reduction of cupric oxide in methanol catalysts. J. Catal. 83: 469-471; 1983.

Hollins, P.; Pritchard, J. Interactions of CO molecules adsorbed on Cu(111). Surface Sci. 89: 486-495; 1979.

Horn, K.; Pritchard, J. Infrared spectrum of CO chemisorbed on Cu(100). Surface Sci. 55: 701-704; 1976.

Hotan, W.; Göpel, W.; Haul, R. Interaction of CO_2 and CO with nonpolar zinc oxide surfaces. Surface Sci. 83: 162-180; 1979.

Hougen, O. A.; Watson, K. M. Solid catalysts and reaction rates. Ind. Eng. Chem. 35: 529-541; 1943.

Hougen, O. A.; Watson, K. M.; Ragatz, R. A. Chemical process principles charts. 2nd ed. New York: John Wiley & Sons; 1960.

Ito, K.; Bernstein, H. J. The vibrational spectra of the formate, acetate, and oxalate ions. Can. J. Chem. 34: 170-178; 1956.

Ivanov, K. N. Mem. Inst. Chem. Ukr. Akad. Sci. U.R.S.S. 1: 49; 1934a.

Ivanov, K. N. Acta Physicochim. U.R.S.S. 1: 493; 1934b.

John, C. S. Catalysis by zinc oxide. Catalysis 3: 169-188; 1980.

Kagan, Yu. B.; Lin, G. I.; Rozovskii, A. Ya.; Loktev, S. M.; Slivinskii, E. V.; Bashkirov, A. N.; Naumov, I. P.; Khludenev, I. K.; Kudinov, S. A.; Golovkin, Yu. I. The mechanism of the synthesis of methanol from carbon dioxide and hydrogen I. Kinetic regularities. Kinet. Catal. 17: 380-384; 1976. Translated from Kinet. Katal. 17: 440-446; 1976.

Kagel, R. O. Infrared investigation of the adsorption and surface reactions of the C_1 through C_4 normal alcohols on γ-alumina. J. Phys. Chem. 71: 844-850; 1967.

Kauffe, K.; Pschera, K. Z. Anorg. Allgem. Chem. 262: 147; 1950.

Ketchik, S. V.; Minyukova, T. P.; Plyasova, L. M.; Yurieva, T. M.; Boreskov, G. K. Peculiarities of formation of ZnO and CuO-based solid solutions. React. Kinet. Catal. Lett. 19: 345-349; 1982.

Kieffer, R.; Ramaroson, E.; Deluzarche, A.; Trambouze, Y. A comparison of reactivity in the synthesis of methanol from $CO_2 + H_2$ and $CO + H_2$ (catalysts $Cu,Zn/Al_2O_3$, $P = 515 \times 10^4$ Pa). React. Kinet. Catal. Lett. 16: 207-212; 1981.

King, R. B.; King, A. D., Jr.; Iqbal, M. Z.; Frazier, C. C. Transition metal alkyl chemistry at elevated carbon monoxide pressures. An infrared spectroscopic study of systems related to catalytic intermediates in homogeneous hydroformylation reactions. J. Am. Chem. Soc. 100: 1687-1694; 1978.

King, S. T. An infrared spectroscopic flow reactor for in situ studies of heterogeneous catalytic reactions at high temperature and the reactions of CO_2 and benzyl benzoate on alumina. Appl. Spectrosc. 34: 632-636; 1980.

Kiselev, A. V.; Lygin, V. I. Infrared spectra of surface compounds. New York: John Wiley & Sons; 1975. Translated from the Russian by N. Kaner.

Klier, K. Methanol synthesis. Adv. Catal. 31: 243-313; 1982.

Klier, K.; Chatikavanij, V.; Herman, R. G.; Simmons, G. W. Catalytic synthesis of methanol from CO/H_2 IV. The effects of carbon dioxide. J. Catal. 74: 343-360; 1982.

Kohn, Philip M. Bright future for CO feed. Chem. Eng. 86 (Jan. 29): 49-52; 1979.

Kokes, R. J.; Dent, A. L.; Chang, C. C.; Dixon, L. T. Infrared studies of isotope effects for hydrogen adsorption on zinc oxide. J. Am. Chem. Soc. 94: 4429-4436; 1972.

Kotera, Y.; Oba, M.; Ogawa, K.; Shimomura, K.; Uchida, H. The preparation of the catalysts for methanol synthesis and their characteristics. Delmon, B.; Jacobs, P. A.; Poncelet, G. eds. Preparation of catalysts. Amsterdam: Elsevier Scientific; 1976; 589-599.

Kung, Harold H. Methanol synthesis. Catal. Rev. — Sci. Eng. 22 (2): 235-259; 1980.

Kuznetsov, V. A.; Gerei, S. V.; Gorokhovat-skii, Ya. B.; Rozhkova, É. V. Interaction of hydrocarbons with oxide catalyst surfaces I. Infrared spectroscopic study of the reaction of hydrocarbons with chromic oxide. Kinet. Catal. 18: 355-359; 1977. Translated from Kinet. Katal. 18: 418-423; 1977.

Kuznetsov, V. D.; Shub, F. S.; Temkin, M. I. Role of carbon dioxide in methanol synthesis on the copper catalyst SNM-1. Kinet. Catal. 23: 788-791; 1983. Translated from Kinet. Katal. 23: 932-935; 1982.

Kuznetsova, L. I.; Yurieva, T. M.; Minyukova, T. P.; Ketchik, S. V.; Plyasova, L. M.; Boreskov, G. K. Nature of the active component of copper-zinc-aluminum catalyst for methanol synthesis. React. Kinet. Catal. Lett. 19: 355-359; 1982.

Lander, Elliot P.; Hubbard, J. Nathan; Smith, Lawrence A., Jr. Revving-up refining profits with catalytic distillation. Chem. Eng. 90 (Apr. 18): 36-39; 1983.

Lange's handbook of chemistry. 11th ed. Dean, John A. ed. New York: McGraw-Hill Book Co.; 1973; 3.118-3.123.

Larson, Alfred T., inventor. Production of methanol and other carbon compounds and catalytic agents for use therein. U.S. patent 2,061,470. 1936 Nov. 17.

Little, L. H. Infrared spectra of adsorbed species. New York: Academic Press; 1966.

London, Jack W.; Bell, Alexis T. Infrared spectra of carbon monoxide, carbon dioxide, nitric oxide, nitrogen dioxide, nitrous oxide, and nitrogen adsorbed on copper oxide. J. Catal. 31: 32-40; 1973.

Ludlum, K. H.; Eischens, R. P. Carbonyl formation in stainless steel infrared cells. Surface Sci. 40: 397-398; 1973.

Lüth, H.; Rubloff, G. W.; Grobman, W. D. Ultraviolet-photoemission studies of formic acid decomposition on ZnO nonpolar surfaces. Solid State Commun. 18: 1427-1430; 1976.

Matsushita, Sanjuro; Nakata, Toshiko. Infrared absorption of zinc oxide and of adsorbed CO_2. II. J. Chem. Phys. 36: 665-669; 1962.

McClellan, M. R.; Trenary, M.; Shinn, N. D.; Sayers, M. J.; D'Amico, K. L.; Solomon, Edward I.; McFeely, F. R. An angle resolved photoemission determination of the coordination of CO to the ZnO (0001) surface. J. Chem. Phys. 74: 4726-4731; 1981.

McIntyre, N. S. Analysis of corrosion films using XPS: Advantages and limitations. Windawi, Hassan; Ho, Floyd F.-L. eds. Applied electron spectroscopy for chemical analysis. New York: John Wiley & Sons; 1982; 99-101.

Mehta, S.; Simmons, G. W.; Klier, K.; Herman, R. G. Catalytic synthesis of methanol from CO/H_2 II. Electron microscopy (TEM, STEM, microdiffraction, and energy dispersive analysis) of the Cu/ZnO and $Cu/ZnO/Cr_2O_3$ catalysts. J. Catal. 57: 339-360; 1979.

Metallgesellschaft, assignee. Methanol production from carbon monoxide/dioxide and hydrogen. French patent 2,049,193. 1971 March 26.

Miyata, Hisashi; Nakajima, Takashi; Kubokawa, Yutaka. Infrared studies of oxidation of 2-butanol and 2-methyl-2-propanol adsorbed on ZnO. J. Catal. 69: 292-298; 1981.

Molstad, M. C.; Dodge, B. F. Zinc oxide — Chromium oxide catalysts for methanol synthesis. Ind. Eng. Chem. 27: 134-140; 1935.

Morimoto, Tetsuo; Morishige, Kunimitsu. Interaction between carbon dioxide and the zinc oxide surface. Bull. Chem. Soc. Japan 47: 92-94; 1974.

Morimoto, Tetsuo; Morishige, Kunimitsu. Relation between amounts of chemisorbed water and carbon dioxide on zinc oxide. J. Phys. Chem. 79: 1573-1577; 1975.

Morimoto, Tetsuo; Nagao, Mahiko. Adsorption anomaly in the system zinc oxide-water. J. Phys. Chem. 78: 1116-1120; 1974.

Morimoto, Tetsuo; Yanai, Hiromi; Nagao, Mahiko. Infrared spectra of ammonia adsorbed on zinc oxide. J. Phys. Chem. 80: 471-475; 1976.

Morterra, C.; Coluccia, S.; Ghiotti, G.; Zecchina, A. An IR spectroscopic characterization of alpha alumina surface properties. Carbon dioxide adsorption. Z. Phys. Chem. Neue Folge 104: 275-290; 1977.

Nagao, Mahiko; Morimoto, Tetsuo. Adsorption of alcohols on zinc oxide surfaces. J. Phys. Chem. 84: 2054-2058; 1980.

Nagao, Mahiko; Morishige, Kunimitsu; Takeshita, Toshie; Morimoto, Tetsuo. Porous structure formed by the decomposition of the surface product on ZnO preserved in the atmosphere. Bull. Chem. Soc. Japan 47: 2107-2110; 1974.

Nagao, Mahiko; Yunoki, Koji; Muraishi, Haruto; Morimoto, Tetsuo. Differential heat of chemisorption. I. Chemisorption of water on zinc oxide and titanium oxide. J. Phys. Chem. 82: 1032-1035; 1978.

Nakamoto, Kazuo. Infrared and Raman spectra of inorganic and coordination compounds. 3rd ed. New York: John Wiley & Sons; 1978; 243-245.

Natta, G. Synthesis of methanol. Emmett, P. H. ed. Catalysis. Vol. 3. New York: Reinhold; 1955; 349-411.

Natta, G.; Pino, P.; Mazzanti, G.; Pasquon, I. Kinetic interpretation of the heterogeneous catalysis of high pressure reactions — Synthesis of methanol. Chim. Ind. (Milan) 35: 705-725; 1953.

Newman, Roger. Polarized infrared spectrum of sodium formate. J. Chem. Phys. 20: 1663-1664; 1952.

Newsome, David S. The w[illegible]er-gas shift reaction. Catal. Rev. — Sci. Eng. 21 (2): 275-318; 1980.

Nguyen, Tam T.; Sheppard, Norman. The adsorption of allylbenzene on zinc oxide: An infrared spectroscopic study. J. Catal. 67: 402-409; 1981.

Noto, Yuko; Fukuda, Kenzo; Onishi, Takaharu; Tamaru, Kenzi. The dehydrogenation of formic acid over zinc oxide. Bull. Chem. Soc. Japan 40: 2722; 1967.

Oba, M. Zinc oxide catalysts. V. Catalytic activity for methanol synthesis of catalysts prepared by precipitation method. Tokyo Kogyo Shikensho Kokoku 60: 121-123; 1965.

Okamoto, Yasuaki; Fukino, Kiyotaka; Imanaka, Toshinobu; Teranishi, Shiichiro. A study of the catalytically active copper species in the synthesis of methanol on Cu-ZnO by x-ray photoelectron spectroscopy. J. Chem. Soc., Chem. Commun.: 1405-1407; 1982.

Okamoto, Yasuaki; Fukino, Kiyotaka; Imanaka, Toshinobu; Teranishi, Shiichiro. Surface characterization of CuO-ZnO methanol-synthesis catalysts by x-ray photoelectron spectroscopy. 1. Precursor and calcined catalysts. J. Phys. Chem. 87: 3740-3747; 1983a.

Okamoto, Yasuaki; Fukino, Kiyotaka; Imanaka, Toshinobu; Teranishi, Shiichiro. Surface characterization of CuO-ZnO methanol-synthesis catalysts by x-ray photoelectron spectroscopy. 2. Reduced catalysts. J. Phys. Chem. 87: 3747-3754; 1983b.

Ostrovskii, V. E.; Dyatlov, A. A.; Ogneva, T. P. Adsorption of carbon monoxide on the low-temperature methanol synthesis catalyst. Kinet. Catal. 19: 410-413; 1978. Translated from Kinet. Katal. 19: 514-518; 1978.

Parkinson, Gerald; Skole, Robert; McQueen, Silke; Payne, Adam. California puts methanol plan into high gear. Chem. Eng. 89 (Nov. 1): 30-33; 1982.

Parkyns, N. D. Surface properties of metal oxides. Part I. Infrared studies of the adsorption and oxidation of carbon monoxide on alumina. J. Chem. Soc. (A): 1910-1913; 1967.

Parkyns, N. D. The surface properties of metal oxides. Part II. An infrared study of the adsorption of carbon dioxide on γ-alumina. J. Chem. Soc. (A): 410-417; 1969.

Pasquali, Marco; Marchetti, Fabio; Floriani, Carlo. Synthesis, properties, and x-ray structure of (diethylenetriamine)copper(I) carbonyl: A highly thermally stable copper(I) amine carbonyl. Inorg. Chem. 17: 1684-1688; 1978.

Pasquali, Marco; Marini, Giuliana; Floriani, Carlo; Gaetani-Manfredotti, Amelia. The role of halide ligands in copper(I) carbonyl chemistry: Synthesis of monohalogen-bridged dinuclear copper(I) carbonyls, and x-ray crystal structure of $(Cu_2(Me_2NCH_2CH_2NMe_2)_2(CO)_2Cl)(BPh_4)$. J. Chem. Soc., Chem. Commun.: 937-938; 1979.

Pasquali, Marco; Floriani, Carlo; Gaetani-Manfredotti, Amelia. Copper-amine-carbonyl chemistry. Solution and solid-state studies of the copper(I)-ethylenediamine-carbon monoxide system: Synthesis and x-ray structures of mononuclear and binuclear copper(I)-carbonyl complexes. Inorg. Chem. 19: 1191-1197; 1980a.

Pasquali, Marco; Marini, Giuliana; Floriani, Carlo; Gaetani-Manfredotti, Amelia; Guastini, Carlo. Model compounds for copper(I) sites in hemocyanins: Synthesis, structure, and properties of copper(I) — Histamine complexes. Inorg. Chem. 19: 2525-2531; 1980b.

Pasquali, M.; Fiaschi, P.; Floriani, C.; Zanazzi, P. F. Copper(I) binds carbon monoxide in a cubane-like structure: Chemistry and x-ray crystal structure of tetrakis((2-methylquinolin-8-olato)-carbonylcopper(I)). J. Chem. Soc., Chem. Commun.: 613-614; 1983.

Penninger, Johannes M. L. A spectroscopic flow reactor for *in situ* studies of heterogeneous catalysts at elevated pressure and temperature by means of IR transmission spectroscopy. J. Catal. 56: 287-289; 1979.

Peri, J. B. Infrared and gravimetric study of the surface hydration of γ-alumina. J. Phys. Chem. 69: 211-219; 1965.

Pinchas, S.; Laulicht, I. Infrared spectra of labelled compounds. New York: Academic Press; 1971.

Plotnikov, V. A.; Ivanov, K. N.; Pospekhov, D. A. J. Chem. Ind. (Moscow) 8: 119, 472; 1931.

Pritchard, J.; Sims, M. L. Infra-red reflection spectra of adsorbed CO on copper. Trans. Faraday Soc. 66: 427-433; 1970.

Pritchard, J.; Catterick, T.; Gupta, R. K. Infrared spectroscopy of chemisorbed carbon monoxide on copper. Surface Sci. 53: 1-20; 1975.

Rálek, M.; Gunsser, W.; Knappwost, A. ESR studies on $ZnO-Cr_2O_3$ catalysts. J. Catal. 11: 317-325; 1968.

Reid, Robert C.; Prausnitz, John M.; Sherwood, Thomas K. The properties of gases and liquids. 3rd ed. New York: McGraw-Hill Book Co.; 1977; Appendix A.

Rozovskii, A. Ya. New data on the mechanism of catalytic reactions with the participation of carbon oxides. Kinet. Catal. 21: 78-87; 1980. Translated from Kinet. Katal. 21: 97-107; 1980.

Rozovskii, A. Ya.; Kagan, Yu. B.; Lin, G. I.; Slivinskii, E. V.; Loktev, S. M.; Liberov, L. G.; Bashkirov, A. N. Mechanism for the synthesis of methanol from carbon monoxide and hydrogen. Kinet. Catal. 16: 706; 1975. Translated from Kinet. Katal. 16: 810; 1975.

Rozovskii, A. Ya.; Lin, G. I.; Loktev, S. M.; Kagan, Yu. B.; Bashkirov, A. N. Transformations of methanol on a copper-containing oxide catalyst. Kinet. Catal. 17: 933; 1976a. Translated from Kinet. Katal. 17: 1071; 1976.

Rozovskii, A. Ya.; Kagan, Yu. B.; Lin, G. I.; Slivinskii, E. V.; Loktev, S. M.; Liberov, L. G.; Bashkirov, A. N. Mechanism of methanol synthesis from carbon dioxide and hydrogen II. Selection of the reaction mechanism. Kinet. Catal. 17: 1132-1138; 1976b. Translated from Kinet. Katal. 17: 1314-1320; 1976.

Rozovskii, A. Ya.; Lin, G. I.; Liberov, L. G.; Slivinskii, E. V.; Loktev, S. M.; Kagan, Yu. B.; Bashkirov, A. N. Mechanism of methanol synthesis from carbon dioxide and hydrogen III. Determination of rates of individual stages using ^{14}CO. Kinet. Catal. 18: 578-585; 1977. Translated from Kinet. Katal. 18: 691-699; 1977.

Rubloff, G. W.; Lüth, H.; Grobman, W. D. Orbital energy shifts associated with chemical bonding of organic molecules on ZnO nonpolar surfaces. Chem. Phys. Lett. 39: 493-496; 1976.

Rudnitskii, L. A.; Maksimova, N. P.; Alekseev, A. M. Investigation of the adsorption isotherms of hydrogen on zinc-chromium and zinc-chromium-copper catalysts. Kinet. Catal. 14: 1331-1337; 1973. Translated from Kinet. Katal. 14: 1505-1513; 1973.

Ruggeri, O.; Trifirò, F.; Vaccari, A. Catalysts for low-temperature methanol synthesis I. A study of the reduction process. J. Solid State Chem. 42: 120-124; 1982.

Ryberg, Roger. Carbon monoxide adsorbed on Cu(100) studied by infrared spectroscopy. Surface Sci. 114: 627-641; 1982.

Saussey, Jacques; Lavalley, Jean-Claude; Lamotte, Jean; Rais, Taoufik. I.R. spectroscopic evidence of formyl species formed by CO and H_2 co-adsorption on ZnO and Cu-ZnO. J. Chem. Soc., Chem. Commun.: 278-279; 1982.

Sayers, M. J.; McClellan, M. R.; Gay, R. R.; Solomon, Edward I.; McFeely, F. R. Angle resolved photoemission investigation of the bonding geometry of CO to ZnO ($10\bar{1}0$). Chem. Phys. Lett. 75: 575-578; 1980.

Sayers, M. J.; McClellan, M. R.; Shinn, N. D.; Trenary, M.; McFeely, F. R. A novel bonding geometry of CO on Cu(311) as determined by angle-resolved photoemission spectroscopy. Chem. Phys. Lett. 80: 521-525; 1981.

Scholten, J. J. F.; van Montfoort, A. An I.R. and volumetric study of hydrogen chemisorption on zinc oxide. Hightower, Joe W. ed. Proceedings of the 5th International Congress on Catalysis. New York: Elsevier Scientific; 1973; 385-395.

Semenova, T. A.; Lyudkovskaya, B. G.; Markina, M. I.; Volynkina, A. Ya.; Cherkasov, G. P.; Sharkina, V. I.; Khitrova, N. F.; Shpiro, G. P. Phase transformations and properties of the low-temperature carbon monoxide conversion catalyst during the time of its reduction and operations. Kinet. Catal. 18: 834-838; 1977. Translated from Kinet. Katal. 18: 1014-1020; 1977.

Sexton, Brett A. Surface vibrations of adsorbed intermediates in the reaction of alcohols with Cu(100). Surface Sci. 88: 299-318; 1979.

Shannon, R. D.; Prewitt, C. T. Effective ionic radii in oxides and fluorides. Acta Cryst. B25: 925-946; 1969.

Shimomura, Kin'ya; Ogawa, Kiyoshi; Oba, Masaaki; Kotera, Yoshihide. Copper oxide-zinc oxide-alumina catalyst: The structure of a copper oxide-zinc oxide-alumina catalyst for methanol synthesis. J. Catal. 52: 191-205; 1978.

Shishkov, D. S.; Kasabova, N. A.; Gatev, E. M. Aging processes in low-temperature catalysts for carbon monoxide conversion and methanol synthesis. Kinet. Catal. 20: 429-432; 1979. Translated from Kinet. Katal. 20: 521-524; 1979.

Smith, Garry; Cole-Hamilton, David J. Cationic formyl complexes of ruthenium(II). J. Chem. Soc., Chem. Commun.: 490-491; 1982.

Stiles, Alvin B., inventor. Methanol synthesis catalyst. U.S. patent 4,111,847. 1978 Sep. 5.

Strelzoff, Samuel. Methanol: Its technology and economics. Danner, G. A. ed. Methanol technology and economics. Chem. Eng. Progr. Symposium Ser. No. 98 66: 54-68; 1970.

Taylor, J. H.; Amberg, C. H. Infrared spectra of gases chemisorbed on zinc oxide I. CO and CO_2. Can. J. Chem. 39: 535-539; 1961.

Thomas, W. J.; Portalski, Stanislaw. Thermodynamics in methanol synthesis. Ind. Eng. Chem. 50: 967-970; 1958.

Thorn, David L. Hydrido-formyl complexes of iridium. The first cationic formyl complex and its reduction to a stable cis-hydrido-methyl compound. J. Am. Chem. Soc. 102: 7109-7110; 1980.

Tinker, H. Burnham; Morris, Donald E. High-pressure, high-temperature spectrophotometer cell for in situ catalyst identification. Perkins, A. J.; Grove, E. L.; Kaelble, Emmett F.; Westermeyer, Joan E. eds. Developments in applied spectroscopy. Vol. 10. New York: Plenum Press; 1972; 123-135.

Tsuchiya, Susumu; Shiba, Tadao. Mutual influence of adsorption of hydrogen and carbon monoxide on a methanol synthesis catalyst. J. Catal. 4: 116-122; 1965.

Ueno, Akifumi; Onishi, Takaharu; Tamaru, Kenzi. Dynamic technique to elucidate the reaction intermediate in surface catalysis. Trans. Faraday Soc. 66: 756-763; 1970.

Ueno, Akifumi; Onishi, Takaharu; Tamaru, Kenzi. Reaction intermediates in methyl alcohol decomposition on ZnO. Trans. Faraday Soc. 67: 3585-3589; 1971.

van Herwijnen, T.; de Jong, W. A. Kinetics and mechanism of the CO shift on Cu/ZnO I. Kinetics of the forward and reverse CO shift reactions. J. Catal. 63: 83-93; 1980.

van Herwijnen, T.; Guczalski, R. T.; de Jong, W. A. Kinetics and mechanism of the CO shift on Cu/ZnO II. Kinetics of the decomposition of formic acid. J. Catal. 63: 94-101; 1980.

Veltistova, M. V.; Dolgov, B. N.; Karpov, A. Z. J. Chem. Ind. (9): 24; 1934.

Vlasenko, V. Catalytic activity of precipitated zinc-chromium catalyst of various chemical compositions in the methanol synthesis. Ukr. Khim. Zh. 32: 348-353; 1966.

Wachs, Israel E.; Madix, Robert J. The selective oxidation of CH_3OH to H_2CO on a copper(110) catalyst. J. Catal. 53: 208-227; 1978.

Wachs, Israel E.; Madix, Robert J. The oxidation of H_2CO on a copper(110) surface. Surface Sci. 84: 375-386; 1979.

Wadayama, Toshimasa; Monma, Kiyoshi; Suĕtaka, Wataru. Multiple adsorbates on copper surfaces in formic acid vapor observed by polarization modulation infrared spectroscopy. J. Phys. Chem. 87: 3181-3183; 1983.

Wagner, C. D.; Riggs, W. M.; Davis, L. E.; Moulder, J. F.; Muilenberg, G. E. eds. Handbook of x-ray photoelectron spectroscopy. Eden Prairie, MN: Perkin-Elmer; 1979; 171.

Wayland, Bradford B.; Woods, Bruce A. Observation of a neutral metallo-formyl complex formed by the reaction of rhodium octaethylporphyrin hydride with carbon monoxide. J. Chem. Soc., Chem. Commun.: 700-701; 1981.

Weismantel, Guy E. Methanol supplies: Too much or too little? Chem. Eng. 87 (July 14): 75-78; 1980.

Williams, Roberto J. J.; Cunningham, Roberto E. Noncatalytic gas-solid reaction. Chromium oxide catalyst in methanol synthesis. Ind. Eng. Chem., Prod. Res. Develop. 13: 49-60; 1974.

Wood, Bernard J.; Isakson, William E.; Wise, Henry. Kinetic studies of catalyst poisoning during methanol synthesis at high pressures. Ind. Eng. Chem., Prod. Res. Develop. 19: 197-204; 1980.

Zecchina, A.; Coluccia, S.; Guglielminotti, E.; Ghiotti, G. An infrared study of surface properties of α-chromia. I. Preparation and adsorption of water, heavy water, and carbon monoxide. J. Phys. Chem. 75: 2774-2783; 1971a.

Zecchina, A.; Coluccia, S.; Guglielminotti, E.; Ghiotti, G. An infrared study of surface properties of α-chromia. III. Adsorption of carbon dioxide. J. Phys. Chem. 75: 2790-2798; 1971b.

ACKNOWLEDGMENTS

I am grateful to Professor Glenn Schrader for the opportunity to work on this research at the University of Delaware and Iowa State University. I am also indebted to the many colleagues at both of these institutions who have been helpful and cooperative during my professional activities. In particular, I thank Mr. David Studer for the construction of the high pressure infrared cell, Dr. John McClellan for use of his photoacoustic cell, Mr. Jim Anderegg for obtaining the XPS-Auger measurements, and Dr. Bernard Harbrecht for assistance with the Guinier X-ray technique. The encouragement and advice of Professor Alvin Stiles for catalyst preparation have been invaluable.

The pursuit of this degree has been more than a technical task; it has been a way of life for the last five years. Therefore, it is appropriate also to acknowledge the support and fellowship provided by my family and friends which have sustained me toward my goal.

APPENDIX A.

CALCULATION OF XPS BINDING ENERGIES

The calculations involved in the analysis of XPS and AES data from an oxidized 67/33 Zn/Cu oxide are carried through in detail. Table 5 gives a value of 1191.2 eV for the C 1s photoelectron. The correction term for this sample is calculated from the Einstein relation using a value of 285.0 eV for the binding energy of the C 1s electron:

$$\phi = h\nu - E_K - E_B = 1486.6 - 1191.2 - 285.0 = 10.4 \text{ eV}$$

Using this value for the correction term, the binding energy of the Zn $2P_{3/2}$ photoelectron is calculated from the Einstein relation using the value of 454.4 eV for the kinetic energy obtained from Table 5:

$$E_B = h\nu - E_K - \phi = 1486.6 - 454.4 - 10.4 = 1021.8 \text{ eV}$$

In the same manner, the Cu $2P_{3/2}$ photoelectron is evaluated using the kinetic energy value of 542.8 eV:

$$E_B = h\nu - E_K - \phi = 1486.6 - 542.8 - 10.4 = 933.4 \text{ eV}$$

These binding energies can be compared to values reported in the literature.

From Figure 12, the experimental kinetic energy of the Cu $L_3M_{4,5}M_{4,5}$ Auger electron can be determined to be 908.2 eV. A correction term is added to this value to adjust the kinetic energy value with respect to the Fermi level:

$$E_K^* = E_K + \phi = 908.2 + 10.4 = 918.6 \text{ eV}$$

This Auger kinetic energy can be compared to values reported in the literature.

APPENDIX B.

CALCULATION OF BET SURFACE AREA AND MICROPORE DISTRIBUTION

The procedures for analyzing physical adsorption/desorption processes on catalysts using the Accusorb 2100E instrument have been described in detail for a sample of 95/5 ZnO/CuO catalyst which had been removed from the reactor after activity tests. The catalyst, having a weight (W_s) of 0.5220 g, was placed into a BET bulb and heated overnight at 190°C under vacuum to remove adsorbed gases. Then, the sample was cooled to liquid nitrogen temperature (T_s) for adsorption measurements. The dead space (V_s) in the bulb varies with the amount of sample used, so the first measurement utilizes helium (a nonadsorbing gas) to determine the value of V_s. The system is composed of three sections: a manifold (V_D) held at a constant temperature (T_D) of 307.2°K, the dead space in the bulb, and the interconnecting tubing (V_i) which has a temperature (T_i) taken as the average of the manifold and liquid nitrogen temperatures. The initial manifold pressure (H_1) was 550 mmHg and the final pressure (H_2) in the system was 148.7 mmHg. The dead space was calculated from a material balance based on the ideal gas law:

$$V_s = (T_s/H_2)[(V_D/T_D)(H_1 - H_2) - V_i H_2/T_i]$$

$$V_s = (77.40^{\circ}K/148.7\ mmHg)[(29.79\ ml/307.2^{\circ}K)(550.0 - 148.7\ mmHg) - (3.65\ ml)(148.7\ ml)/192.3^{\circ}K]$$

$$= 18.79\ ml$$

After pumping off the helium in the bulb, the adsorption of nitrogen was measured. Because the nitrogen gas in the bulb does not behave ideally, a correction term of $(1 + \alpha P_e)$ is applied to the dead space. The perfect gas law correction factor, α, for nitrogen is 6.6×10^{-5} $mmHg^{-1}$. The volume of nitrogen adsorbed on the catalyst (V_a), which is given at STP conditions (760 mmHg and 273.1°K), can be calculated from a material balance:

$$V_a = \frac{273.1^{\circ}K}{760\ mmHg}\left[\frac{V_D}{T_D}(P_1 - P_2) - \left(\frac{V_s}{T_s} + \frac{V_i}{T_i}\right)(P_2 - P_e) - \frac{V_s}{T_s}\alpha(P_2^2 - P_e^2)\right]$$

where the initial manifold pressure (P_1), the final system pressure (P_2), and the final system pressure from the previous measurement (P_e) are experimental values. Usually, four or five sets of pressure readings are obtained in the range from 0.05 to 0.3 P_2/P_s, where P_s is the saturation pressure of nitrogen at 77.40°K (765 mmHg). Table 26 gives experimental values for P_1 and P_2, and the calculated values for the normalized volume of adsorbed nitrogen and the relative pressure. The BET equation utilizes this information to determine the monolayer volume (V_m):

$$(W_s/V_a)(P_2/P_s - P_2) = C/V_m + [(C - 1)/CV_m](P_2/P_s)$$

A plot of $(W_s/V_a)(P_2/P_s - P_2)$ vs. P_2/P_s will yield a straight line with a slope of $W_s(C - 1)/CV_m$ and an intercept of W_s/CV_m. The value of V_m is simply $(\text{slope plus intercept})^{-1}$. A least-squares linear regression of the data points yielded a slope of 0.1681 and an intercept of 0.0012; the initial pair of data points were not used because the relative pressure was 0.0206 which was outside the linear region. The BET

Table 26. BET pressure readings and volume adsorbed

P_1 (mm Hg)	P_2 (mm Hg)	$\Sigma V_a/W_s$ (ml/g)	(P_2/P_s)
130.54	15.76	4.816	0.0206
151.36	48.92	5.654	0.0639
174.08	80.52	6.159	0.1053
197.82	110.20	6.597	0.1441
222.30	138.34	7.053	0.1808

surface area is the unit area per nitrogen molecule (S) times the number of molecules in a monolayer, which can be determined from the monolayer volume and the ideal gas law (the volume adsorbed was expressed at STP conditions). The BET surface area (S_w) was calculated to be:

$$S_w = SV_m(P/RT)_{STP}$$

$$= (16.2\ \text{Å}^2)(0.1681+0.0012)^{-1}(82.06 \times 273.1)^{-1}$$

$$(6.023 \times 10^{23}/10^{20}\ \text{Å}^2/\text{m}^2)$$

$$= 26\ \text{m}^2$$

Additional adsorption increments were made until the relative pressure (P_2/P_s) approached unity. Adsorbed nitrogen gradually filled the micropores during the adsorption process, with smaller pores filling before larger pores. Then, the pressure in the system was decreased by increments and a material balance made to determine the amount of nitrogen desorbed ($-V_a$) after each step. Both the adsorption and desorption isotherms were nearly the same, indicating that the desorption isotherm should be used for calculating the pore size distribution. A cylindrical pore model was utilized which assumes that the catalyst has

a distribution of pores of radii r_c with condensate of thickness t. The free radius, r, was determined from the Kelvin equation:

$$r = - 2\sigma M \cos\theta/(RT\rho \ln (P_2/P_s))$$

where σ is the surface tension of nitrogen, ρ is the density of liquid nitrogen, M is the molecular weight of nitrogen, and θ is the contact angle of the condensate (taken as zero). The condensate thickness was calculated from a Halsey-type expression:

$$t = 3.54[- 5/\ln (P_2/P_s)]^{0.33}$$

The pore radius was determined simply as:

$$r_c = r + t$$

Table 27 gives relative pressures, normalized volume of adsorbed nitrogen, pore radii, the change in pore radii between increments, the change in adsorbed nitrogen between increments, and the surface area of unfilled micropores ($\Sigma \Delta S_p$). The pore size distribution was plotted as $\Delta V/\Delta r$ vs. r_c. The surface area was calculated for each increment from geometrical considerations to be:

$$(\Sigma \Delta S_p)_i = \Sigma 2\Delta V_{p,i}/r_{c,i}$$

where

$$\Delta V_{p,i} = [\Delta V_i - \Delta t_i(\Sigma \Delta S_p)_{i-1}][r_c/(r_c - t)]_i^2$$

The total surface area of the micropores was determined to be 45 m^2/g, which is much higher than the BET surface area of 26 m^2/g. This

discrepancy indicates that the cylindrical pore model is not a true representation of the pore structure.

Table 27. Desorption pressure readings and volume desorbed

P_2/P_s	$\Sigma(V_a/W_s)$ (ml/g)	r_c (Å)	Δr (Å)	ΔV (ml)	$\Sigma \Delta S_p$ (m^2/g)
0.954	132.99	–	–	–	–
0.939	127.70	170	–	–	1.2
0.926	109.47	140	30	18.2	6.2
0.914	84.49	120	20	25.0	14
0.898	54.68	100	20	29.8	26
0.854	27.49	74	26	27.2	41
0.776	19.43	47	27	8.1	45

APPENDIX C.

THERMODYNAMICS OF METHANOL SYNTHESIS

A. $CO + 2H_2 = CH_3OH$ at 200°C and 50 atm

The standard-state free energy of formation for the reaction is

$$\Delta G^o = \Delta G^o_{CH_3OH} - \Delta G^o_{CO} - 2\Delta G^o_{H_2}$$
$$= -38.6 + 32.8 - 0.0 = -5.8 \text{ kcal/g mol}$$

The standard-state equilibrium constant is

$$K^o = \exp[-\Delta G^o/RT_o]$$
$$= \exp[5800/(1.99)(298)] = 1.8 \times 10^4$$

The standard-state heat of formation is

$$\Delta H^o = \Delta H^o_{CH_3OH} - \Delta H^o_{CO} - 2\Delta H^o_{H_2}$$
$$= -41.8 + 26.4 - 0.0 = -21.7 \text{ kcal/g mol}$$

The constants for the heat capacity expression are

$$\Delta a = \Sigma \nu_i a_i = a_{CH_3OH} - a_{CO} - 2a_{H_2}$$
$$= 5.052 - 7.373 - 2(6.483) = -15.287$$

$$\Delta b = \Sigma \nu_i b_i = b_{CH_3OH} - b_{CO} - 2b_{H_2}$$
$$= (1.694 + 0.307 - 2(0.2215)) \times 10^{-2} = 1.558 \times 10^{-2}$$

$$\Delta c = \Sigma \nu_i c_i = c_{CH_3OH} - c_{CO} - 2c_{H_2}$$
$$= (0.6179 - 0.6662 + 2(0.3298)) \times 10^{-5} = 0.6113 \times 10^{-5}$$

$$\Delta d = \Sigma \nu_i d_i = d_{CH_3OH} - d_{CO} - 2d_{H_2}$$
$$= (-6.811 + 3.037 - 2(1.826)) \times 10^{-9} = -7.426 \times 10^{-9}$$

The equilibrium constant at 473°K, using Equation 26, is

$$\ln K = 9.78 - (15.287/1.99) \ln (473/298) + (0.01558/2(1.99))$$
$$(473 - 298) + (0.6113 \times 10^{-5}/6(1.99))(473^2 - 298^2)$$
$$- (7.426 \times 10^{-9}/12(1.99))(473^3 - 298^3) + (1/1.99)$$

$$(21{,}700 - 15.287(298) + (.01558/2)(298)^2$$

$$+ (0.6113 \times 10^{-5}/3)(298)^3 - (7.426 \times 10^{-9}/4)(298)^4)$$

$$(1/473 - 1/298)$$

$$\ln K = -4.39$$

$$K = 0.0124$$

Using the fugacity coefficients from Table 22 and Equation 28,

$$y_1 = y_2 y_3^2 (0.0124)(0.98)(1.03)^2(50)^2/0.70$$

For an initial stoichiometric mixture of CO and H_2, the mole fraction of CO at equilibrium is $(1 - X)/(3 - 2X)$, the mole fraction of H_2 is $2(1 - X)/(3 - 2X)$, and the mole fraction of CH_3OH is $X/(3 - 2X)$. Substituting and solving for X,

$$X^3 - 3.01X^2 + 3.02X - 1 = 0$$

$$X \approx 0.82$$

$$y_1 = X/(3 - 2X) = .82/(3 - 1.64) = 0.60$$

B. $CO_2 + 3H_2 = CH_3OH + H_2O$ at 200°C and 50 atm

The standard-state free energy of formation for the reaction is

$$\Delta G^o = \Delta G^o_{CH_3OH} + \Delta G^o_{H_2O} - \Delta G^o_{CO_2} - 3\Delta G^o_{H_2}$$

$$= -38.62 - 54.64 + 94.26 - 0.0 = 1.00 \text{ kcal/g mol}$$

The standard-state equilibrium constant is

$$K^o = \exp[-1000/(1.99)(298)] = 0.185$$

The standard-state heat of formation is

$$\Delta H^o = \Delta H^o_{CH_3OH} + \Delta H^o_{H_2O} - \Delta H^o_{CO_2} - 3\Delta H^o_{H_2}$$

$$= -48.1 - 57.8 + 94.1 - 0.0 = -11.8 \text{ kcal/g mol}$$

The constants for the heat capacity expression are

$$\Delta a = a_{CH_3OH} + a_{H_2O} - a_{CO_2} - 3a_{H_2}$$

$$= 5.052 + 7.701 - 4.728 - 3(6.483) = -11.424$$

$$\Delta b = b_{CH_3OH} + b_{H_2O} - b_{CO_2} - 3b_{H_2}$$
$$= (1.694 + .046 - 1.754 - 3(0.2215)) \times 10^{-2} = - 0.679 \times 10^{-2}$$

$$\Delta c = c_{CH_3OH} + c_{H_2O} - c_{CO_2} - 3c_{H_2}$$
$$= (0.6179 + 0.2521 + 1.338 + 3(0.3298)) \times 10^{-5} = 3.197 \times 10^{-5}$$

$$\Delta d = d_{CH_3OH} + d_{H_2O} - d_{CO_2} - 3d_{H_2}$$
$$= (- 6.811 - 0.859 - 4.097 - 3(1.826)) \times 10^{-9} = - 17.25 \times 10^{-9}$$

The equilibrium constant at 473°K, using Equation 26, is

$$\ln K = - 1.686 - (11.424/1.99) \ln (473/298) - (0.00679/2(1.99))$$
$$(473 - 298) + (3.197 \times 10^{-5}/6(1.99))(473^2 - 298^2)$$
$$- (17.25 \times 10^{-9}/12(1.99))(473^3 - 298^3) + (1/1.99)$$
$$(11{,}800 - 11.424(298) - (0.00679/2)(298)^2 + (3.197 \times 10^{-5}/3)$$
$$(298)^3 - (17.25 \times 10^{-9}/4)(298)^4)(1/473 - 1/298)$$

$$\ln K = - 9.54$$

$$K = 7.21 \times 10^{-5}$$

Using the fugacity coefficients from Table 22 and Equation 27,

$$y_{CH_3OH} = y_{CO_2} y_{H_2}^3 \, (7.21 \times 10^{-5})(0.96)(1.03)^3(50)^2 / y_{H_2O}(0.70)(0.38)$$

For an initial stoichiometric mixture of CO_2 and H_2, the mole fraction of CO_2 at equilibrium is $(1 - X)/2(2 - X)$, the mole fraction of H_2 is $3(1 - X)/2(2 - X)$, the mole fraction of CH_3OH is $X/2(2 - X)$, and the mole fraction of H_2O is $X/2(2 - X)$. Substituting and solving for X,

$$X^4 - 21X^3 + 35X^2 - 27X + 6.7 = 0$$

$$X \approx .44$$

$$y_{CH_3OH} = X/2(2 - X) = .44/2(2 - .44) = 0.14$$

C. $HCOOH + 2H_2 = CH_3OH + H_2O$ at 200°C and 50 atm

The standard-state free energy of formation for the reaction is

$$\Delta G^o = \Delta G^o_{CH_3OH} + \Delta G^o_{H_2O} - \Delta G^o_{HCOOH} - 2\Delta G^o_{H_2}$$
$$= -38.62 - 54.64 + 80.24 - 0.0 = -13.02 \text{ kcal/g mol}$$

The standard-state equilibrium constant is

$$K^o = \exp[13020/(1.99)(298)] = 3.43 \times 10^9$$

The standard-state heat of formation is

$$\Delta H^o = \Delta H^o_{CH_3OH} + \Delta H^o_{H_2O} - \Delta H^o_{HCOOH} - 2\Delta H^o_{H_2}$$
$$= -48.1 - 57.8 + 86.7 - 0.0 = -19.2 \text{ kcal/g mol}$$

The constants for the heat capacity expression are

$$\Delta a = a_{CH_3OH} + a_{H_2O} - a_{HCOOH} - 2a_{H_2}$$
$$= 5.052 + 7.701 - 2.798 - 2(6.483) = -3.011$$

$$\Delta b = b_{CH_3OH} + b_{H_2O} - b_{HCOOH} - 2b_{H_2}$$
$$= (1.694 + 0.046 - 3.243 - 2(0.2215)) \times 10^{-2} = -0.01946$$

$$\Delta c = c_{CH_3OH} + c_{H_2O} - c_{HCOOH} - 2c_{H_2}$$
$$= (0.6179 + 0.2521 + 2.009 + 2(0.3298)) \times 10^{-5} = 3.539 \times 10^{-5}$$

$$\Delta d = d_{CH_3OH} + d_{H_2O} - d_{HCOOH} - 2d_{H_2}$$
$$= (-6.811 - 0.859 - 4.187 - 2(1.826)) \times 10^{-9} = -15.51 \times 10^{-9}$$

The equilibrium constant at 473°K, using Equation 26, is

$$\ln K = 21.96 - (3.011/1.99) \ln (473/298) - (0.01946/2(1.99))$$
$$(473 - 298) + (3.539 \times 10^{-5}/6(1.99))(473^2 - 298^2)$$
$$- (1.551 \times 10^{-8}/12(1.99))(473^3 - 298^3)$$
$$+ (1/1.99)(19200 - 3.011(298) - (0.01946/2)(298)^2$$
$$+ (3.539 \times 10^{-5}/3)(298)^3 - (1.551 \times 10^{-8}/4)(298)^4)(1/473 - 1/298)$$

$$\ln K = 9.69$$

$$K = 1.62 \times 10^4$$

Using the fugacity coefficients from Table 22 and Equation 27,

$$y_{CH_3OH} = y_{HCOOH} y_{H_2}^2 (1.62 \times 10^4)(50)(0.30)(1.03)^2 / y_{H_2O}(0.70)(0.38)$$

For an initial stoichiometric mixture of HCOOH and H_2, the mole fraction of HCOOH at equilibrium is $(1 - X)/(3 - X)$, the mole fraction of H_2 is $2(1 - X)/(3 - X)$, the mole fraction of H_2O is $X/(3 - X)$, and the mole fraction of CH_3OH is $X/(3 - X)$. Substituting and solving for X,

$$X \approx 0.999$$

$$y_{CH_3OH} = 0.999/(3 - 0.999) = 0.50$$

D. $HCHO + H_2 = CH_3OH$ at 200°C and 50 atm

The standard-state free energy of formation for the reaction is

$$\Delta G^o = \Delta G^o_{CH_3OH} - \Delta G^o_{HCHO} - \Delta G^o_{H_2}$$
$$= - 38.62 + 26.88 - 0.0 = - 11.74 \text{ kcal/g mol}$$

The standard-state equilibrium constant is

$$K^o = \exp[11740/(1.99)(298)] = 3.96 \times 10^8$$

The standard-state heat of formation is

$$\Delta H^o = \Delta H^o_{CH_3OH} - \Delta H^o_{HCHO} - \Delta H^o_{H_2}$$
$$= - 48.1 + 28.3 - 0.0 = - 19.8 \text{ kcal/g mol}$$

The constants for the heat capacity expression are

$$\Delta a = a_{CH_3OH} - a_{HCHO} - a_{H_2}$$
$$= 5.052 - 5.607 - 6.483 = - 7.038$$

$$\Delta b = b_{CH_3OH} - b_{HCHO} - b_{H_2}$$
$$= (1.694 - 0.754 - 0.222) \times 10^{-2} = .00718$$

$$\Delta c = c_{CH_3OH} - c_{HCHO} - c_{H_2}$$
$$= (0.6179 - 0.7130 + 0.3298) \times 10^{-5} = 2.347 \times 10^{-6}$$

$$\Delta d = d_{CH_3OH} - d_{HCHO} - d_{H_2}$$
$$= (- 6.811 + 5.494 - 1.826) \times 10^{-9} = - 3.143 \times 10^{-9}$$

The equilibrium constant at 473°K, using Equation 26, is

$$\ln K = 19.80 - (7.038/1.99)\ln(473/298) + (0.00718/2(1.99))(473 - 298) + (2.347 \times 10^{-6}/6(1.99))(473^2 - 298^2) - (3.143 \times 10^{-9}/12(1.99))(473^3 - 298^3) + (1/1.99)(19800 - 7.038(298) + (0.00718/2)(298)^2 + (2.347 \times 10^{-6}/3)(298)^3 - (3.143 \times 10^{-9}/4)(298)^4)(1/473 - 1/298)$$

$$\ln K = 7.26$$

$$K = 1.42 \times 10^3$$

Using the fugacity coefficients from Table 22 and Equation 27,

$$y_{CH_3OH} = y_{HCHO}y_{H_2}(1.42 \times 10^3)(50)(0.85)(1.03)/(0.70)$$

For an initial stoichiometric mixture of HCHO and H_2, the mole fraction of HCHO at equilibrium is $(1 - X)/(2 - X)$, the mole fraction of H_2 is $(1 - X)/(2 - X)$, and the mole fraction of CH_3OH is $X/(2 - X)$.

Substituting and solving for X,

$$X \approx 1.00$$

$$y_{CH_3OH} = 1.00$$

APPENDIX D.

THERMODYNAMICS OF THE WATER-GAS SHIFT REACTION

$CO + H_2O = CO_2 + H_2$ at 200°C and 50 atm

The standard-state free energy of formation for the reaction is:

$$\Delta G^o = \Delta G^o_{CO_2} + \Delta G^o_{H_2} - \Delta G^o_{CO} - \Delta G^o_{H_2O}$$
$$= - 94.26 + 0.0 + 32.81 + 54.64$$
$$= - 6.81 \text{ kcal/g mol}$$

The standard-state equilibrium constant is

$$K^o = \exp[- \Delta G^o/RT]$$
$$= \exp[6810/(1.99)(298)] = 9.71 \times 10^4$$

The standard-state heat of formation is

$$\Delta H^o = \Delta H^o_{CO_2} + \Delta H^o_{H_2} - \Delta H^o_{CO} - \Delta H^o_{H_2O}$$
$$= - 94.1 + 0.0 + 26.4 + 57.8 = - 9.9 \text{ kcal/g mol}$$

The constants for the heat capacity expression are

$$\Delta a = a_{CO_2} + a_{H_2} - a_{CO} - a_{H_2O}$$
$$= 4.728 + 6.483 - 7.373 - 7.701 = - 3.863$$

$$\Delta b = b_{CO_2} + b_{H_2} - b_{CO} - b_{H_2O}$$
$$= (1.754 + 0.222 + 0.307 - 0.046) \times 10^{-2} = 2.237 \times 10^{-2}$$

$$\Delta c = c_{CO_2} + c_{H_2} - c_{CO} - c_{H_2O}$$
$$= (- 1.338 - 0.330 - 0.666 - 0.252) \times 10^{-5} = - 2.586 \times 10^{-5}$$

$$\Delta d = d_{CO_2} + d_{H_2} - d_{CO} - d_{H_2O}$$
$$= (4.097 + 1.826 + 3.037 + 0.859) \times 10^{-9} = 9.819 \times 10^{-9}$$

The equilibrium constant at 473°K, using Equation 26, is

$$\ln K = 11.48 - (3.863/1.99) \ln (473/298) + (0.02237/2(1.99))$$
$$(473 - 298) - (2.586 \times 10^{-5}/6(1.99))(473^2 - 298^2)$$

$$+ (9.819 \times 10^{-9}/12(1.99))(473^3 - 298^3) + (1/1.99)(9900$$

$$- 3.863(298) + (0.02237/2)(298)^2 - (2.586 \times 10^{-5}/3)(298)^3$$

$$+ (9.819 \times 10^{-9}/4)(298)^4)(1/473 - 1/298)$$

$$\ln K = 5.33$$

$$K = 206.$$

Using the fugacity coefficients from Table 22 and Equation 27,

$$y_{CO_2} = y_{CO}y_{H_2O}(206)(0.98)(0.38)/y_{H_2}(1.03)(0.96)$$

For an initial stoichiometric mixture of CO and H_2O, the mole fractions of CO and H_2O at equilibrium are $(1 - X)/2$ and the mole fractions of CO_2 and H_2 are $X/2$. Substituting and solving for X,

$$X^2 = 2.03X + 1.01 = 0$$

$$X \approx 0.95$$

$$y_{CO_2} = X/2 = 0.95/2 = 0.48$$

APPENDIX E.

MASS FLOW CONTROLLER CALIBRATION CURVES

Although the manufacturer provided a calibration curve for each mass flow controller, flowrates were measured with a wet test meter at several pressures after the flow controllers had been installed in the flow system. Each flow setting was based on the digital indicator reading and not the potentiometer set point. Every point on a curve was an average of two flowrate measurements. Some of the low flowrates (< 200 cc/min STP) were checked with a bubble meter to ensure the accuracy of the results.

Calibration curves for nitrogen, hydrogen, and carbon monoxide at pressures of 1, 10, 30, and 50 atm are given in Figures 80, 81, and 82, respectively. The Brooks calibration curve, which was measured at 100 atm, has been included for comparison. The hydrogen line was also used with the premixed cylinder of hydrogen (90%) and carbon dioxide (10%); the calibration curve for this gas mixture at 1 and 50 atm is given in Figure 83. The curves for each gas show that the slope of each curve was pressure-dependent. This effect would not result from leakage because a leak would simply cause a shift in the entire curve without affecting the slope.

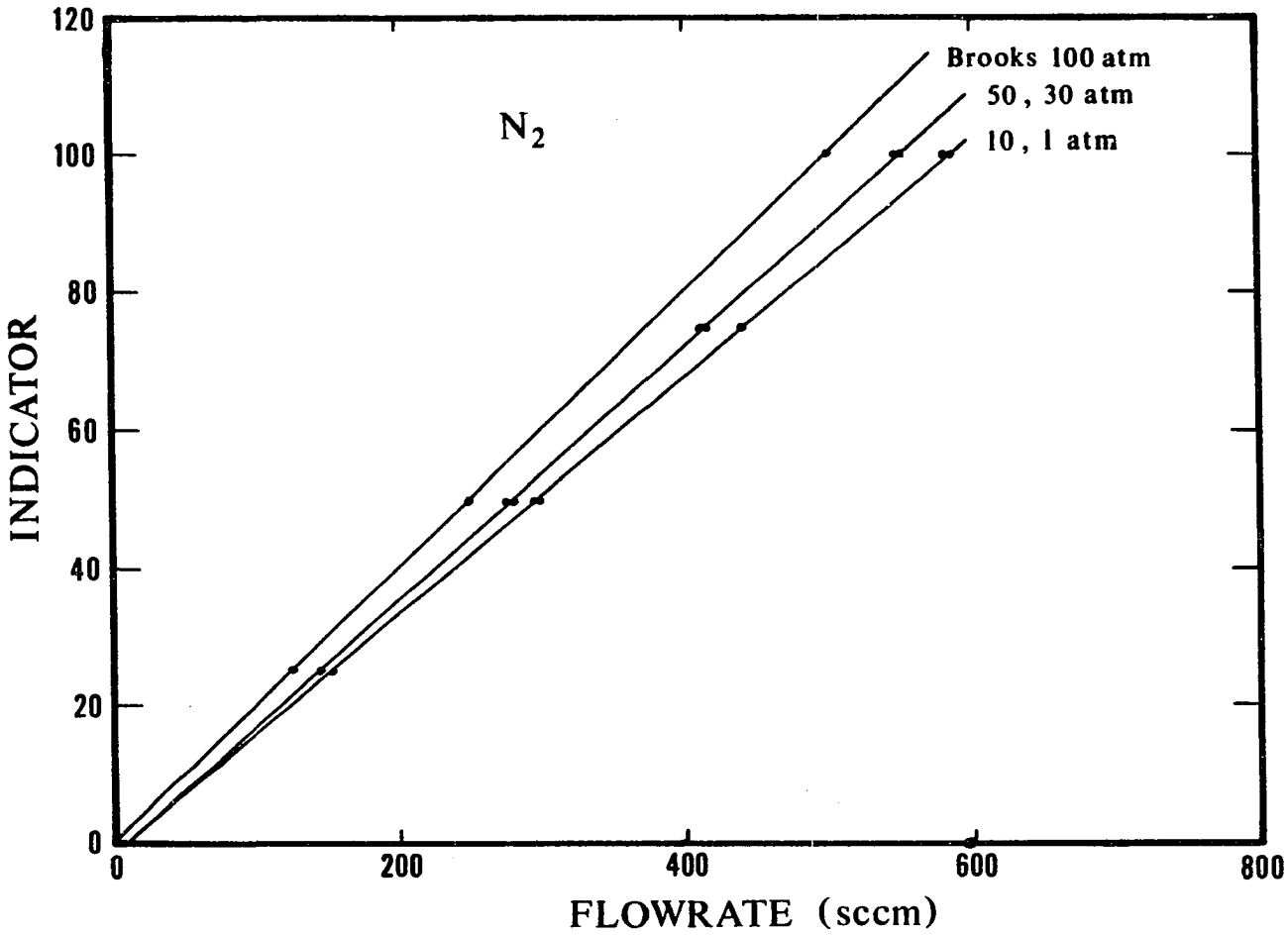

Figure 80. Calibration curves for nitrogen flowrates

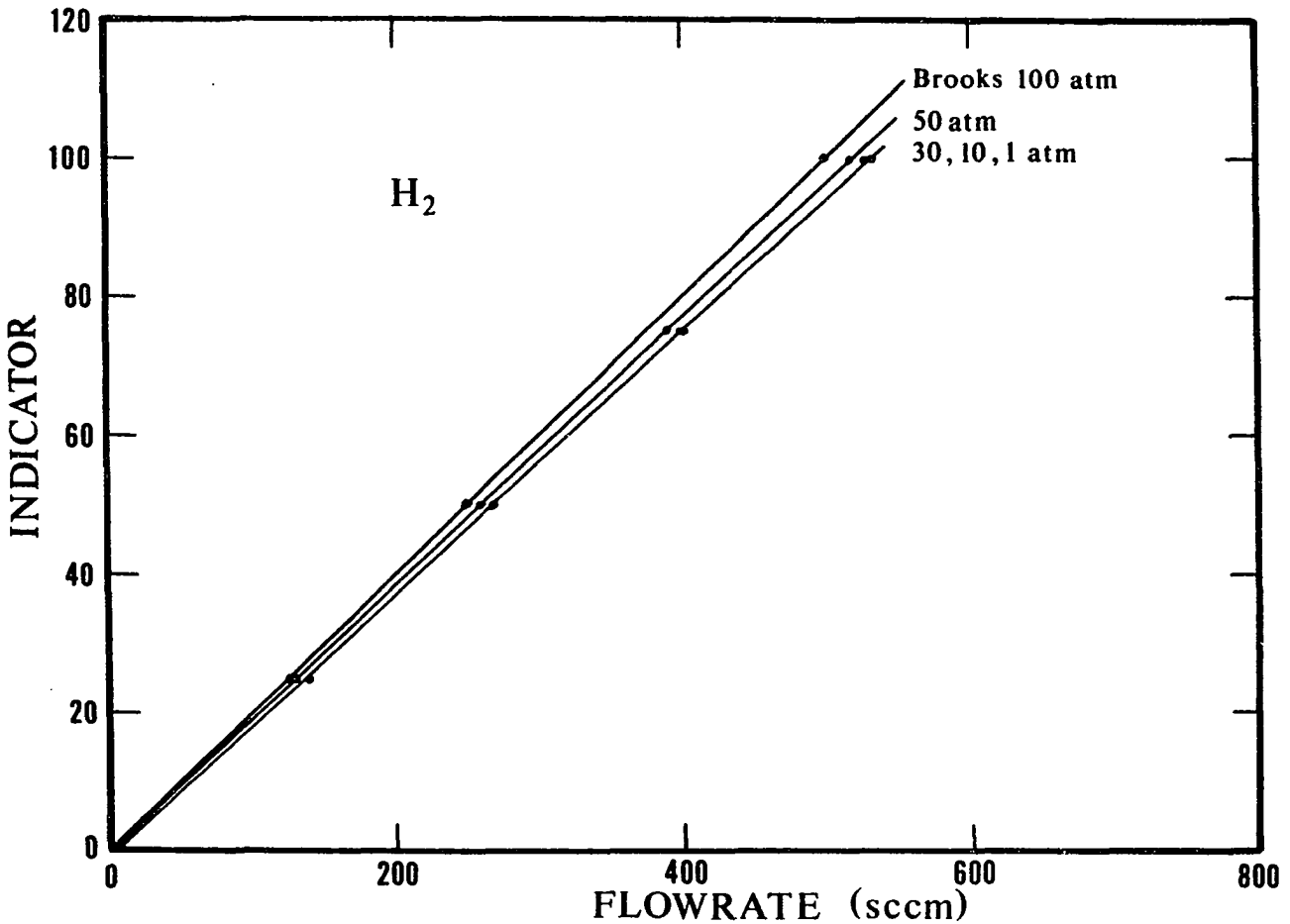

Figure 81. Calibration curves for hydrogen flowrates

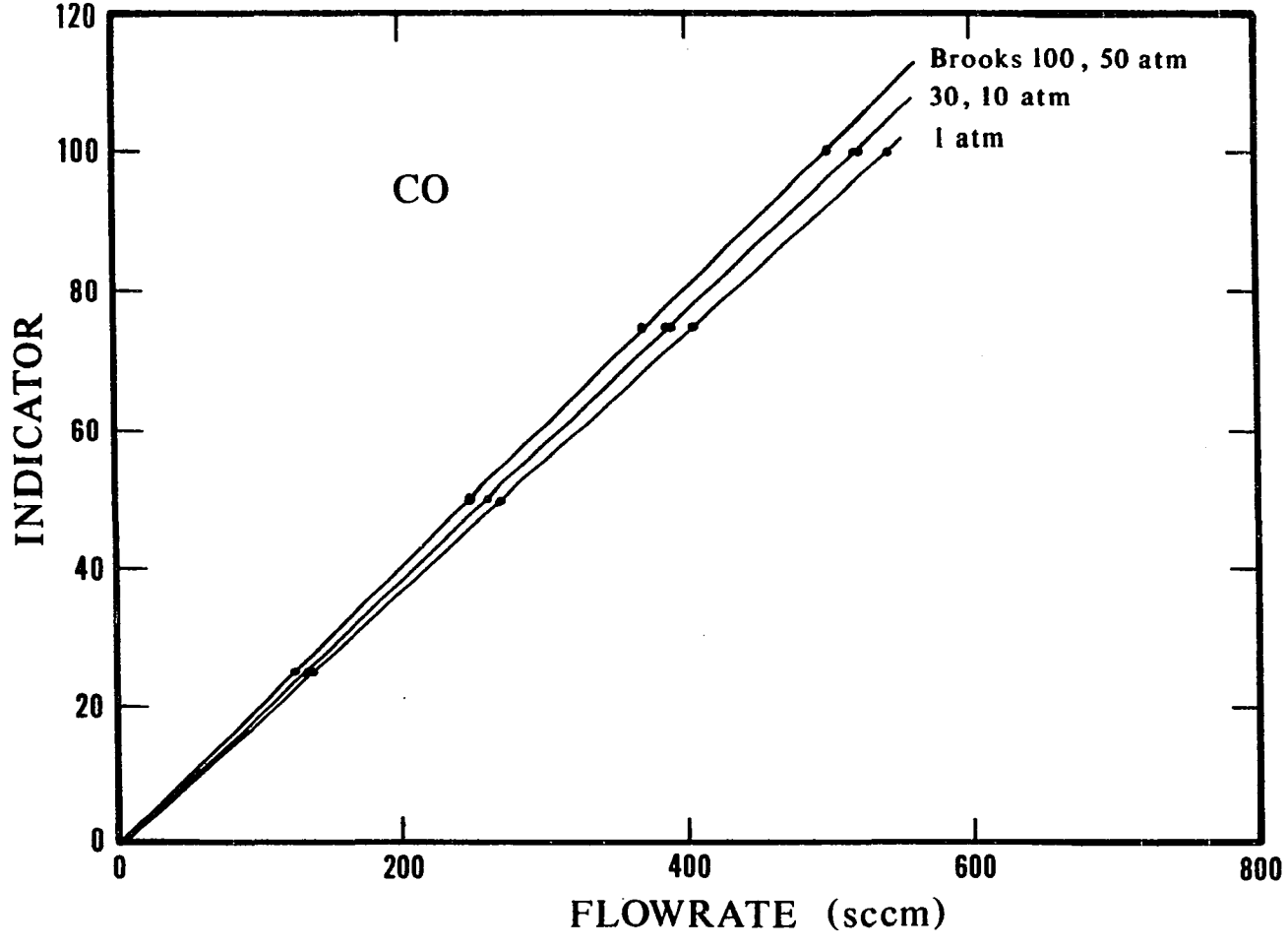

Figure 82. Calibration curves for carbon monoxide flowrates

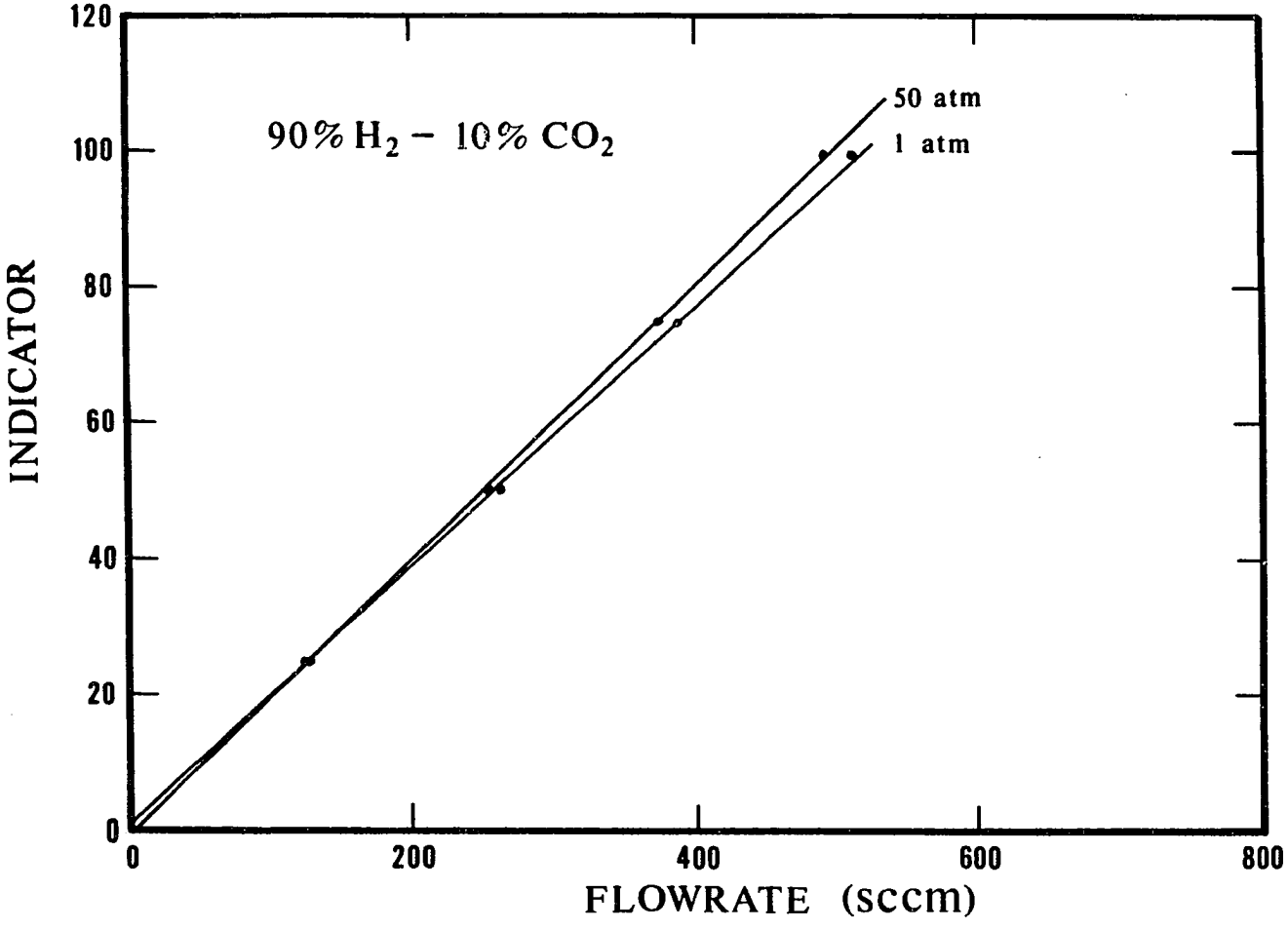

Figure 83. Calibration curves for 90% hydrogen-10% carbon dioxide flowrates

APPENDIX F.

RELATIVE RESPONSE FACTORS

A mixture of 95% CO, 4% CH_3OH, and 1% H_2O was prepared by injecting 17.6 µl of CH_3OH and 1.9 µl of H_2O into 250 cc of CO. After allowing enough time for the components to evaporate and mix, 0.5 cc samples were injected into the gas chromatograph. The response factor of CH_3OH was determined to be 1.11 and the response factor of H_2O to be 0.91. A mixture of 97.2% CO and 2.8% CH_3OH was prepared by injecting 12.0 µl of CH_3OH into 250 cc of CO. The response factor of CH_3OH was determined to be 1.19. A mixture of 99.0% CO and 1.0% CO_2 was prepared by injecting 2.5 cc of CO_2 into 250 cc of CO. The response factor of CO_2 was determined to be 0.98. A mixture of 52.9% CO and 47.1% N_2 was prepared by blending 35.5 cc/min CO with 31.6 cc/min N_2 and using the sampling loop to take samples. The response factor of N_2 was determined to be 1.10. Peak areas and relative response factor determinations have been given in Table 28.

Table 28. Relative response factors

1. 95% CO, 4% CH_3OH, 1% H_2O

   Area CO: 95.4, 95.2, 95.2, 95.4, 95.3; avg. = 95.3
   Area CH_3OH: 3.61, 3.66, 3.65, 3.54, 3.58; avg. = 3.61
   Area H_2O 1.01, 1.15, 1.13, 1.08, 1.14; avg. = 1.10

   $RF_{CH_3OH} = (4.0/95)(95.3/3.61) = 1.11$
   $RF_{H_2O} = (1.0/95)(95.3/1.10) = 0.91$

2. 97.2% CO, 2.8% CH_3OH

   Area CO: 97.6, 97.5, 97.6, 97.5, 97.6; avg. = 97.6
   Area CH_3OH: 2.40, 2.32, 2.38, 2.30, 2.43; avg. = 2.37

   $RF_{CH_3OH} = (2.8/97.2)(97.6/2.37) = 1.19$

3. 99.0% CO, 1.0% CO_2

   Area CO: 98.99, 98.98, 98.98, 98.98, 98.98; avg. = 98.98
   Area CO_2: 1.01, 1.02, 1.02, 1.02, 1.02; avg. = 1.02

   $RF_{CO_2} = (1.0/99.0)(98.98/1.02) = 0.98$

4. 52.9% CO, 47.1% N_2

   Area CO: 54.99, 55.18, 55.20, 54.90, 55.28; avg. = 55.11
   Area N_2: 44.94, 44.73, 44.72, 45.00, 44.66; avg. = 44.81

   $RF_{N_2} = (47.1/52.9)(55.11/44.81) = 1.10$